MeerKAT S-band calibrators candidates extension report

Document number	
Revision	A
Classification	Public
Released by	S Passmoor
Release Date	28 May 2026

Organisation	:	NRF (National Research Foundation)
Facility	:	SARAO (South African Radio Astronomy Observatory)
Project	:	MeerKAT
Document Type	:	Report (REP)
Function/Discipline	:	Commissioning, Science Operations

DOCUMENT APPROVALS

	Name	Designation	Affiliation	Date	Signature
Released by	Miriam Nyamai	Associate Operation Scientist	SARAO	n/a	n/a
Released by	Samuel Legodi	Operation Scientist	SARAO		
Released by	Sean Passmoor	Senior Operation Scientist	SARAO		

DOCUMENT HISTORY

Revision	Date of issue	Prepared by	Comments (e.g. ECN Number or changes to document)
01	28 May 2026	Miriam Nyamai	First Release Part of the effort to ensure legacy documents get put into document storage. Dr Miriam Nyamai prepared the report and calibrators were added to the Telescope database but left the Organisation before the report was signed.

DOCUMENT DISTRIBUTION

Publish:	Please publish documents once Approved in Key360 and the Internal Comms Portal were applicable.
Distribute:	Approved Record to be distributed to all signatories, relevant line managers, and Internal staff were applicable.

DOCUMENT SOFTWARE

Package		Version	Filename
Word Processor	Google Doc		

COMPANY DETAILS

Name	SARAO, Cape Town (Observatory, Cape Town)	SARAO, HartRAO (Hartebeesthoek, Gauteng)	SARAO, Karoo Astronomy Reserve (Northern Cape)
Physical / Postal Address	Liesbeek House Building, River Park, River Lane, Gloucester Road, Mowbray, 7700, South Africa	P.O. Box 443, Krugersdorp, 1740, South Africa	Posbus 69, Carnarvon, 8925, South Africa
Tel	+27 21 506 7300	+27 12 301 3100	+27 21 506 7300
Fax	+27 21 506 7375	+27 12 301 3300	+27 86 538 6836
Website	www.sarao.ac.za	www.hartrao.ac.za	www.sarao.ac.za

TABLE OF CONTENTS

LIST OF TABLES

LIST OF FIGURES

ABBREVIATIONS

CASA	Common Astronomy Software Applications
VLA	The Very Large Array
VLBA	The Very Long Baseline Array
ATCA	Australia Telescope Compact Array
SARAO	South African Radio Astronomy Observatory

1 INTRODUCTION

Phase calibration in a radio interferometry is the process of correcting the observed phases of signals received by an array of antennas. Complex gain in this context refers to the gain of an antenna system represented as a complex number. It consists of two components. The amplitude gain which refers to how much the signal strength is amplified or attenuated by the system and phase gain which determines how much the phase of the signal is shifted. A source with a known flux density, structure and position (a calibrator) is observed. The expected response from the calibrator is compared with the actual observed data and the difference between the two values, provides complex gain for each antenna. I.e, the amplitude gain and the phase shift. The complex gains calculations are done using CASA, which iteratively solves the gain equation for all antennas and baseline combinations.

In addition, a calibrator should be located close to the target object, ideally less than 5 degrees (Beasley et.a al, 1994) in the sky to experience similar atmospheric conditions and be observed regularly during an observation run. This concept was not investigated in this project. The phase errors introduced by the atmosphere are estimated by comparing the observed phase from the calibrator source to the expected phase (based on its known position). The phase corrections derived from the calibrator source are applied to the target source. This corrects for any distortions that occurred during the observation. Radio observations rely on interferometric combinations of signals from many antennas, and correct phase data ensures that the position and structure of observed targets are accurate.

An ideal calibrator for MeerKAT S band should therefore have:

- S-band flux densities above 0.5 Jy to ensure high signal-to-noise (S/N) ratio
- to be a point source
- to have inverted, flat and steep spectrum in-band spectrum but images are not fuzzy
- have closure phases less than 2°

NB: The calibrator sources should have known parameters such as flux, shape and spectrum

2 Analysis

In the following section, we provide background information of the analysis tools used.

2.1 Sample

A long list of the VLA Calibrator List (https://science.nrao.edu/facilities/vla/observing/callist) from declination of +40° to -40° . Each of the sources has a little 'matrix' listed, giving its suitability as a calibrator in a given band/configuration combination. MeerKAT's size is between the VLA's 'C' and 'B' configurations, so sources that were suitable calibrators in these configurations were used in the sample for MeerKAT. The VLA database makes recommendations (P = primary, the best, S = secondary, sources which are weaker, 'W' = weak, used only at Q-band, and 'X' = don't use, meaning it is too weak or is resolved) indicating whether one can use a point-source model or not. This was the initial list that was selected. All the sources in the VLA database were considered as potential calibrators. Some sources were considered from the VLBA database (https://www.vlba.nrao.edu/astro/calib/vlbaCalib_allfreq_cut_2025a.txt).

There was a next list made from the Australia Telescope Compact Array (ATCA;https://www.narrabri.atnf.csiro.au/calibrators/calibrator_database.html) calibrators with flux densities > 5 Jy between 2.1 GHz and 5.5 GHz bands and declinations below -40°to - 90°. The ATCA database lists of calibrators considered for MeerKAT observations are between RA 00 and 09. The remaining sources between RA 10 and 23 will be considered in the next project to include more sky coverage for MeerKAT.

2.2 Observations

Each source was observed with the MeerKAT radio telescope for three 5-minute scans and a phase calibrator was observed for 2 minutes every 30 minutes. Depending on the LST range available, the observations lasted between 4 hrs and 6 hrs. At least one of the flux calibrators was always present every 3 hrs. Sources were observed at the S3 sub-band (2406 MHz to 3281 MHz). MeerKAT S-band (https://skaafrica.atlassian.net/wiki/spaces/ESDKB/pages/277315585/MeerKAT+specifications) is divided into four sub-bands; S0: 1750 - 2625 MHz, S1: 1968 - 2843 MHz, S2: 2187 - 3062 MHz, S3: 2406 - 3281 MHz and S4: 2625 - 3500 MHz. The observations were taken between July, 2023 and April, 2024. The data is recorded under the following capture IDs, 169151138, 1690821078, 1690738463, 1690630277, 1699645638, 1701306207, 1702818796, 1703338876, 1704077799, 1704174687, 1706448981.

2.3 Calibration, imaging, rms

Calibration and imaging was done using the OxKAT (Heywood 2020; Heywood et al. 2022) pipeline (https://github.com/IanHeywood/oxkat). OxKAT uses several existing radio astronomy packages including CASA for tasks such as gain and bandpass calibration, self-calibration, and

flagging, CUBICAL (Kenyon et al. 2018) for further self-calibration procedures, TRICOLOUR (Hugo et al. 2022) for further flagging, and WSCLEAN (Offringa et al. 2014) for imaging. These steps are broken into first-generation calibration (1GC; direction-independent effects), flagging and self-calibration (2GC) based on closure phases in the target image itself. Oxkat generates images with WSClean, at the 1CG level and at the 2GC level with a robust weighting of -0.5.

Data products are continuum images provided for each calibrator source reported. To determine the flux density, we used the CASA task imfit to fit a two-dimensional Gaussian model to an emission region in an image. For each source we define a rectangle region around the source position. The Gaussian is described by the peak intensity (amplitude), position (right ascension and declination), Full width at half maximum (FWHM) in both major and minor axes, position angle which is the orientation of the major axis. The image to be fit is specified with the emission region within the region also specified. CASA performs the fitting by estimating an initial guess of parameters based on the intensity distribution in the image region. Using non-linear least-squares minimization to refine the estimates of the Gaussian parameters by comparing the observed data to the Gaussian model. The output of the fit are parameters such as the peak flux (the maximum brightness of the Gaussian at the centre), integrated flux density (the product of the peak intensity times the area of the Gaussian which is defined by the FWHM of the Gaussian), position (the right ascension and declination of the centre of the Gaussian), source size (FWHM of the minor and major axes) and orientation of the major axis relative to the sky (position angle).

Root Mean Square (rms) in the context of flux density considerations is a statistical measure to determine the detection of the noise level in a radio image. The rms value is the detection threshold of a source. If the flux density is above five times the rms, the source can be identified as real. To determine the rms value for each image we define a region (usually a rectangle or circle) very near the target's position, and measure using CASA, the pixel rms value. This value compared with the integrated flux density is used to determine the signal-to-noise (S/N).

3 RESULTS

3.1 Flux density, S/N, rms

In Table 1, is the list of MeerKAT S-band gain calibrators chosen from the VLA and ATCA databases. Initial criteria was that it should be flux density of > 0.5 Jy, centred on the candidate which is a point source. MeerKAT generally spends 2 mins on a known gain calibrator, which is sufficient to get precise measurements of the complex gains (amplitude and phase) for all antennas when using bright sources as calibrators. This also helps if the atmosphere is relatively stable, the calibration remains valid for several minutes before another calibration is needed. A 2 min scan on a source that is bright, ~0.5 Jy, produces theoretical noise of approximately 1e-5 Jy/beam hence signal to noise ratio of 1e4.

The integrated flux density, the ratio of peak flux density and integrated flux density to determine any significant variations between the two fluxes, and signal-to-noise ratio are given in Table 1. The comparison between the integrated flux density and peak flux density is made to determine the morphology or structure of a radio source, as well as its extent (whether it is compact or extended). Peak flux density is the highest observed flux density at a specific point in the radio image, often measured in Jy/beam. It indicates how bright the source appears at its brightest point. The integrated flux density is the total flux density summed over the entire source. The average radial extent measurement, which is the FWHM radius of the Gaussian fits is approximately 3.5 arcseconds**.** It accounts for the total radio emission from the source, not just at the peak, and is typically measured in Jy. By comparing these two values, scientists can determine if a source is point-like (compact) or extended. A compact Source is unresolved (appears as a point source), the peak flux density and integrated flux density will be nearly equal. This is because the source's emission is concentrated in a single, small area. An extended Source is resolved (spread out over a larger area) and the integrated flux density will be significantly higher than the peak flux density. This indicates that the source is not a point source, but has extended structure. A ratio significantly greater than 1 also suggests the source is larger than the beam size of the telescope.

The S/N diagnosis indicates if the calibrator is significantly brighter than the noise in the image. For accurate corrections, the calibrator's signal needs to be strong and easily distinguishable from noise. A high S/N ensures that the measured phase of the calibrator is precise, reducing the uncertainty in the phase corrections applied to the target source. In interferometric observations, you typically switch between the target source and the phase calibrator regularly. To minimise the time spent on calibrator observations (and maximise time on the target), you want the calibrator to have a S/N so that accurate phase solutions can be obtained in a short time. A low-S/N calibrator would require longer observation times to achieve the same level of accuracy, reducing the overall efficiency of the observation.

There is also listed a 'uv-range' plot in Table 3 for each calibrator -- this is the range in baseline spacing for which the source can be considered 'point-like'. This plot represents the distribution of spatial frequencies (UV distances) sampled by the interferometer and shows the amplitude of the observed signal as a function of the UV distance (baseline length in terms of wavelength), allowing astronomers to visualize how much signal is detected at different spatial scales. Shorter UV distances correspond to larger spatial scales (sensitive to extended, diffuse structures in the sky). Longer UV distances correspond to smaller spatial scales (sensitive to finer details or compact structures). The amplitude of the visibility function, which represents the correlated signal strength at each UV distance, provides information about the intensity of the emission from the source at different spatial scales. A higher amplitude at a particular UV range indicates a stronger contribution from that spatial scale.

If the signal amplitude decreases with increasing UV distance, this suggests that the source has more extended structures since more signal is coming from larger structures. If a significant signal is detected at long UV distances, this indicates the presence of compact structures or fine details.

If the amplitude remains relatively constant across UV distances, this means the calibrator is contributing similarly across all spatial scales, thus the source is likely to be compact and unresolved. If the amplitude peaks at specific UV ranges, this suggests the presence of multiple components, like a combination of compact and extended features.

We assumed the sources are not varying at short time scans (5 mins each scan). Variability on long timescales over months or years were not determined in this report.

Table 1: Below is a list of calibrators that are suitable for MeerKAT at S-band. Listed is the name, position, flux density from VLA and ATCA databases, integrated and peak flux density measurement at 2.84 GHz, the root-mean square (rms) flux and signal-to-noise ratio (S/N) of all selected targets (the ratio of integrated flux density and the rms pixel value). Bolded values are originally from the ATCA database of calibrators.

Calibrator Candidate name	RAJ2000	DECJ2000	VLA (3 GHz) Flux density or **ATCA (2.1 GHz) in Jy**	Integrated Flux density (2.84 GHz)/mJy	Peak flux density (2.84 GHz)/mJy	Ratio: Integrated Flux density /Peak flux density	Rms (mJy)	S/N
0012-399	00:12:59.8748	-039:54:25.9396	1.5	709.4 +/- 7.4	710.7 +/- 4.3	0.998	1.93e-2	4.5e4
0048-427	**00:51:09.4792**	**-042:26:33.0066**	**0.813**	**751.2 +/- 9.6**	**751.7 +/- 5.5**	**0.999**	**2.64e-2**	**2.8e4**
0131-522	**01:33:05.7637**	**-052:00:04.0249**	**0.862**	**1.108 +/- 0.011**	**1.1697 +/- 0.0067**	**0.947**	**2.08e-2**	**5.4e4**
0149+059	01:49:22.3695	+005:55:53.6532	0.89	815.1 +/- 2.6	852.9 +/- 1.5	0.955	4.32e-2	1.9e4
0204+152	02:04:50.4137	+015:14:11.0777	3.7	2.837 +/- 0.014	2.8620 +/- 0.0080	0.991	4.14e-2	6.9e4
0222-346	02:22:56.3984	-034:41:28.6523	0.69	788.1 +/- 6.2	784.9 +/- 3.6	1.004	1.66e-2	4.7e4
0308-611	**03:09:56.1019**	**-060:58:39.2968**	**1.018**	**2244.0 +/- 0.031**	**2223.0 +/- 0.018**	**1.01**	**2.7e-2**	**8.2e4**

0332-403	03:34:13.6576	-040:08:25.6207	1.91	1109 +/- 16	1139.4 +/- 9.3	0.973	2.21e-2	5e4
0843-54	**08:45:02.4609**	**-054:58:08.6723**	**0.857**	**943 +/- 14**	**919.1 +/- 7.7**	**1.03**	**1.79e-2**	**5.3e4**
1131-050	11:31:30.5219	-005:00:19.6368	0.9	601.3 +/- 2.9	600.3 +/- 1.7	1.001	3.38e-2	1.8e4
1145-228	11:45:22.0425	-022:50:31.5795	0.6	741.2 +/- 7.3	744.4 +/- 4.2	0.996	2.76e-2	2.7e4
1146-247	11:46:08.1039	-024:47:33.0979	1.1	1395. +/- 0.014	1399.8 +/- 0.0081	0.997	3.5e-2	4e4
1147-074	11:47:51.5523	-007:24:41.1457	1.0	1295.9 +/- 0.0078	1288.6 +/- 0.0045	1.01	4.1e-2	3.2e4
1305-105	13:05:33.01296	-010:33:19.2852	0.8	908.0 +/- 3.7	929.9 +/- 2.2	0.976	2.76e-2	3.3e4
1309+119	13:09:33.93	+011:54:24.71	0.8	732.1 +/- 7.5	732.6 +/- 4.3	0.999	3.75e-2	2e4
1351-018	13:54:06.8969	-002:06:03.1715	0.9	792.9 +/- 2.3	823.5 +/- 1.4	0.962	2.66e-2	3e4
1404-015	14:04:45.8968	-001:30:22.0105	0.6	577.2 +/- 2.5	599.0 +/- 1.5	0.964	2.37e-2	2.4e4
1446+173	14:46:35.3551	+017:21:07.7296	0.8	496.56 +/- 0.11	496.016 +/- 0.065	1.001	1.52e-2	3.3e4
1504+104	15:04:24.9855	+010:29:39.1578	1.5	1183.6 +/- 2.7	1174.1 +/- 1.5	1.008	3.74e-2	3.2e4
1505+034	15:05:06.480	+003:26:30.6184	0.9	702.67 +/- 0.19	700.66 +/- 0.11	1.003	1.59e-2	4.4e4
1507-168	15:07:04.7855	-016:52:30.2762	2.9	1195.6 +/- 1.4	1202.41 +/- 0.80	0.994	1.38e-2	8.7e4
1522-275	15:22:37.6664	-027:30:10.8157	1.93	1045.1 +/- 0.66	1054.61 +/- 0.38	0.991	1.35e-2	7.7e4
1557-000	15:57:51.4339	-000:01:50.5102	0.9	634.9 +/- 2.3	648.4 +/- 1.4	0.979	1.86e-2	3.4e4
1700-261	17:00:53.	-026:10:	0.75	2548.3 +/-	2576.7 +/-	0.989	1.81e-2	1.4e5

	1526	51.6626		4.1	2.4			
1743-038	17:43:58.8599	-003:50:04.5938	2.7	3731.3 +/- 5.6	3774.2 +/- 3.3	0.989	3.74e-2	9.9e4
1745-078	17:45:27.1116	-007:53:03.9886	0.93	1056.7 +/- 1.6	1059.64 +/- 0.92	0.997	1.67e-2	6.3e4
1937-399	19:37:16.2140	-039:58:01.5099	0.7	685.4 +/- 2.1	670.7 +/- 1.2	1.02	1.8e-2	3.8e4
1939-154	19:39:26.6652	-015:25:42.9837	1.3	1826.28 +/- 0.54	1826.08 +/- 0.31	1.00	2.24e-2	8.2e4
1958-179	20:00:57.09002	-017:48:57.7968	1.0	2563.48 +/- 0.59	2562.57 +/- 0.34	1.00	1.6e-2	1.6e5
2011-157	20:11:15.7123	-015:46:40.3466	1.3	1184.72 +/- 0.5	1181.55 +/- 0.29	1.002	1.42e-2	8.3e4
2236-145	22:36:34.0785	-014:33:22.17004	0.84	716.1 +/- 1.8	720.3 +/- 1.0	0.994	1.89e-2	3.8e4
2323-032	23:23:31.9599	-003:17:04.7703	0.8	1.3524 +/- 0.0098	1.3631 +/- 0.0057	0.992	4.78e-2	2.8e4
2324-372	23:24:07.1379	-037:14:22.1658	0.64	646.6 +/- 1.7	630.13 +/- 0.96	1.03	1.72e-2	3.8e4
2333-237	23:33:55.207	-023:43:40.6316	1.0	1094.94 +/- 0.62	1109.29 +/- 0.36	0.987	1.7e-2	6.4e4
2354-152	23:54:30.1905	-015:13:10.943	0.8	788.92 +/- 0.51	790.76 +/- 0.30	0.998	1.62e-2	4.9e4
2359-315	23:59:35.4534	-031:33:43.7766	0.83	584.05 +/- 0.38	589.00 +/- 0.22	0.992	1.54e-2	3.8e4
j0044-8422	**00:44:26.7707**	**-084:22:39.7654**	**0.663**	**591.0 +/- 8.7**	**583.9 +/- 5.0**	**1.01**	**1.93-2**	**3.1e4**
J0211+1051	02:11:13.1737	+010:51:34.7606	0.52	545.54 +/- 0.99	550.44 +/- 0.57	0.991	1.67e-2	3.3e4
j0246-4651	**02:46:00.0913**	**-046:51:17.5322**	**0.959**	**775 +/- 15**	**754.4 +/- 8.5**	**1.03**	**1.93e-2**	**4.0e4**
J0659+0813	06:59:17.9965	+008:13:31.1425	0.75	861.4 +/- 3.5	859.3 +/- 2.0	1.002	2.83e-2	3e4

j0625-5438	**06:25:52.201**	**-054:38:50.6351**	**0.883**	**897 +/- 23**	**908 +/- 13**	**0.989**	**2.07e-2**	**4.3e4**
J0738+1742	07:38:07.3975	+017:42:19.155	0.91	1.5303 +/- 0.0033	1.5155 +/- 0.0019	1.01	1.84e-2	8.3e4
J0745+1011	07:45:33.06	+010:11:12.7	3.47	3945.16 +/- 0.53	3945.78 +/- 0.31	0.999	1.92e-2	2.1e4
J1608+1029	16:08:46.2042	+010.29.07.7034	0.76	1.3647 +/- 0.0053	1.3680 +/- 0.0031	0.998	3.87e-2	3.5e4
J1728+0427	17:28:24.9688	+004:27:05.0447	0.63	595.3 +/- 5.2	597.6 +/- 3.0	0.996	3.7e-2	1.6e4
J1734+0926	17:34:58.3961	+009.26.58.3919	1.18	1.3257 +/- 0.0084	1.3456 +/- 0.0049	0.985	3.64e-2	3.6e4
Negative/steep spectral indices								
0016-002	00:16:11.0889	-000:15:12.4255	0.62	762.644 +/- 0.093	761.783 +/- 0.053	1.001	1.37e-2	5.6e4
0037-593	**00:40:07.8682**	**-059:03:52.734**	**0.7**	**556 +/- 10**	**587.6 +/- 6.3**	**0.946**	**1.58e-2**	**3.5e4**
0048-447	**00:50:52.0318**	**-044:28:37.6621**	**0.863**	**547.0 +/- 8.6**	**486.5 +/- 4.6**	**1.12**	**1.46e-2**	**3.8e4**
0121+043	01:21:56.8606	+004:22:24.7870	0.85	994.3 +/- 3.0	1.0197 +/- 0.0017	0.975	3.03e-2	3.3e4
0203+115	02:03:46.6537	+011:34:45.3628	0.96	600.9 +/- 1.4	604.99 +/- 0.80	0.993	1.98e-2	3e4
0231+133	02:31:45.8913	+013:22:54.7216	2.2	1.7516 +/- 0.0056	1.7383 +/- 0.0032	1.01	3.87e-2	4.5e4
0242-215	02:42:35.9052	-021:32.25.9427	0.79	787 +/- 11	782.1 +/- 6.4	1.01	1.57e-2	5e4
0319+1901	03:19:51.2582	+019.01.31.5691	0.72	615.2 +/- 6.2	617.7 +/- 3.6	0.996	2e-2	3.1e4
0501-019	05:01:12.	-001:59:	2.15	2605 +/-	2560 +/-	1.02	5.3e-2	5e4

	8019	14.3478		20	11			
1034-293	10:37:16.0816	-029:34:02.9699	1.4	1218.8 +/- 10.0	1221.3 +/- 5.8	0.998	6.28e-2	2e4
1051-316	10:51:04.7759	-031:38:14.5458	0.6	737.0 +/- 5.3	731.5 +/- 3.0	1.01	1.83e-2	4e4
1057-245	10:57:55.4153	-024:33:49.0473	0.6	825.5 +/- 3.2	827.4 +/- 1.9	0.998	2.37e-2	3.5e4
1124-186	11:27:04.3840	-018:57:17.5011	1.95	944.3 +/- 6.8	939.2 +/- 3.9	1.01	3.95e-2	2.4e4
1357-177	13:57:06.0650	-017:44:02.0271	1.0	1085.0 +/- 4.7	1118.8 +/- 2.7	0.97	2.33e-2	4.7e4
1415+133	14:15:58.8271	+013:20:23.8875	1.2	767.87 +/- 0.23	767.00 +/- 0.13	1.001	1.55e-2	5e4
1430+107	14:30:09.7456	+010:43:26.9395	1.0	541.848 +/- 0.068	541.798 +/- 0.039	1.0	1.45e-2	3.8e4
1436+233	14:36:40.9928	+023:21:03.6616	0.8	945.28 +/- 0.23	941.94 +/- 0.13	1.0	1.68e-2	5.6e4
1448-163	14:48:15.0523	-016:20:24.5543	0.8	1432.3 +/- 1.1	1441.02 +/- 0.65	0.994	1.66e-2	8.6e4
1543-079	15:43:01.6819	-007:57:06.6796	0.9	1404.6 +/-5.5	1439.9 +/- 3.2	0.975	1.99e-2	7.1e4
1546+004	15:46:09.5267	+000:26:24.6004	0.8	1.3708 +/- 0.0047	1.4066 +/- 0.0028	0.974	2.26e-2	6.1e4
1554-270	15:54:02.4574	-027:04:40.3845	1.25	1.0274 +/- 0.0050	984.6 +/- 2.8	1.04	1.34e-2	7.7e4
1751-253	17:51:51.2557	-025:24:00.2024	0.5	658.4 +/- 1.0	665.85 +/- 0.58	0.989	1.46e-2	4.5e4
1811-209	18:11:06.7942	-020:55:03.33996	0.31	566.4 +/- 1.0	572.48 +/- 0.60	0.989	1.55e-2	3.7e4
1822-096	18:22:28.7256	-009:38:56.7734	5.6	3.724 +/- 0.012	3.7489 +/- 0.0070	0.993	3.58e-2	1e5
1923-210	19:23:32.1994	-021:04:33.3531	2.0 (1.5 GHz)	541.6 +/- 1.5	531.01 +/- 0.83	1.02	1.84e-2	2.9e4

2219-279	22:19:42.5824	-027:56:27.1741	0.46	959.42 +/- 0.26	941.47 +/- 0.15	1.02	1.61e-2	6e4
2248-325	22:48:38.7033	-032:35:51.9217	1.6	1.4978 +/- 0.0011	1.49685 +/- 0.00066	1.00	1.95e-2	7.7e4
2257-364	22:57:10.6103	-036:27:43.7584	1.2	1.18982 +/- 0.00035	1.18981 +/- 0.00020	1.00	1.87e-2	6.4e4
2314-316	23:14:48.5158	-031:38:39.0811	0.5	533.41 +/- 0.23	532.39 +/- 0.13	1.0	1.64e-2	3.3e4
2314-449	23:14:09.3913	-044:55:49.0963	1.0	1.73950 +/- 0.00031	1.7392+/- 0.00018	1.0	1.65e-2	1.1e4
2348-165	23:48:02.5992	-016:31:11.8176	1.9	1.9501 +/- 0.0041	1.9065 +/- 0.0023	1.02	1.96e-2	9.9e4
J0449+1121	04:49:07.6701	+011:21:28.8290	0.92	790 +/- 14	787.1 +/- 8.0	1.0	3.2e-2	2.5e4
J0459+0229	04:59:52.0436	+002:29:31.1273	1.22	1.161 +/- 0.011	1.1624 +/- 0.0064	0.999	3.9e-2	3e4
J0502+0609	05:02:15.4525	+006:09:07.6071	1.03	757.3 +/- 1.5	742.57 +/- 0.83	1.02	2.2e-2	3.4e4
J0505+0459	05:05:23.19	+004:59:42.79	0.71	721.7 +/- 6.9	695.9 +/- 3.9	1.04	1.56e-2	4.6e4
J0509+0541	05:09:25.9717	+005:41:35.4535	0.54	1.0556 +/- 0.0038	1.0523 +/- 0.0022	1.0	3.53e-2	3.0e4
J0522+0113	05:22:17.4681	+001:13:31.2587	0.96	887.2 +/- 1.8	880.0 +/- 1.1	1.01	2.61e-2	3.4e4
J0524-5658	**05:24:40.2533**	**-056:58:51.9492**	**0.844**	**774 +/- 14**	**749.0 +/- 7.8**	**1.03**	**7.2e-2**	**1.1e4**
J0607-6031	**06:07:55.1260**	**-060:31:52.2664**	**0.812**	**696 +/- 18**	**701 +/- 10**	**0.993**	**2.63e-2**	**2.6e4**
J0909+0121	09:09:10.076	+001:21:35.73	1.72	1.127 +/- 0.011	1.2097 +/- 0.0064	0.932	6.42e-2	1.8e4
J0954+1743	09:54:56.81	+017:43:31.49	0.91	840 +/- 12	864.4 +/- 6.9	0.971	3.95e-2	2.1e4
J1109	11:09:28.	+037:44:	0.78	773 +/- 31	769 +/- 18	1.0	3.59e-2	2.2e4

+3744	86	32.4						
J1640 +1220	16:40:47.9402	+012:20:01.9701	1.41	1.523 +/- 0.014	1.5349 +/- 0.0082	0.992	3.92e-2	3.9e4
T0735 +2341	07:35:59.9322	+023:41:03.1138	0.64	691.9 +/- 3.7	685.4 +/- 2.1	1.01	2.13e-2	3.2e4
T0952 +2828	09:52:06.1095	+028:28:32.813	0.8	872 +/- 21	814 +/- 11	1.07	2.44e-2	4.1e4
T1126+3345	11:26:23.6785	+033:45:28.0595	0.63	659 +/- 15	647.8 +/- 8.8	1.02	2.92e-2	2.3e4
T1352+0232	13:52:30.68	+002:32:47.02	0.68	646.2 +/- 7.5	646.4 +/- 4.4	0.999	4.3e-2	1.5e4
1145-071	11:47:51.553	-007:24:41.159	1.0	1301.7 +/- 3.7	1296.1 +/- 2.1	1.004	3.02e-2	4.3e4
1949-199	19:49:53.420	-019:57:13.2776	1.3	1133.77 +/- 0.63	1122.59 +/- 0.36	1.01	1.45e-2	7.8e4
2007-445	20:07:55.1685	-044:34.44.0792	0.5	518.12 +/- 0.12	518.978 +/- 0.071	0.998	1.35e-2	3.8e4
2047-026	20:47:10.3657	-002:36:22.1307	0.9	1488.26 +/- 0.54	1450.39 +/- 0.31	0.103	1.63e-2	9.1e4
2052-474	**20:56:16.3465**	**-047:14:47.7844**	**1.53**	**1814.0 +/- 20**	**1685 +/- 11**	**1.08**	**1.4e-2**	**1.3e5**
2110-103	21:10:00.9812	-010:20:57.3353	1.23	1354.50 +/- 0.25	1354.50 +/- 0.14	1.0	1.47e-2	9.2e4
T0237+0919	02:37:40.524	+009:19:01.526	0.32	528.4 +/- 2.2	531.7 +/- 1.3	0.994	1.86e-2	2.8e4
1432-180	14:32:57.687	-018:01:35.383	0.7	650.1 +/- 2.0	649.5 +/- 1.2	1.001	1.83e-2	3.5e4
J0839+0319	08:39:49.191	+003:19:53.591	0.78	757.5 +/- 7.7	755.8 +/- 4.4	1.002	2.3e-2	3.3e4
0214-522	**02:16:03.1956**	**-052:00:12.4163**	**0.85**	**636.1 +/- 6.3**	**670.2 +/- 3.8**	**0.949**	**2.21e-2**	2.9e4
0407-658	**04:08:20.37**	**-065:45:08.939**	**9.63**	**5878.0 +/- 54**	**5752.0 +/- 31**	**1.022**	**7.9e-2**	**7.4e4**

0606-795	**06:03:06.071**	**-079:34:50.215**	**1.13**	**739.0 +/- 11**	**739.1 +/- 6.2**	**1.0**	**1.75e-2**	**4.2e4**
J1007+1356	10:07:41.495	+013:56:29.644	0.73	514.7 +/- 4.8	531.3 +/- 2.8	0.969	1.9e-2	2.7e4
1534+015	15:34:52.451	+001:31:04.147	0.8	867.8 +/- 3.2	865.2 +/- 1.8	1.003	2.36e-2	3.7e4
1553+129	15:53:32.7	+012:56:51.8	0.7	834.2 +/- 4.2	833.6 +/- 2.4	1.001	2.11e-2	4.0e4
1658+076	16:58:09.01007	+07:41:27.4589	1.5	906 +/- 12	830.5 +/- 6.7	1.09	2.58e-2	3.5e4
2129-156	21:29:12.1716	-015:38:41.0567	1.1	1226.2 +/- 5.0	1225.6 +/- 2.9	1.0	2.46e-2	5.0e4
2129-183	21:29:21.4141	-018:21:22.8163	0.9	1200.2 +/- 3.4	1195.9 +/- 2.0	1.004	1.96e-2	6.1e4
2255-087	22:55:04.2407	-008:44:04.0035	0.6	585.4 +/- 1.5	588.85 +/- 0.90	0.994	1.81e-2	3.2e4
0647-475	**06:48:48.4195**	**-047:34:27.2418**	**1.47**	**1187.0 +/- 27**	**1207.0 +/- 16**	**0.983**	**2.69e-2**	4.4e4
0906-682	**09:06:52.493**	**-068:29:39.9934**	**1.18**	**910.0 +/- 13**	**883.3 +/- 7.6**	**1.03**	**1.87e-2**	**4.9e4**
0731-465	**07:32:44.3119**	**-046:40:17.1418**	**0.85**	**861.4 +/- 9.1**	**855.4 +/- 5.2**	**1.007**	**1.86e-2**	4.6e4
0906-47	**09:08:42.3093**	**-047:36:51.0564**	**0.77**	**657.2 +/- 9.4**	**656.0 +/- 5.4**	**1.002**	**1.96e-2**	3.4e4
J1534+0131	15:34:52.4515	+001:31:04.36	0.98	908.7 +/- 7.9	928.4 +/- 4.6	0.99	3.5e-2	2.6e4
0010+174	00:10:34.0034	+017:24:18.9844	0.98	553.3 +/- 6.6	551.3 +/- 3.8	1.004	3.04e-2	1.8e4
0110-076	01:10:50.0211	-007:41:41.1624	0.78	613.2 +/- 3.3	612.9 +/- 1.9	1.0	1.52e-2	4.0e4
0219+0120	02:19:07.0123	+001:20:59.7055	0.67	704.3 +/- 2.8	690.5 +/- 1.6	1.02	1.71e-2	4.1e4
0249+0619	02:49:18.0069	+006:19:51.8217	0.5	697.3 +/- 4.2	702.1 +/- 2.4	0.993	1.87e-2	3.7e4
0259+074	02:59:27.	+007:47:	0.78	701.7 +/-	693.8 +/-	1.01	2.19e-2	3.2e4

7	0693	39.5259		4.1	2.4			
2138-246	21:38:37.1779	-024:39:54.4430	0.68	577.4 +/- 7.0	593.7 +/- 4.1	0.973	1.35e-2	4.3e4
J0403+2600	04:03:05.59	+026:00:01.497	1.6	979.8 +/- 1.1	981.13 +/- 0.66	0.999	1.36e-2	7.2e4

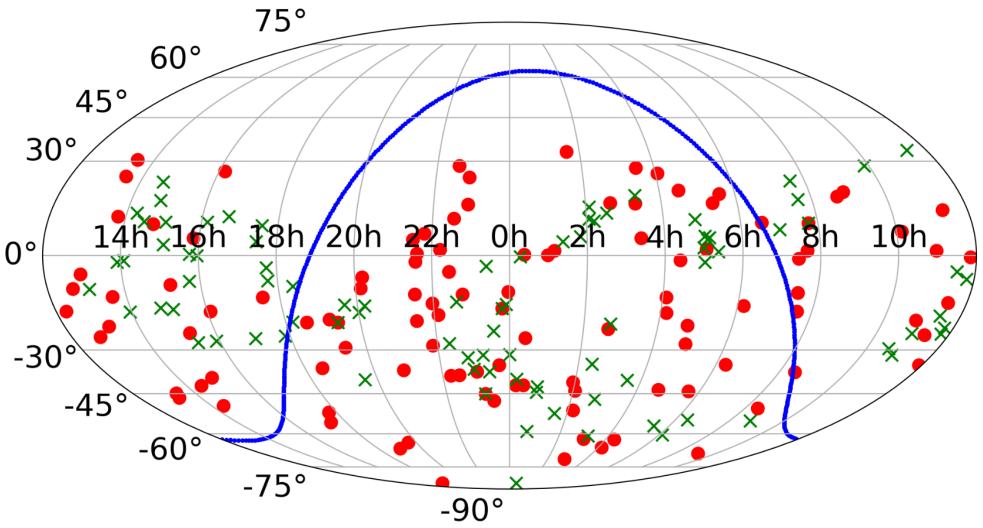

Figure 1: Sky coverage map of S band calibrators

3.2: Spectral index and plotted images

Inverted, and flat, spectrum sources are usually preferred because they are likely to have less visible extended structure (O'Dea & Saikia 2021, Kovalev et al. 2007). Steep-spectrum sources are also considered if they are not resolved as they could also be point sources. This criteria will not be followed in future since all the sources have inverted, flat or steep spectrum. To determine the in-band spectral index of the targets, we subdivided the frequency into 8 channels and imaged each separately. The frequencies are divided such that each point is centred at 2.5 GHz, 2.6 GHz, 2.7 GHz, 2.8 GHz, 2.9 GHz, 3.0 GHz, 3.1 GHz, 3.2 GHz. Given a MeerKAT wide observing band, the channels at ends may often show lower flux densities due to receiver sensitivity and bandpass

shape as the MeerKAT receiver is optimised for the central frequencies. The primary beam response of the antennas also drops off at the edges hence the observed flux density of sources diminishes at the outer frequencies. A region was identified around the target for each channel and fitted separately. The integrated flux density and the error from Imfit were used to determine spectra using the power-law function in python. The respective flux densities and spectra are presented in Table 2.

Table 2: Spectrum and images of selected sources

Table 2: Spectrum derived from fitting a power-law function to integrated flux densities and the respective errors. The images at 2.8 GHz of selected sources are also given. The psf is on the left bottom corner of each image.

Fitted fluxes (2.5-3.2 GHz)/mJy	Images
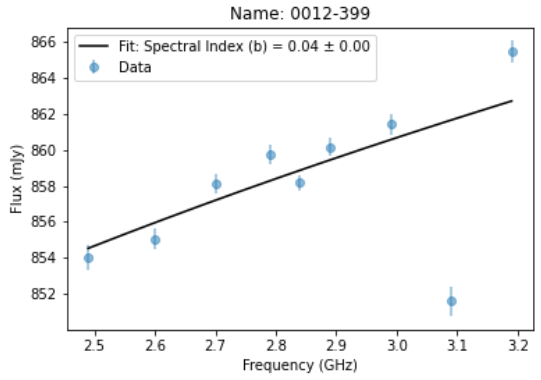	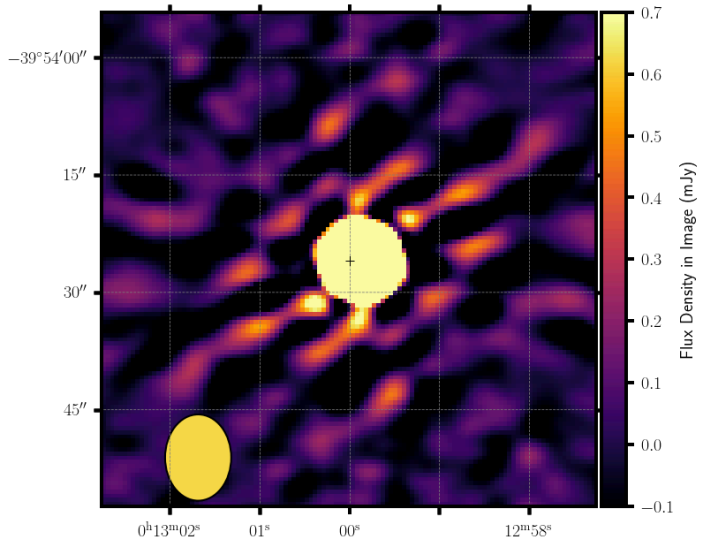
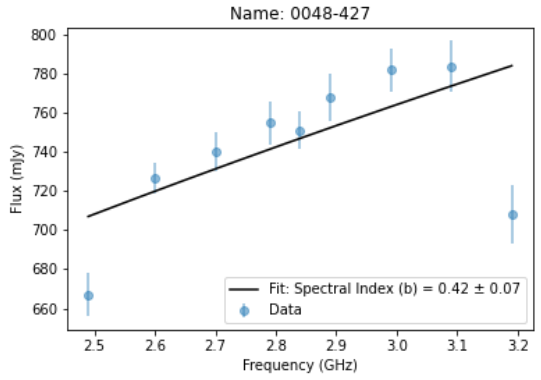	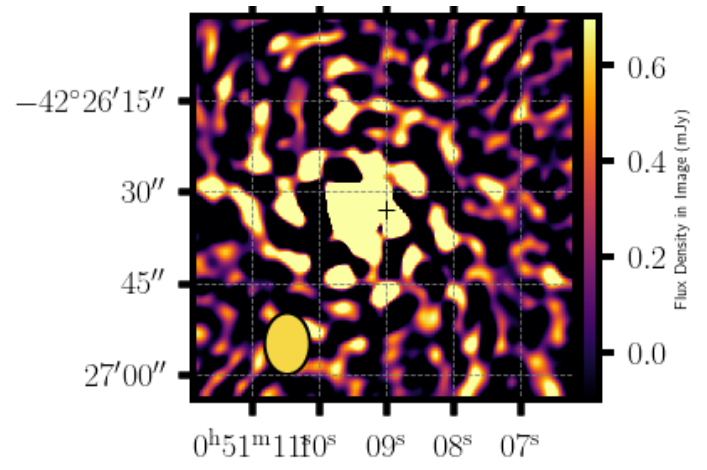

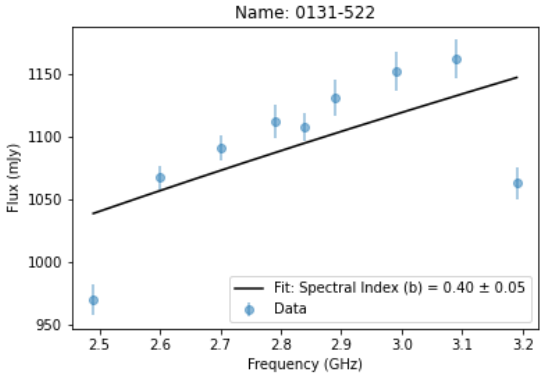

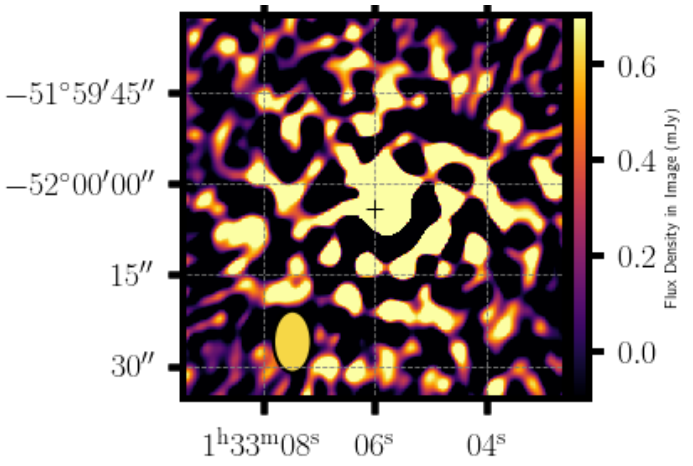

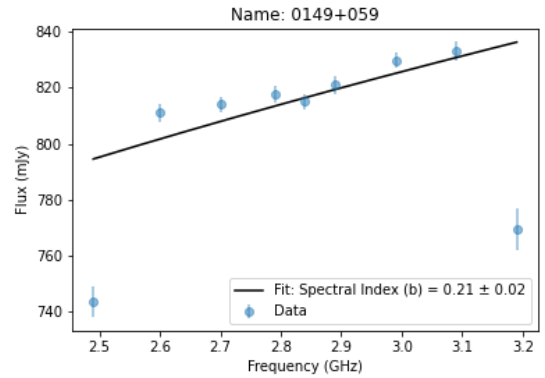

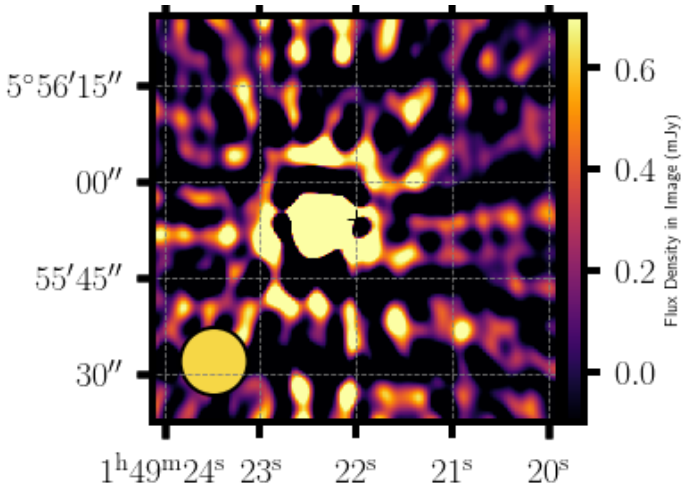

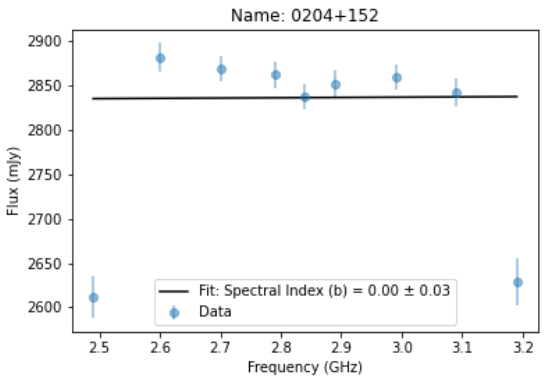

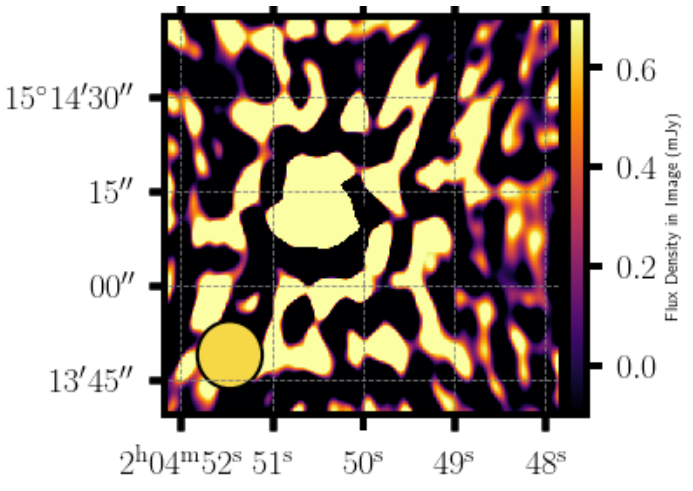

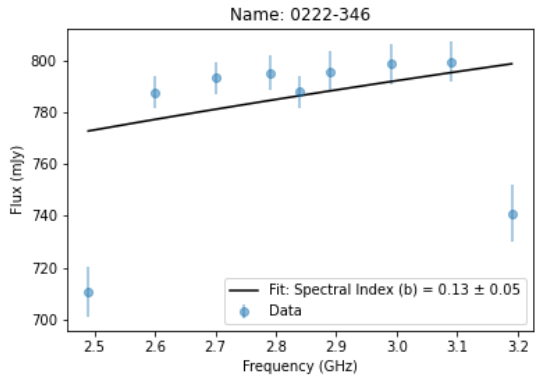

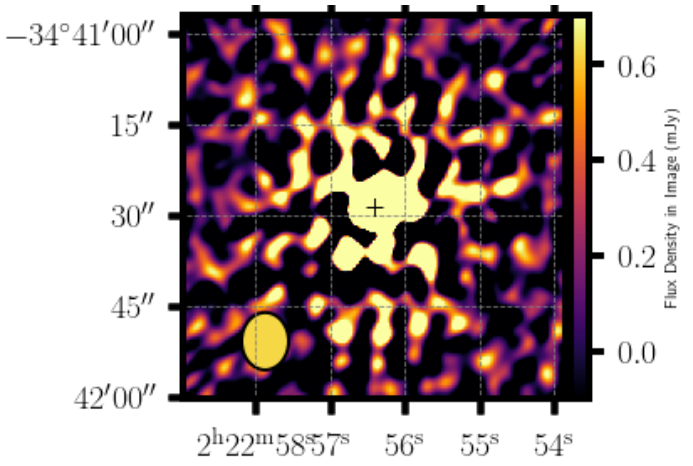

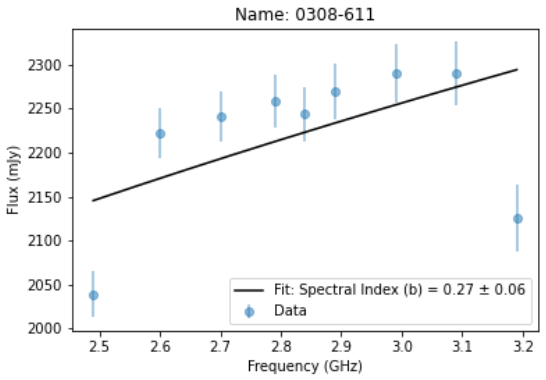

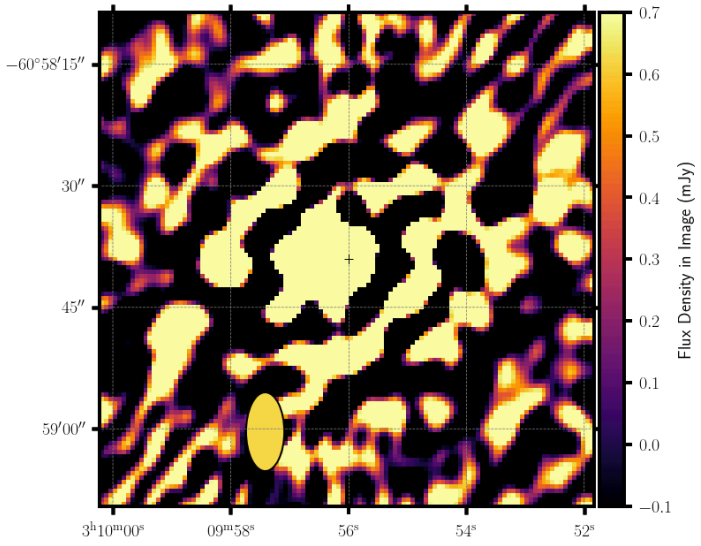

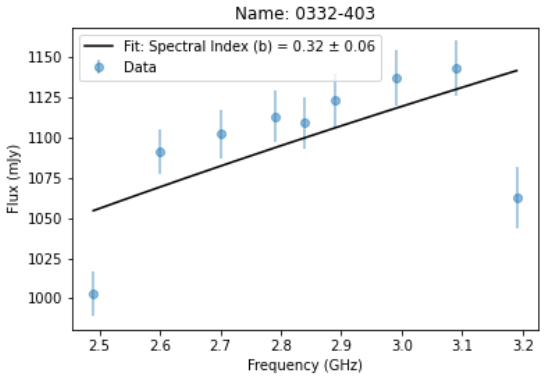

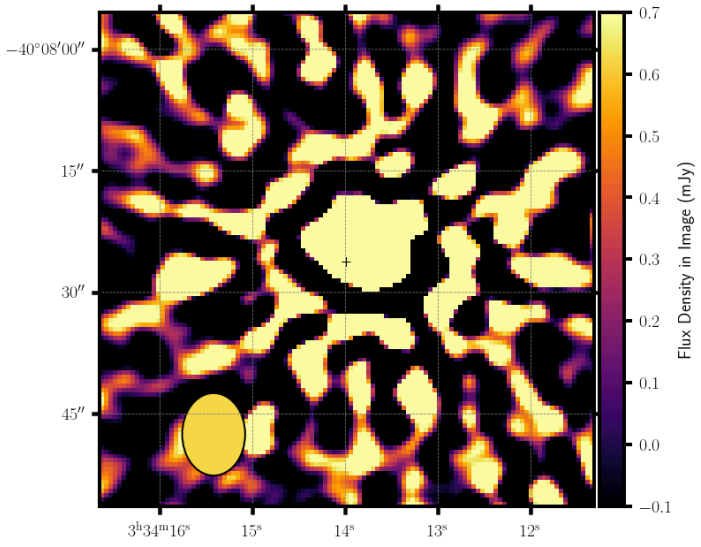

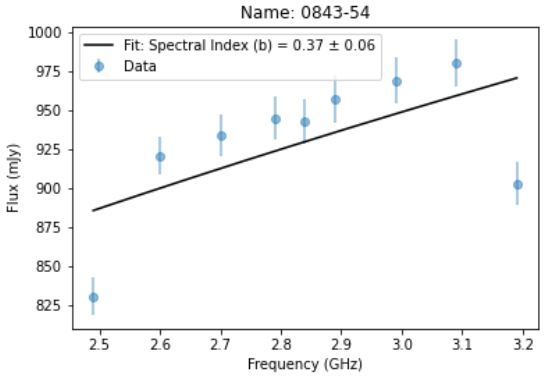

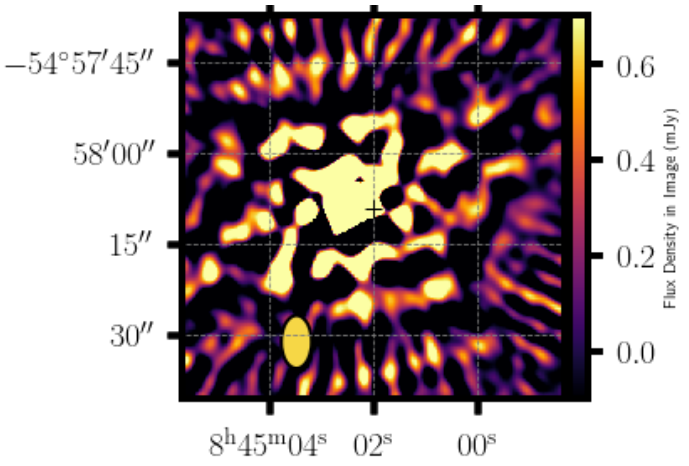

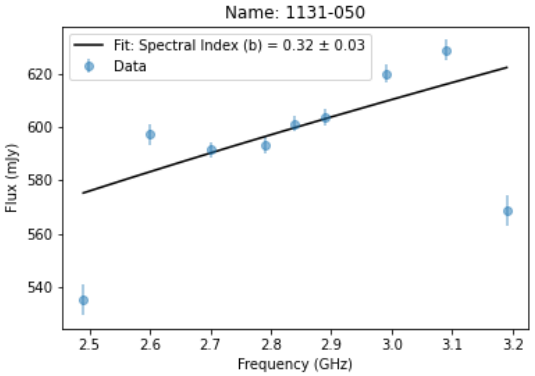

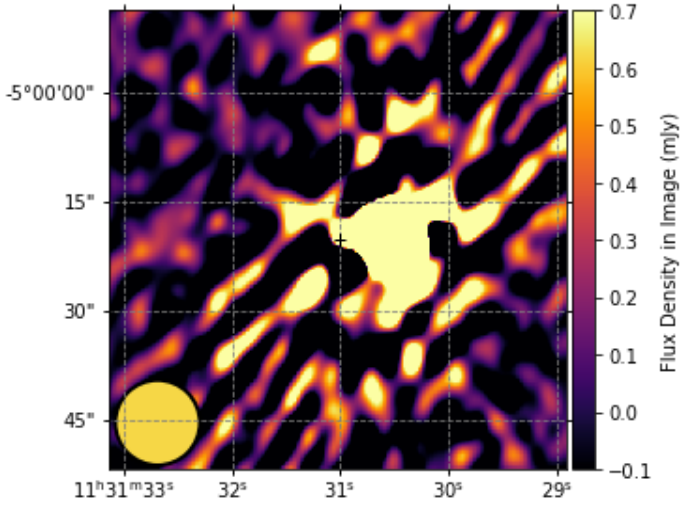

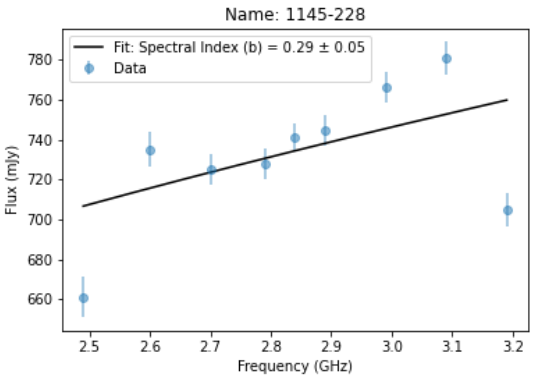

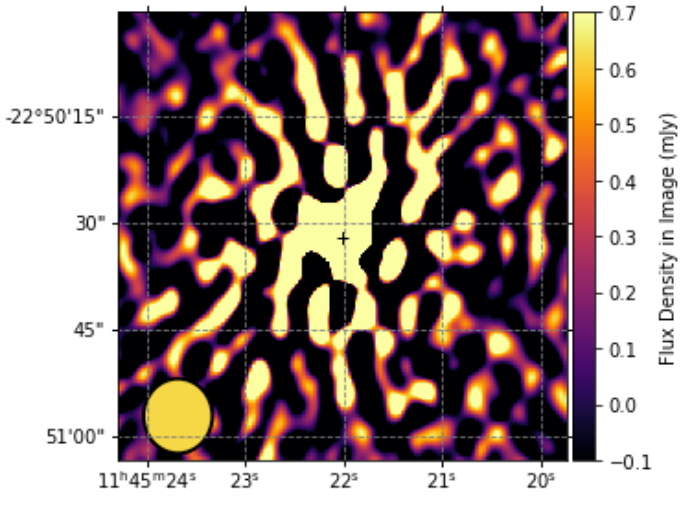

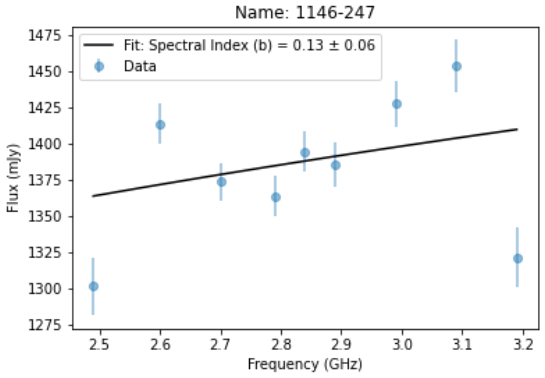

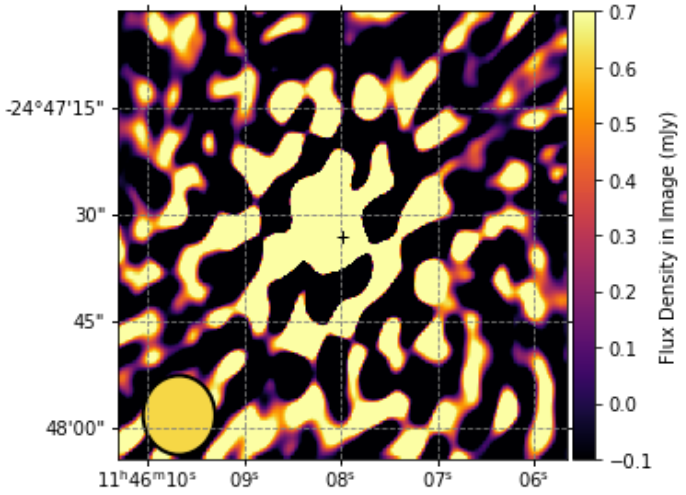

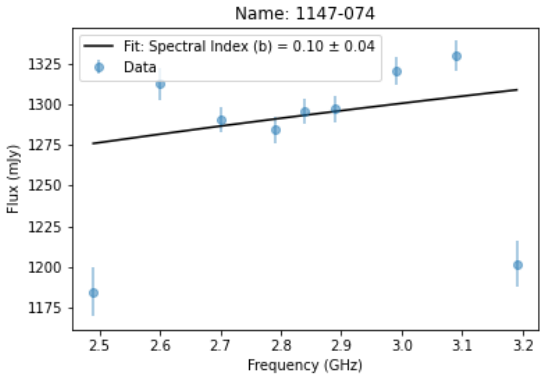

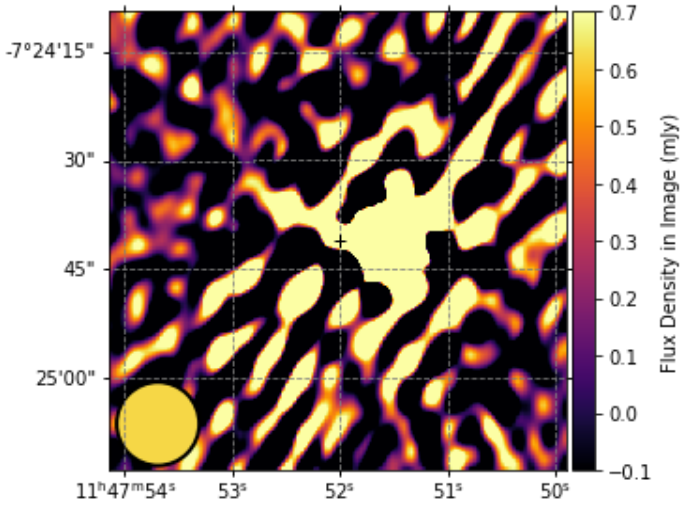

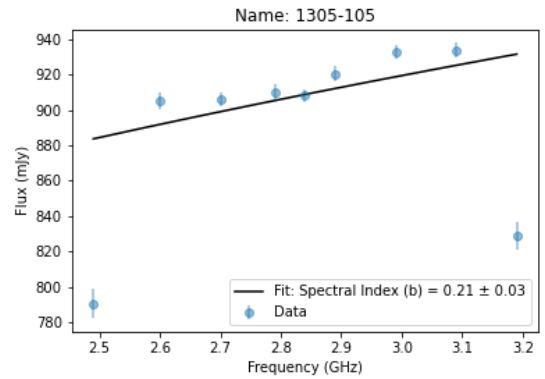

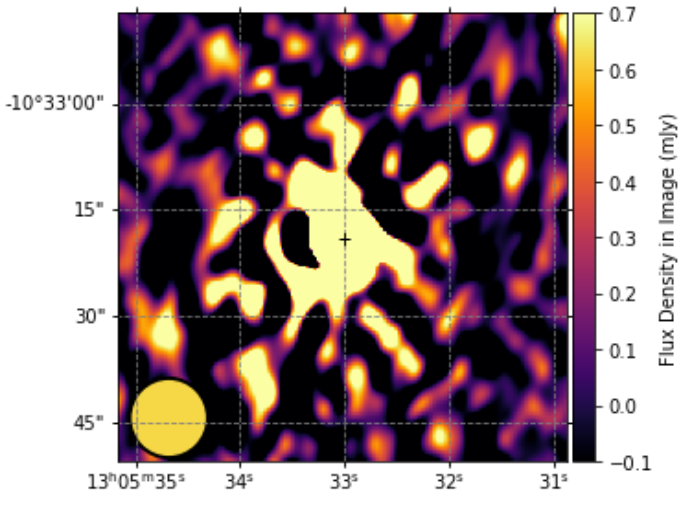

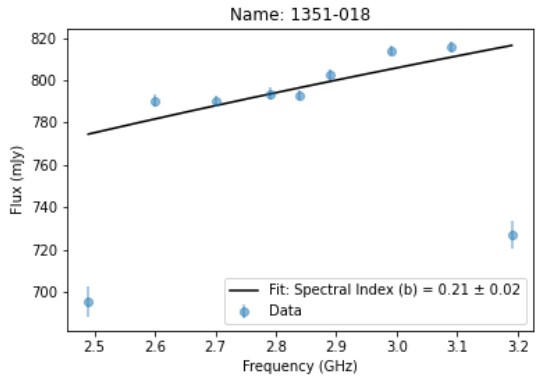

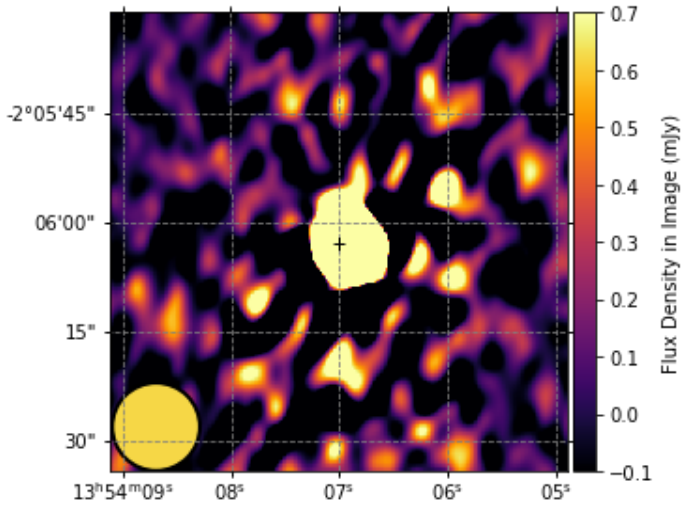

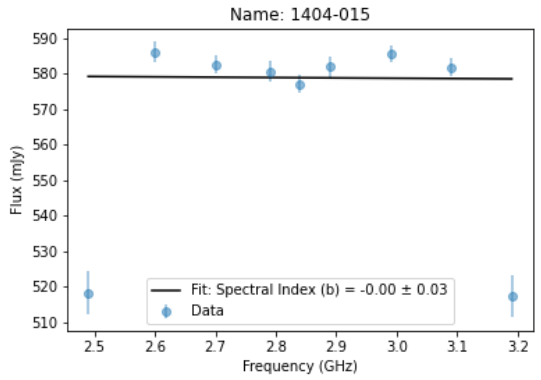

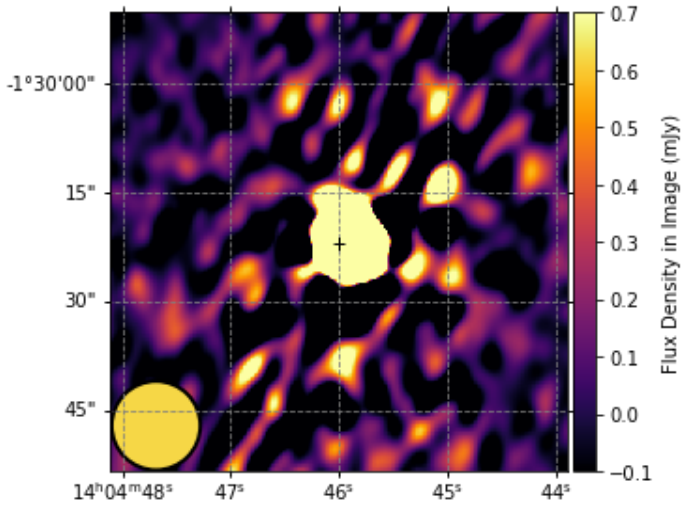

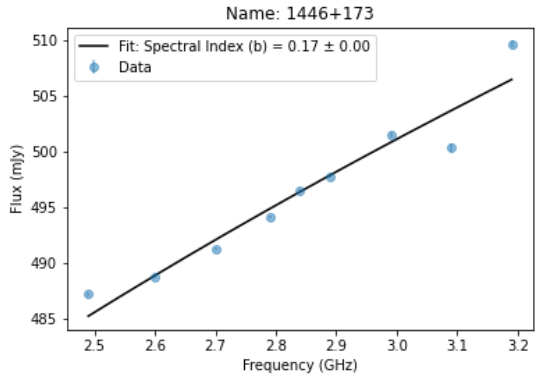

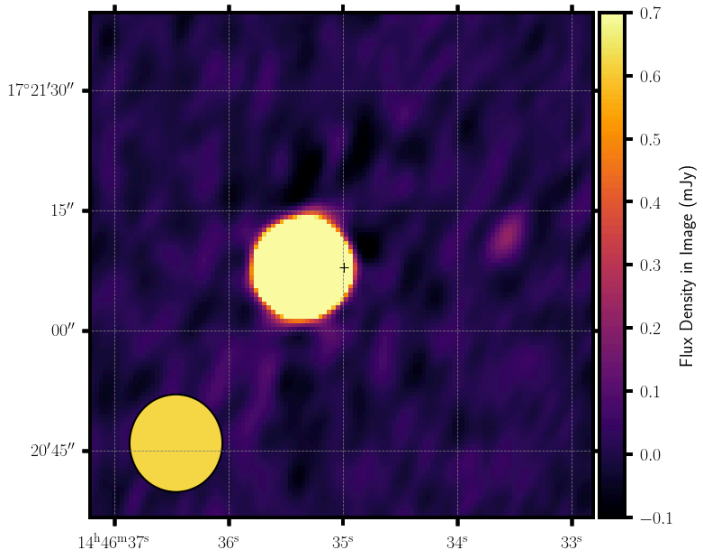

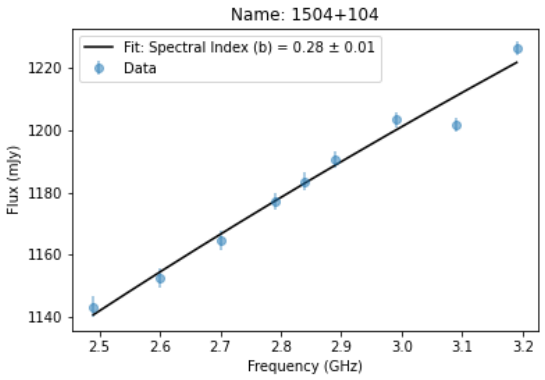

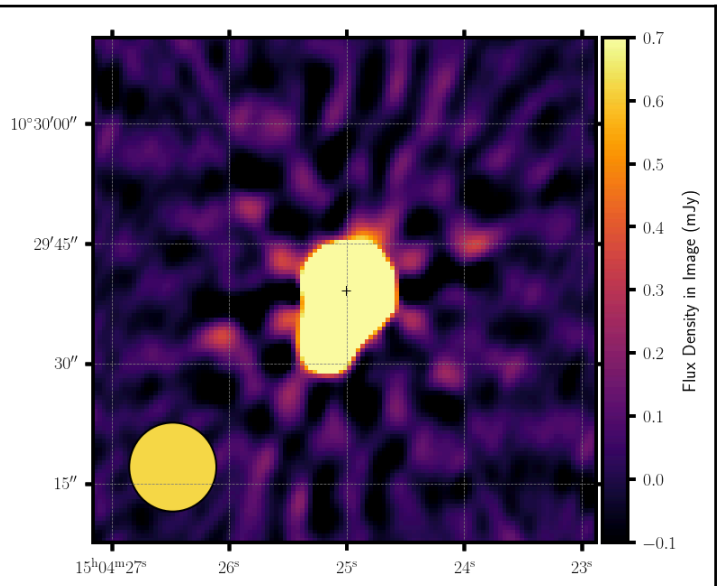

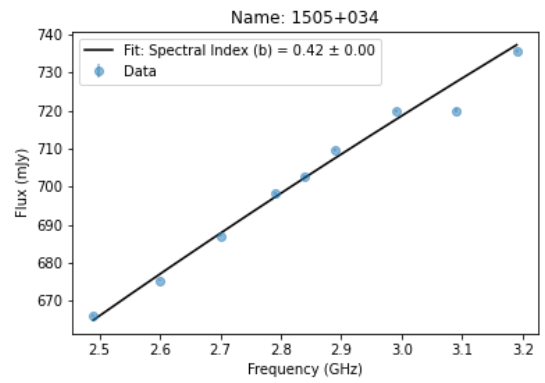

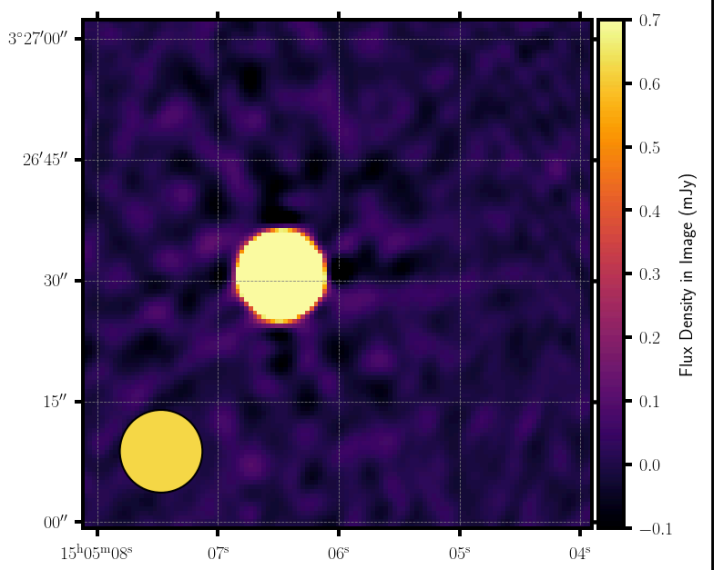

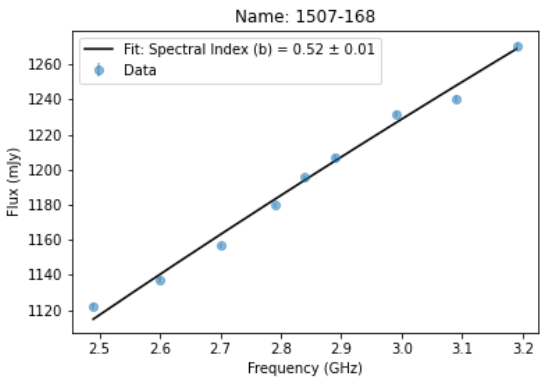

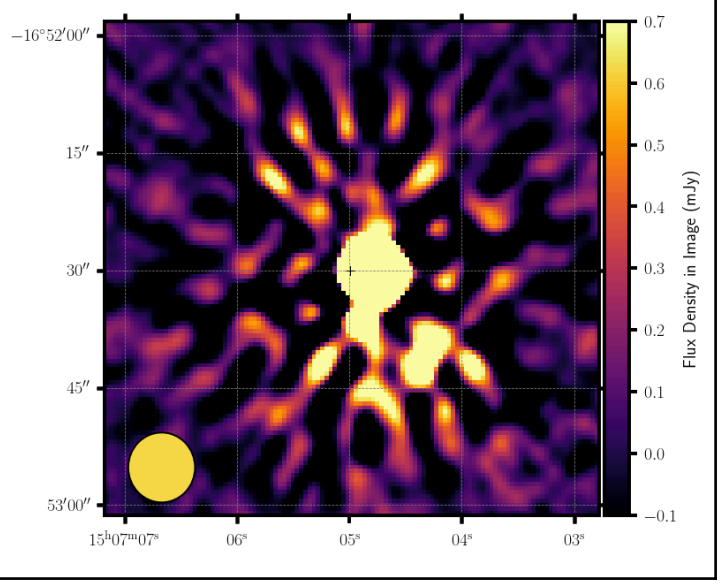

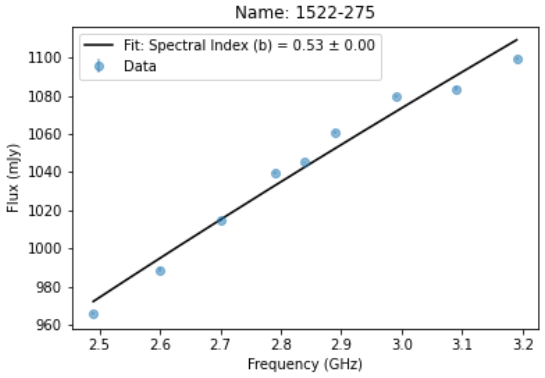

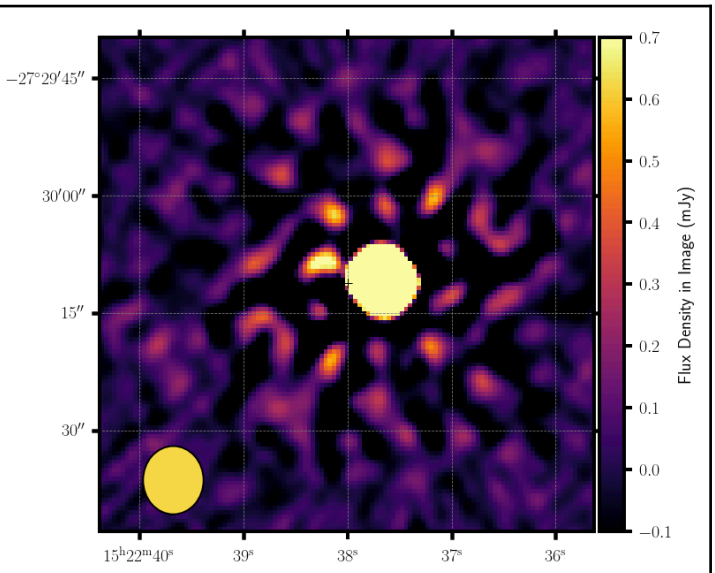

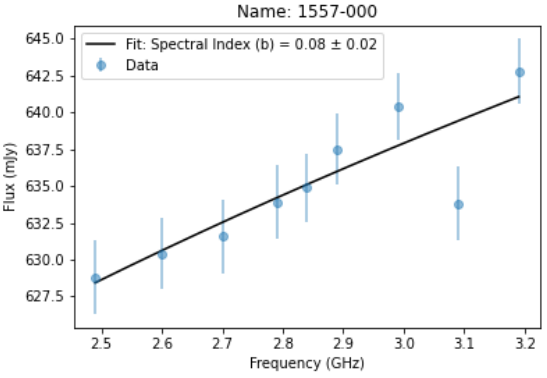

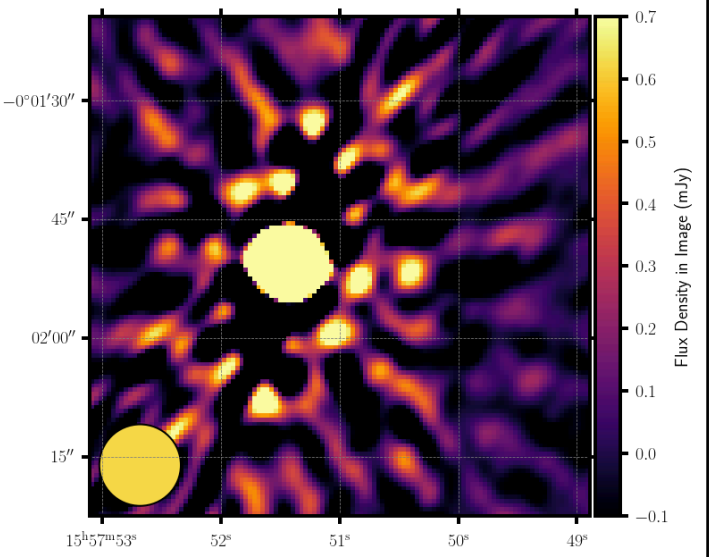

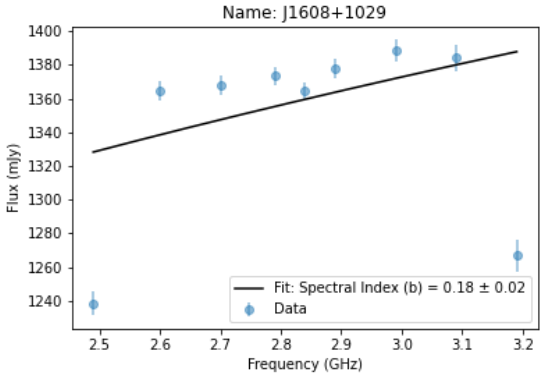

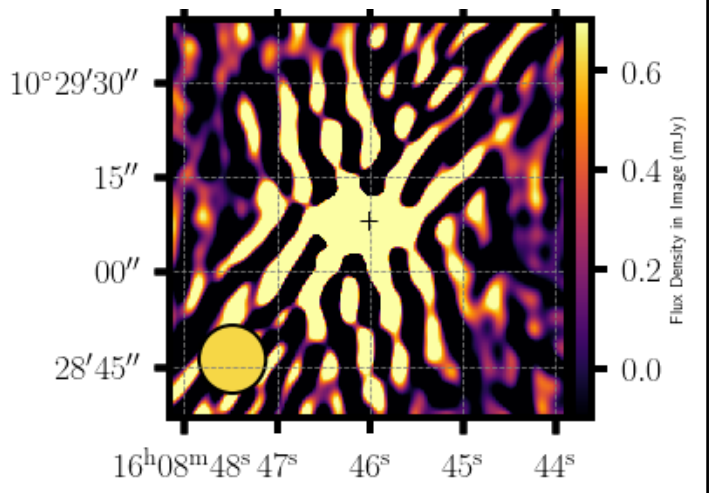

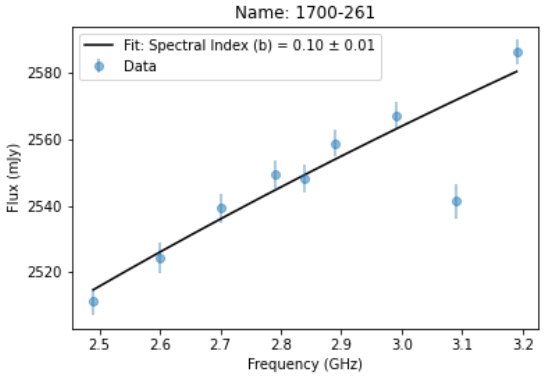

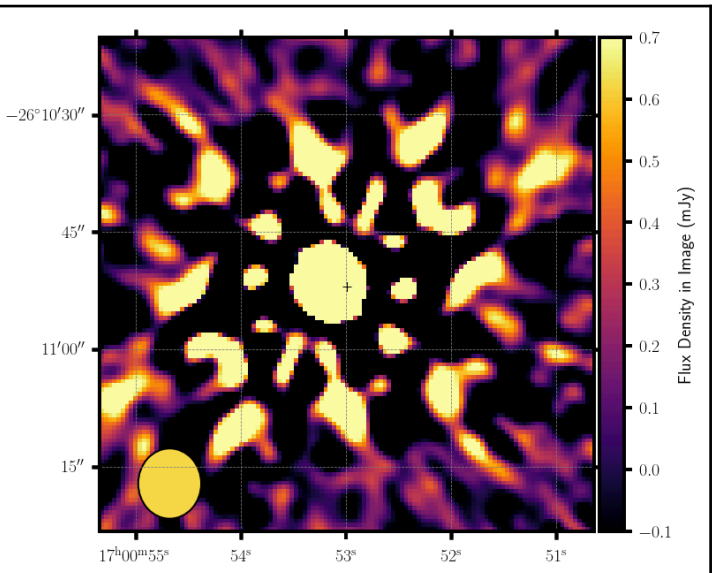

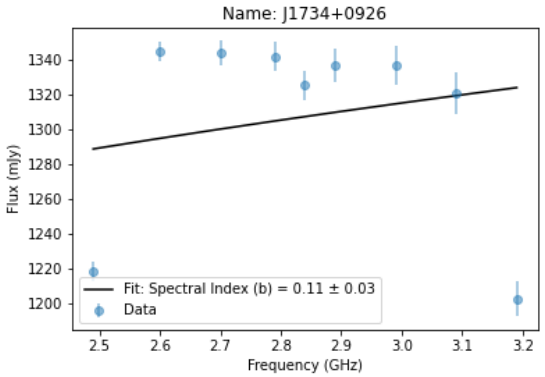

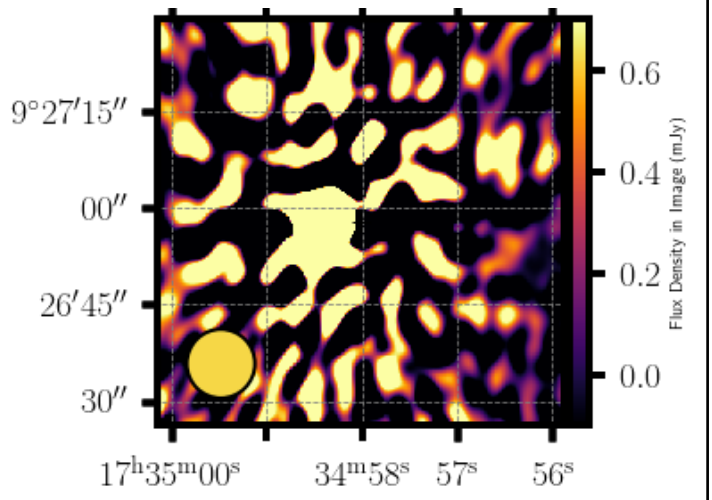

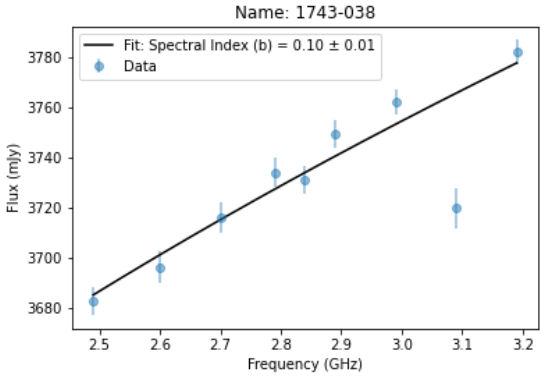

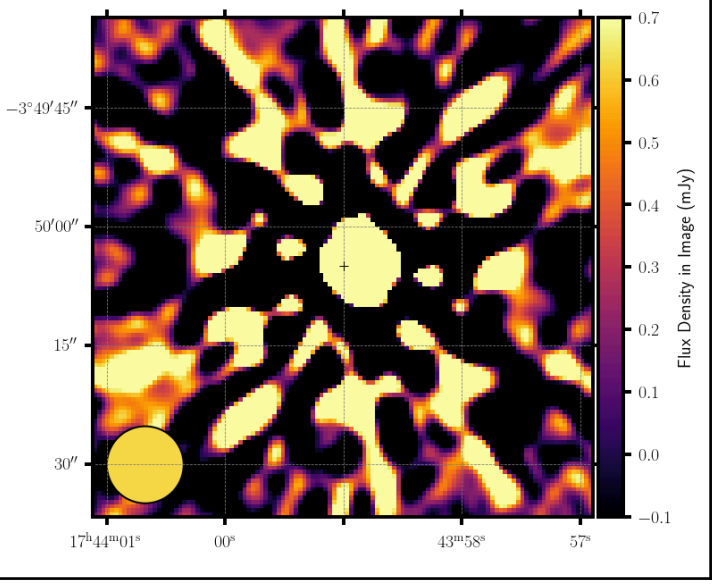

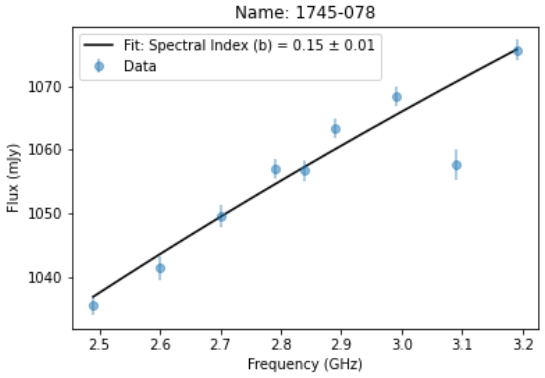

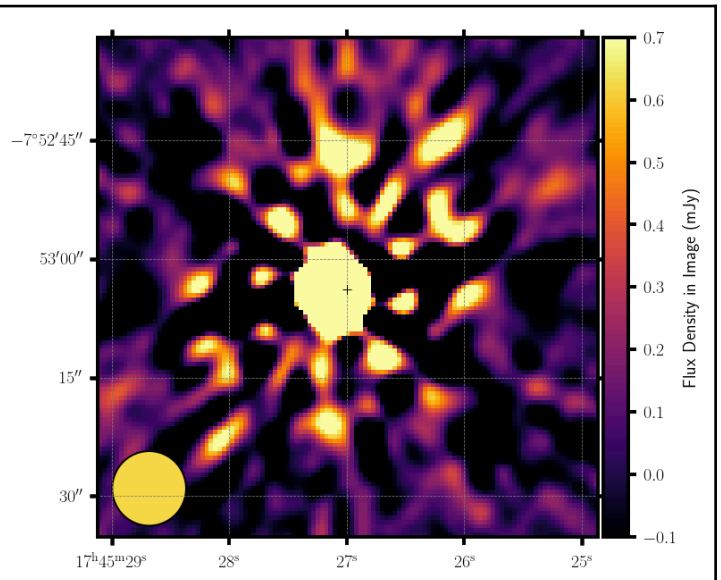

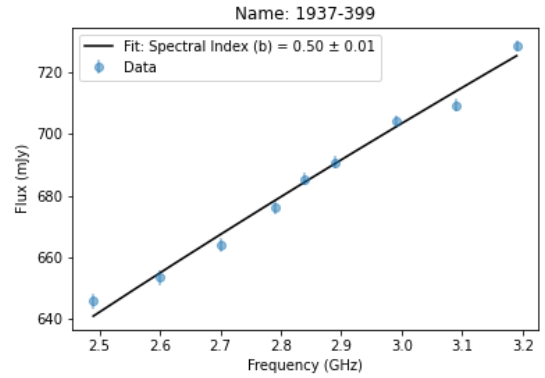

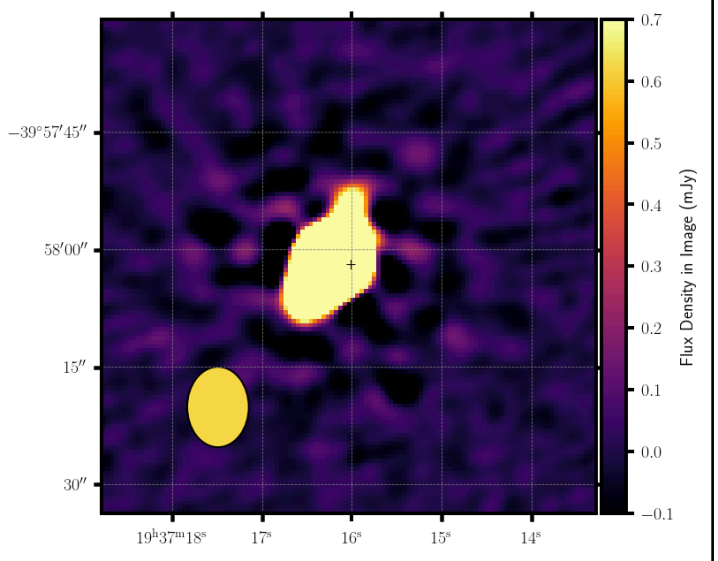

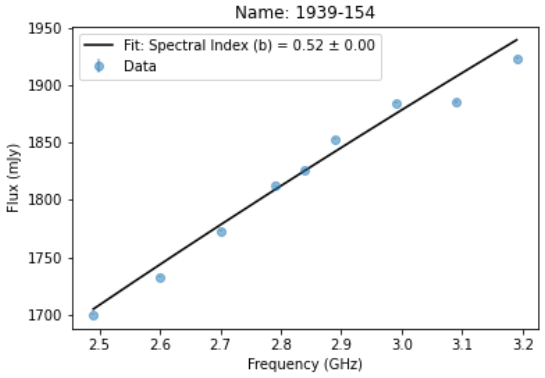

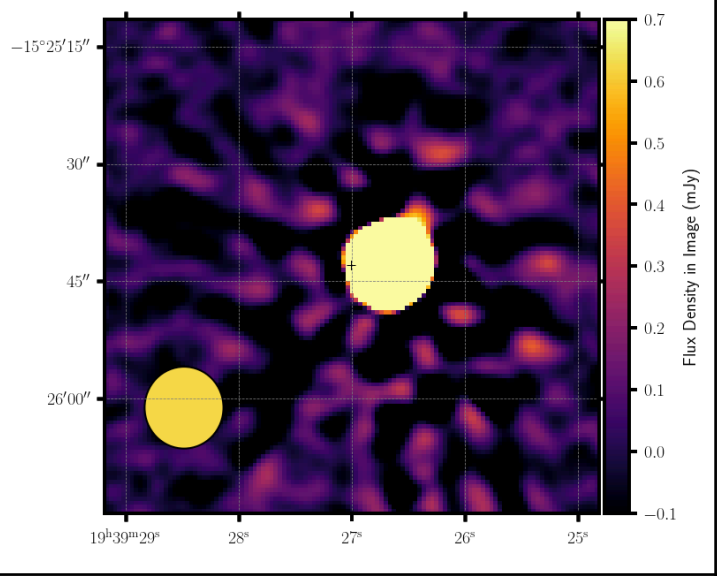

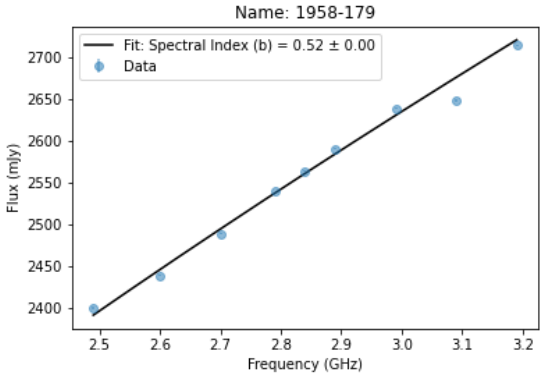

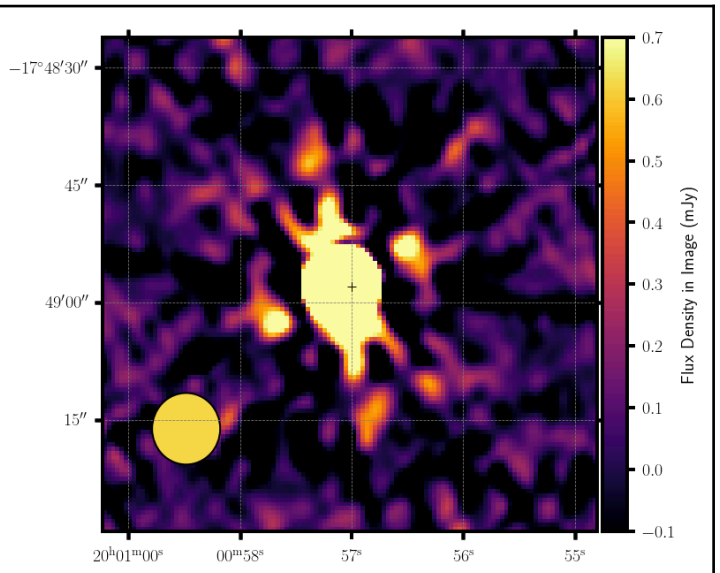

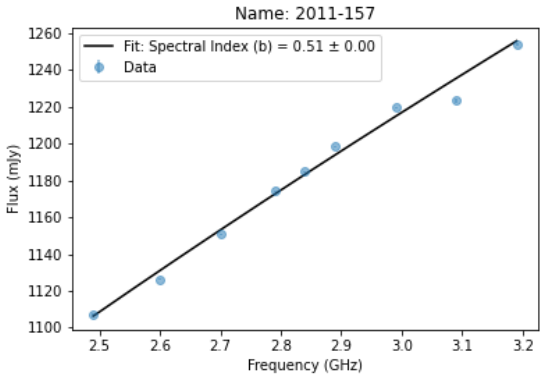

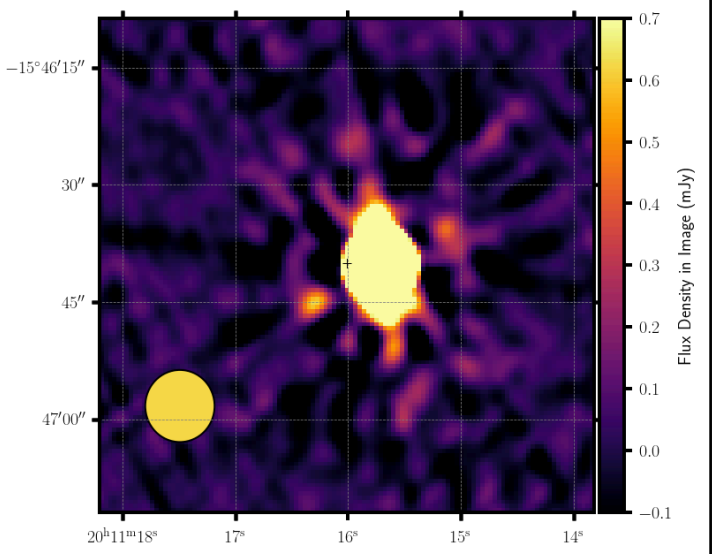

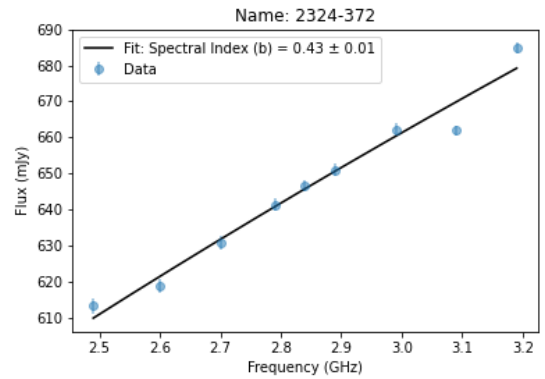

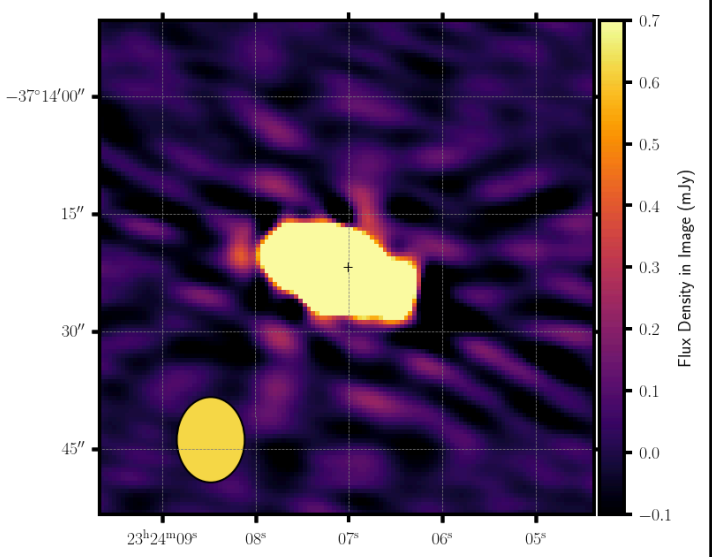

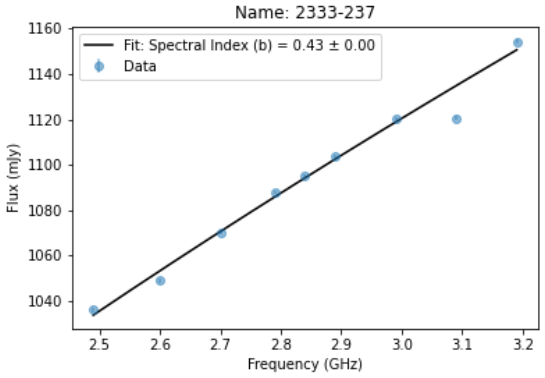

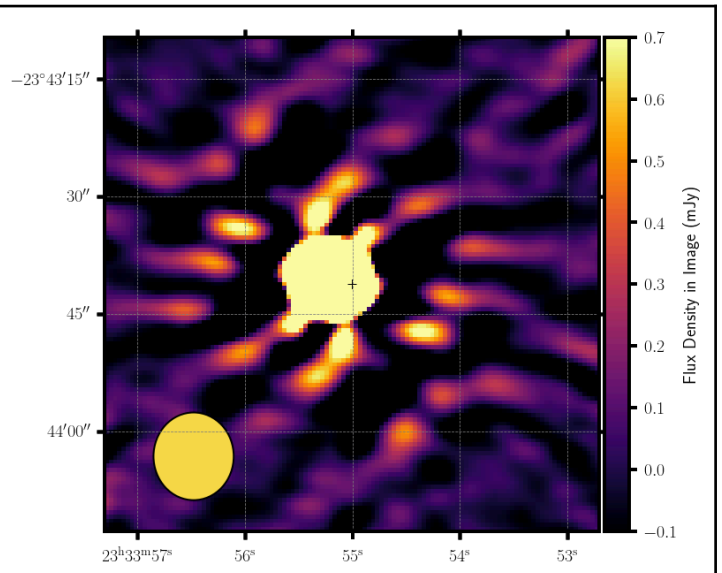

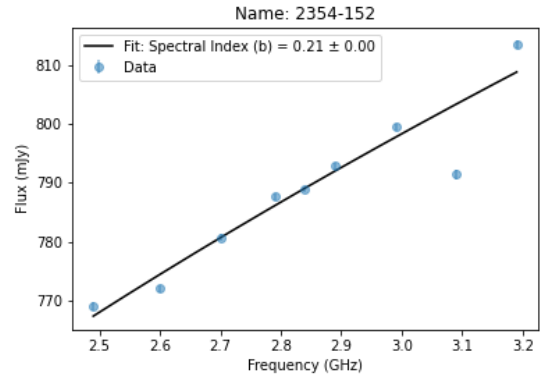

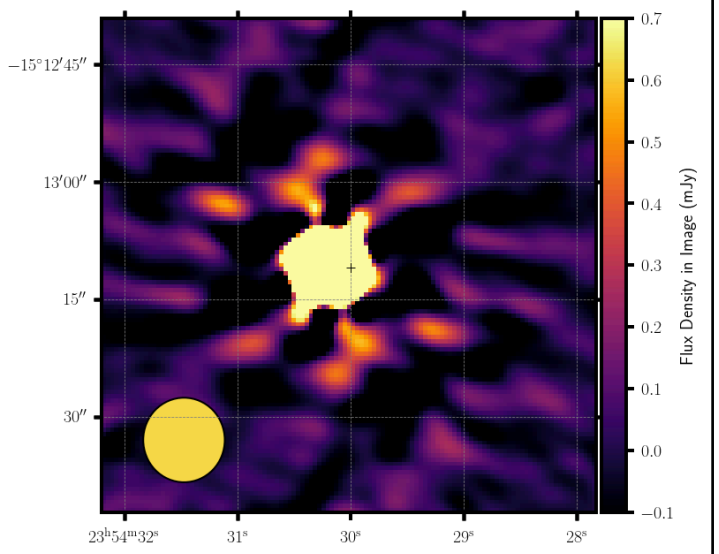

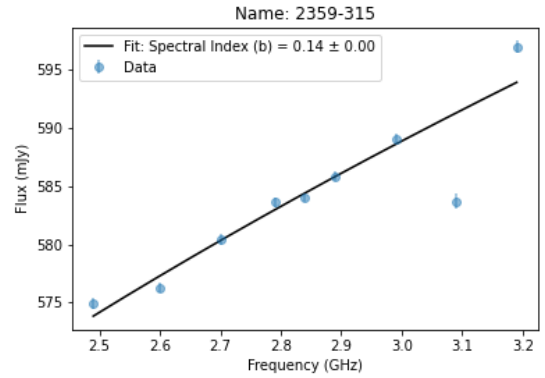

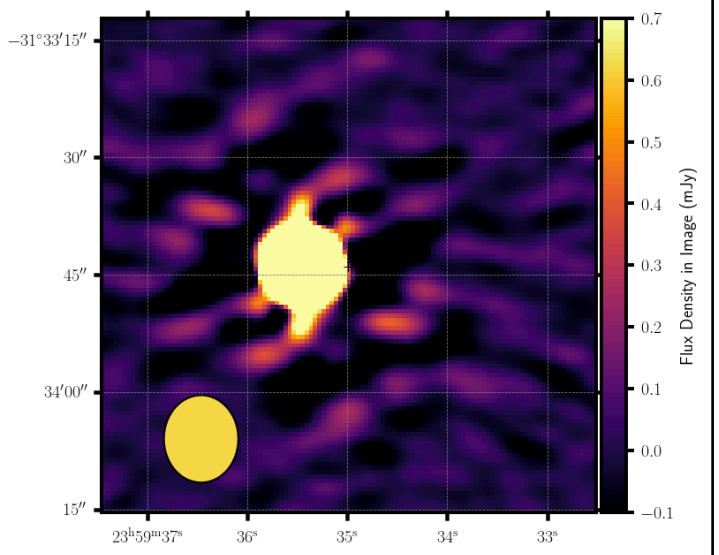

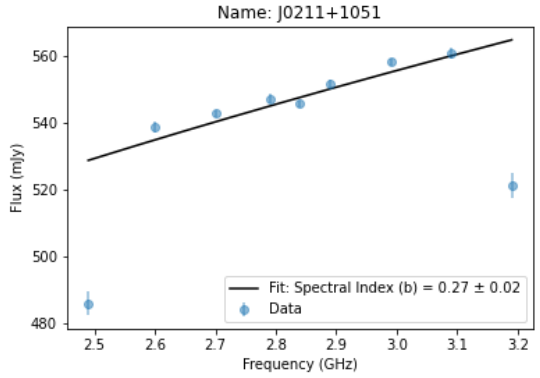

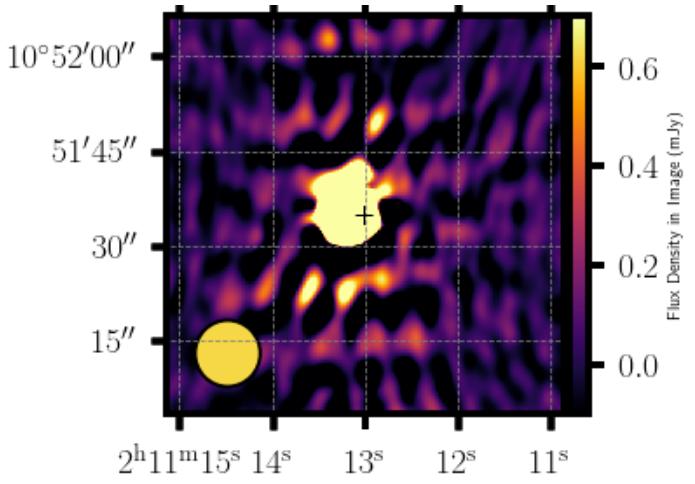

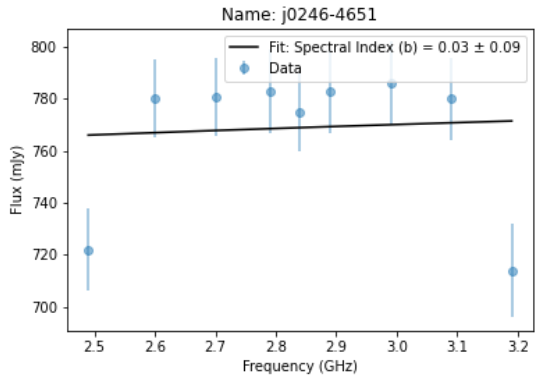

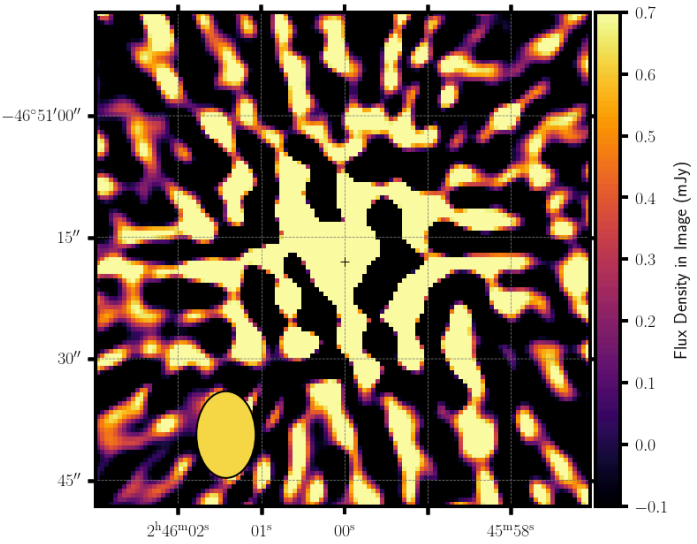

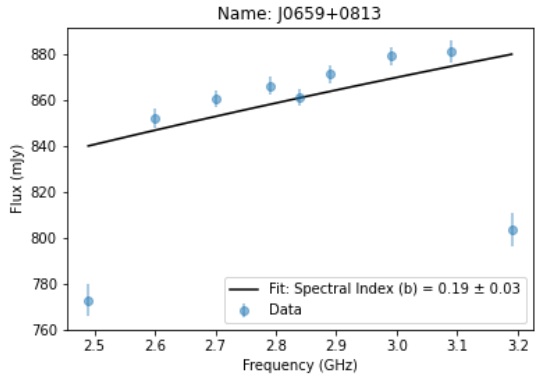

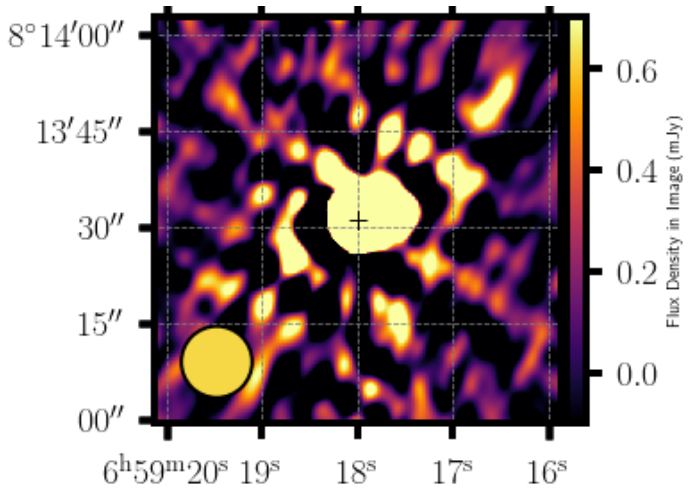

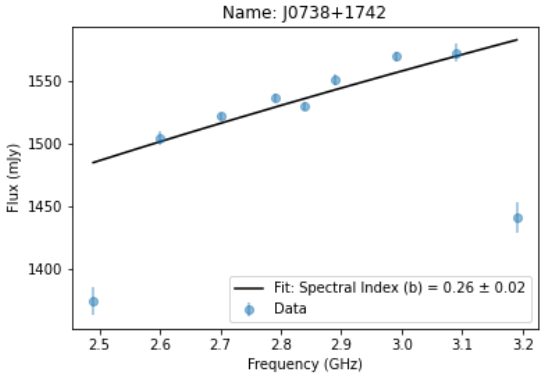

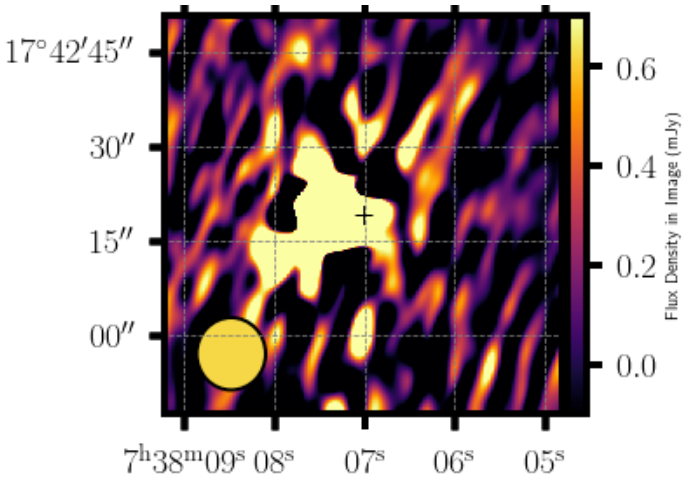

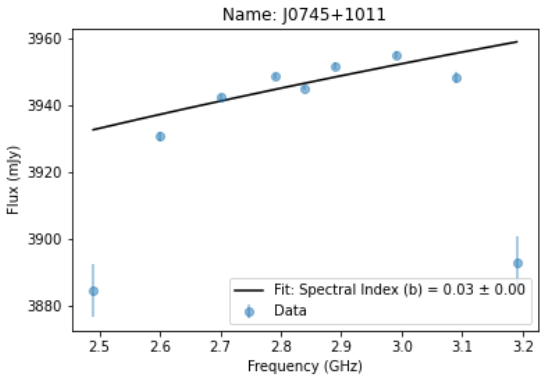

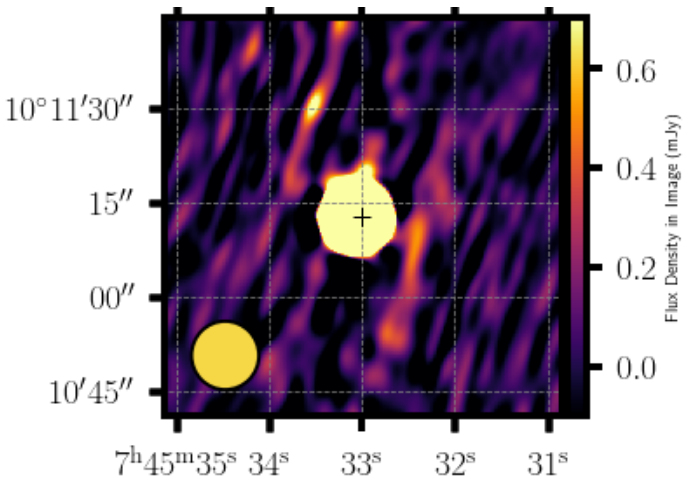

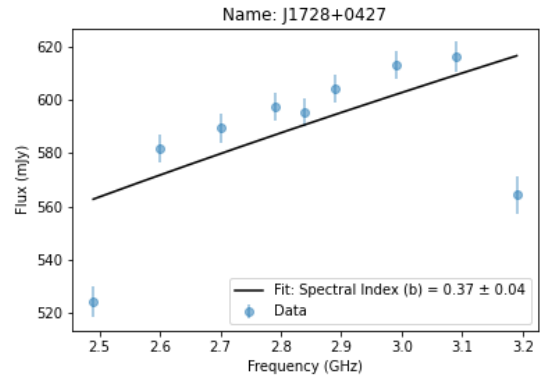

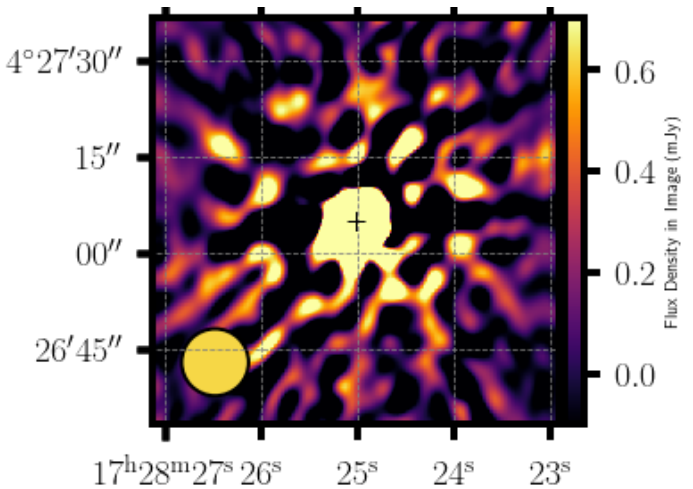

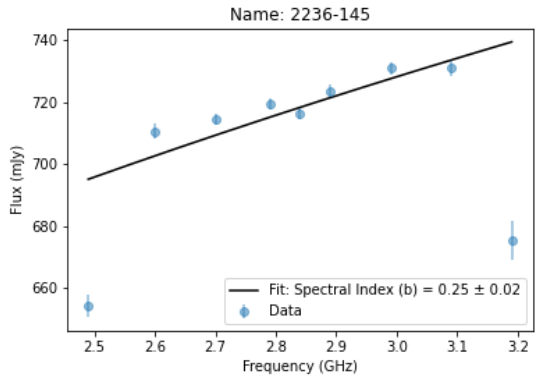

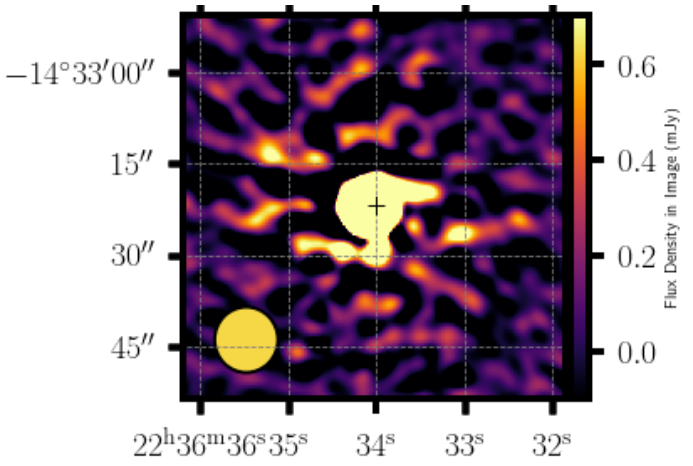

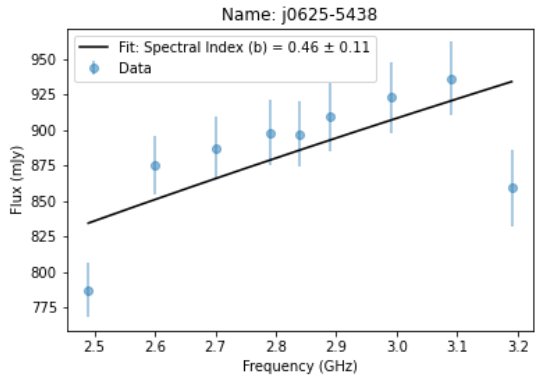

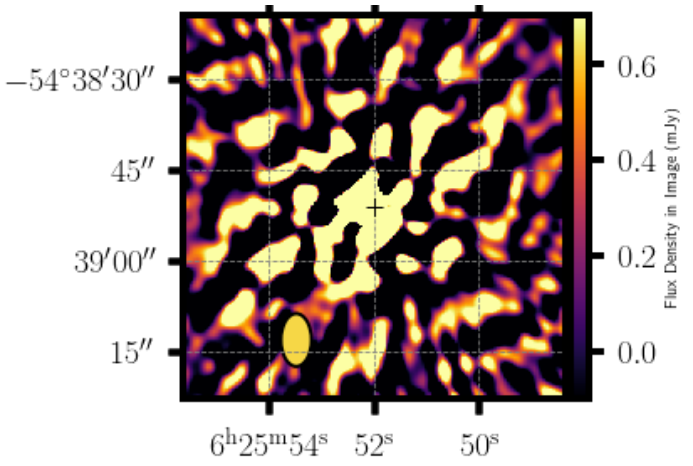

Negative/steep spectral indices

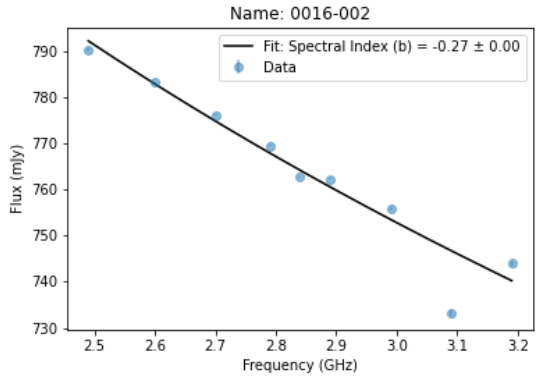

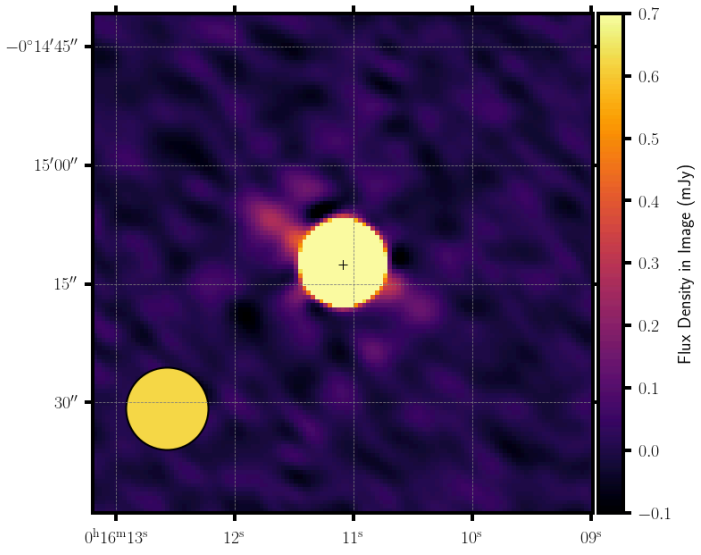

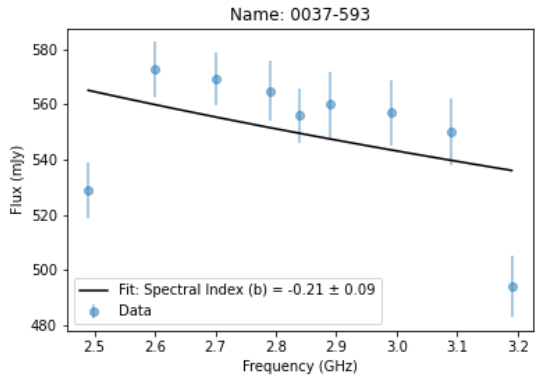

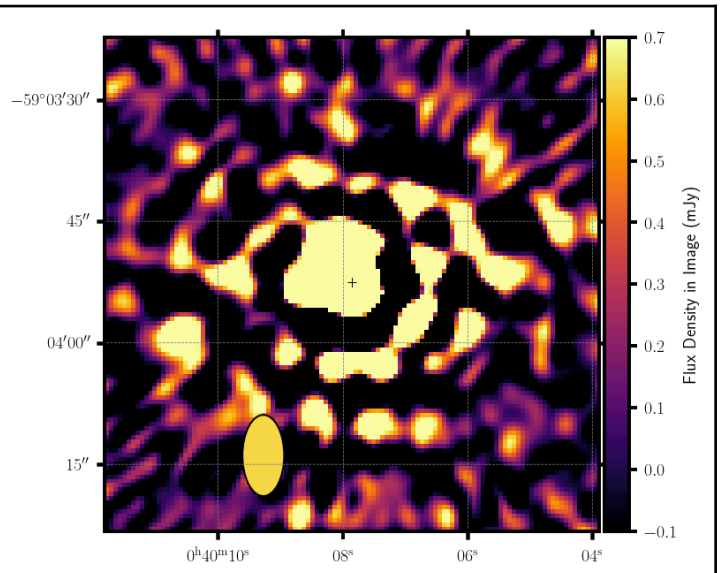

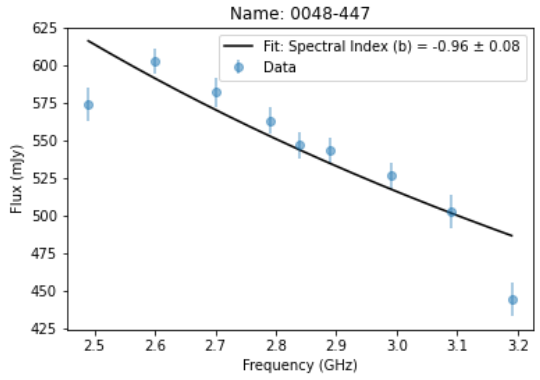

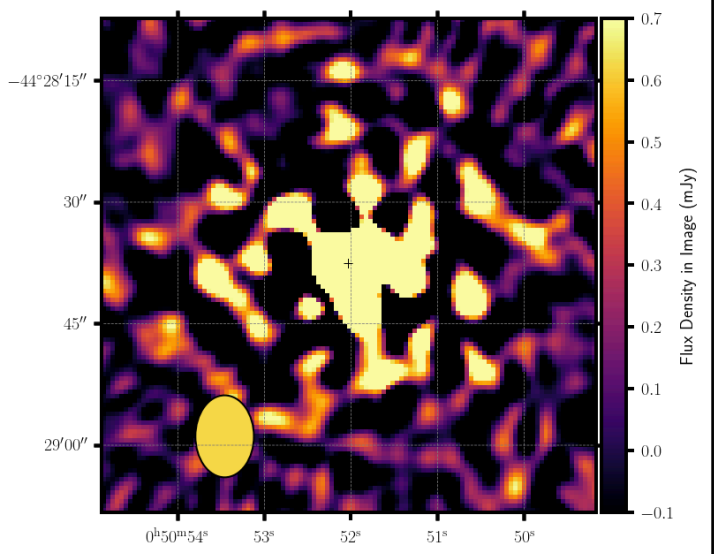

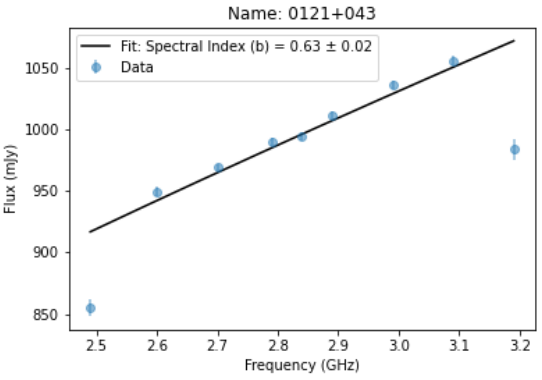

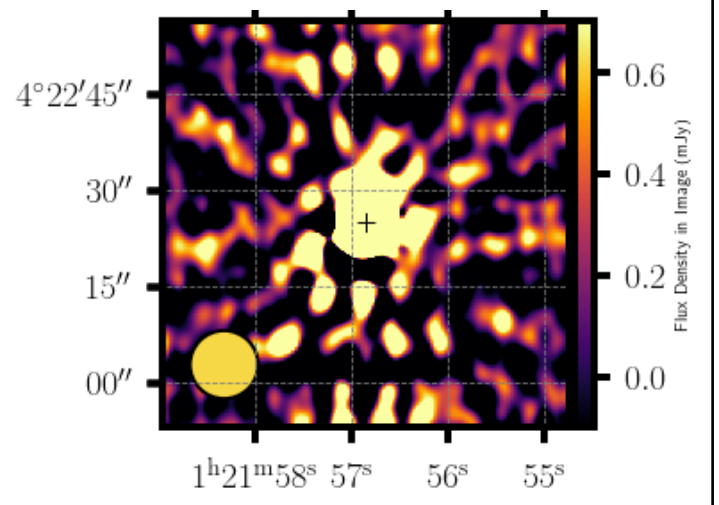

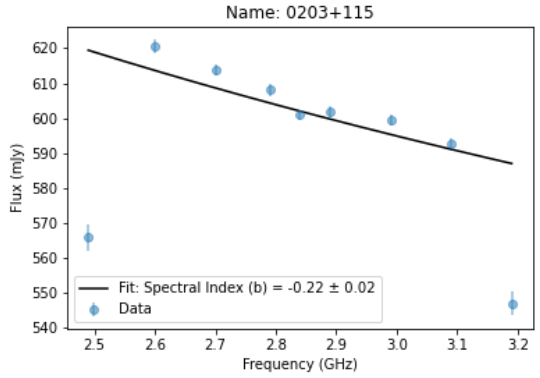

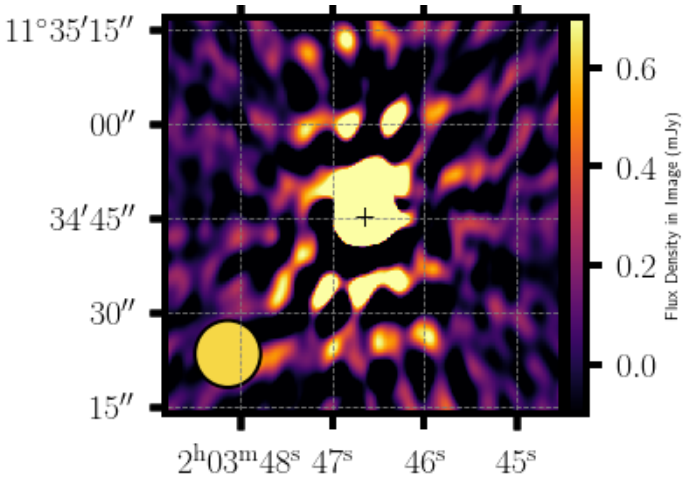

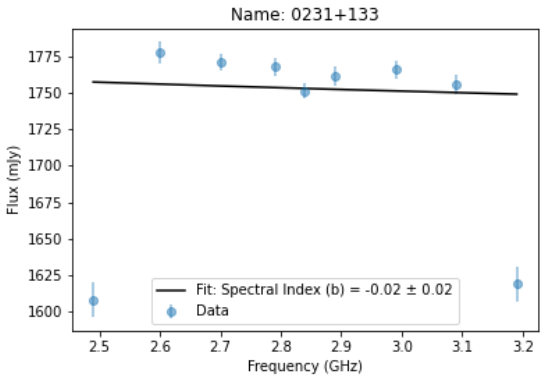

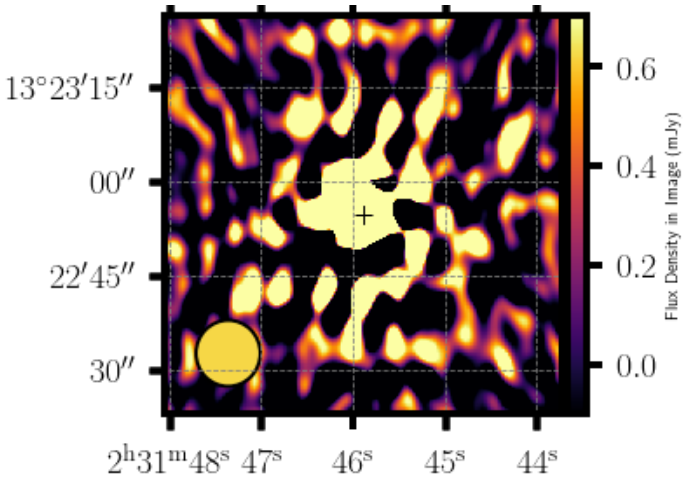

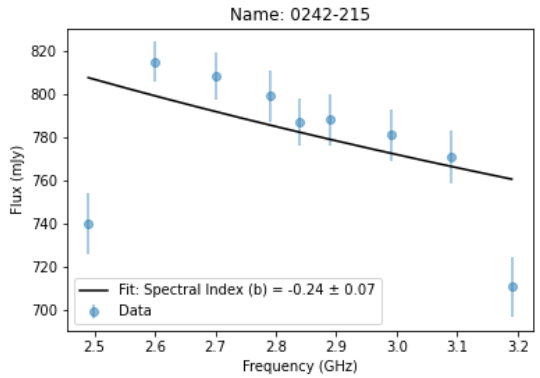

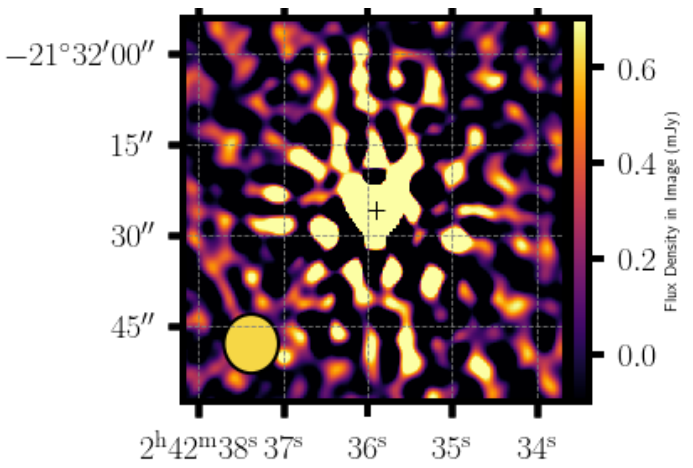

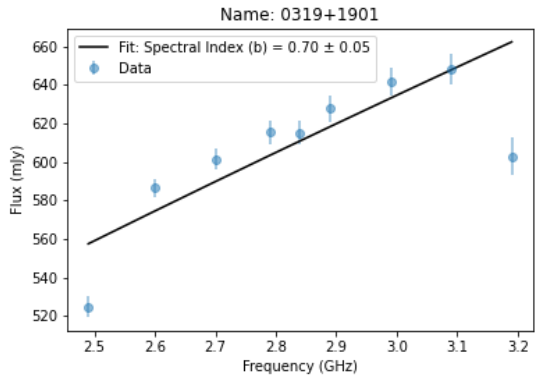

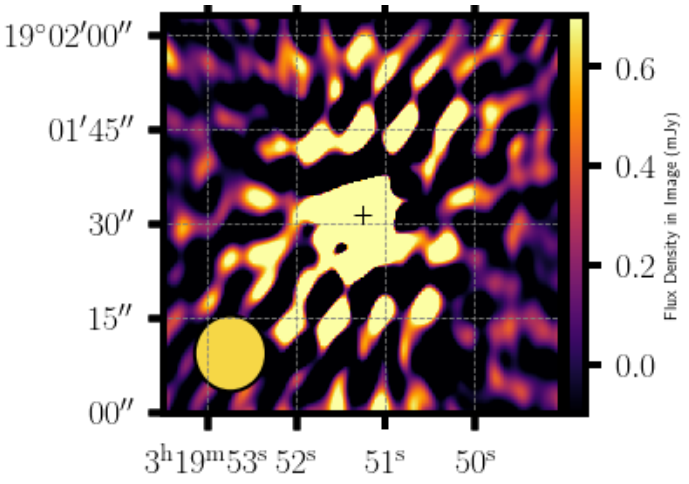

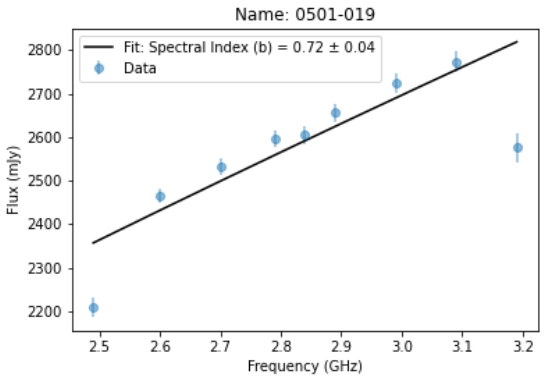

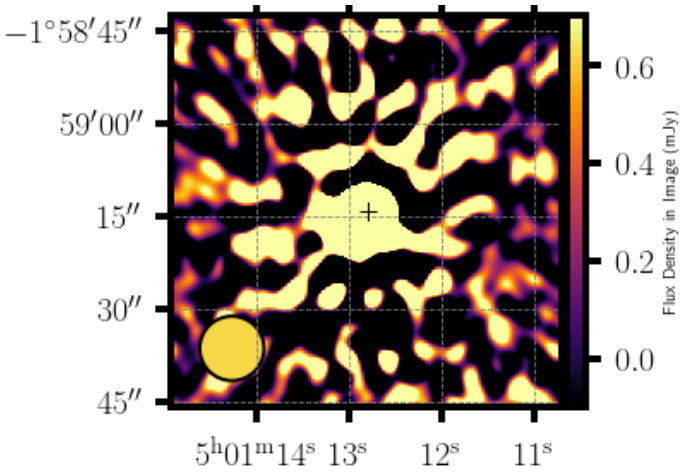

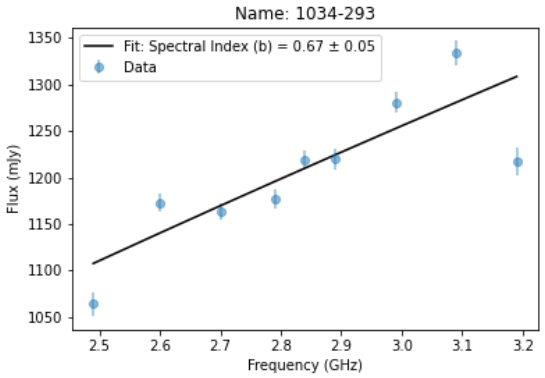

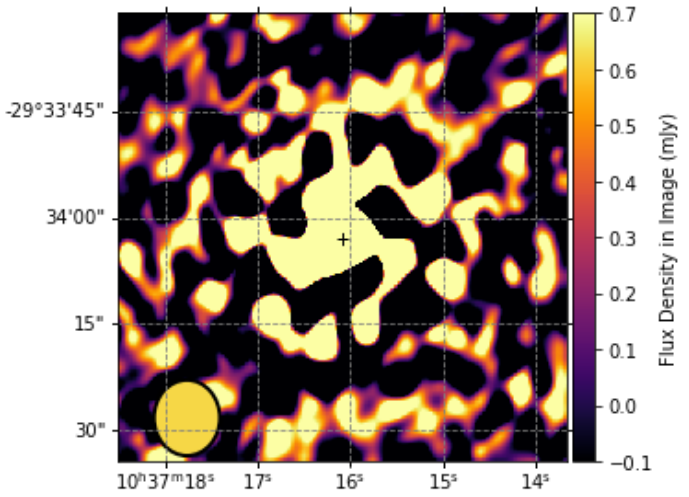

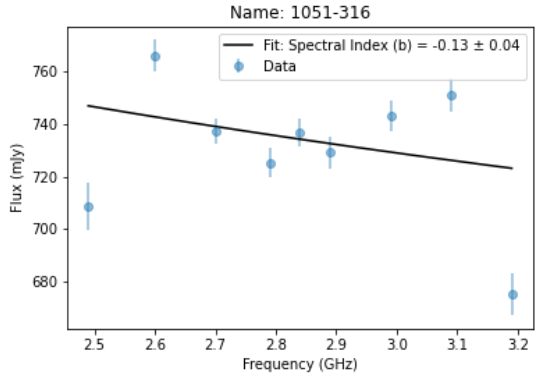

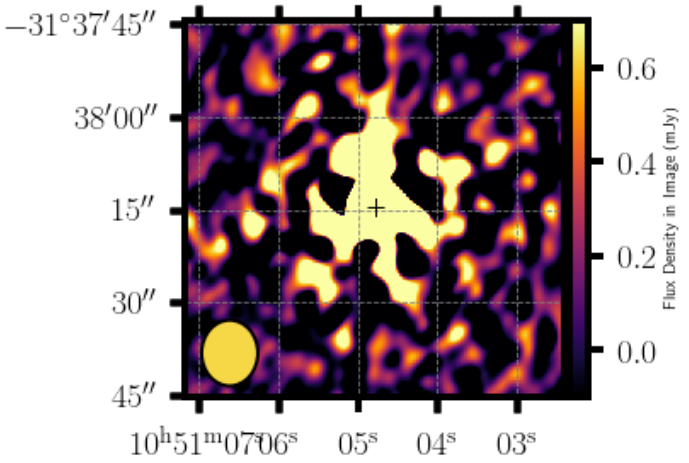

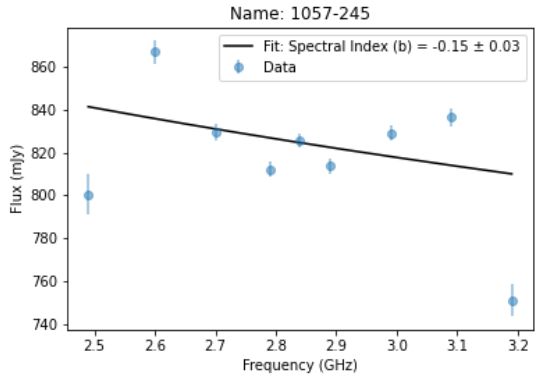

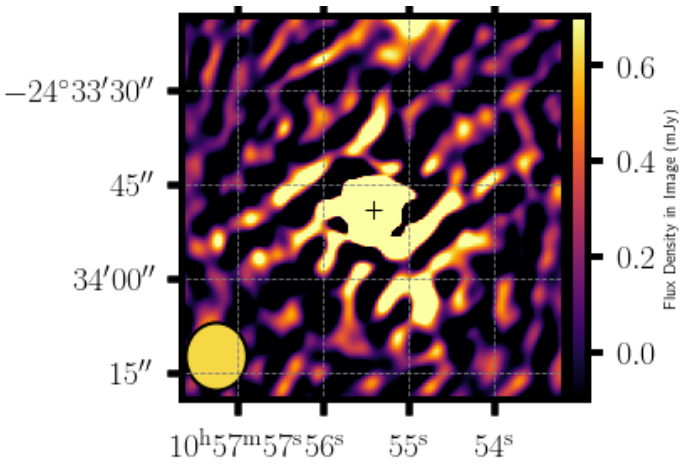

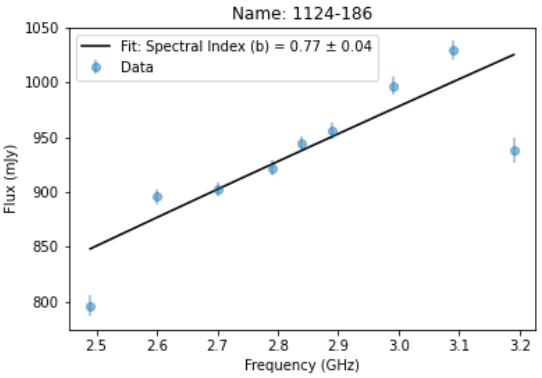

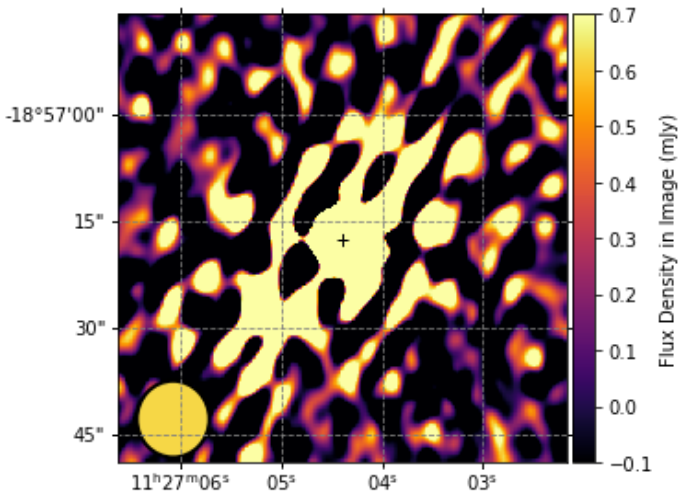

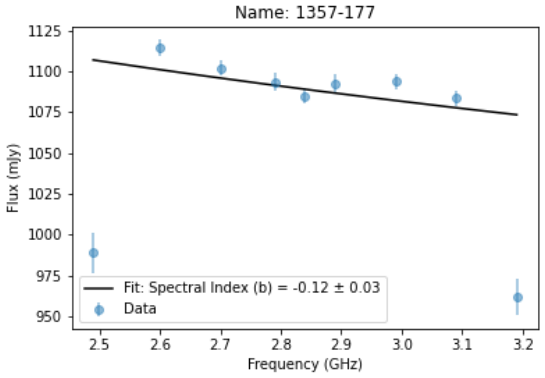

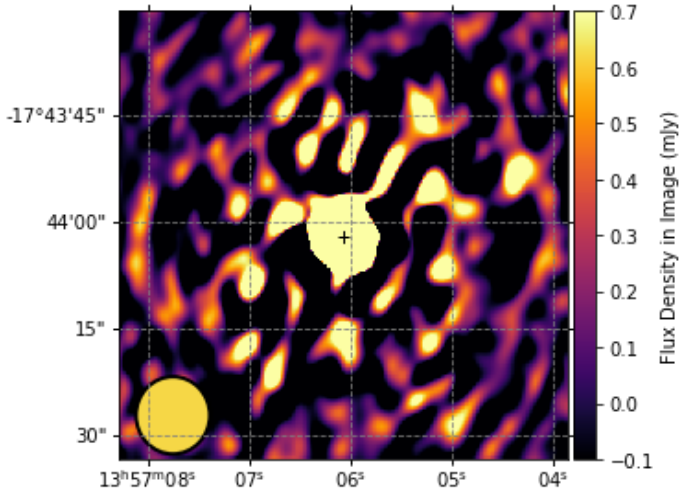

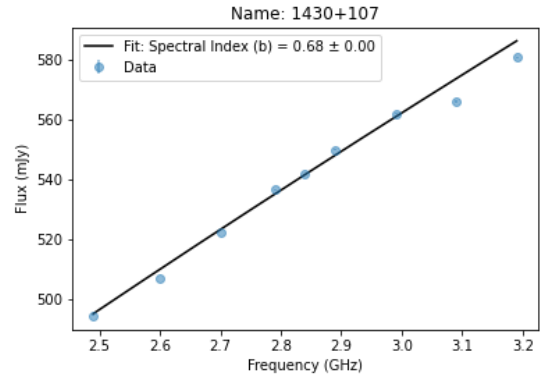

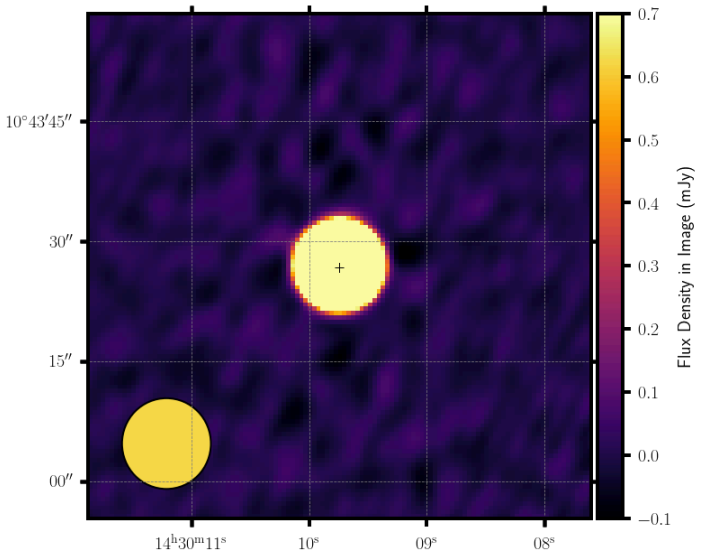

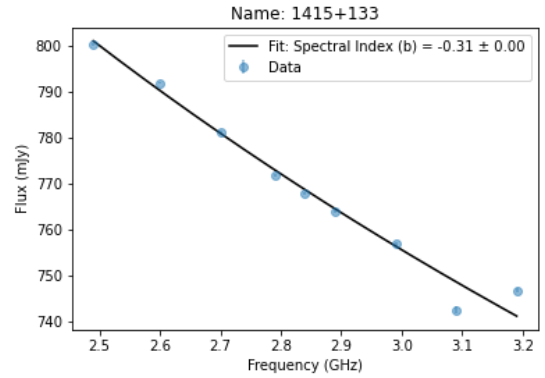

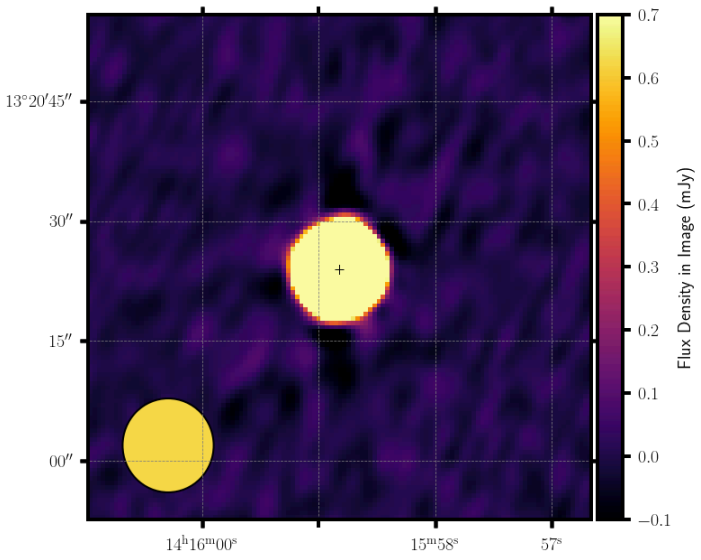

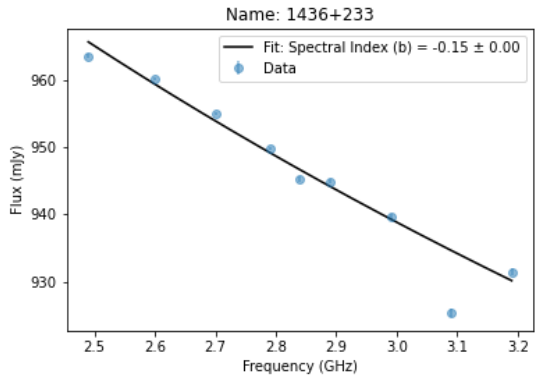

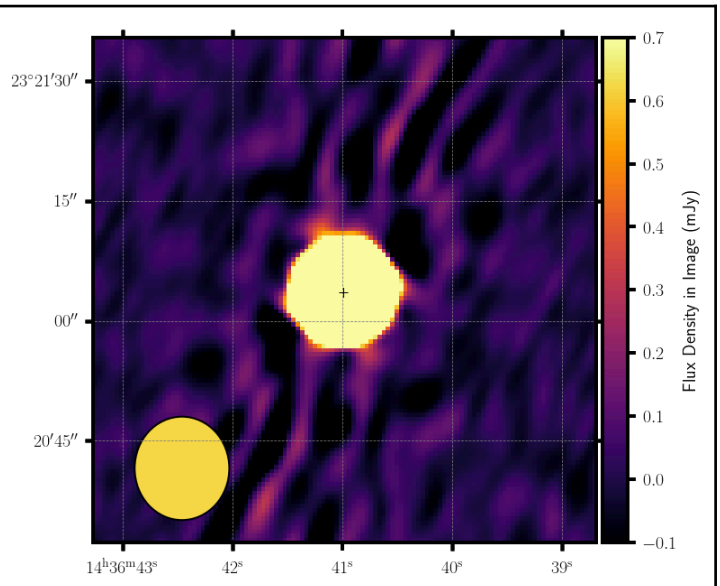

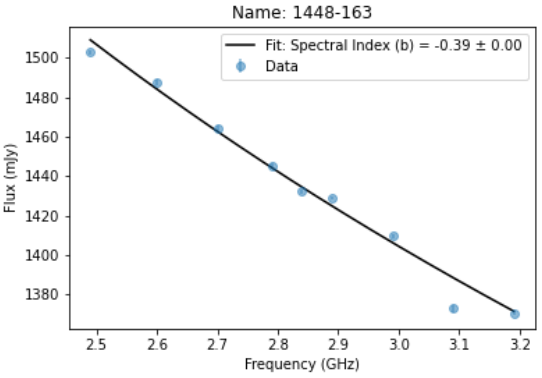

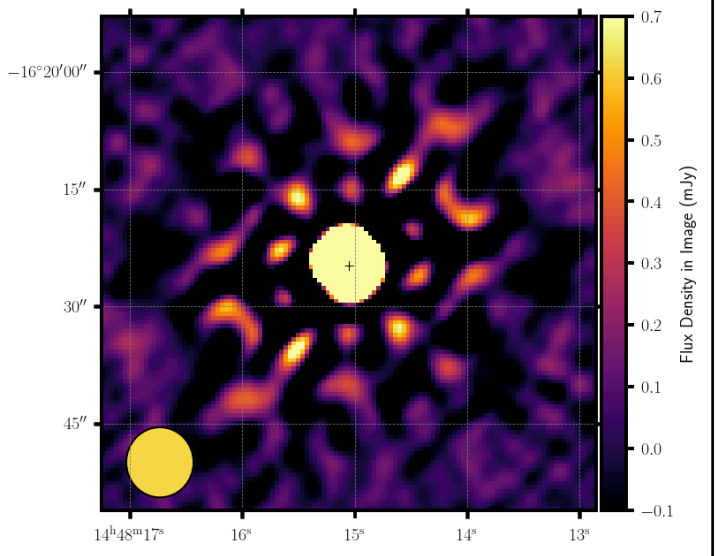

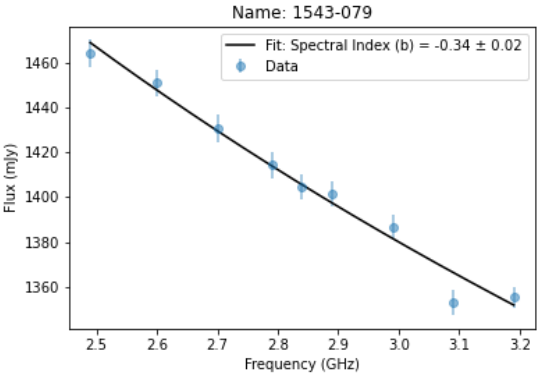

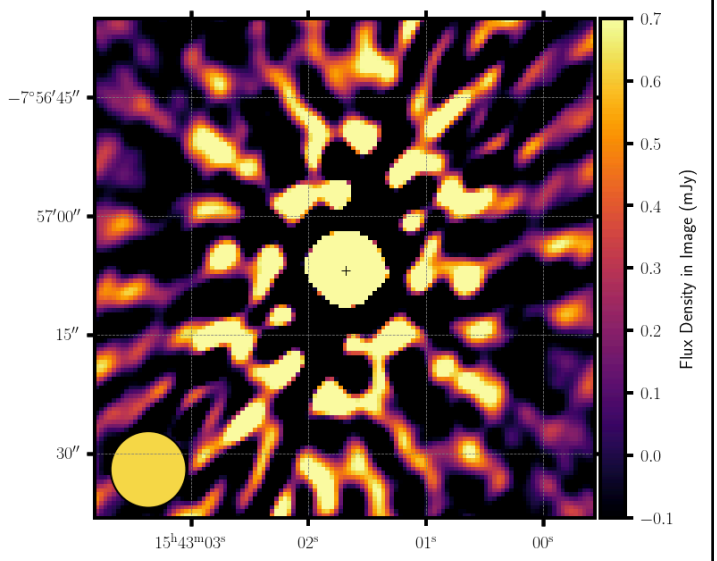

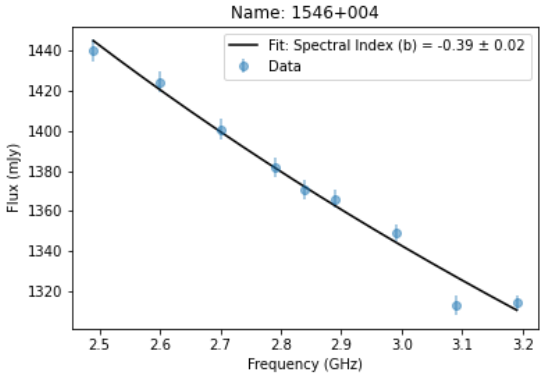

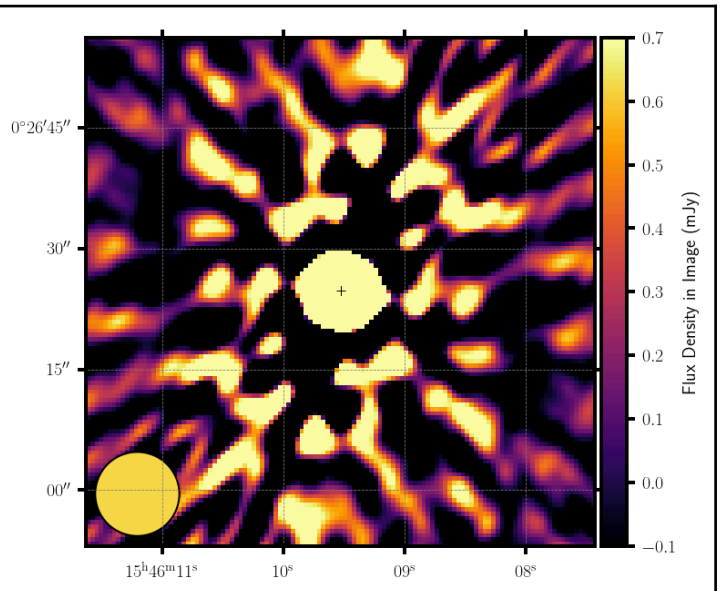

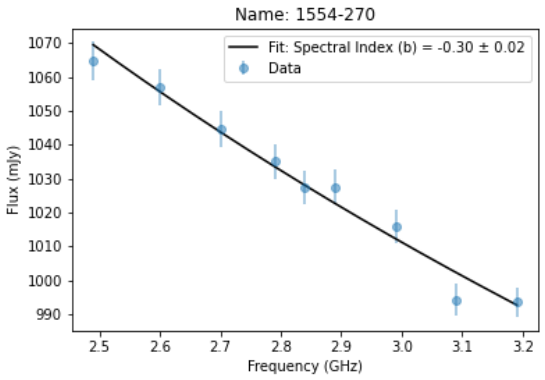

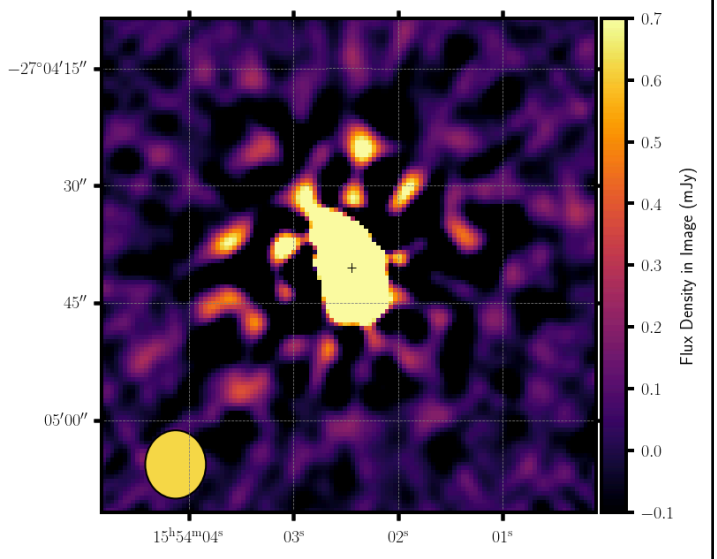

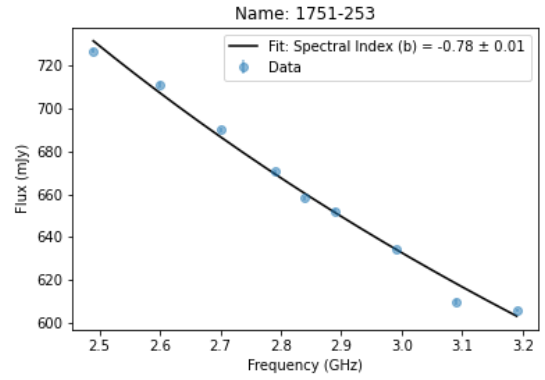

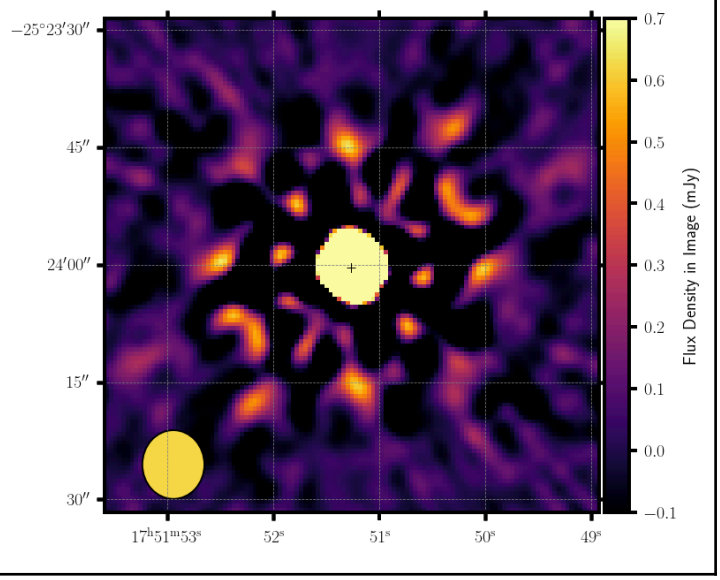

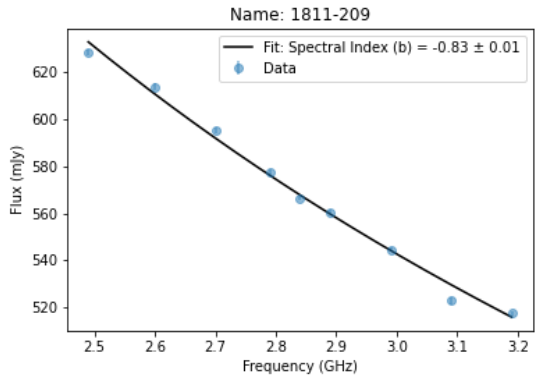

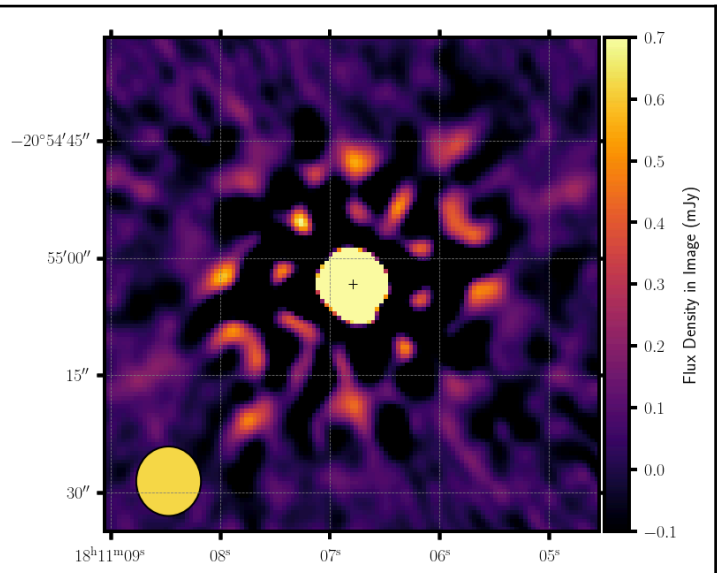

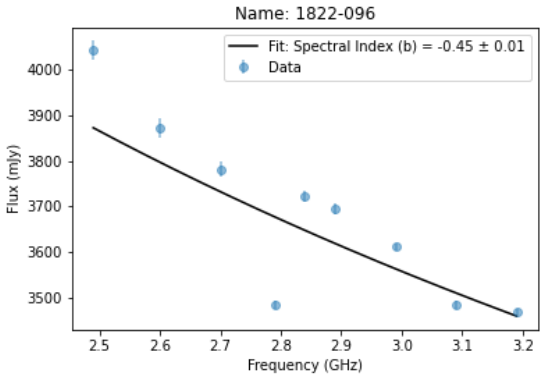

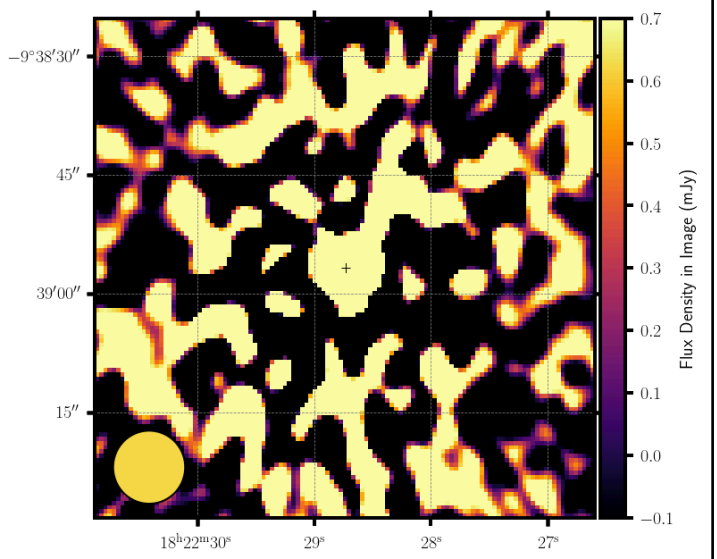

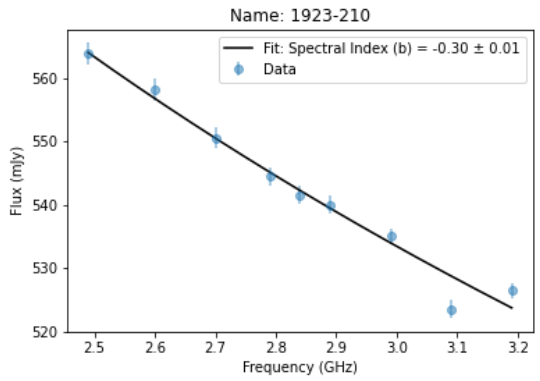

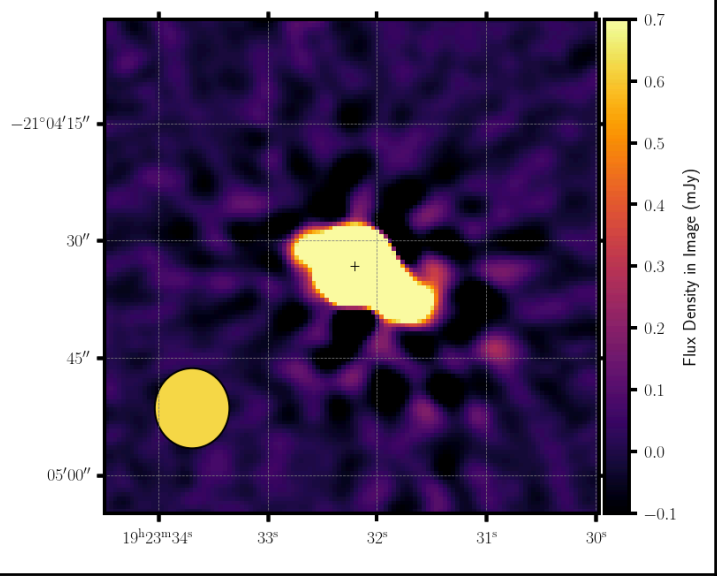

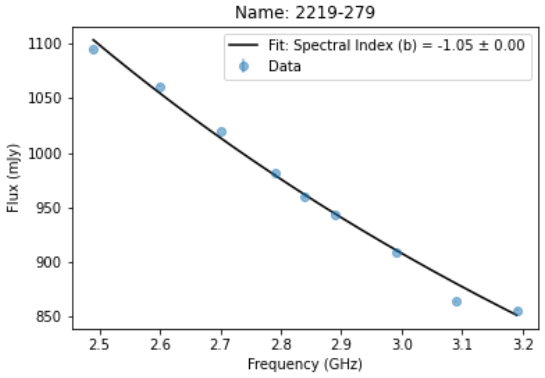

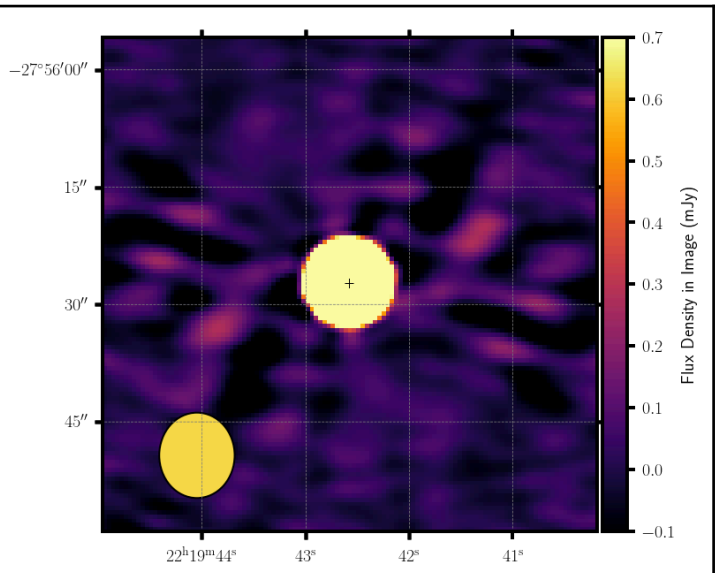

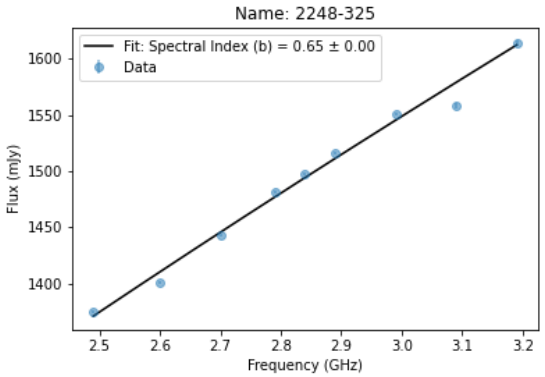

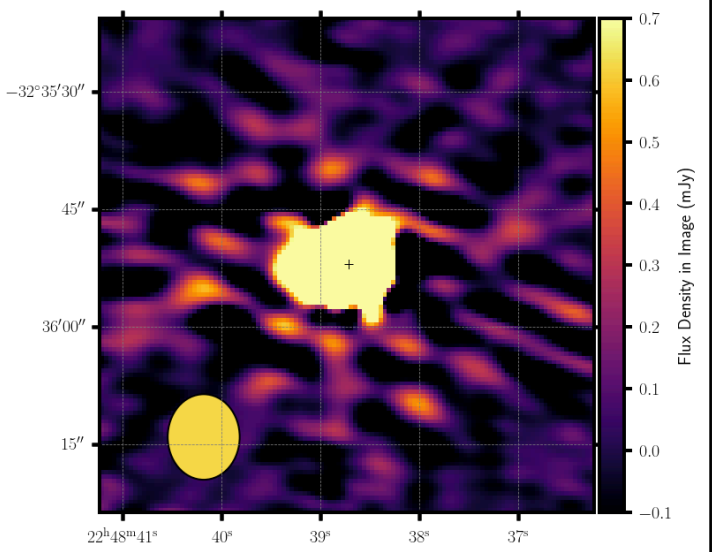

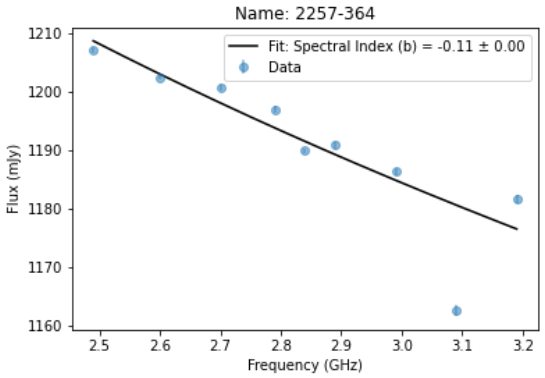

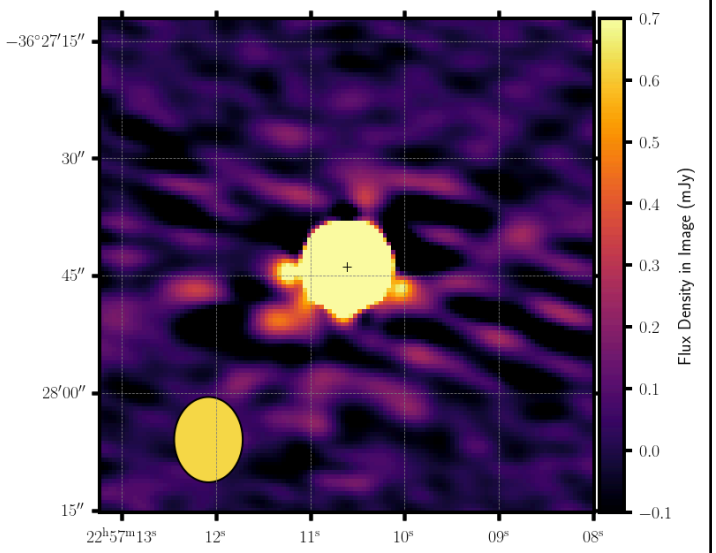

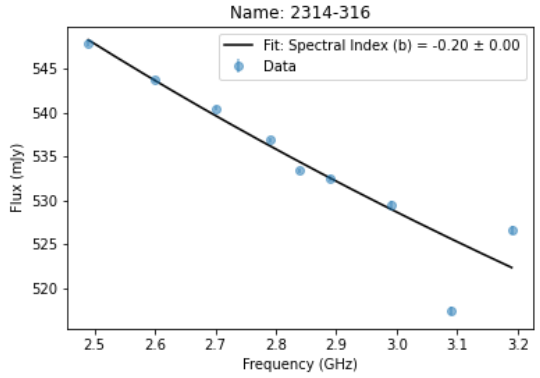

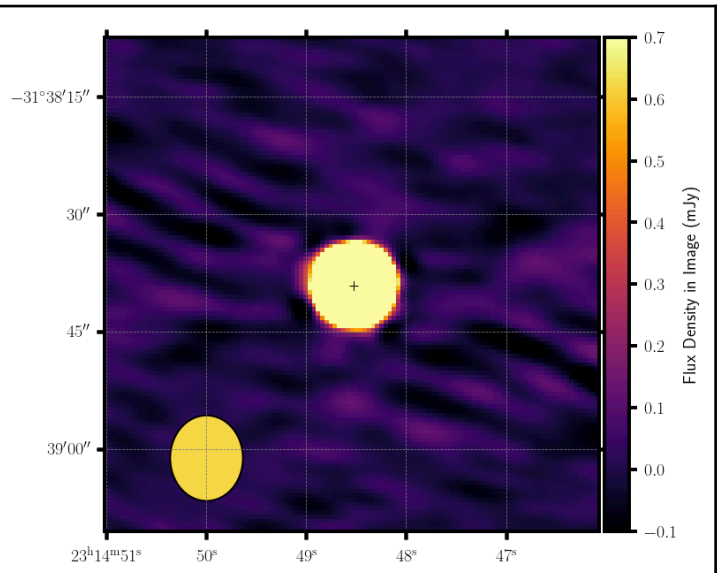

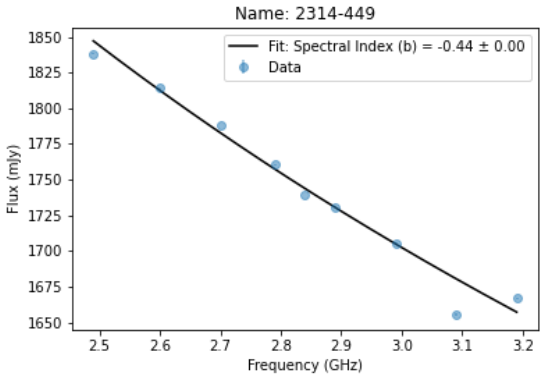

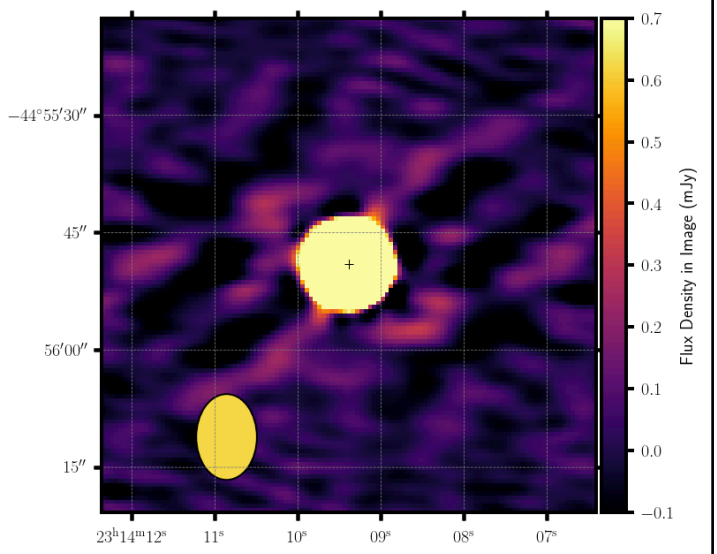

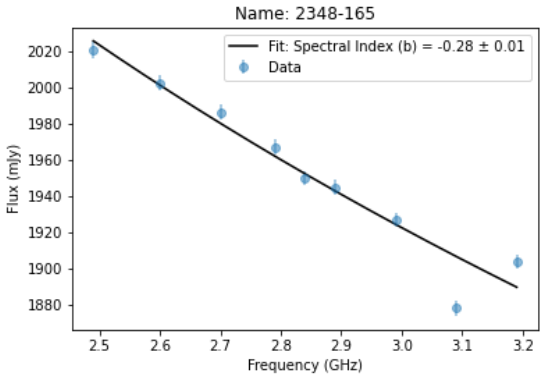

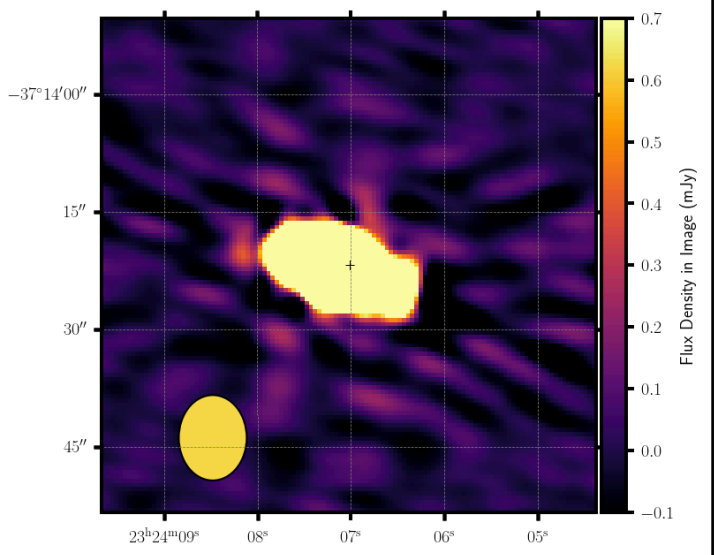

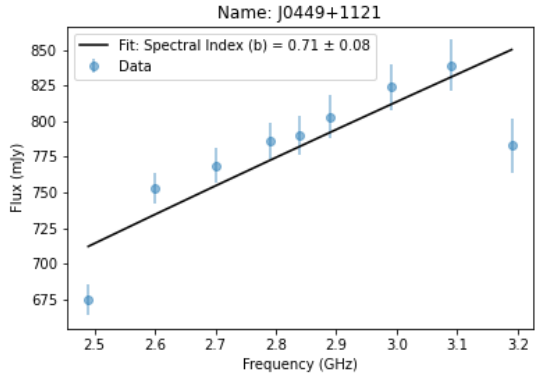

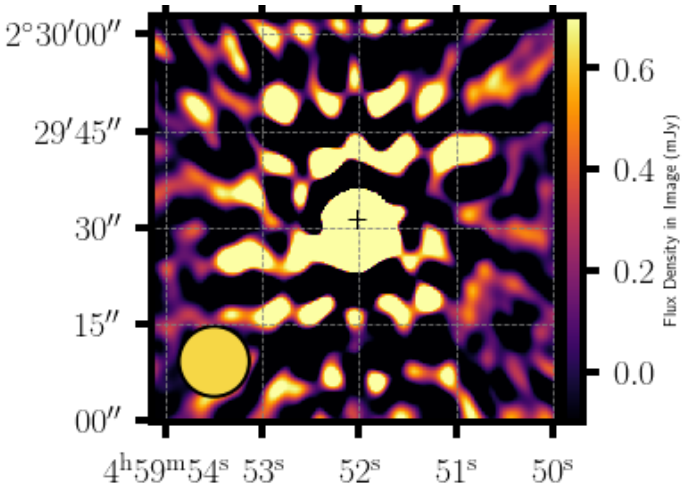

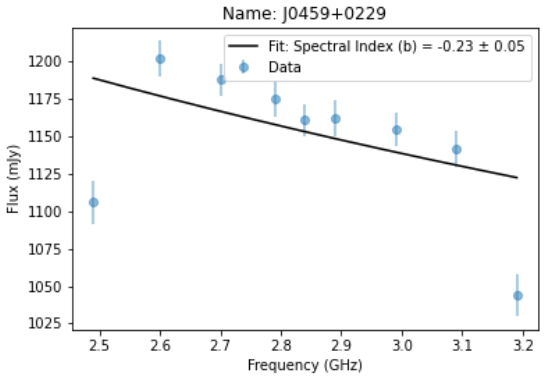

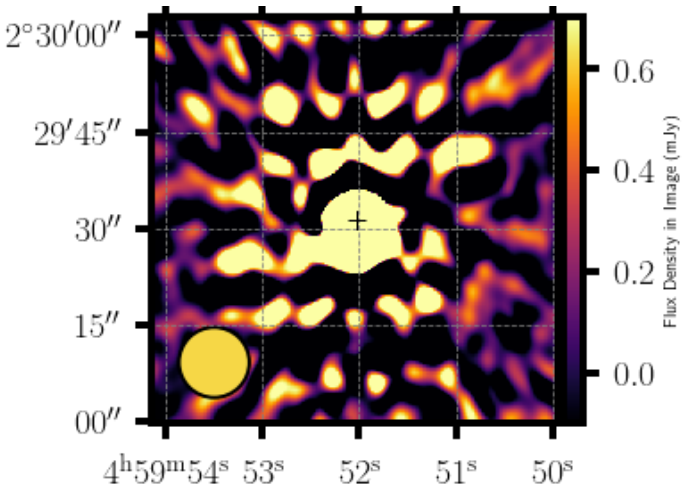

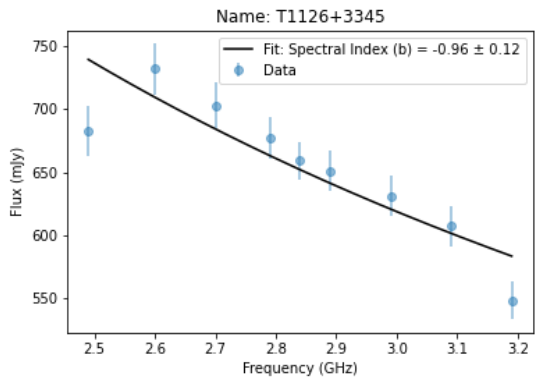

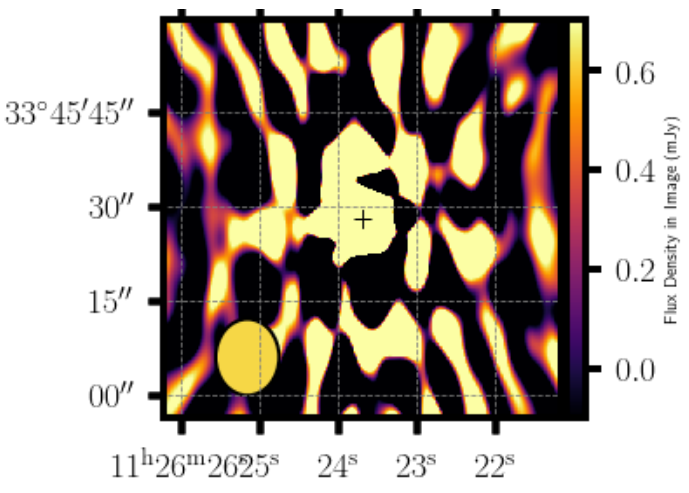

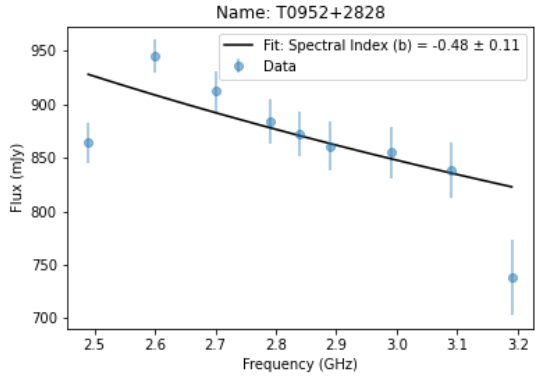

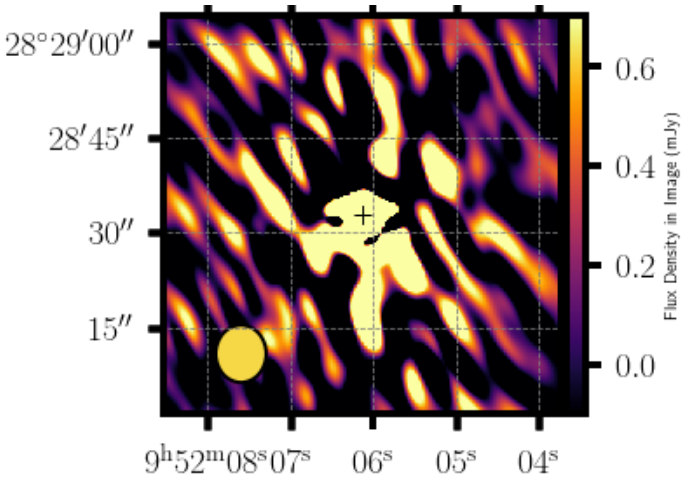

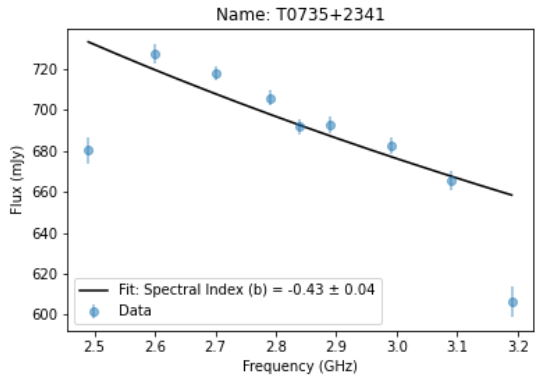

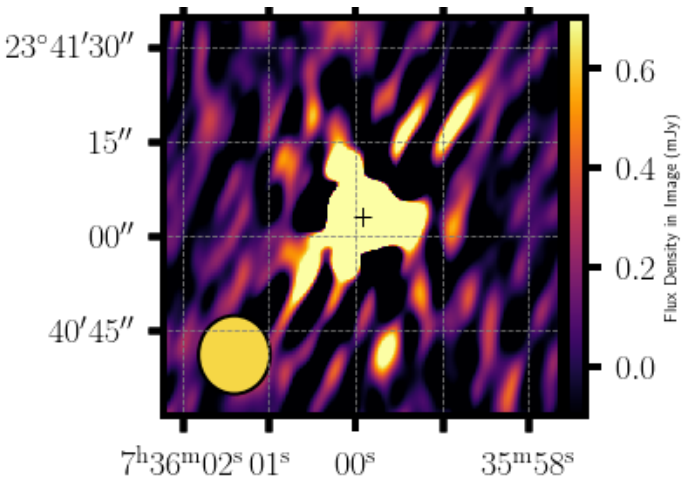

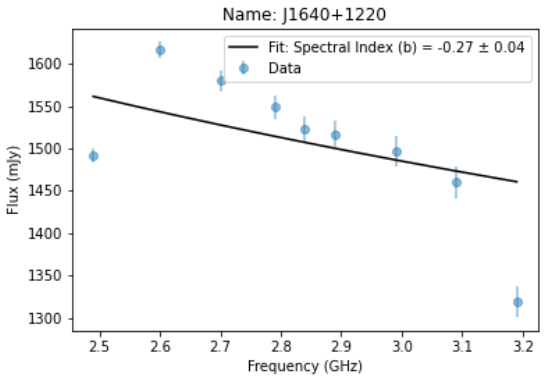

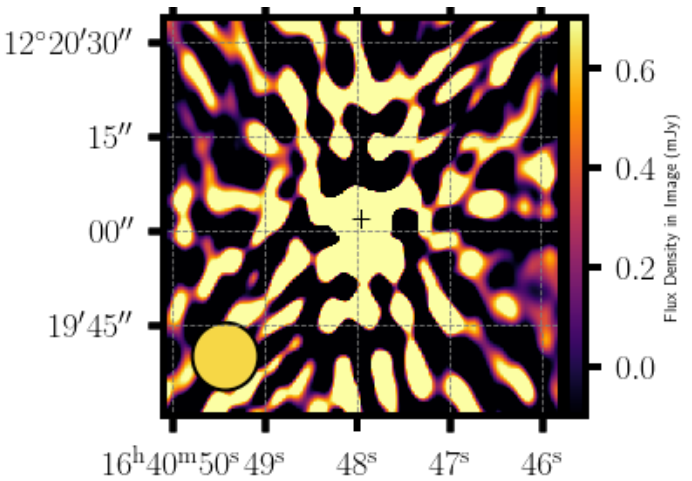

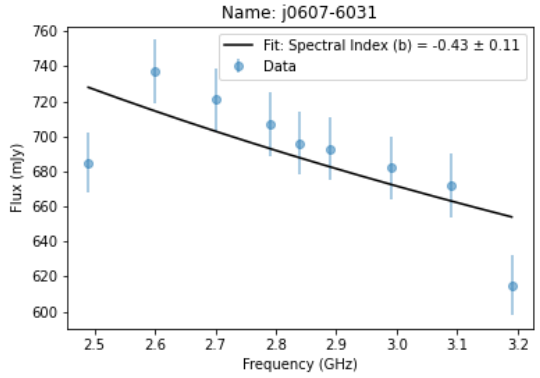

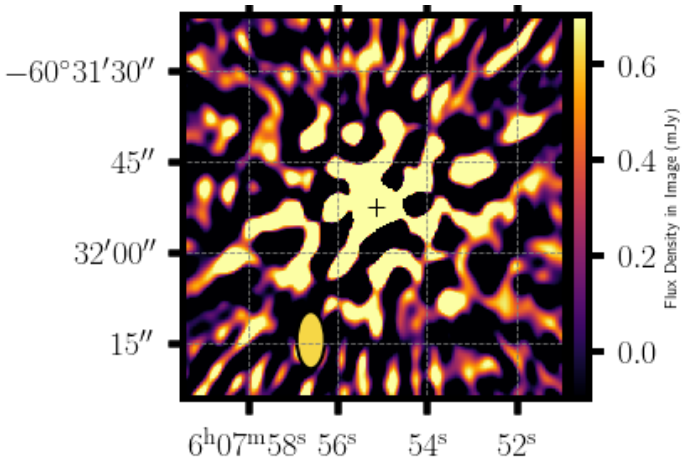

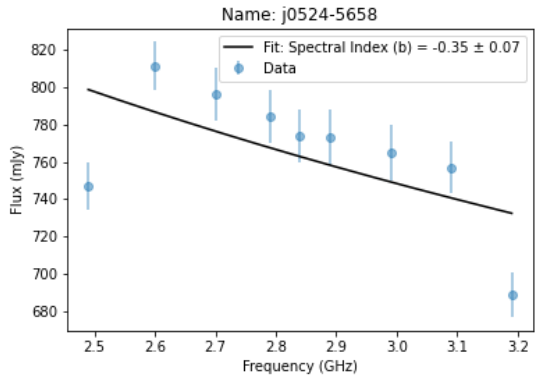

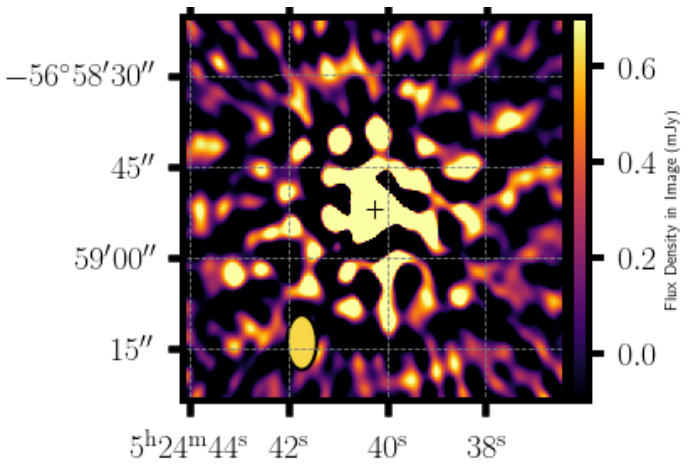

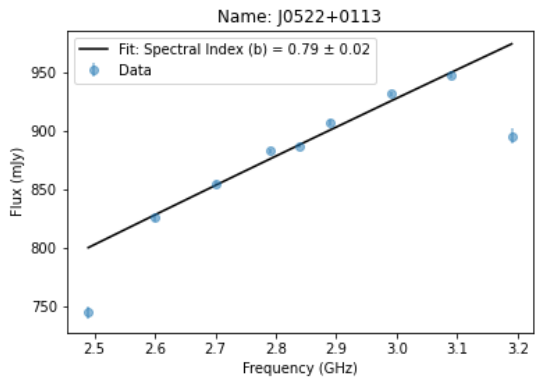

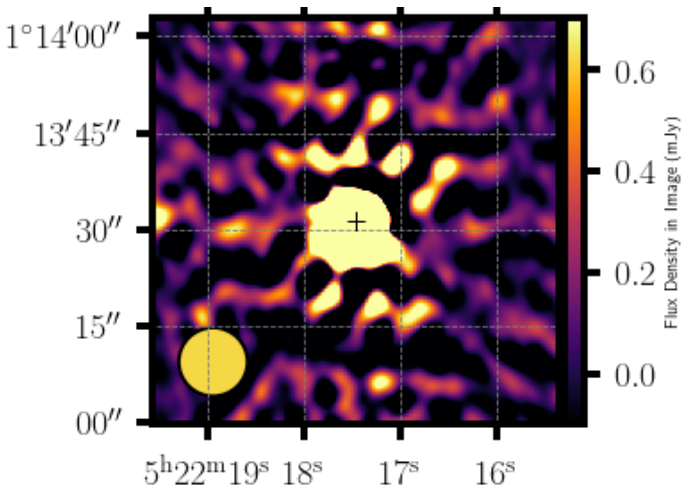

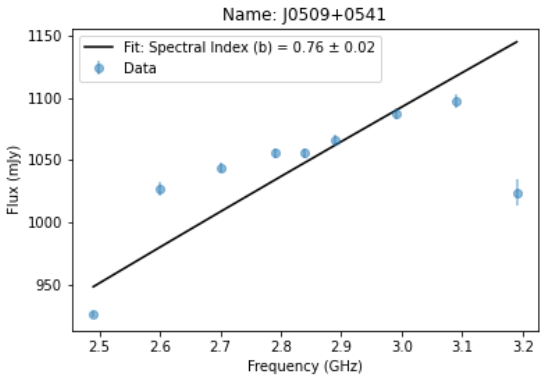

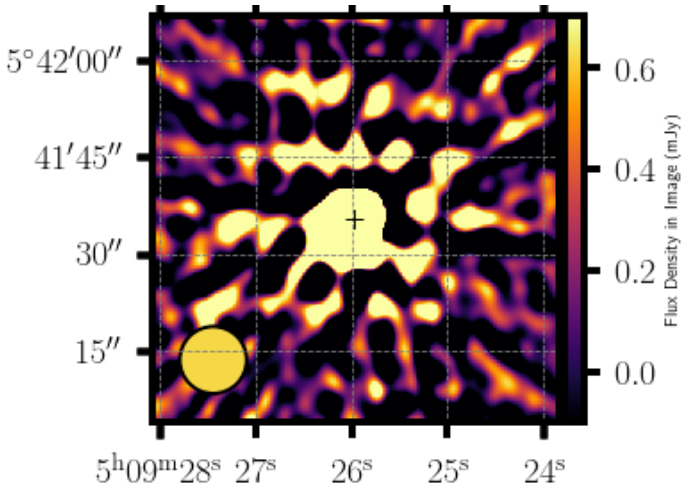

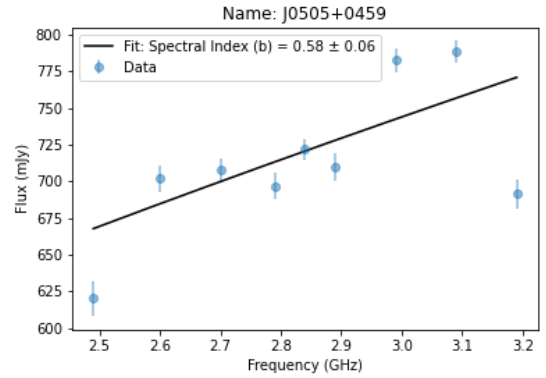

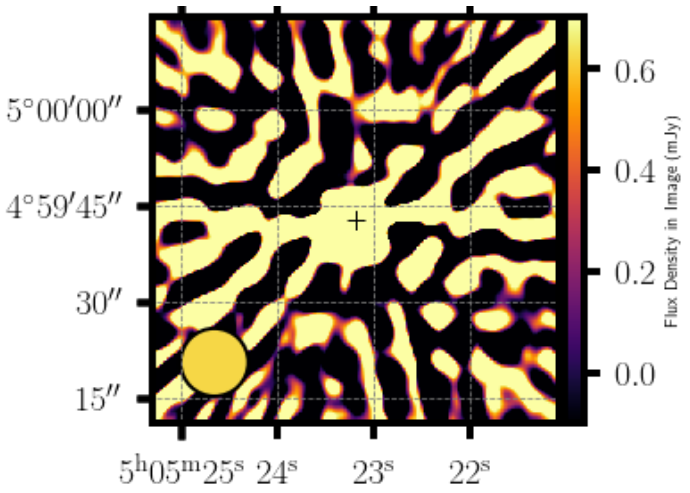

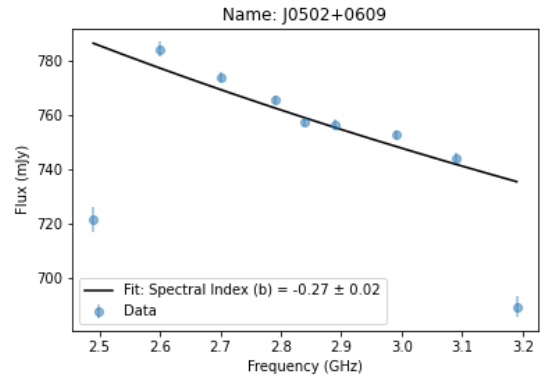

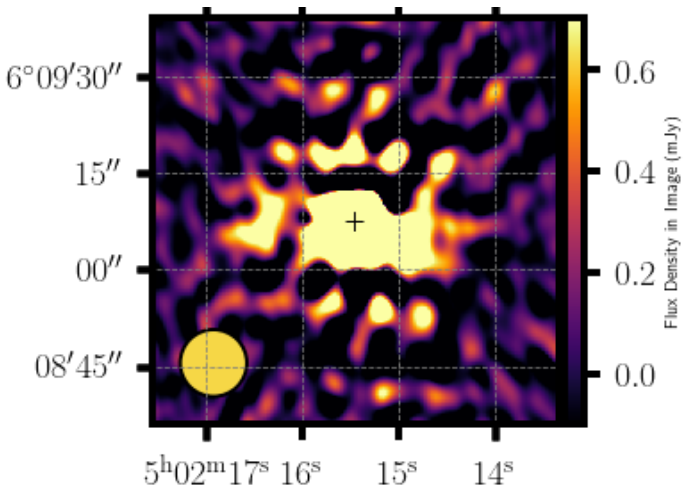

Additional sources

1145-071

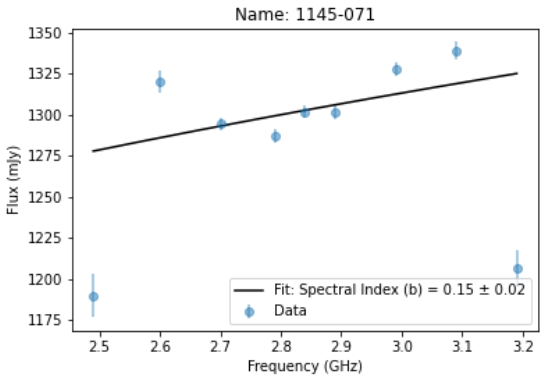

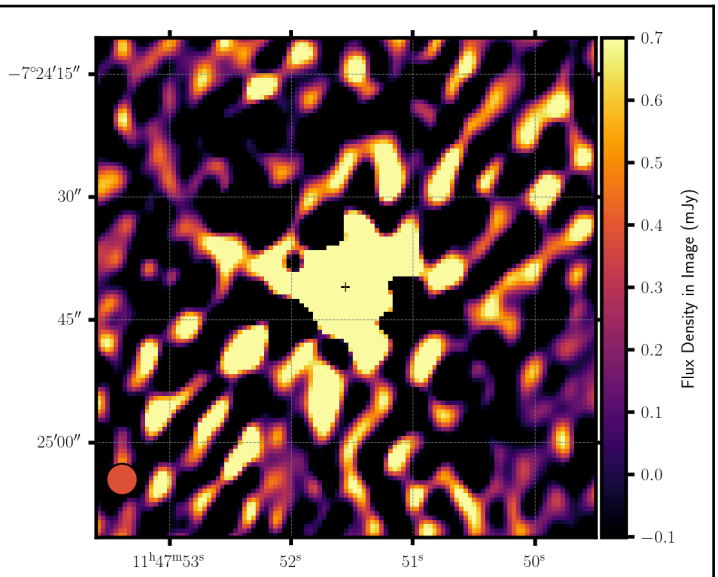

1949-199

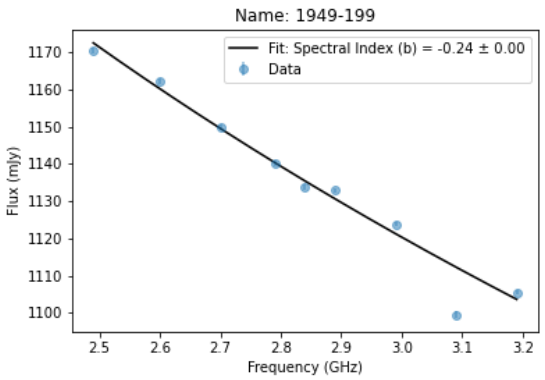

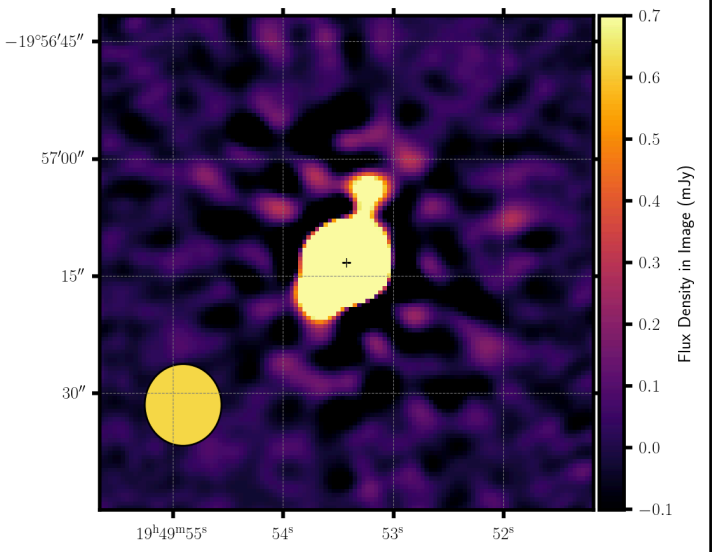

2007-445

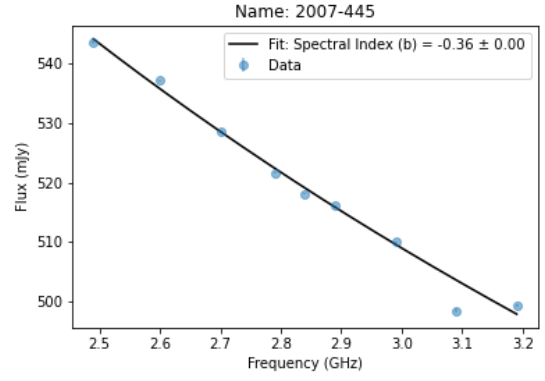

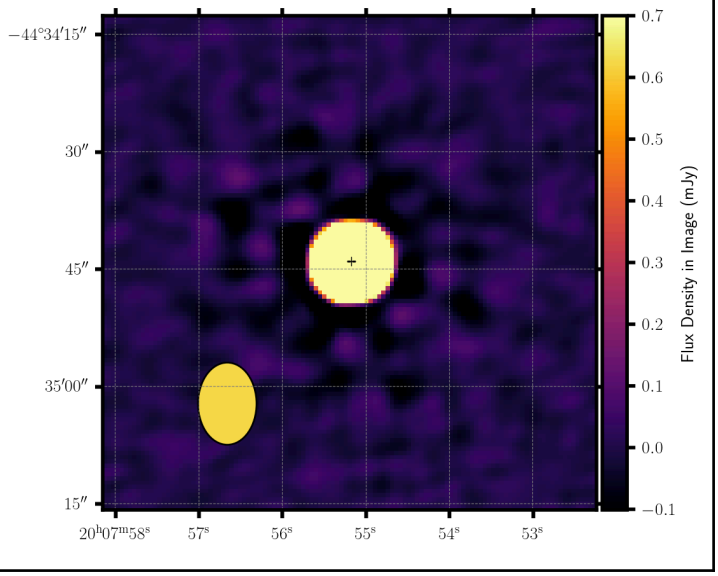

2047-026

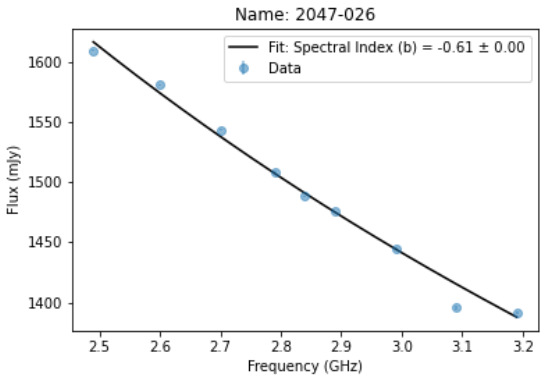

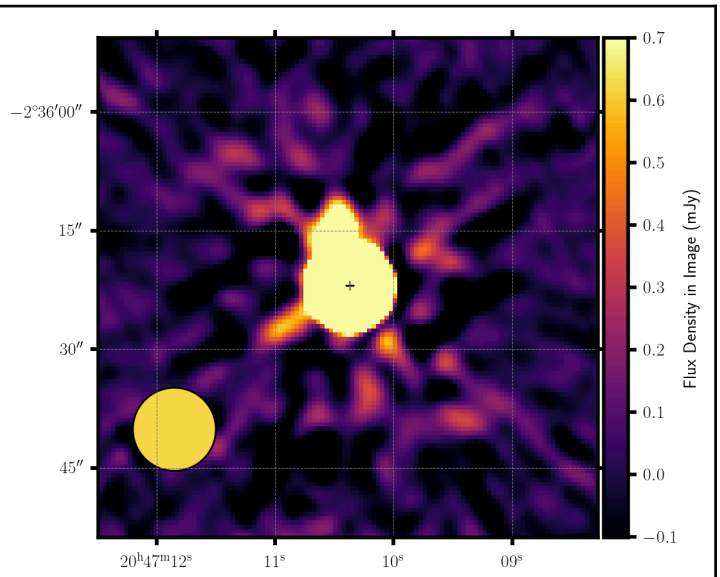

2052-474

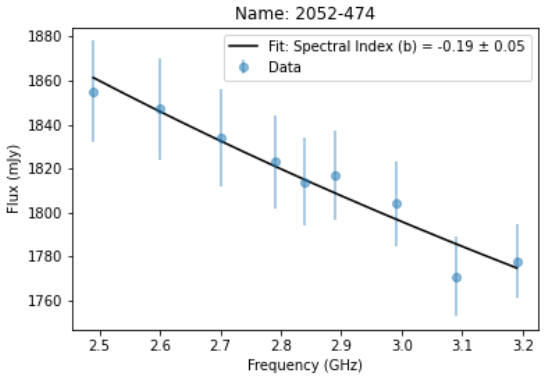

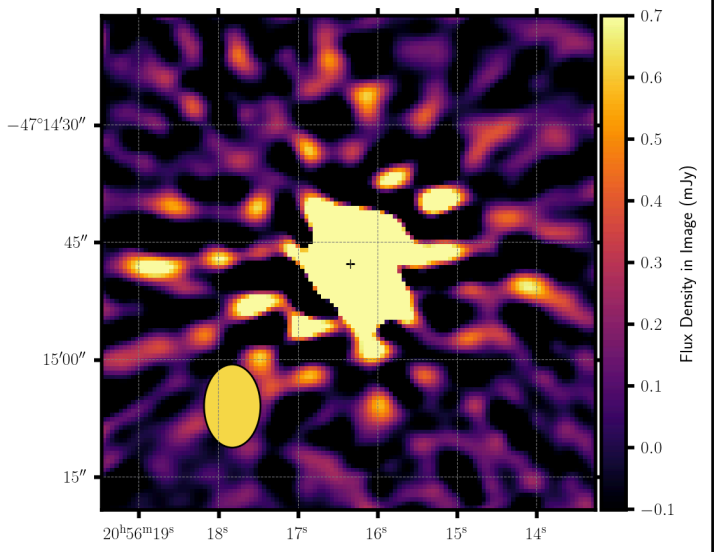

2110-103

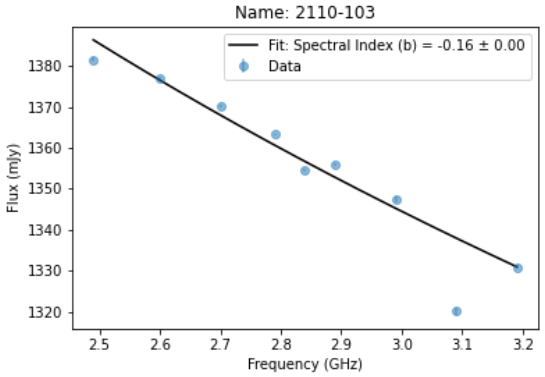

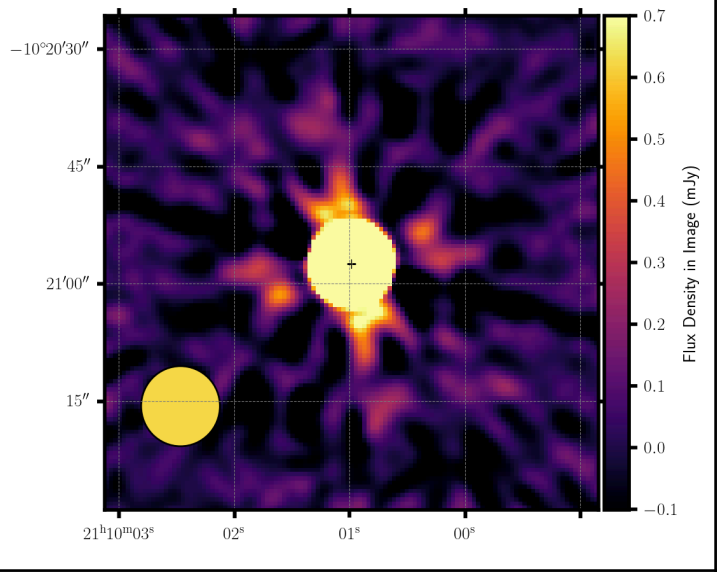

T0237+0919

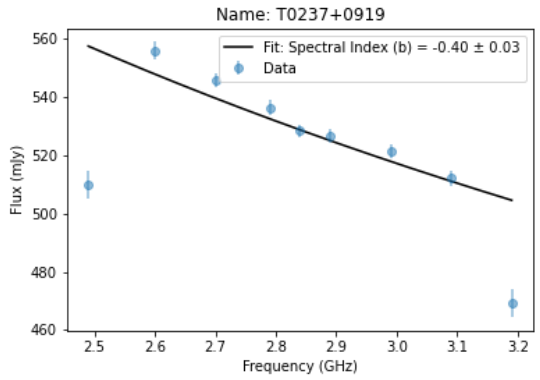

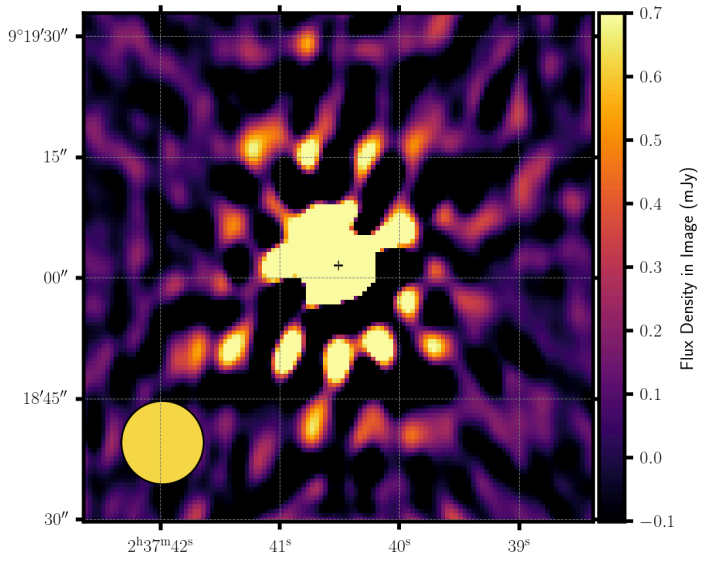

1432-180

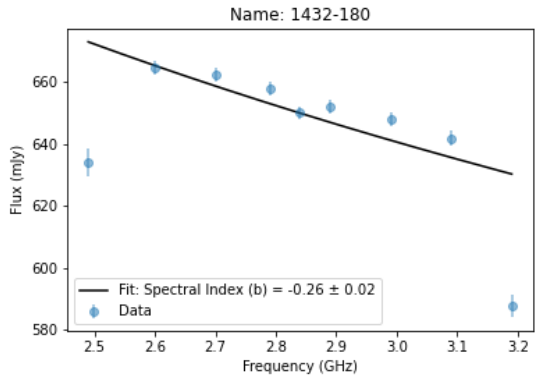

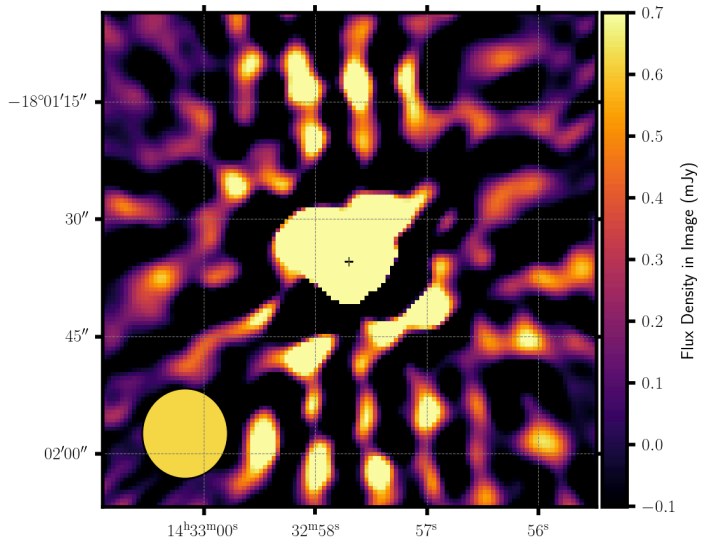

J0839+0319

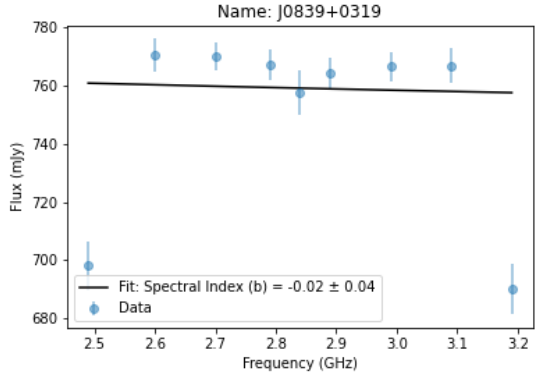

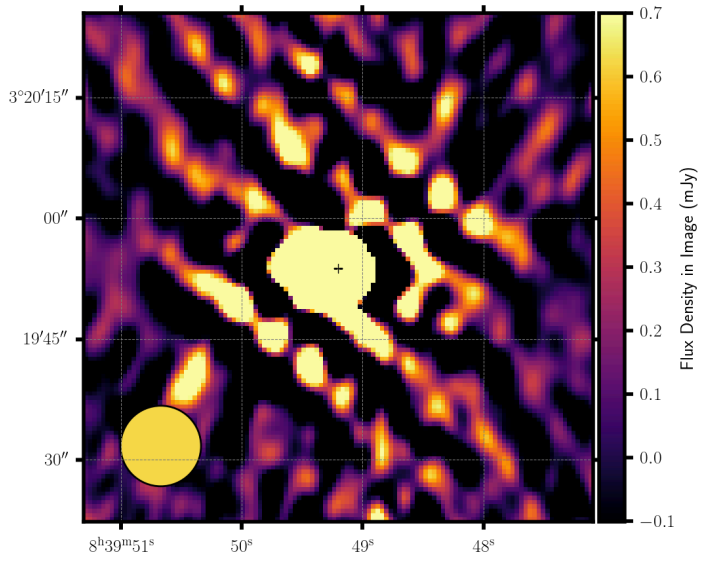

3.3 UV PLOTS

Table 3: Amplitude -UV distance plots of selected targets per antenna using the XX correlation data produced using https://github.com/ratt-ru/shadeMS. The plots indicate that the sources are not resolved at different MeerKAT spatial scales.

0012-399	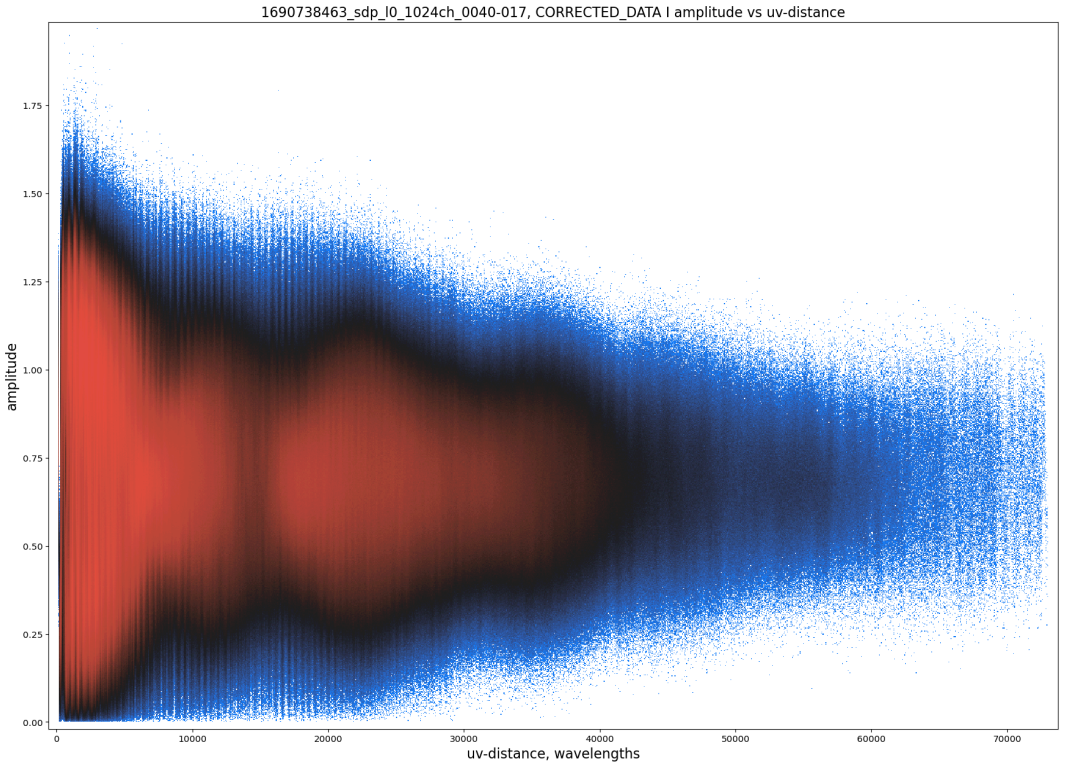

0040-017	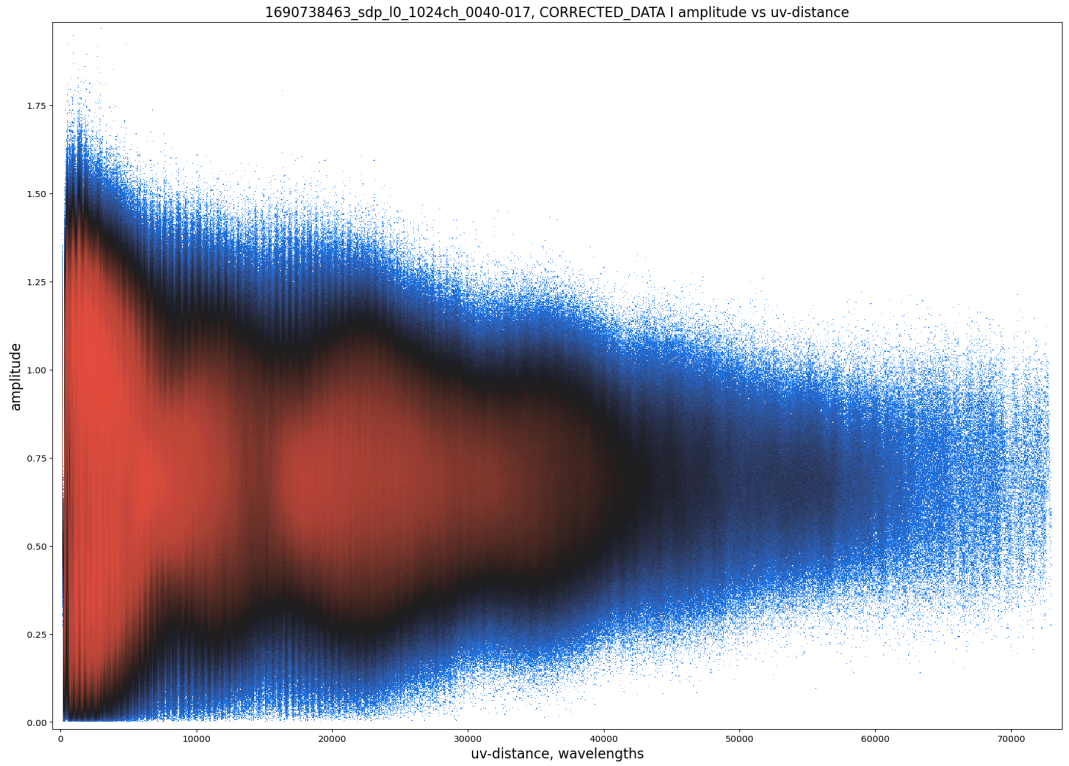
0048-427	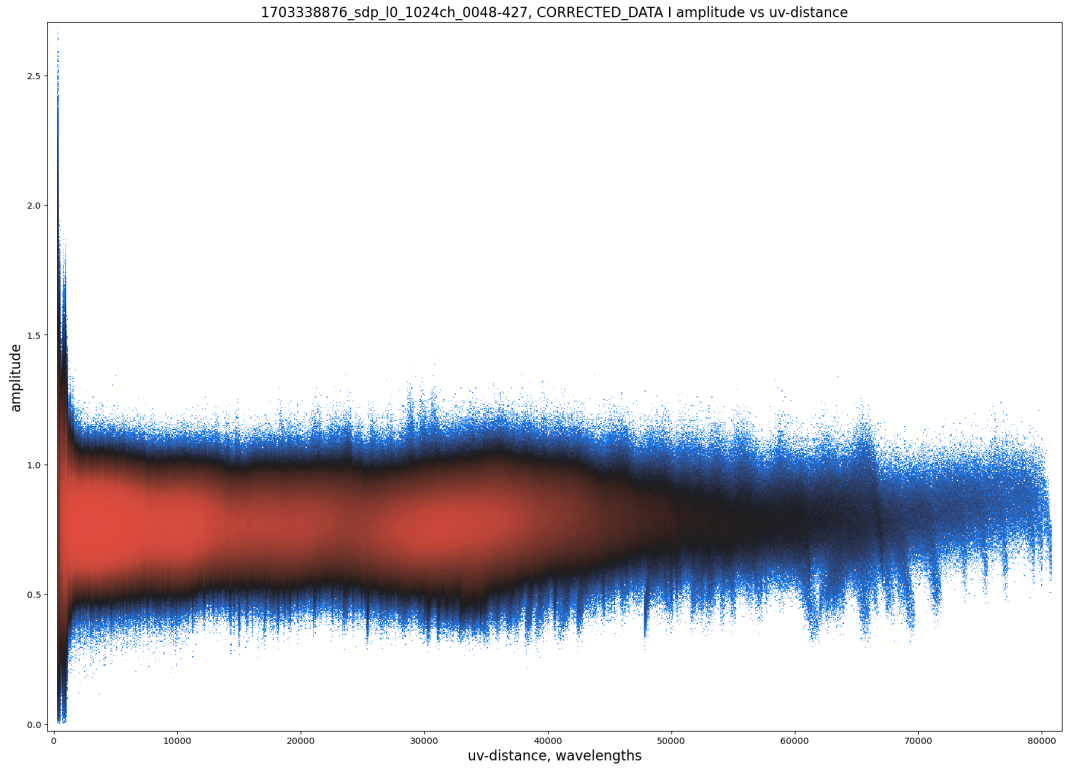

0131-522	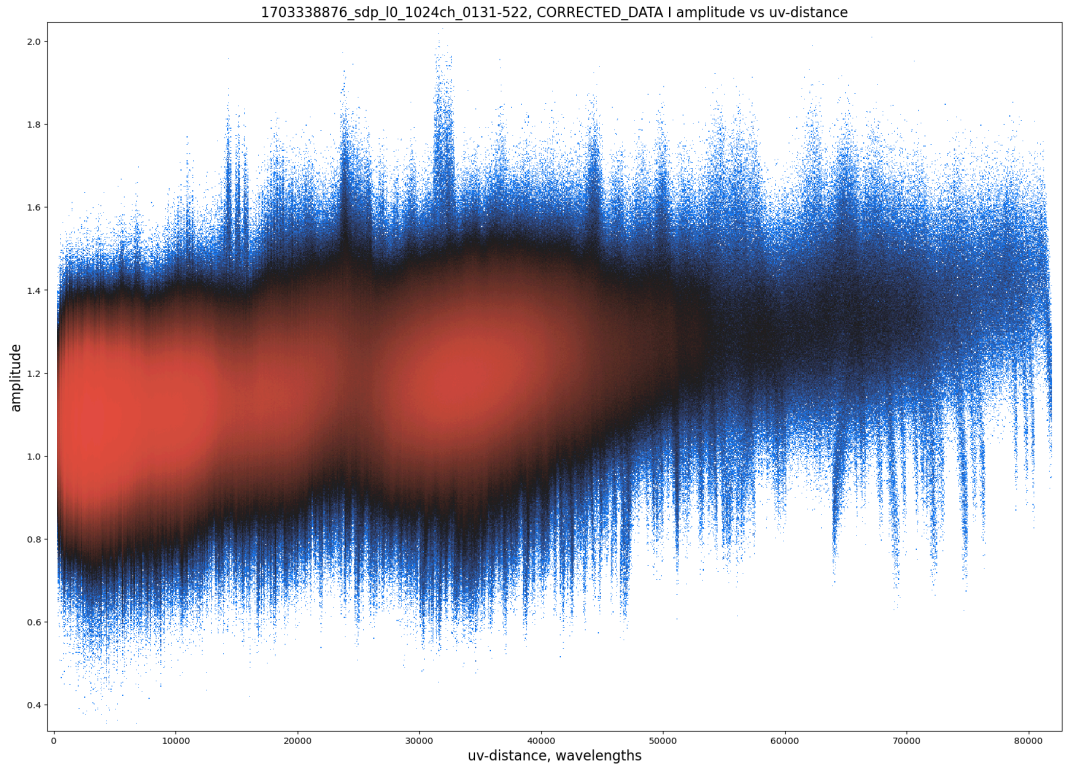
0149+059	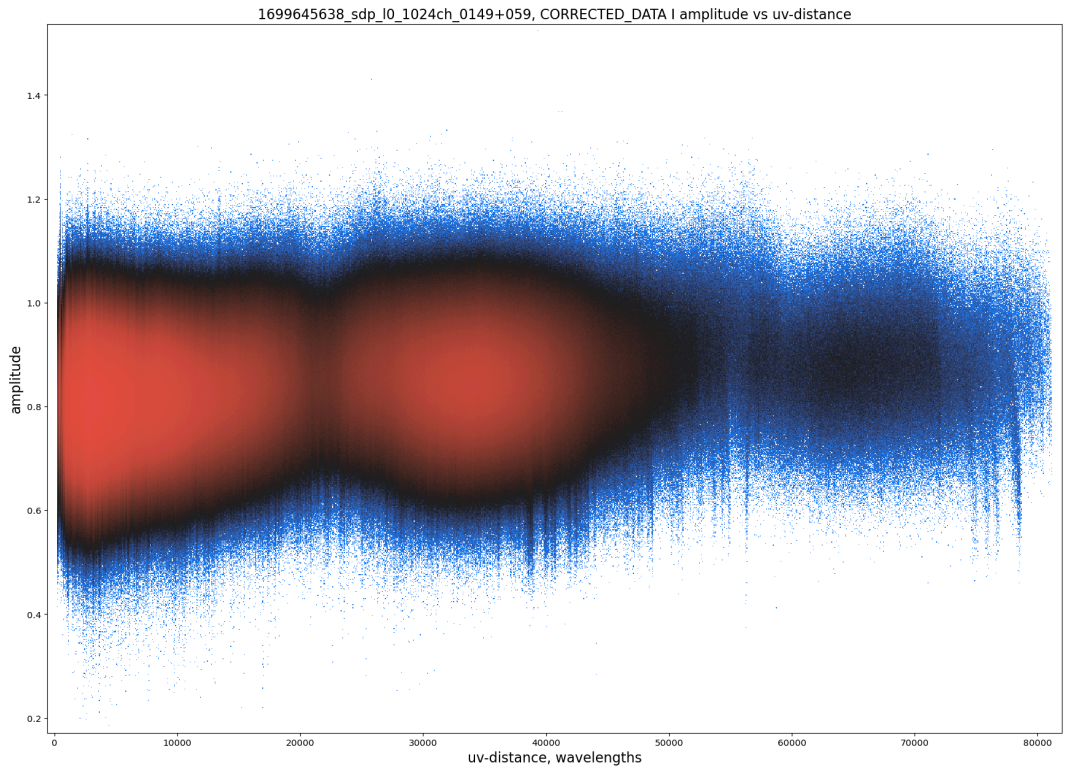

0204+152	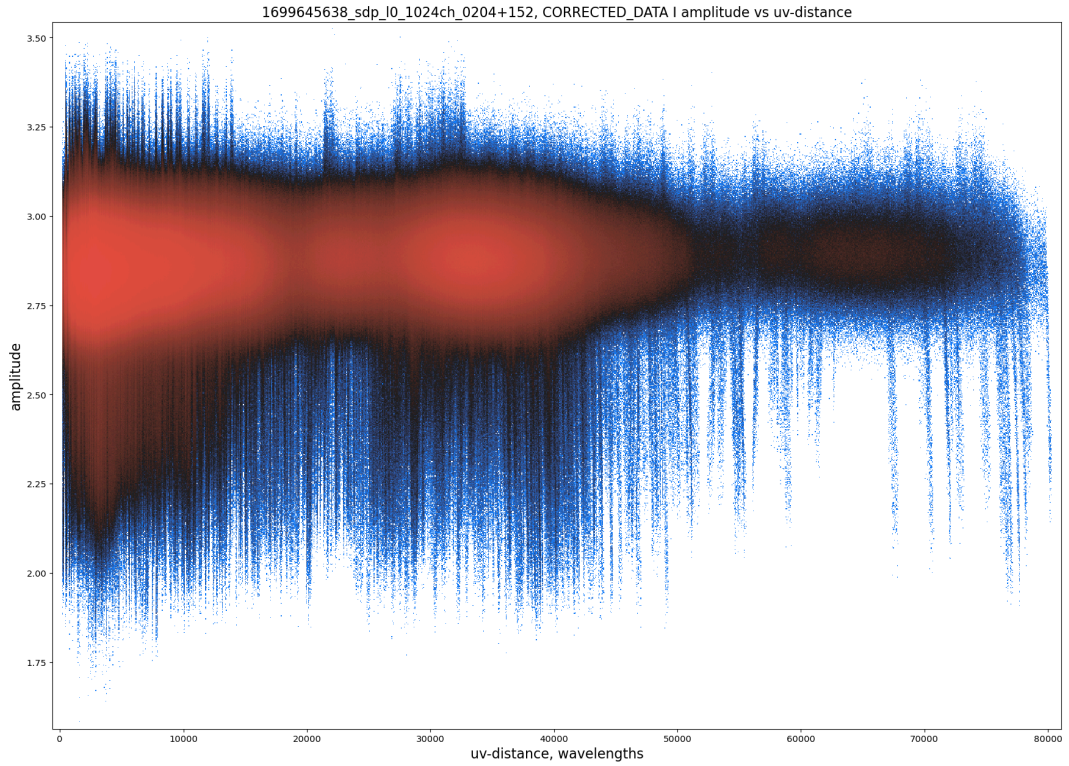
0222-346	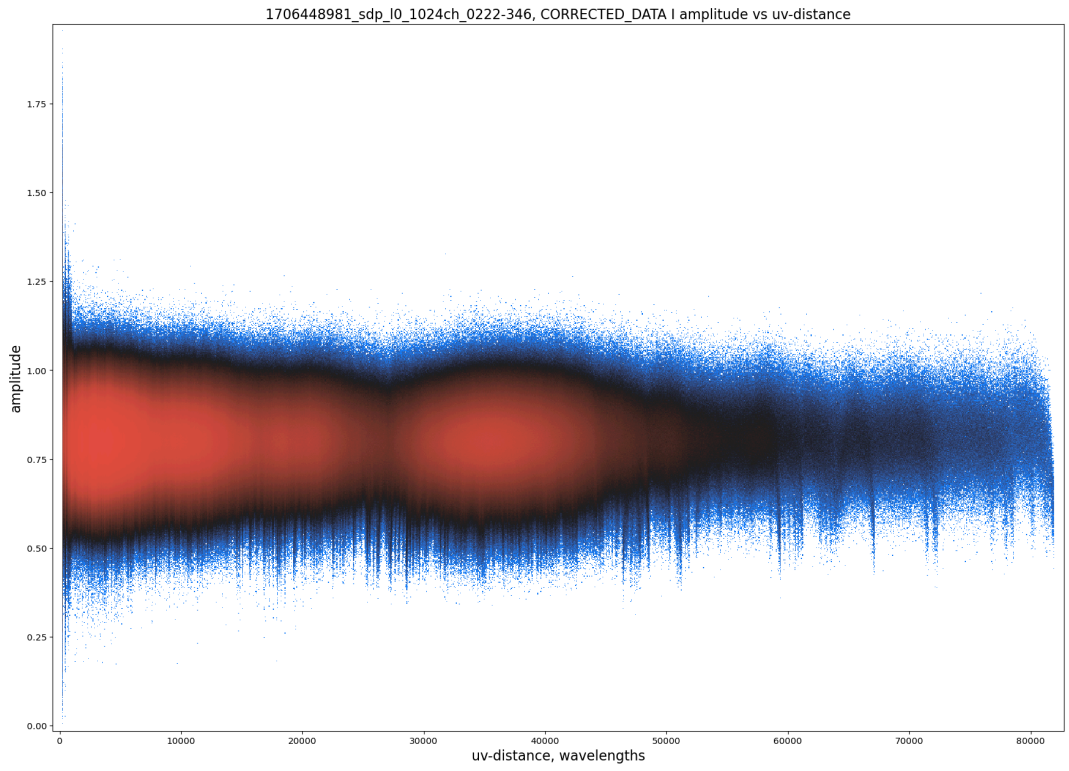

0308-611	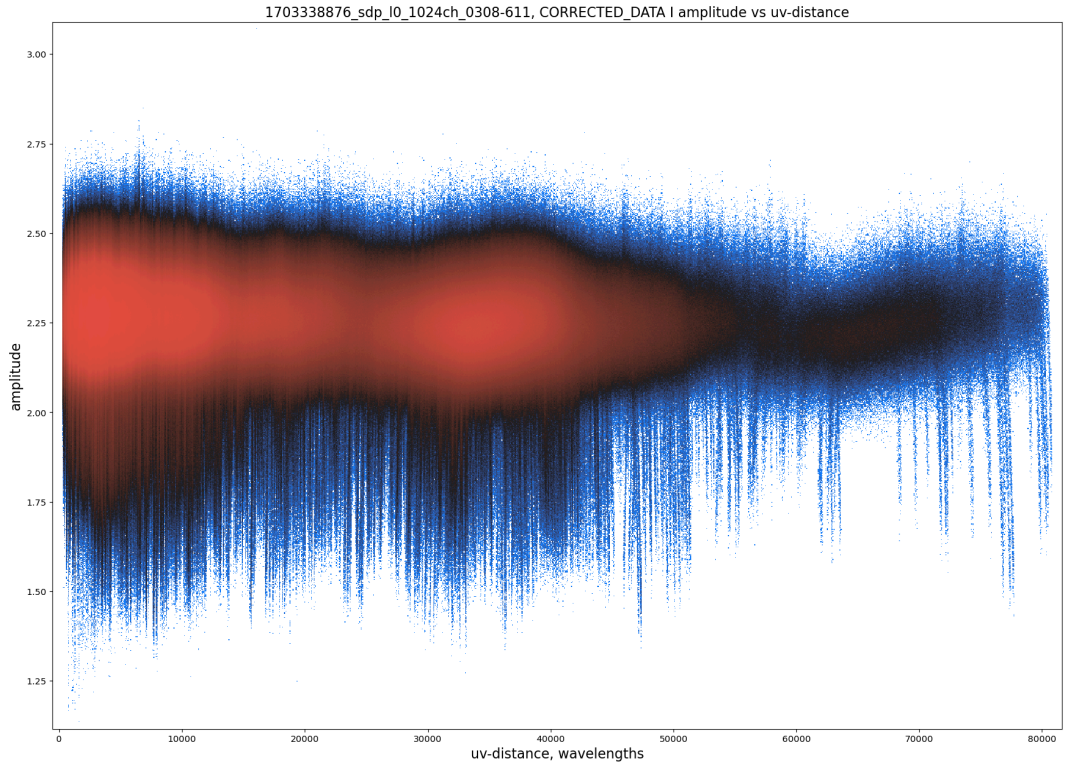
0332-403	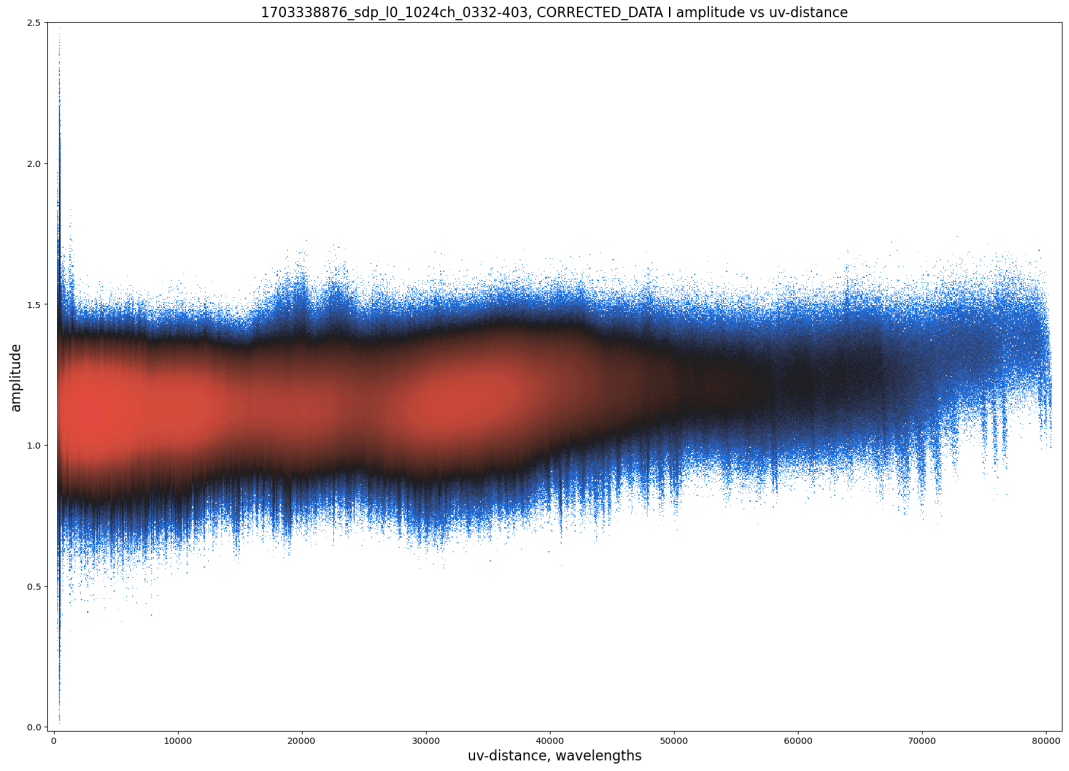

0843-54	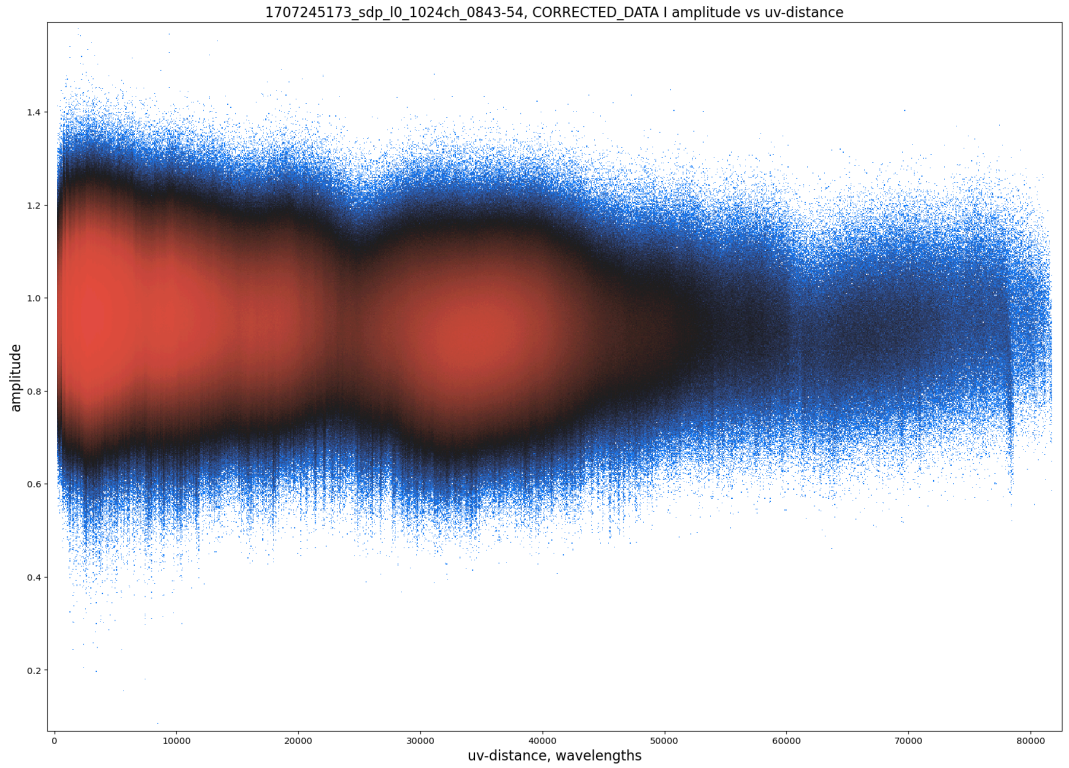
1131-050	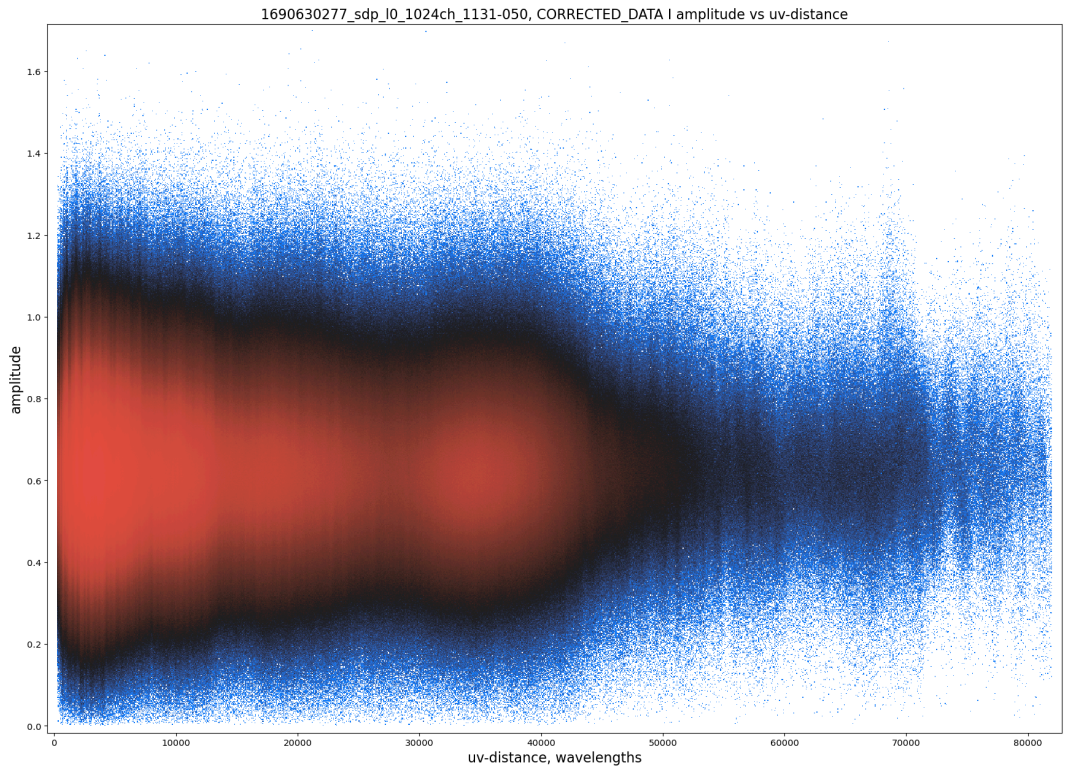

1145-228	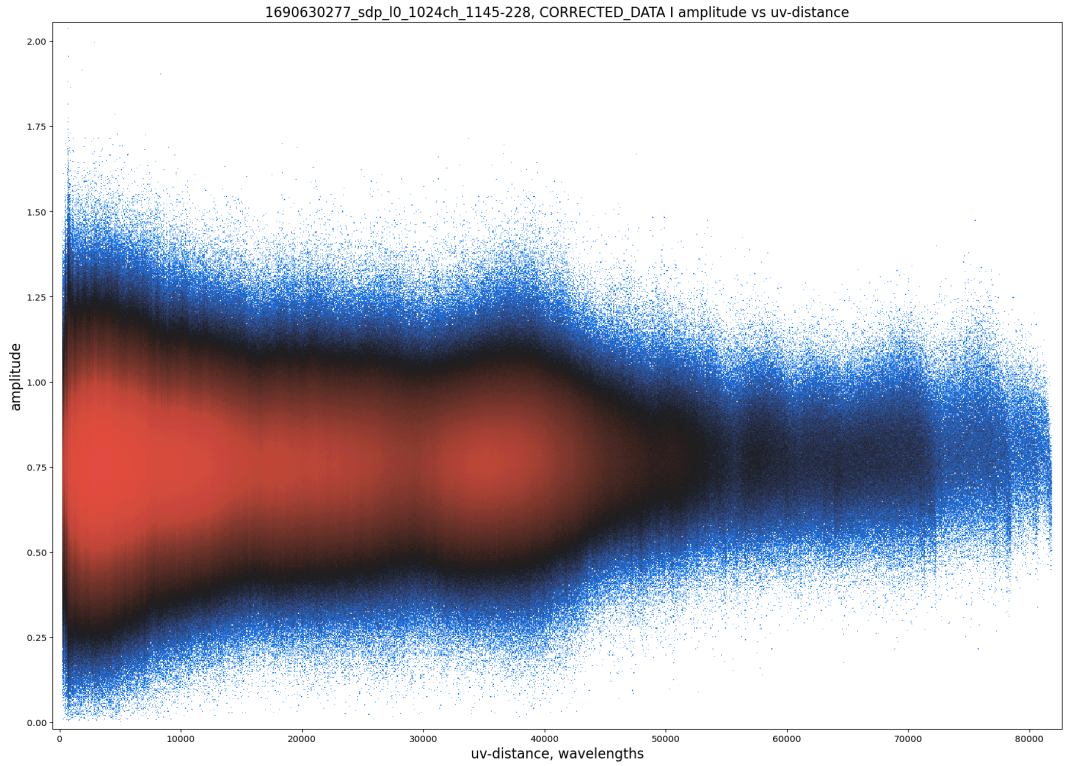
1146-247	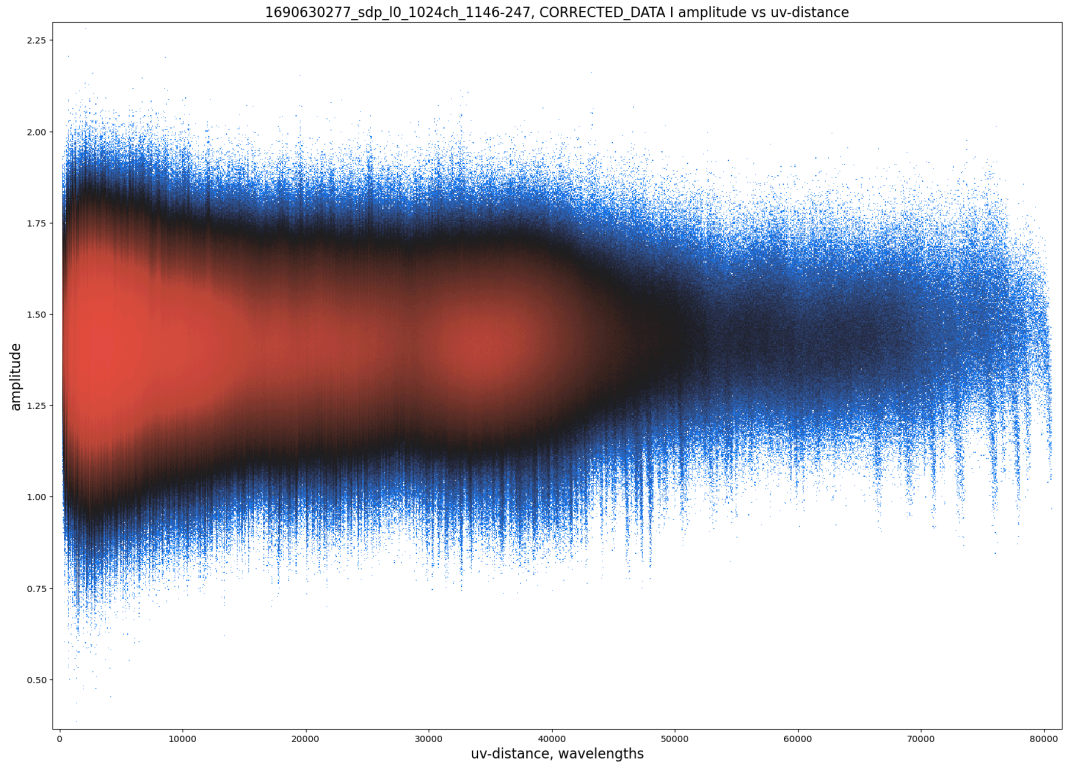

1147-074	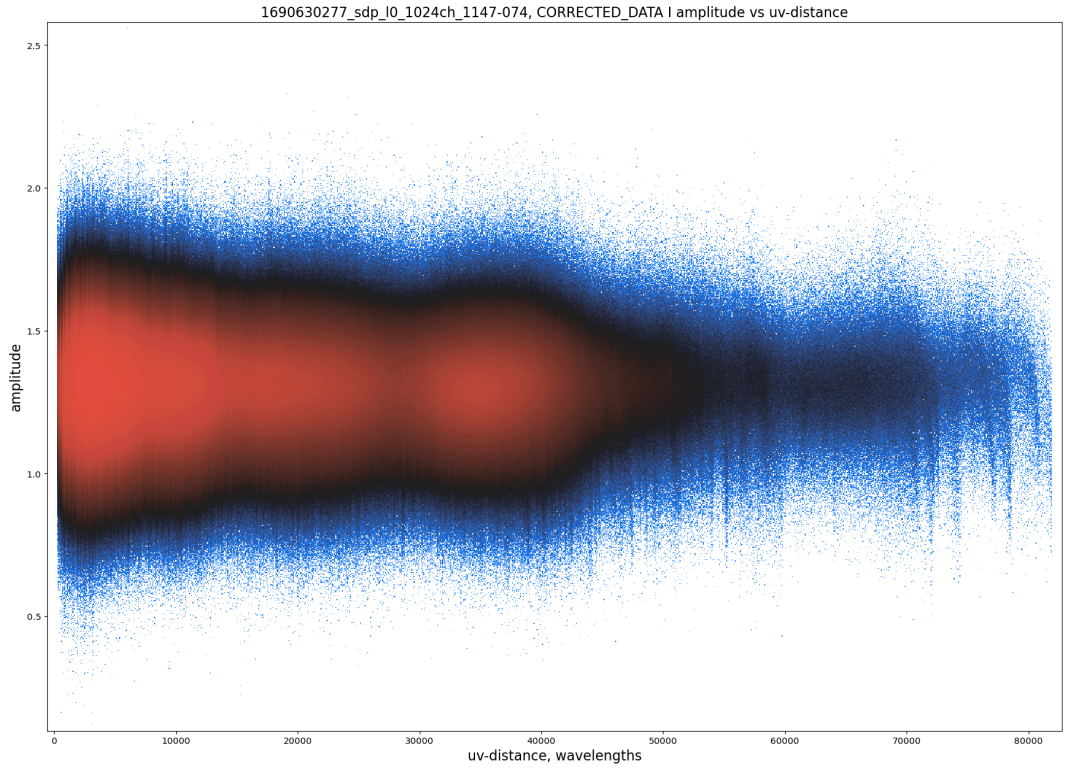
1305-105	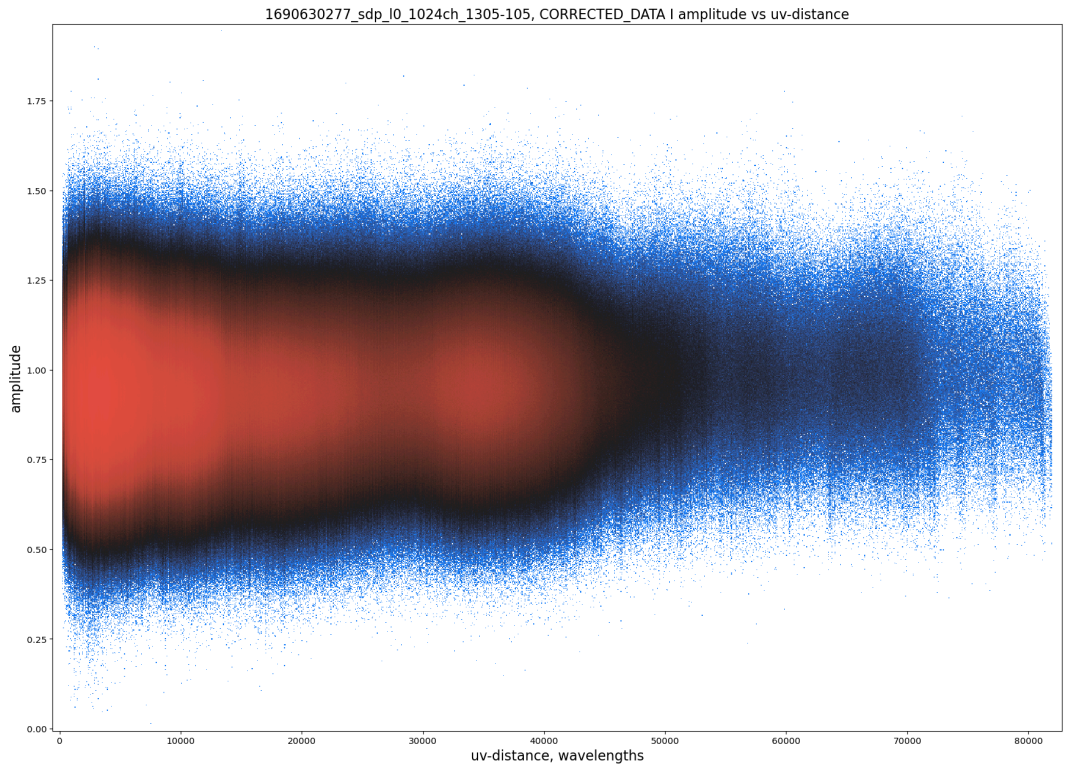

1309+119	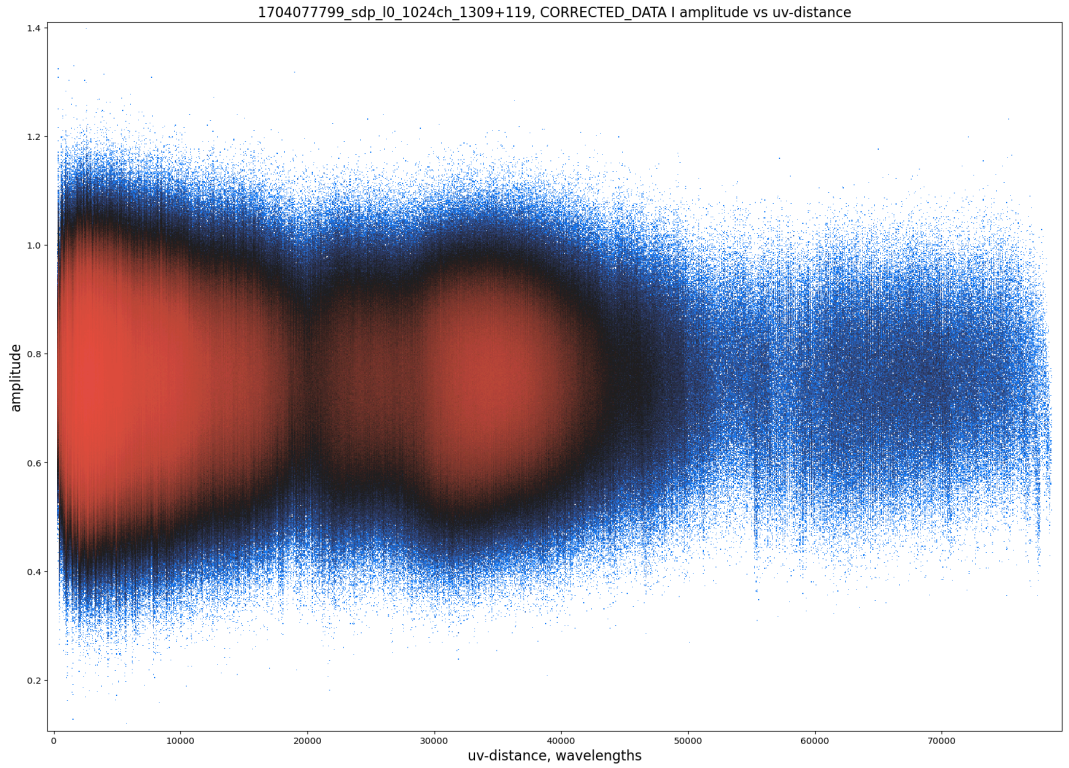
1351-018	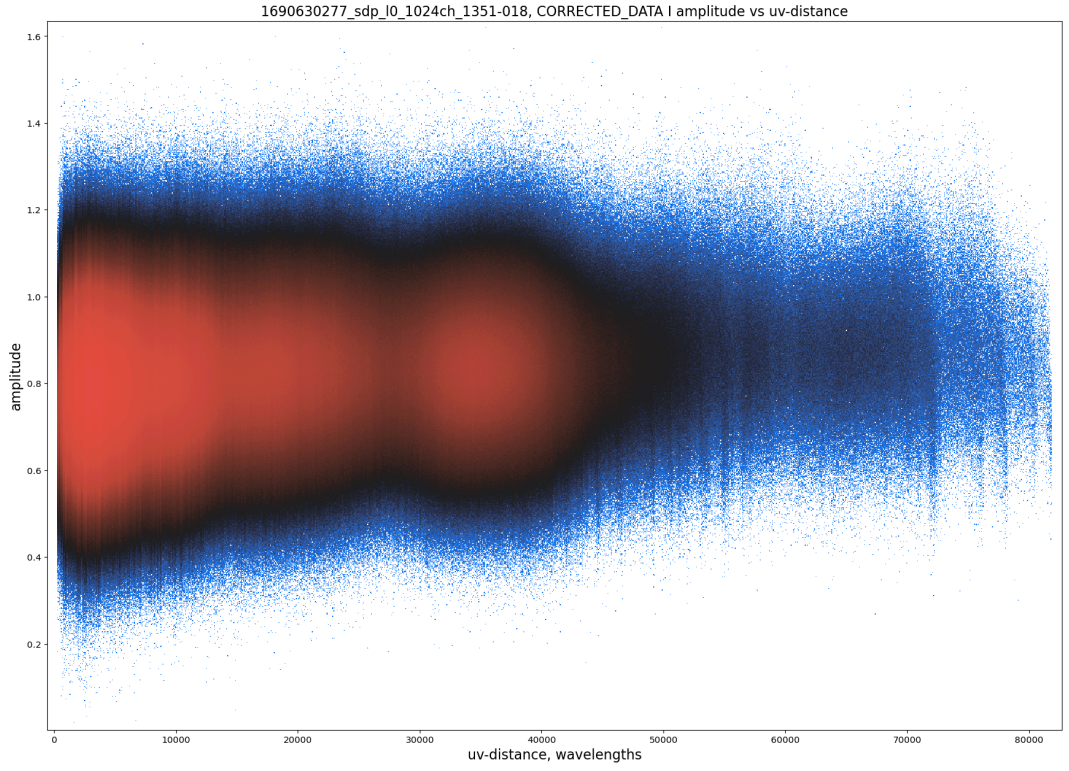

1404-015	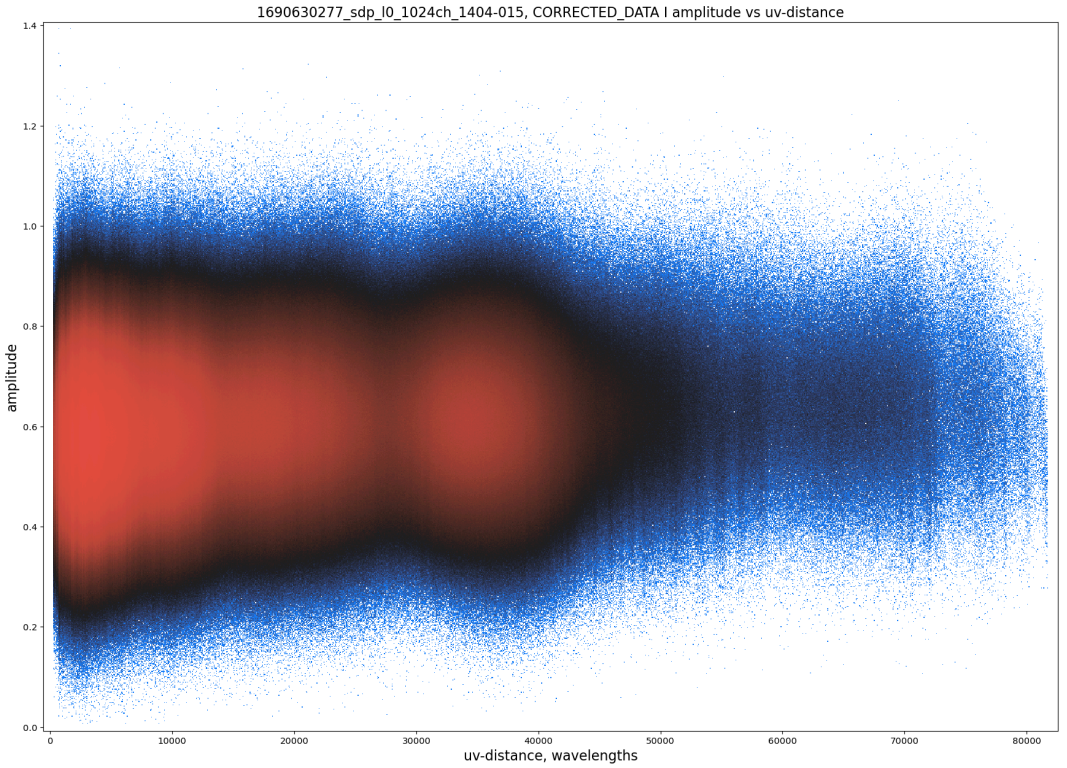
1446+173	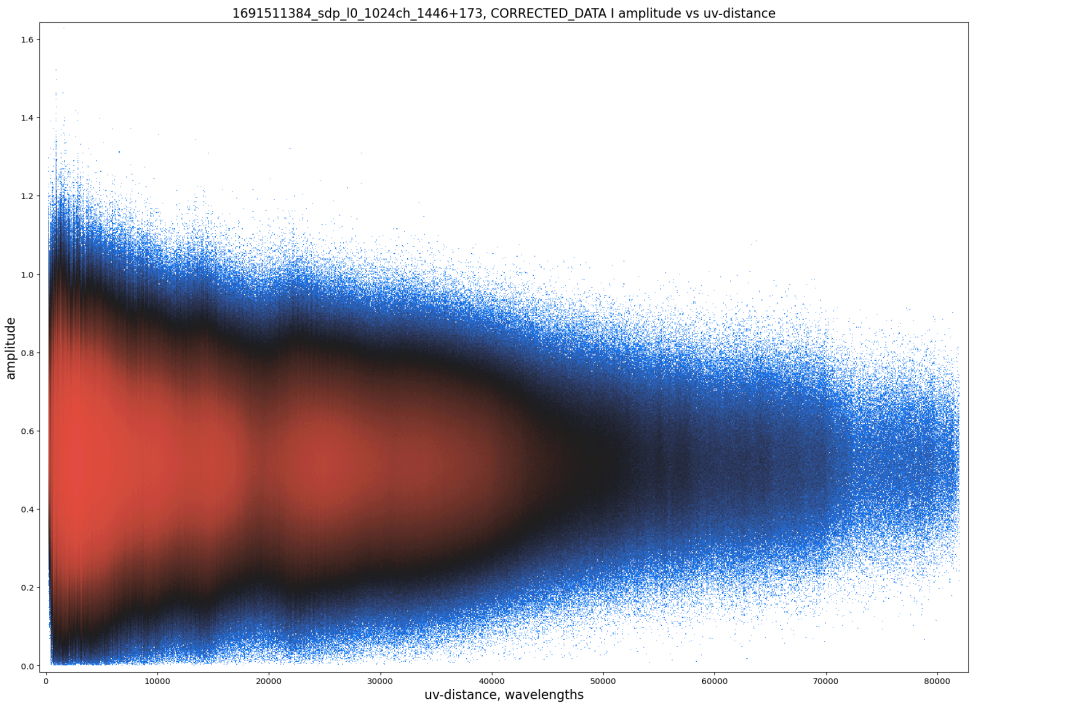

1504+104	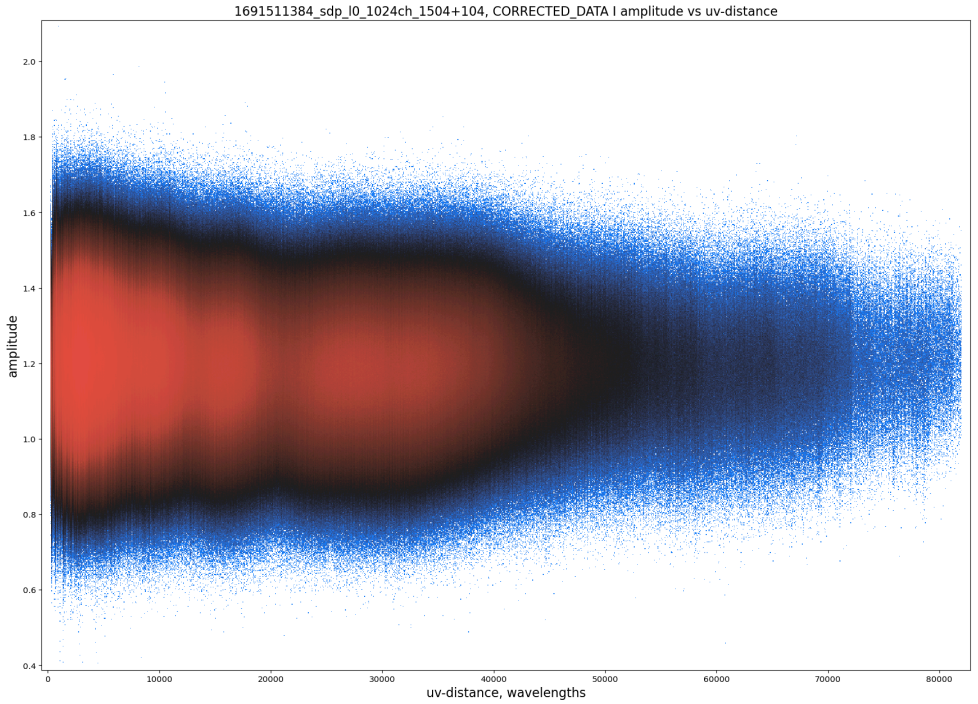
1505+034	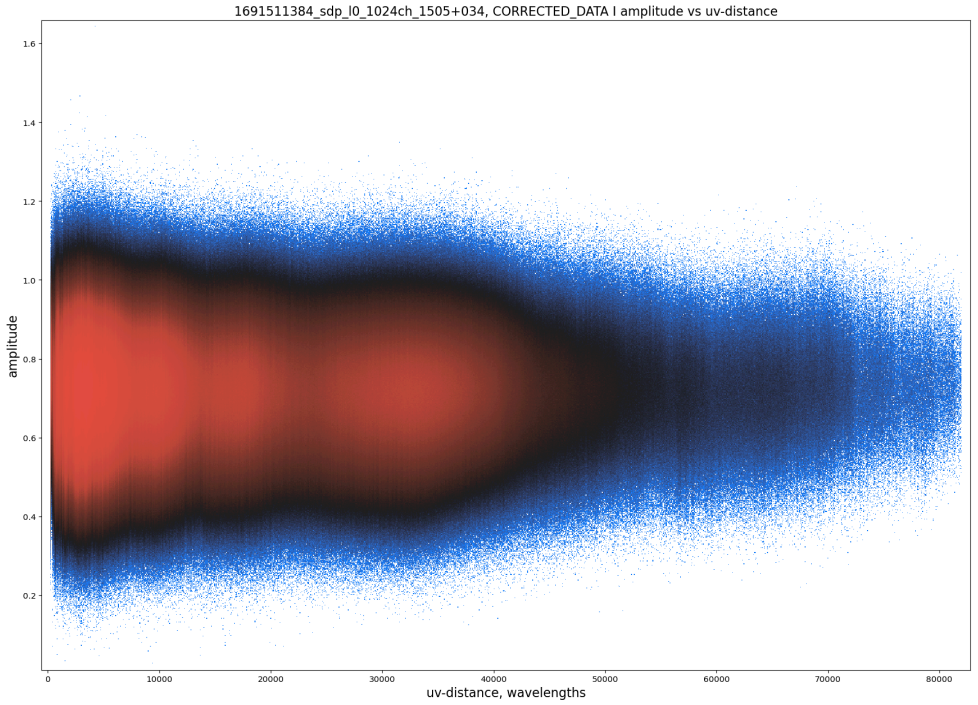

1507-168	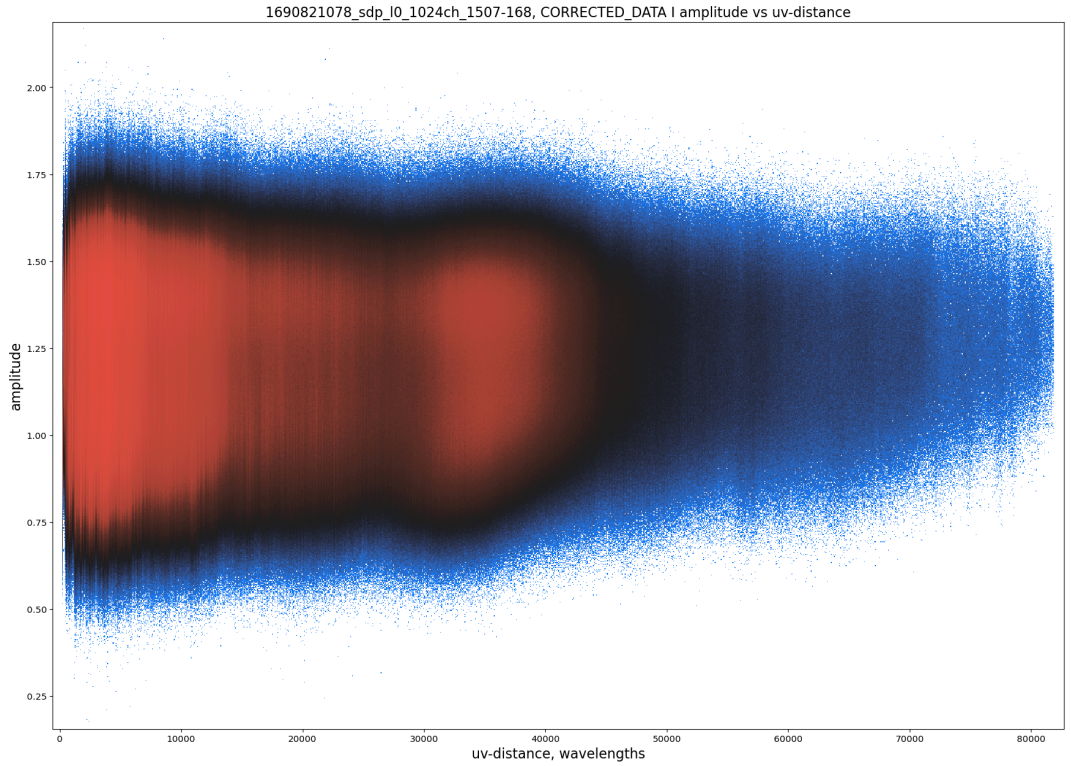
1522-275	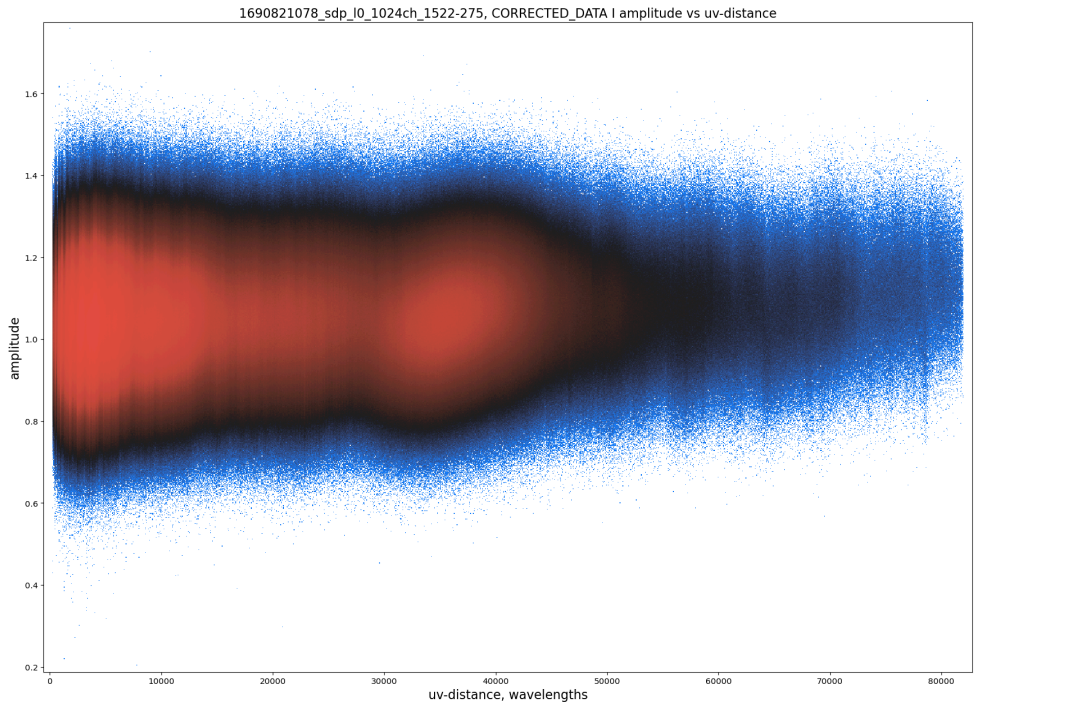

1557-000	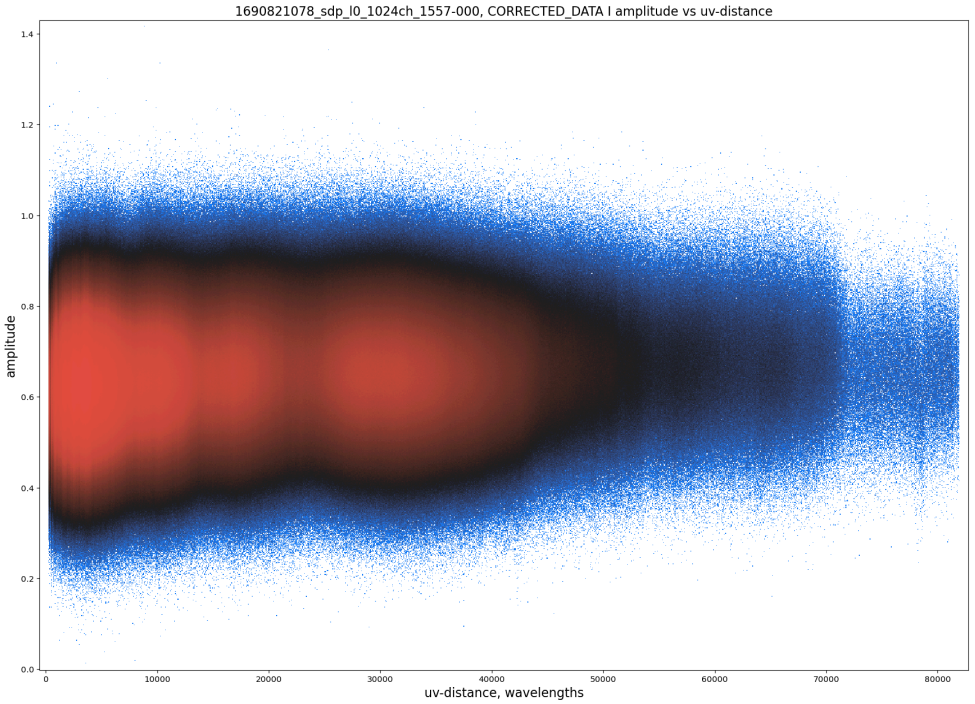
1700-261	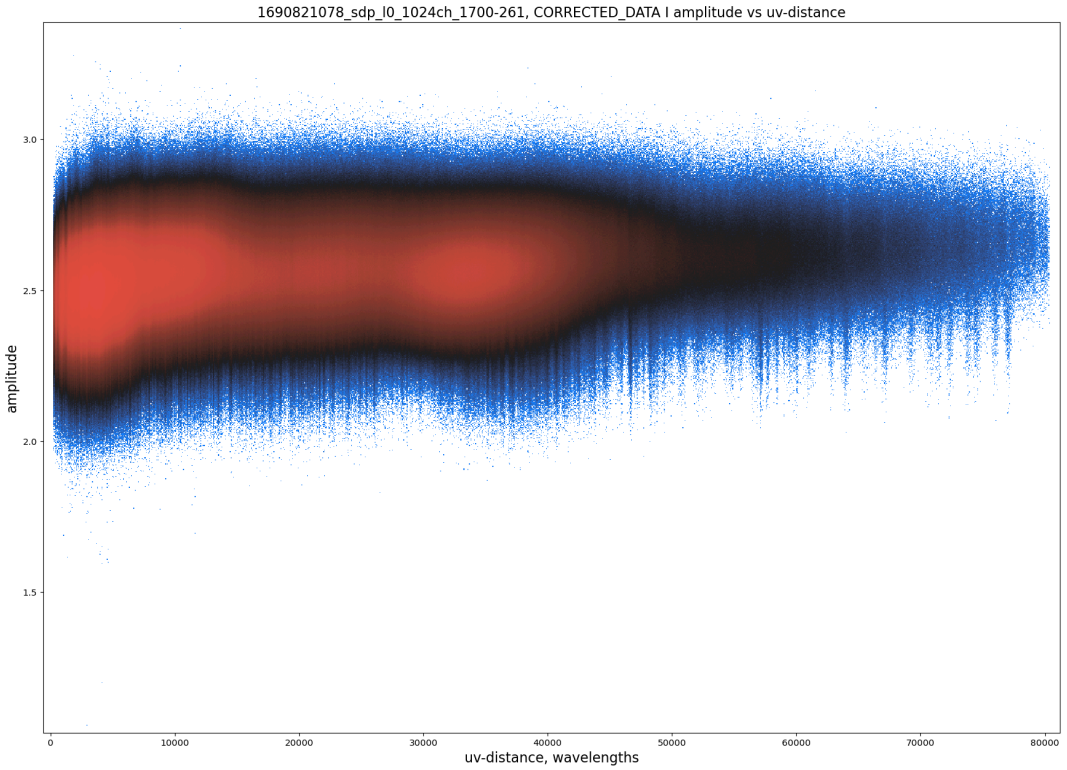

1743-038	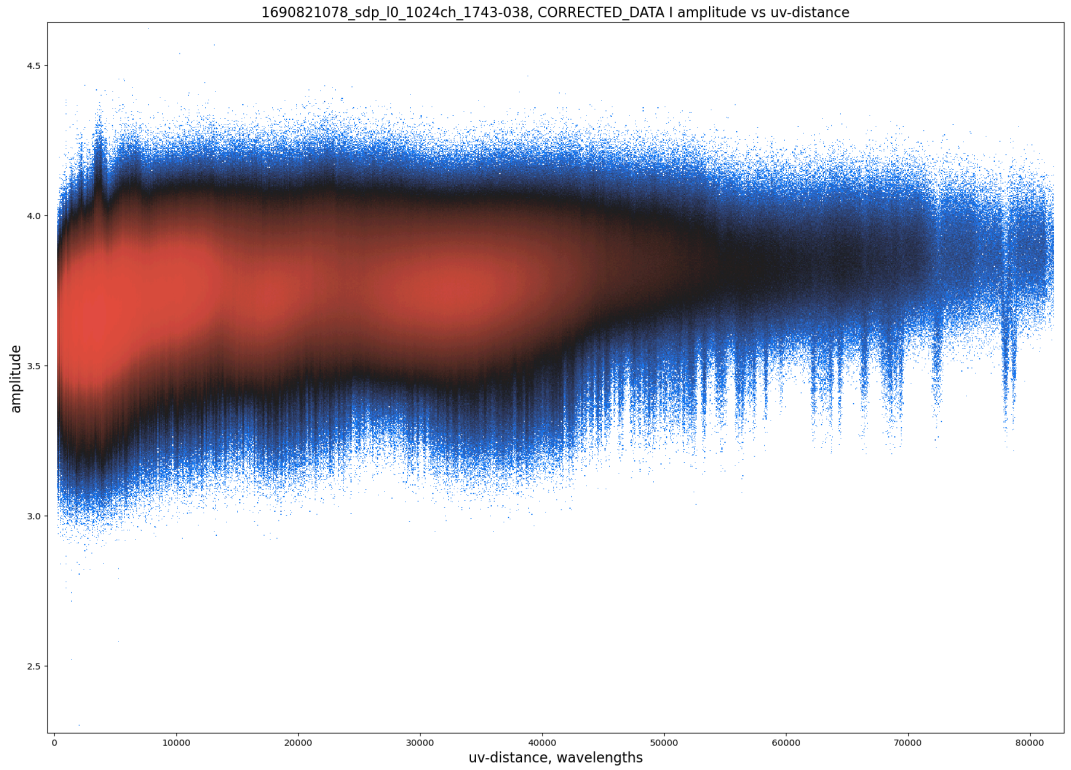
1745-078	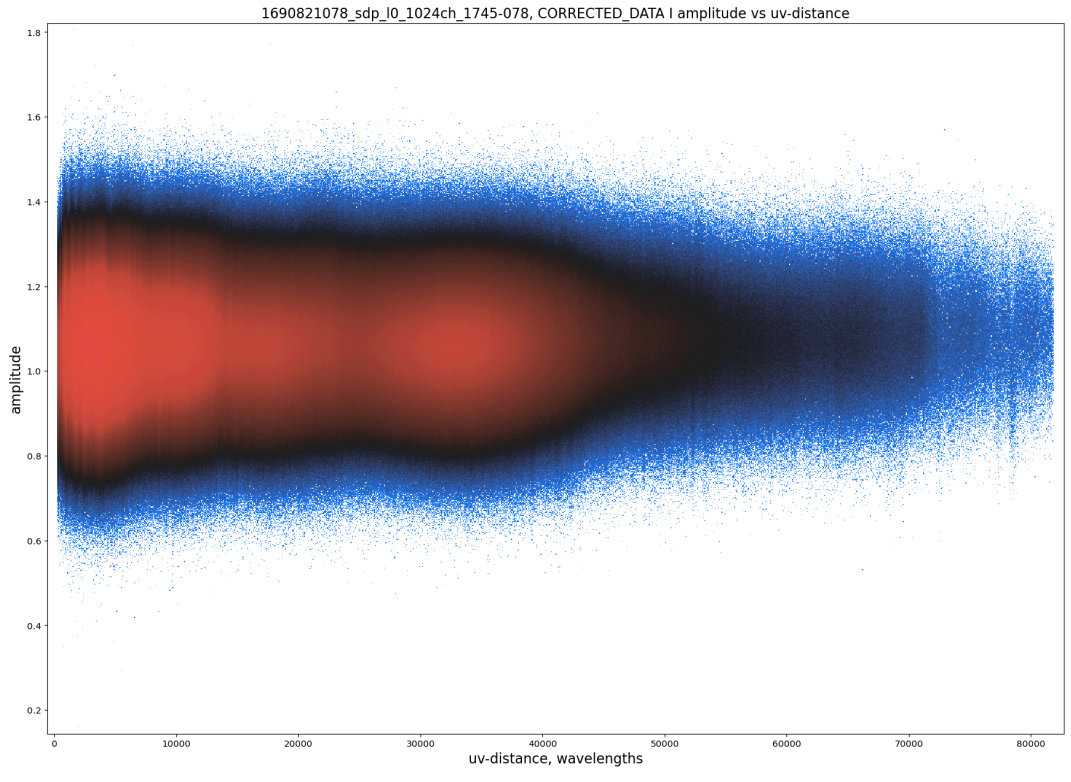

1937-399	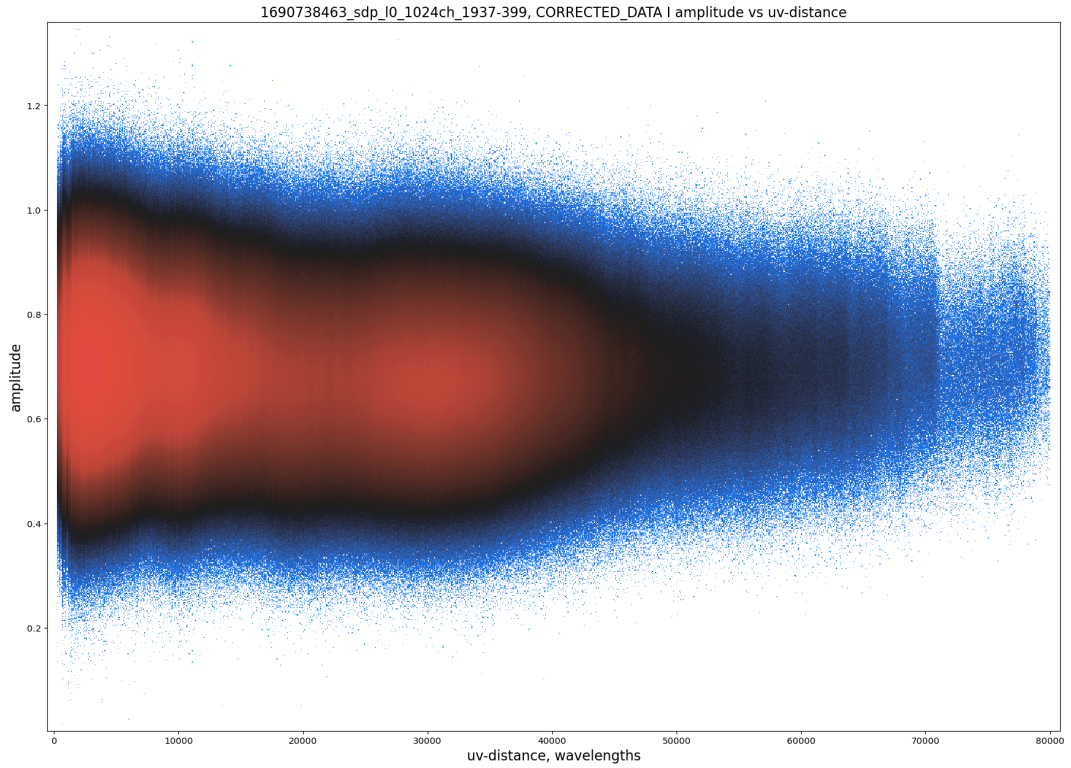
1939-154	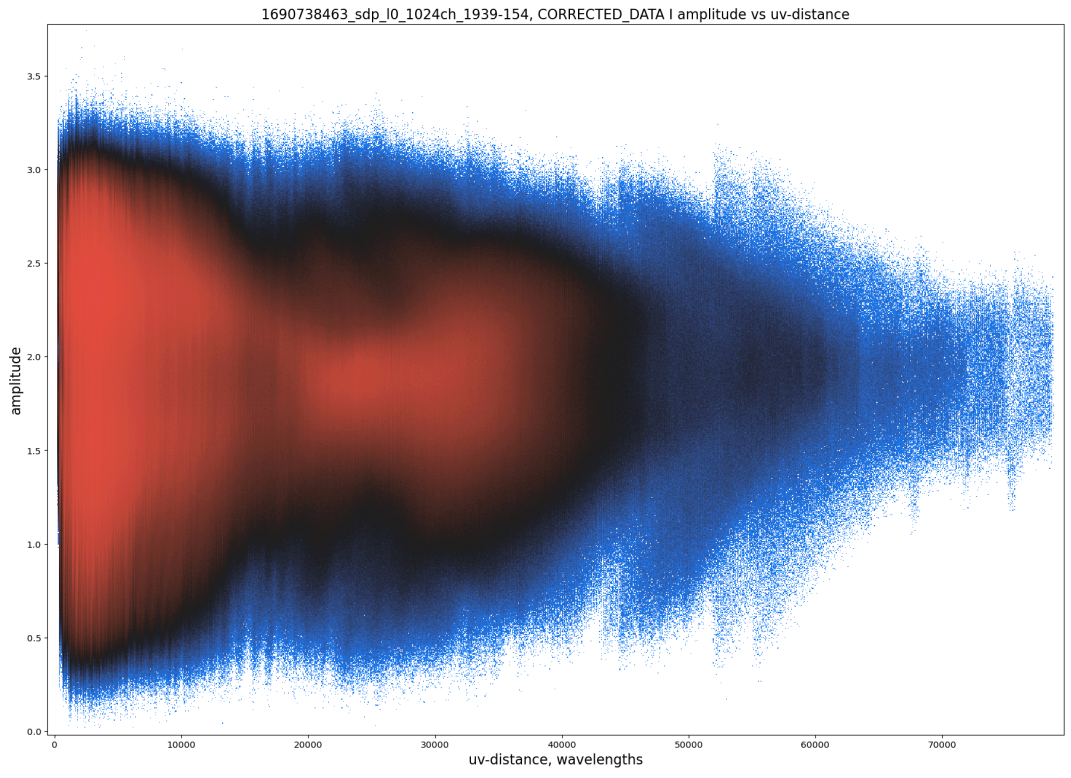

1958-179	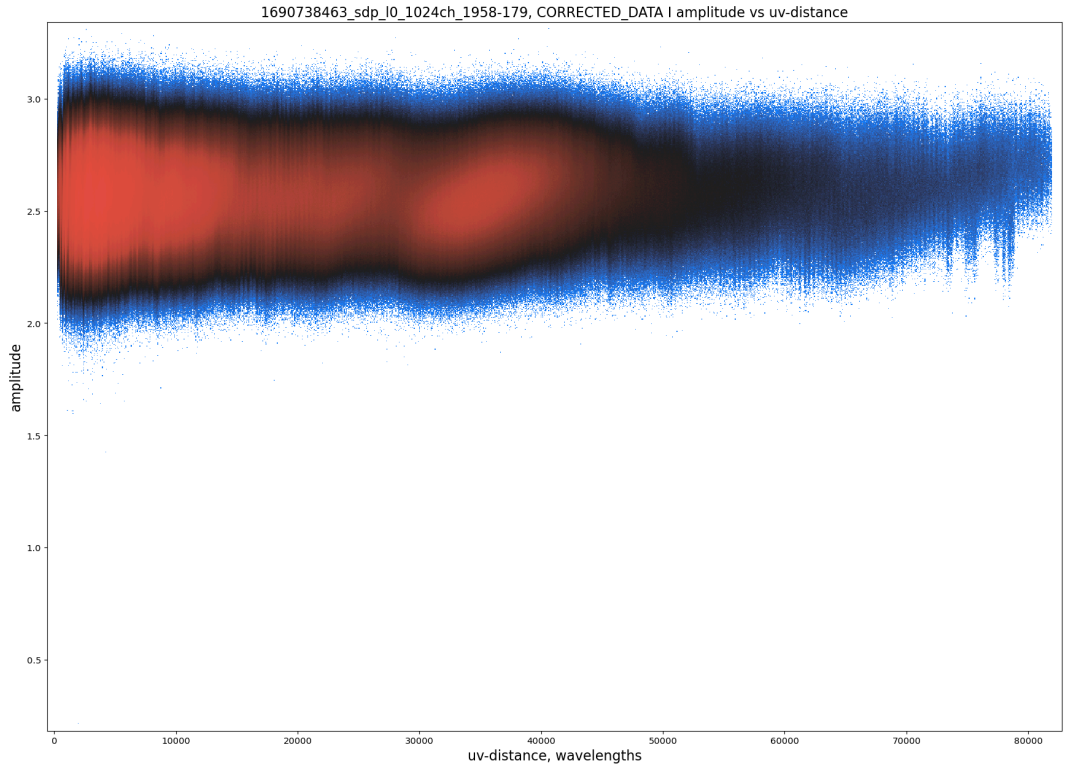
2011-157	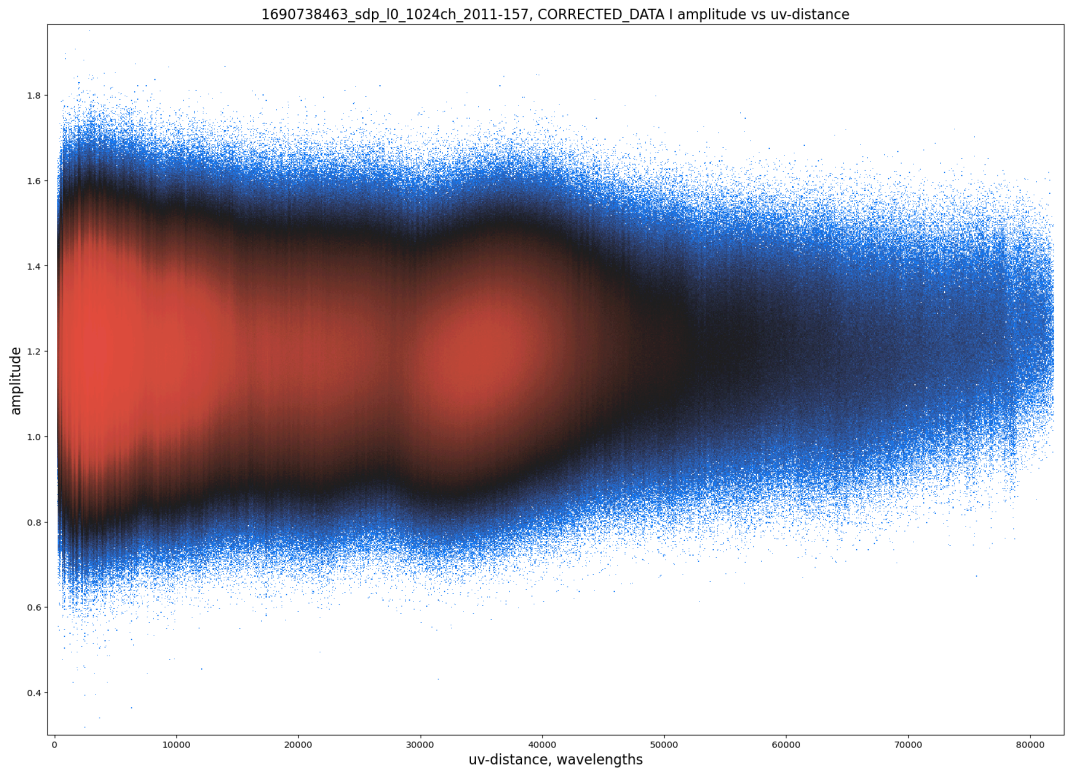

2236-145	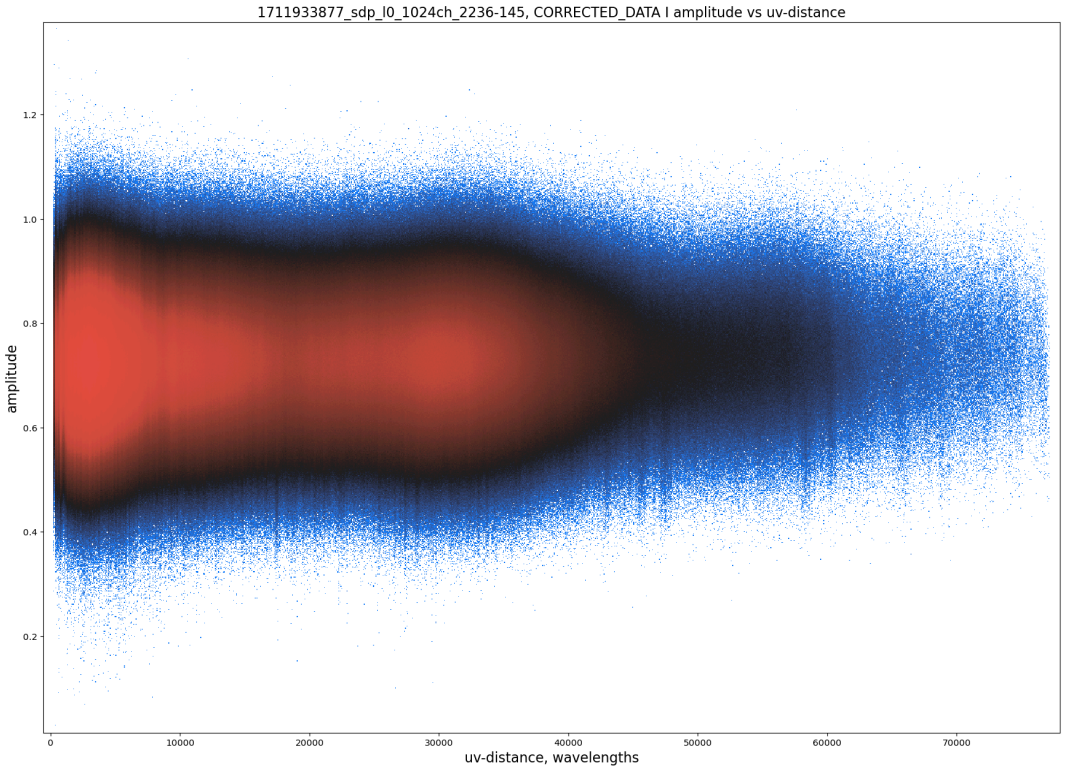
2323-032	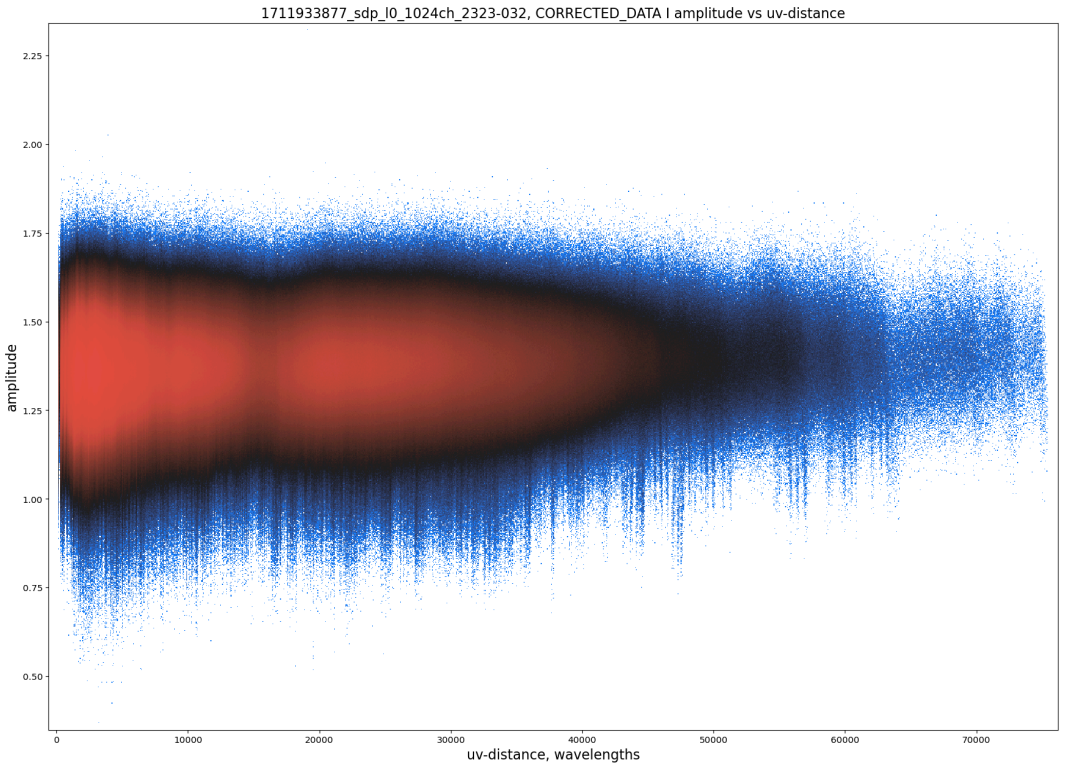

2324-372	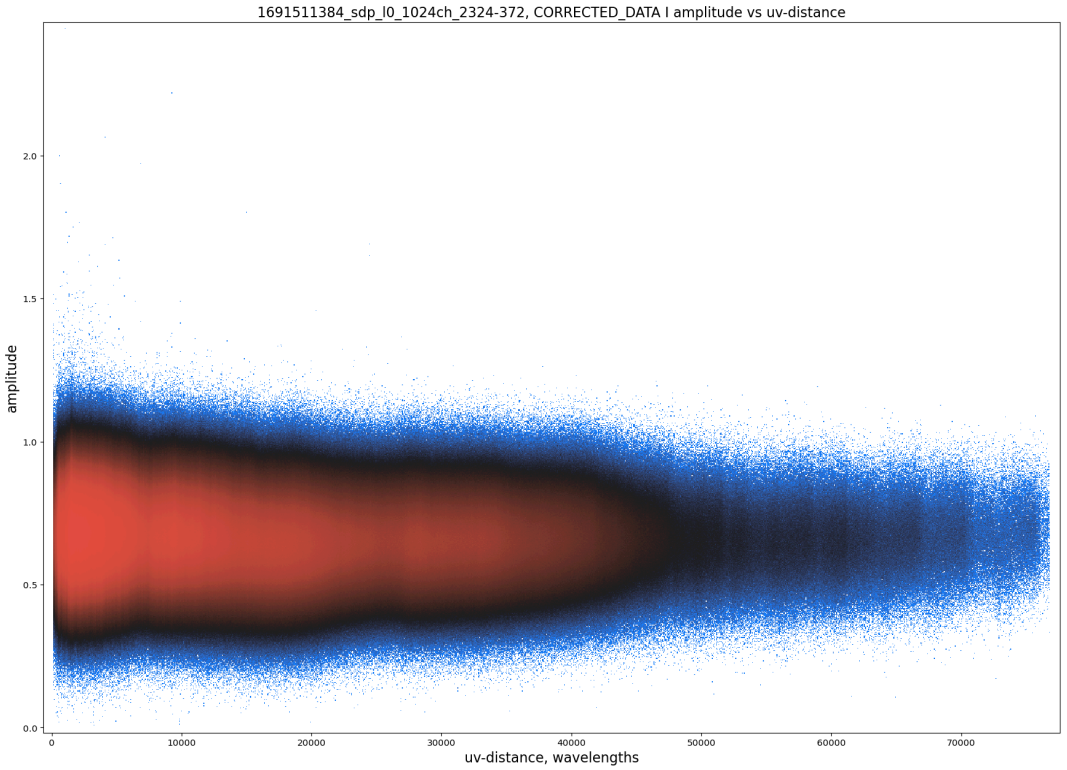
2333-237	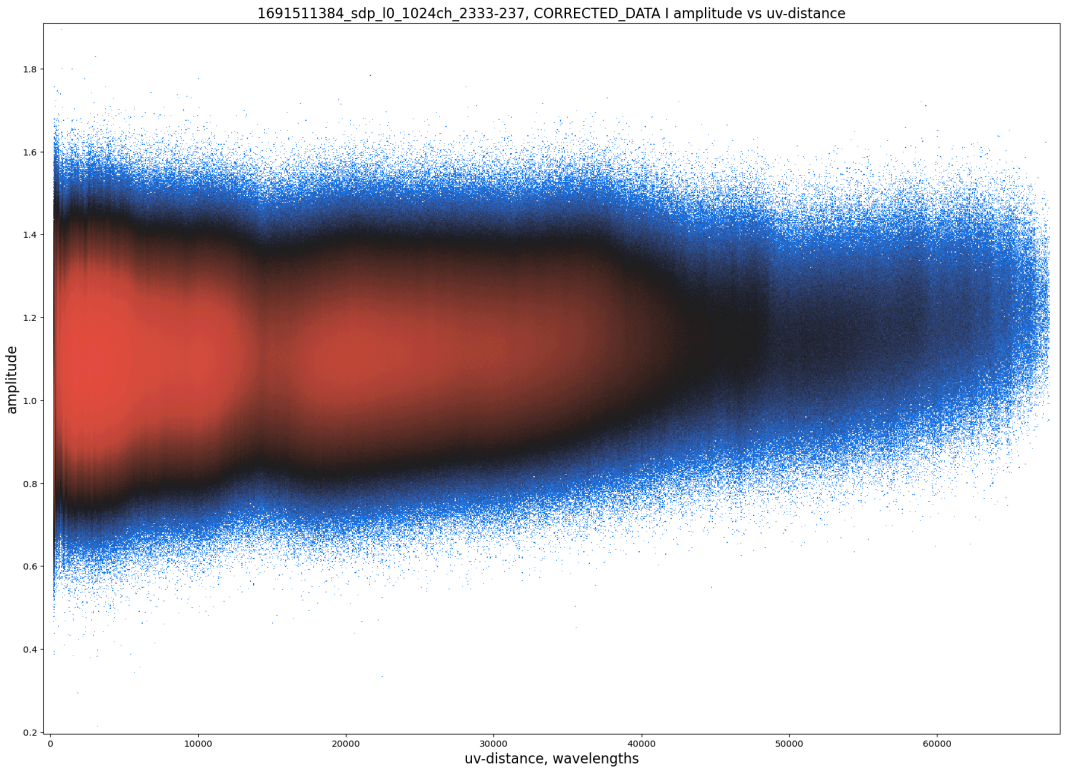

2354-152	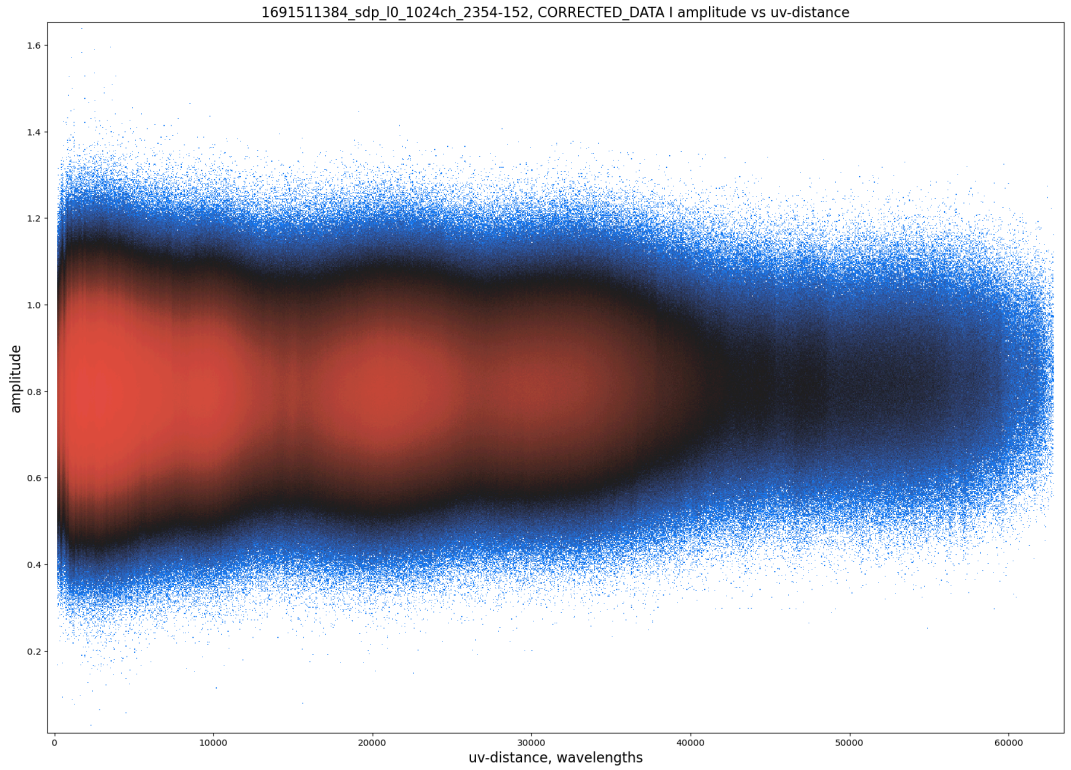
2359-315	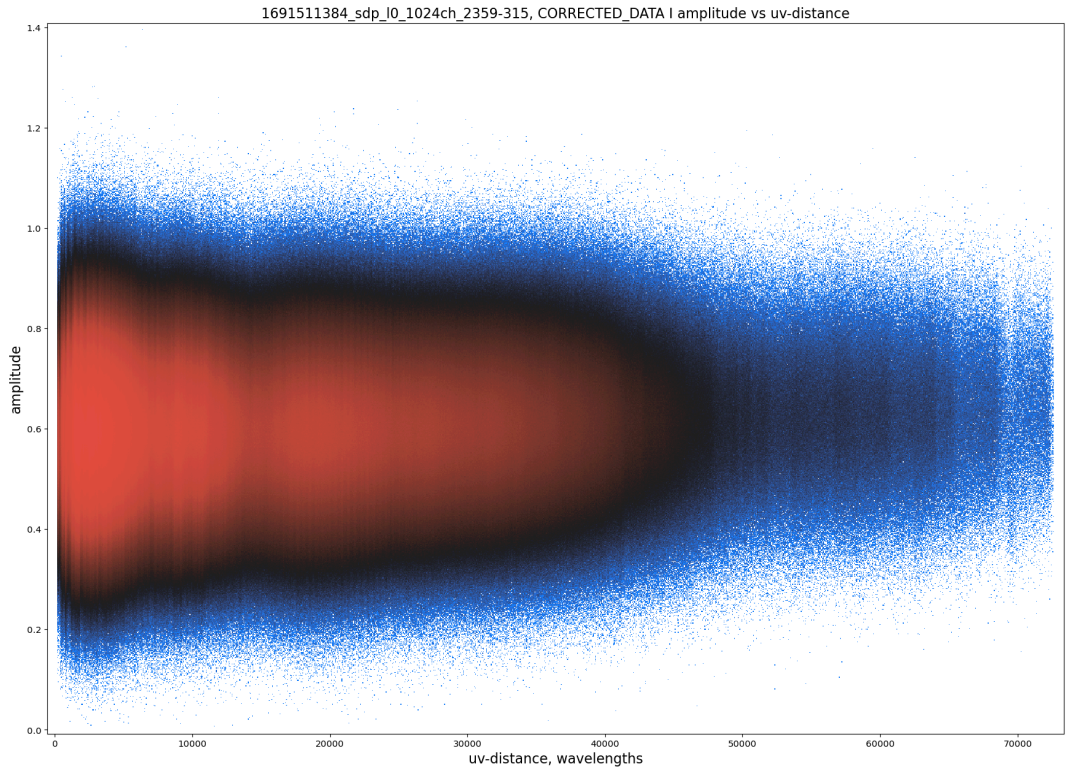

j0044-8422	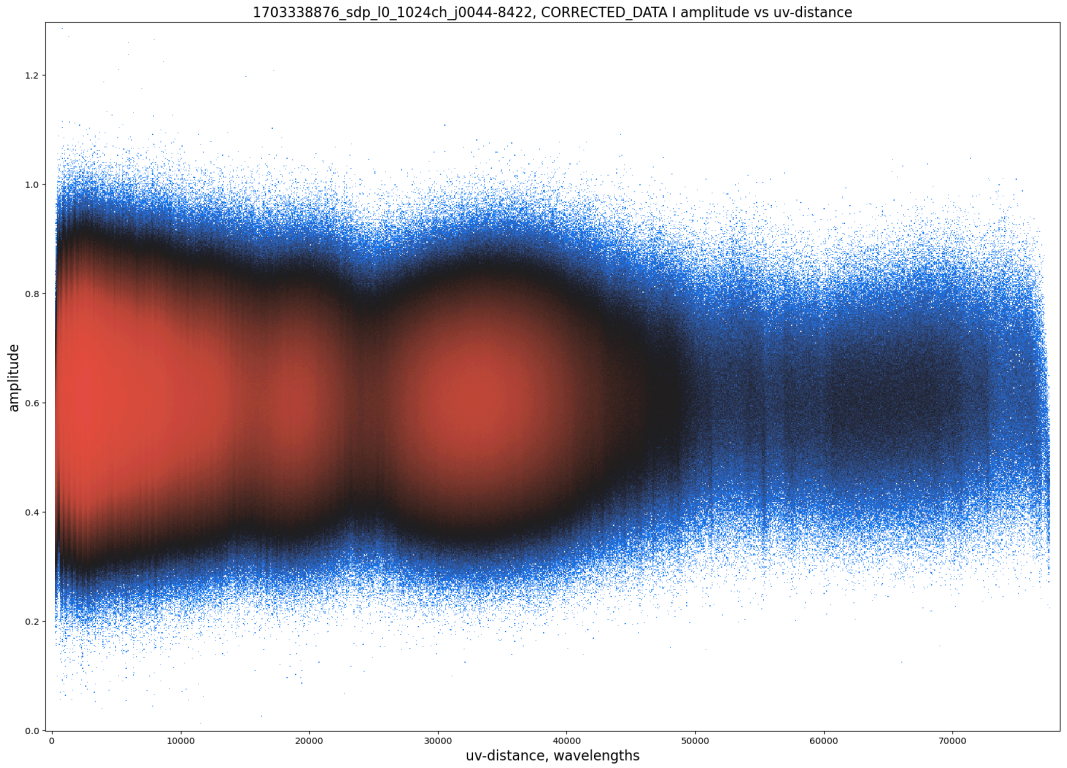
J0211+1051	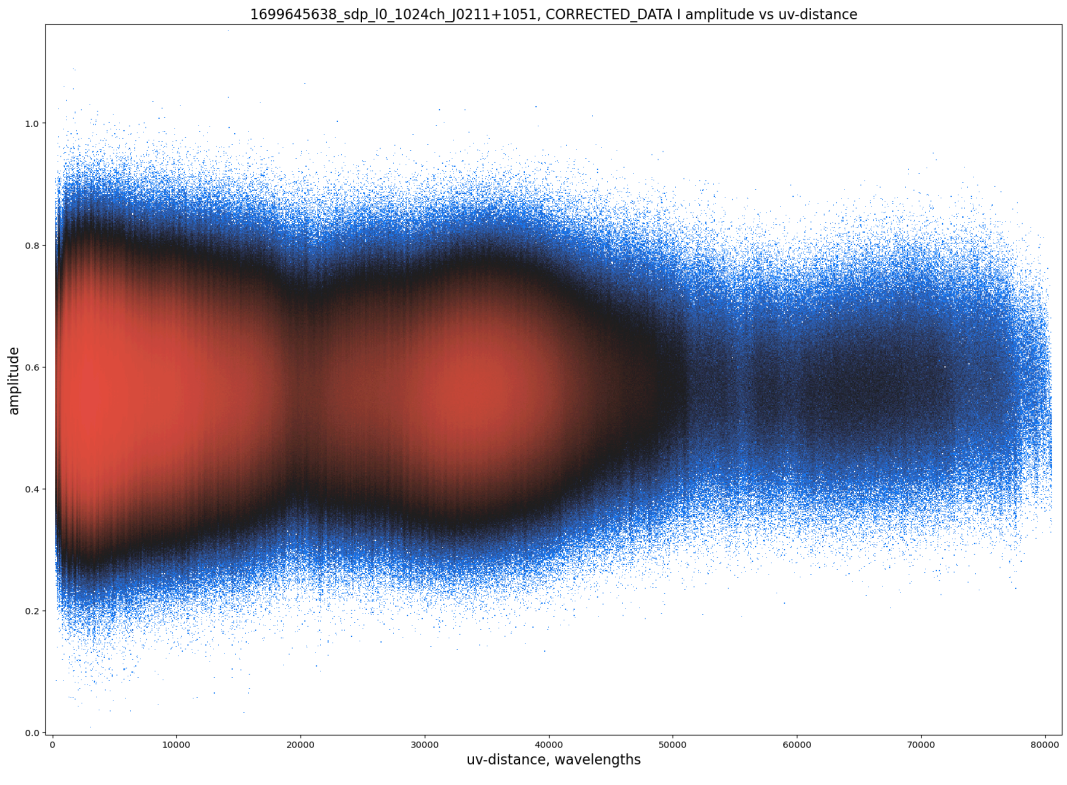

j0246-4651	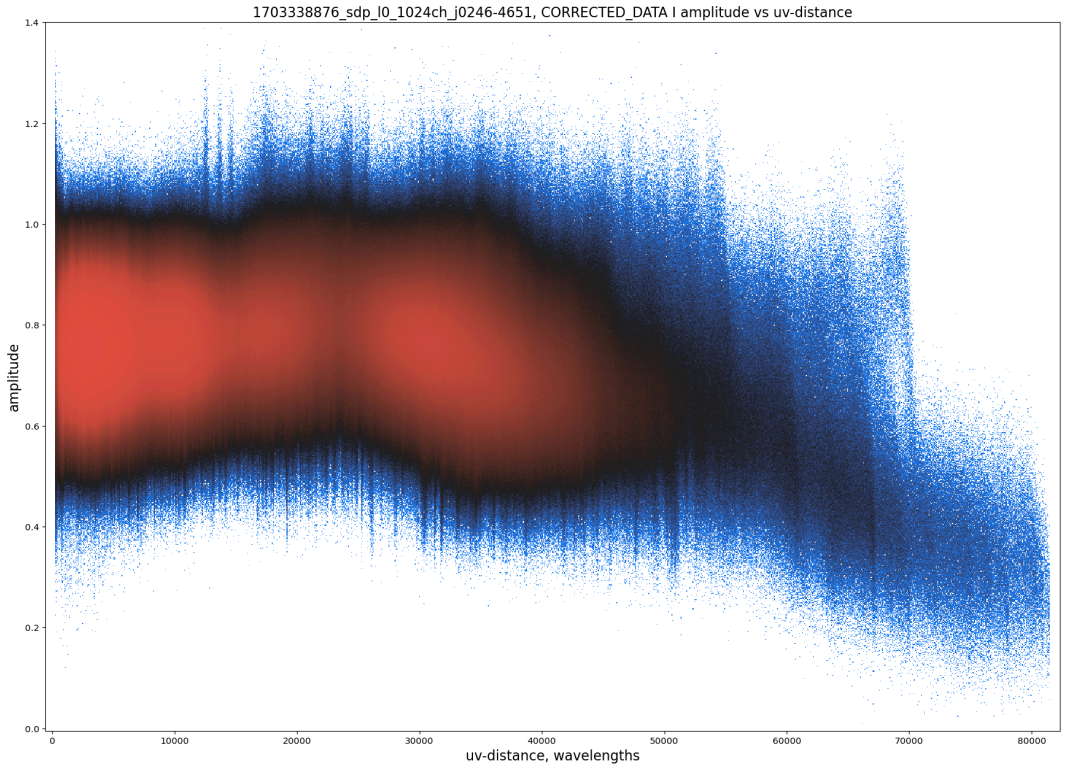
j0625-5438	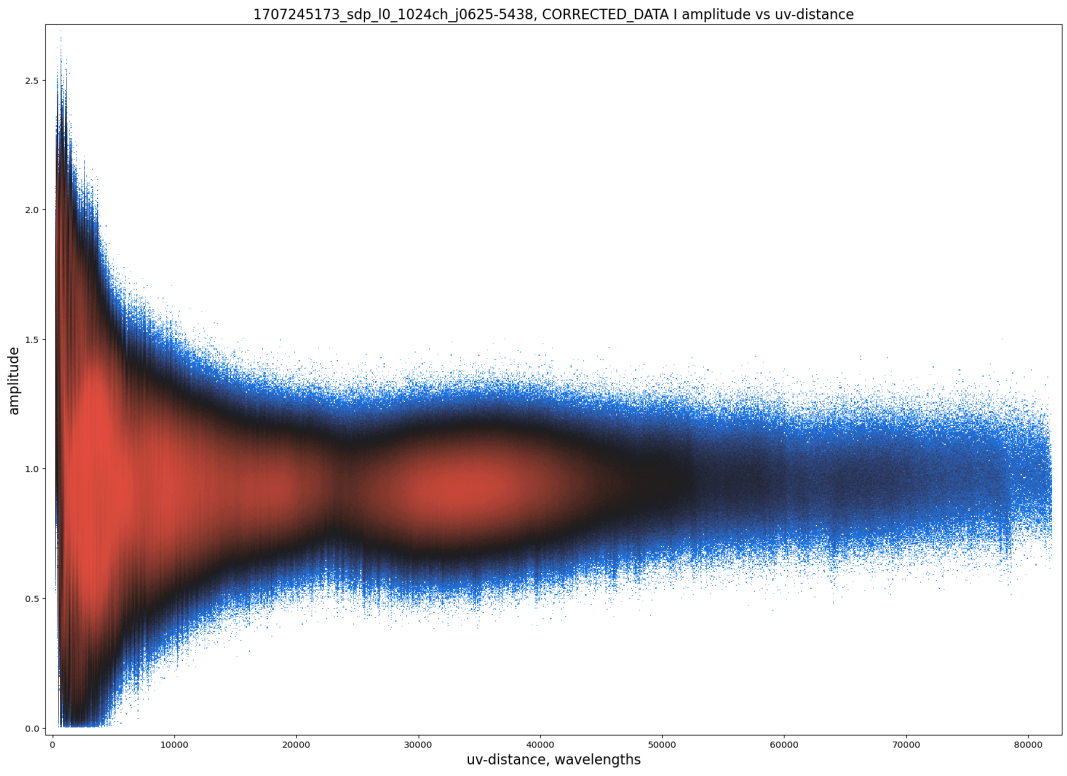

J0659+0813	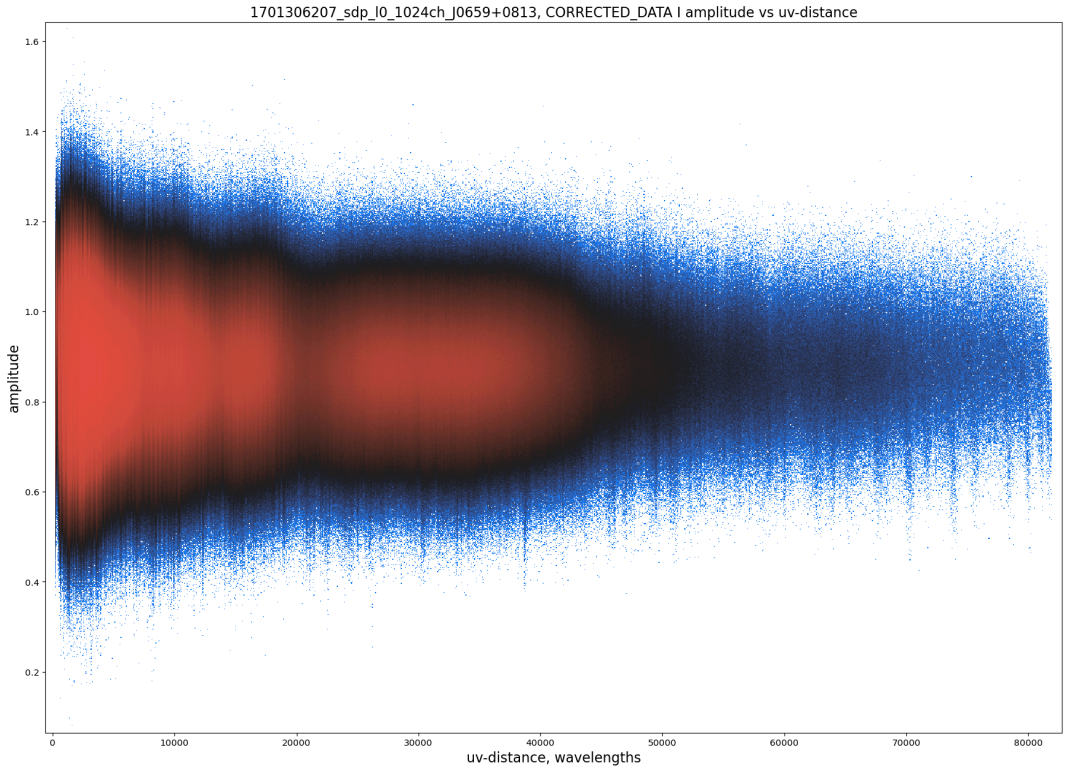
J0738+1742	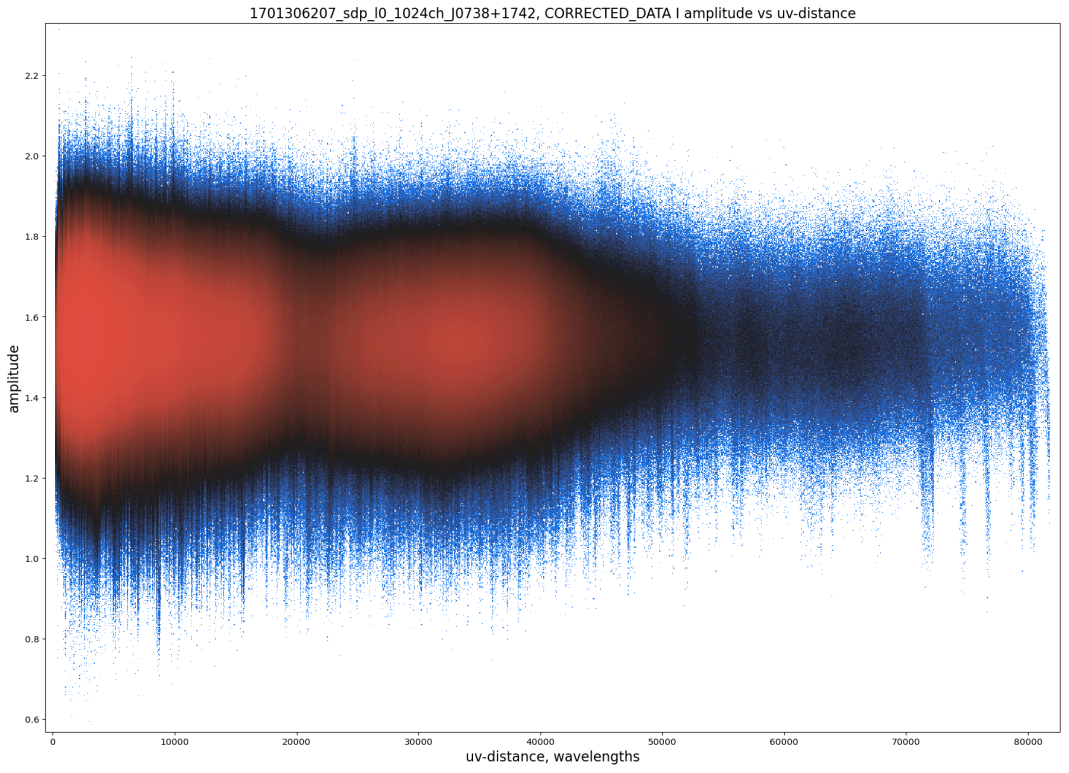

J0745+1011	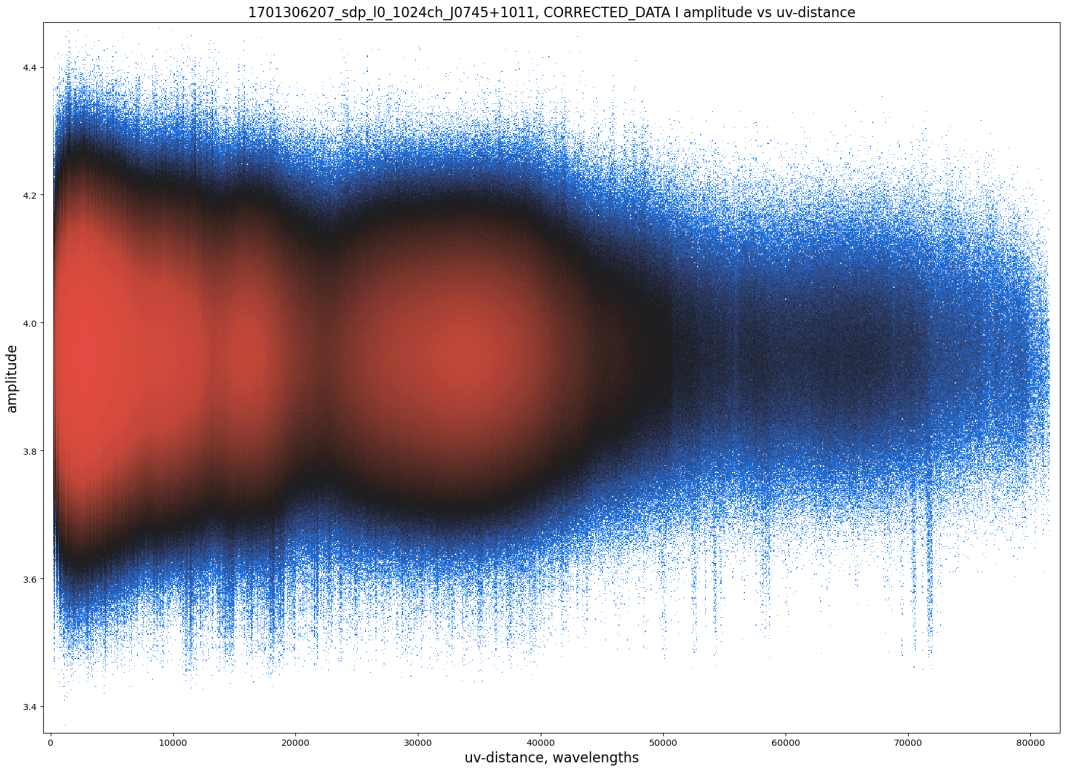
J1608+1029	
J1728+0427	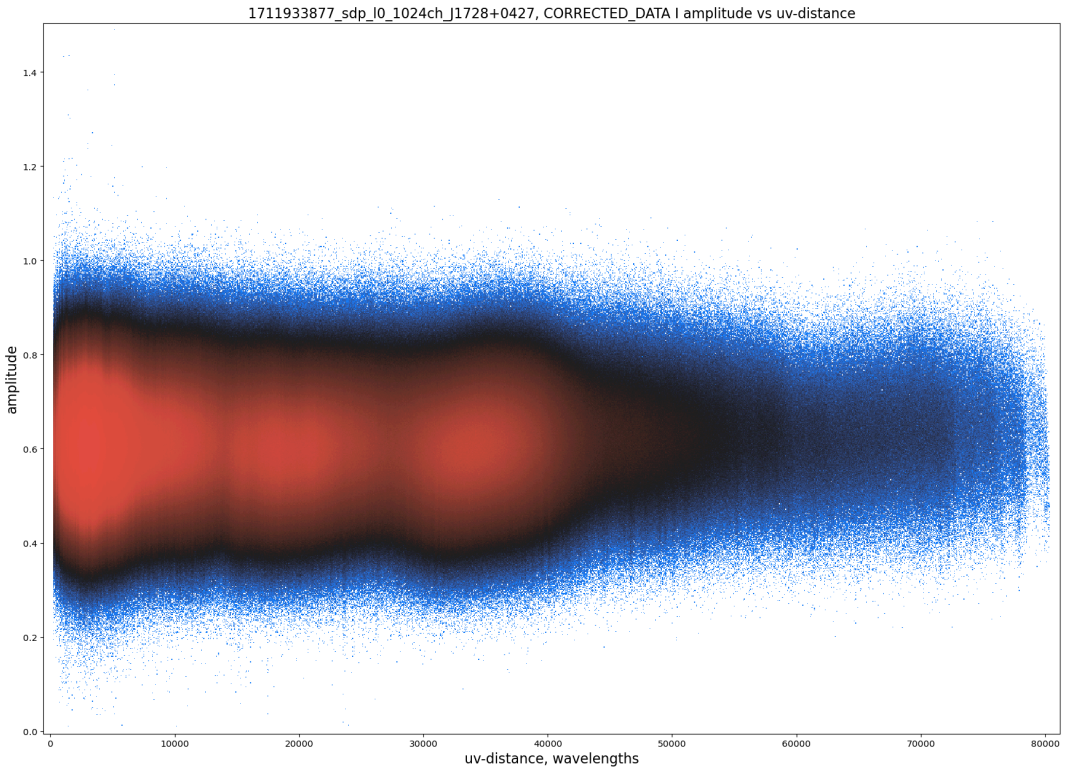

J1734+0926	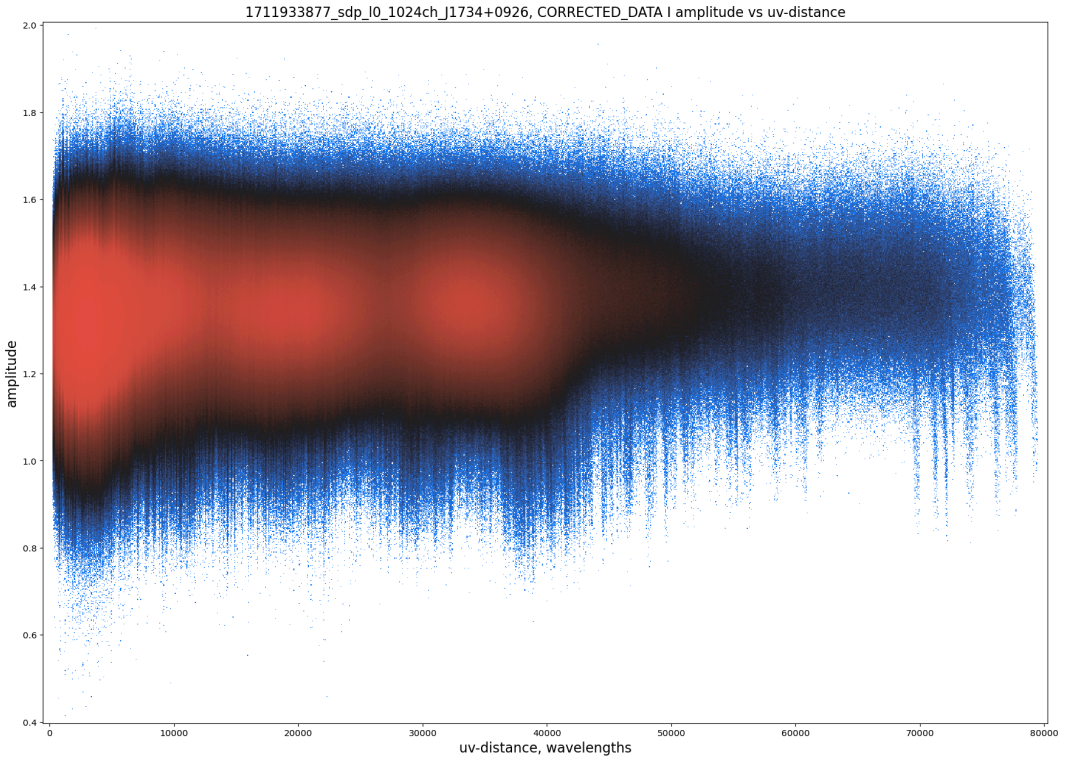
Negative/steep spectral indices	
0016-002	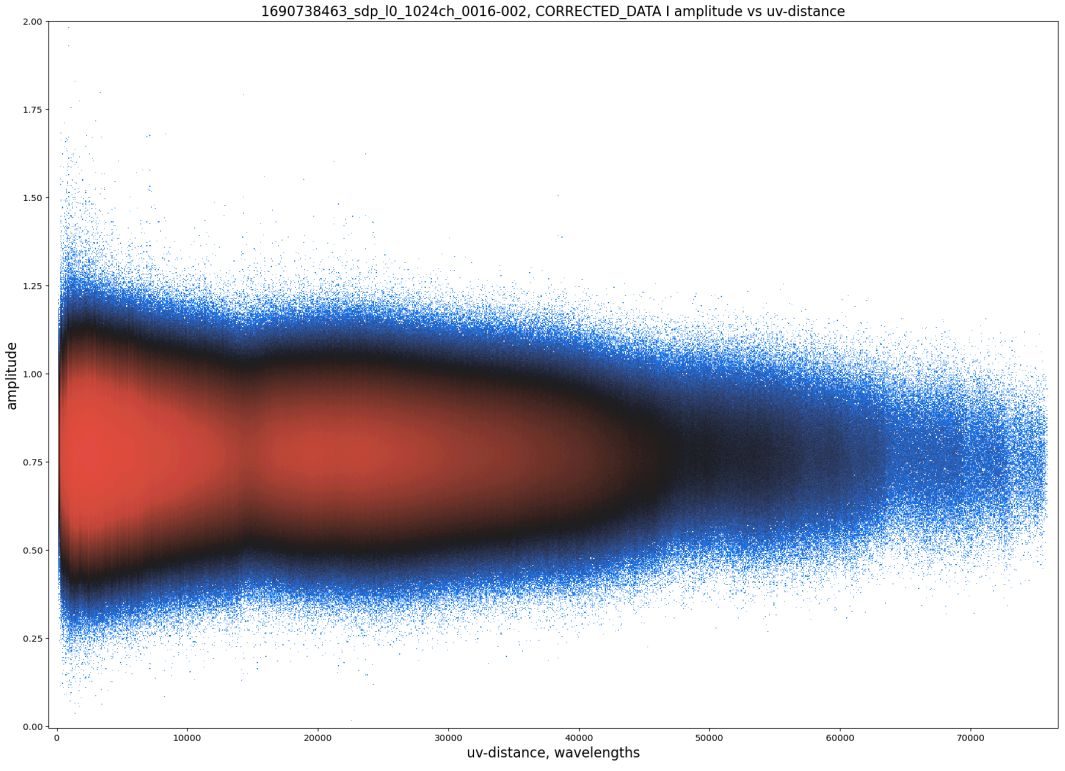

0037-593	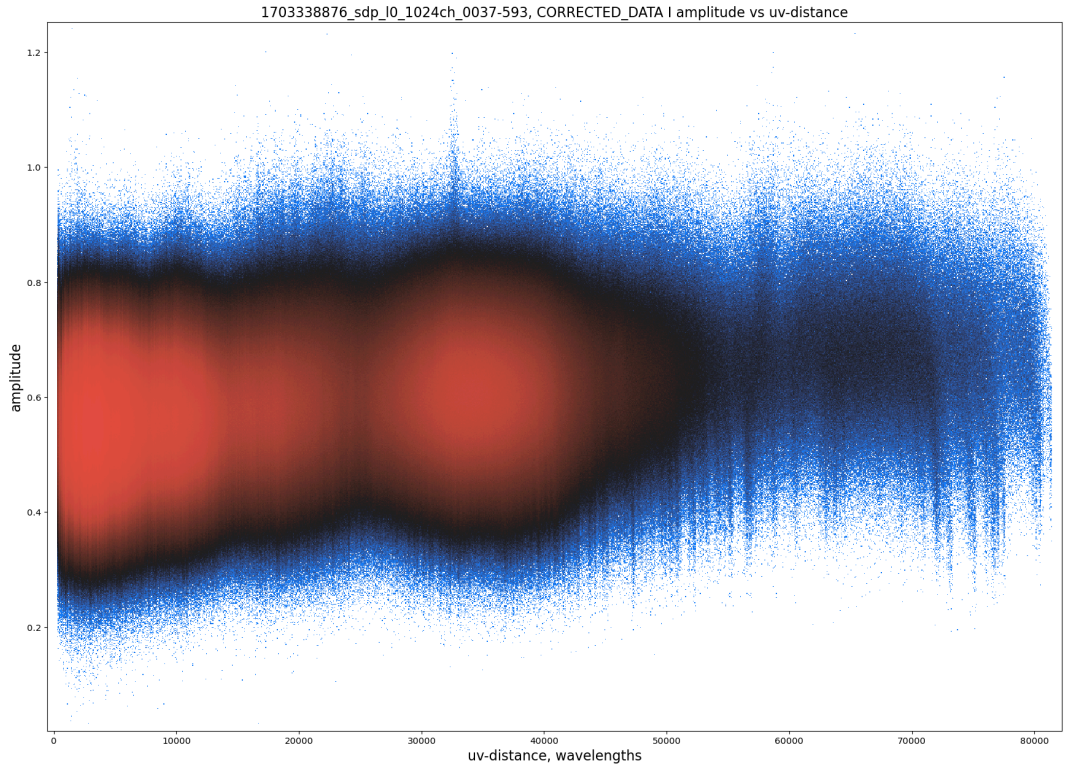
0048-447	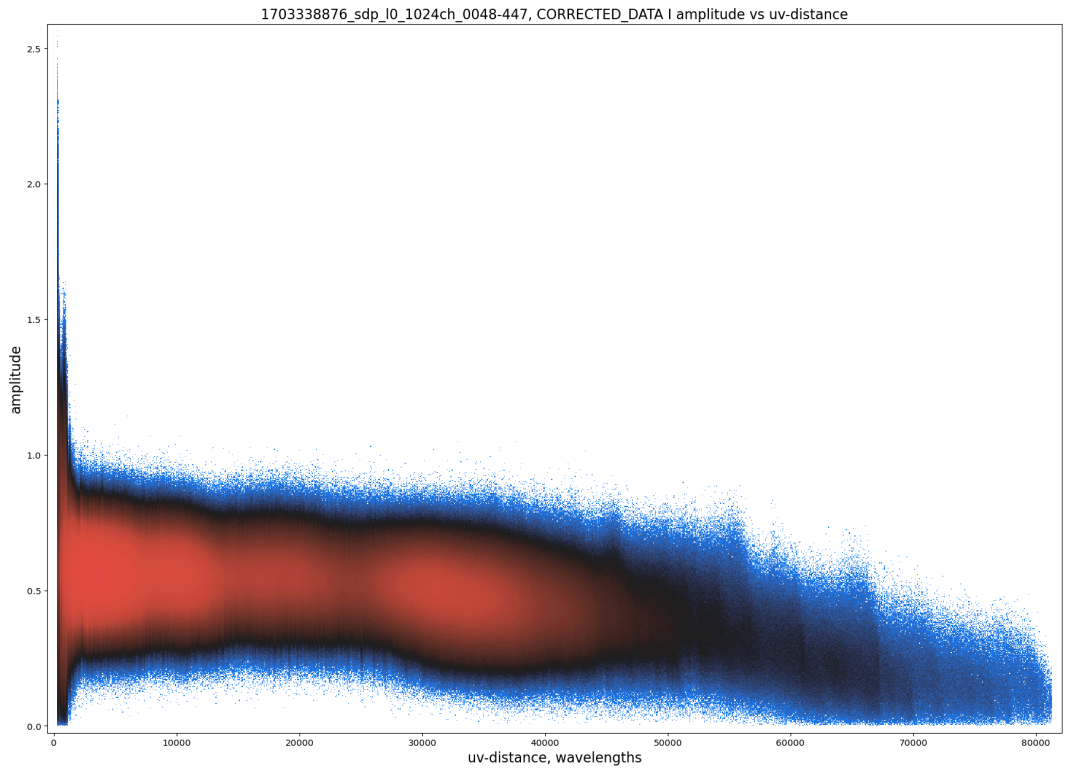

0121+043	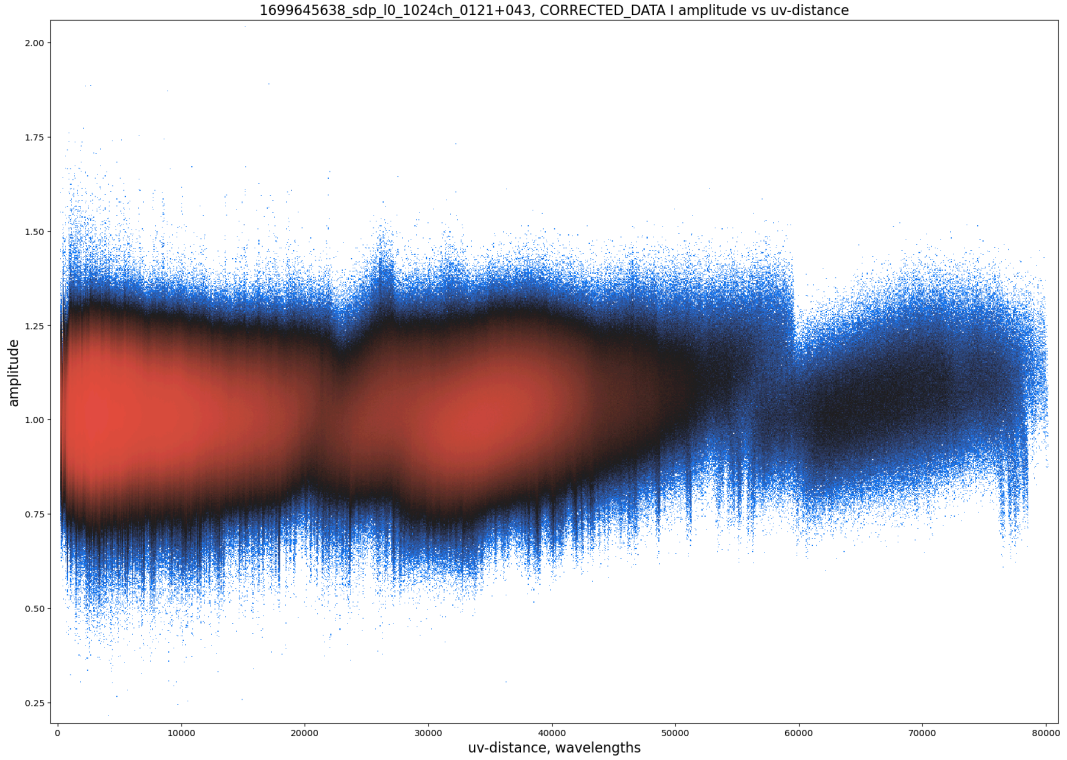
0203+115	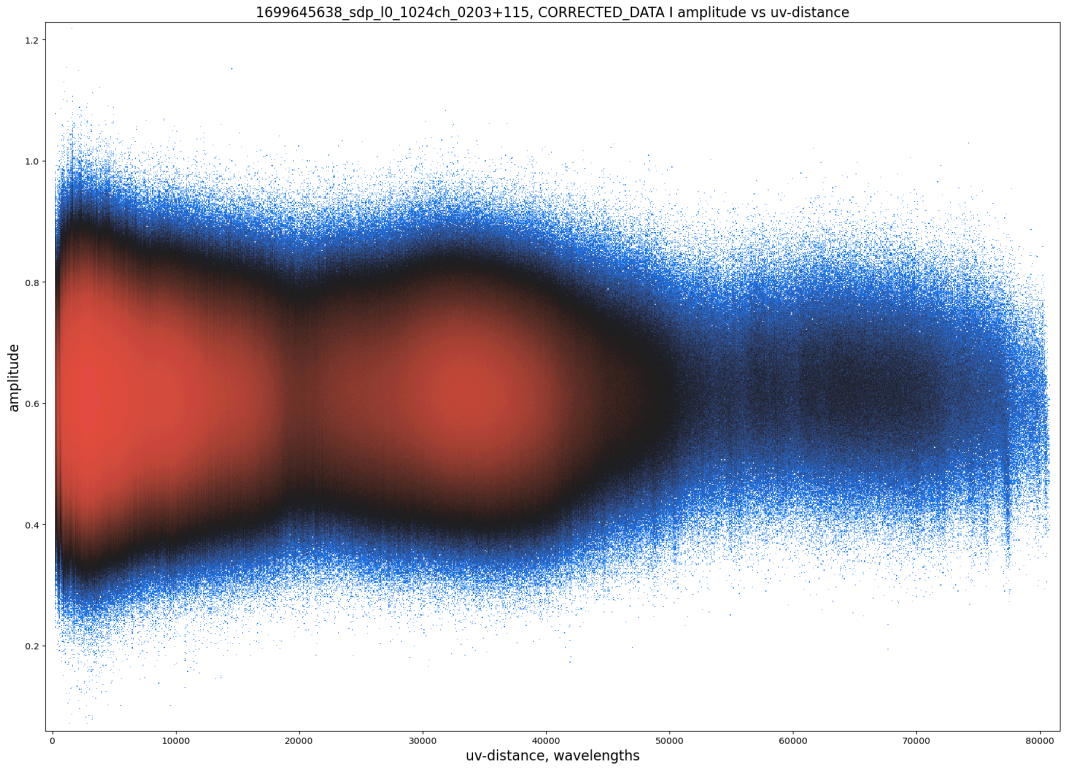

0231 +133	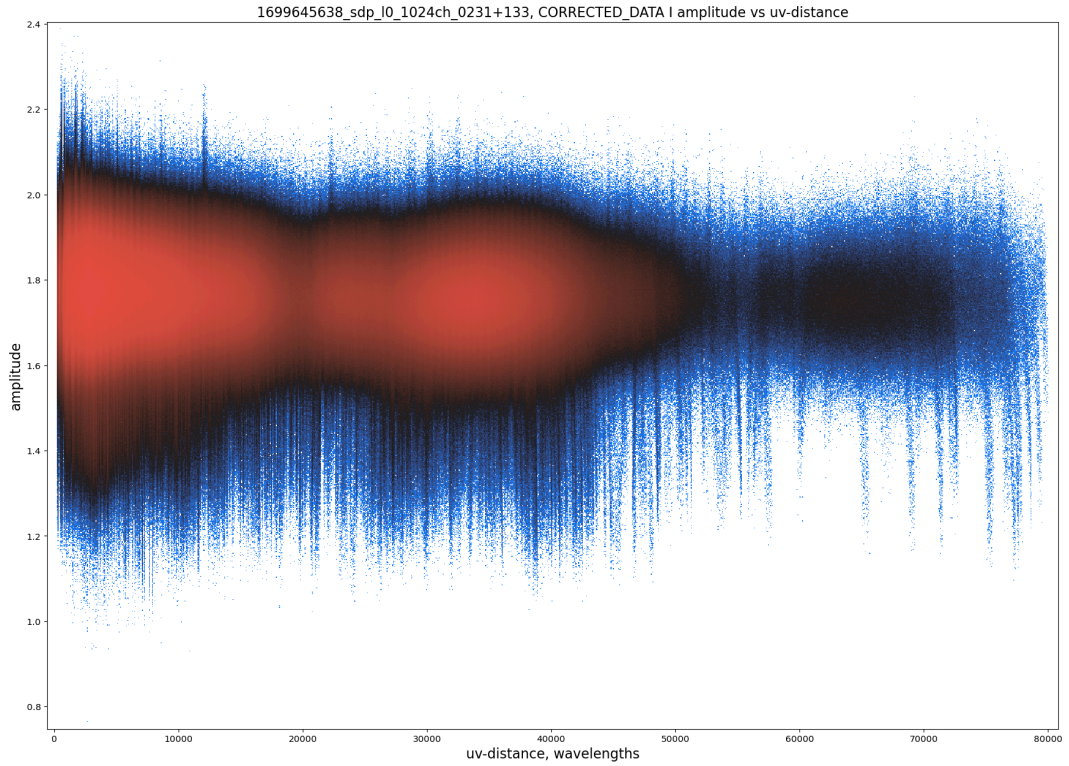
0242-215	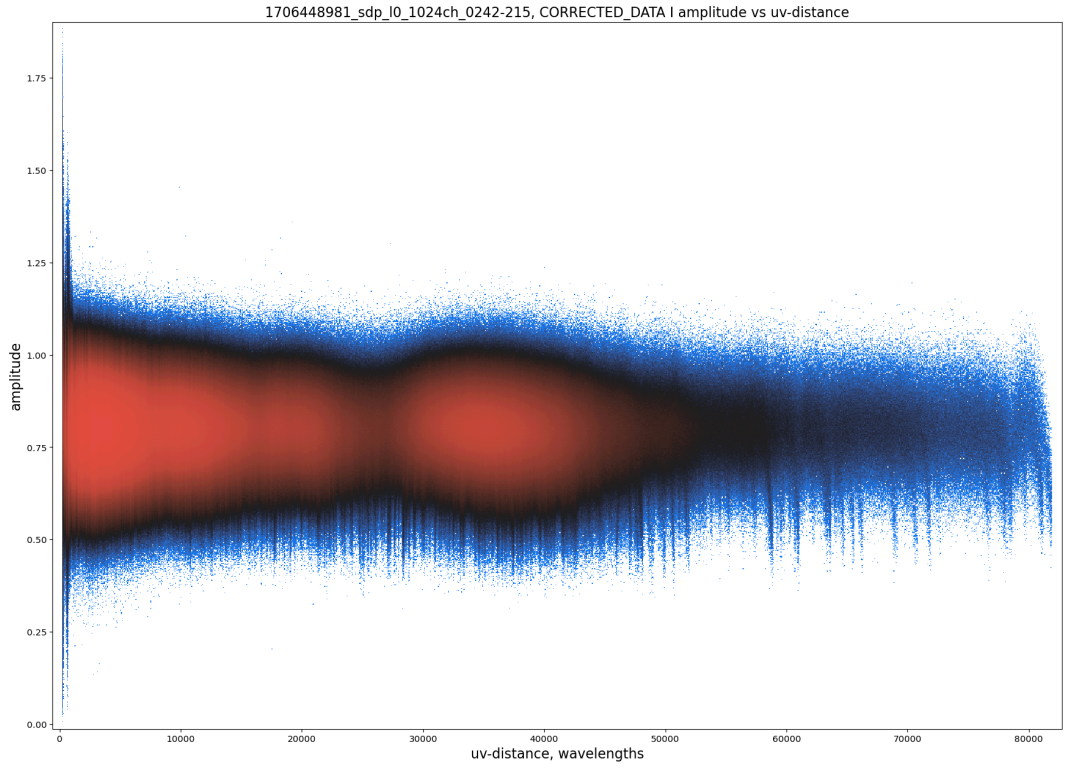

0319+1901	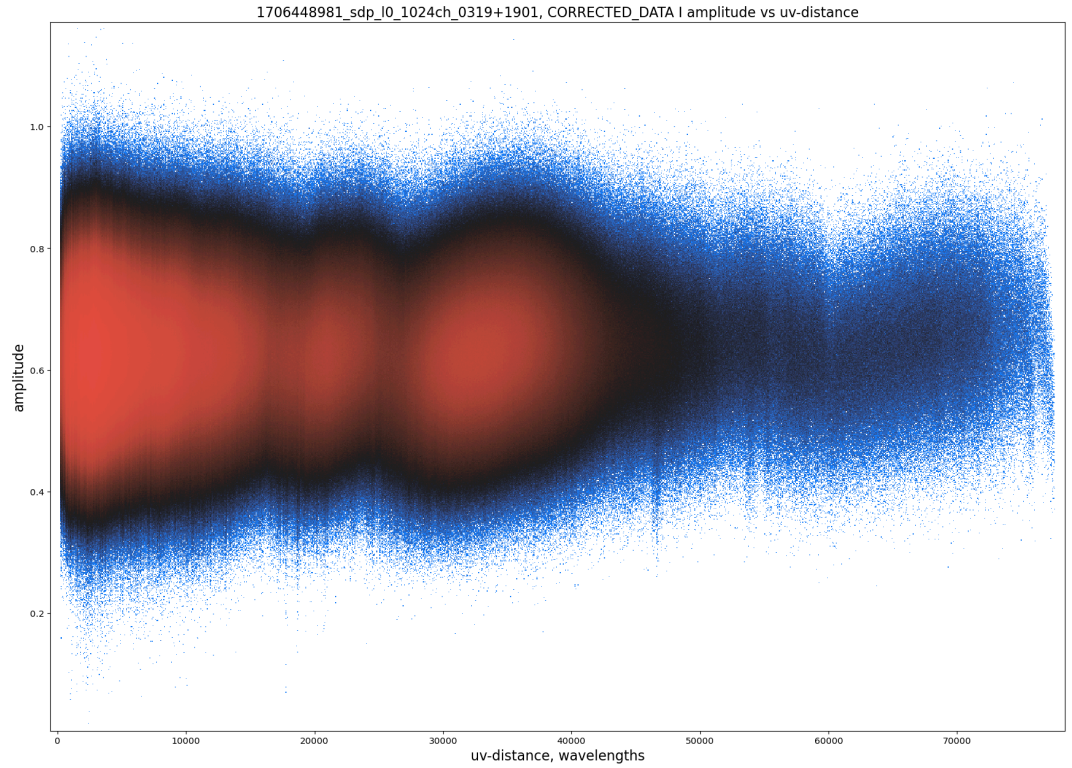
0501-019	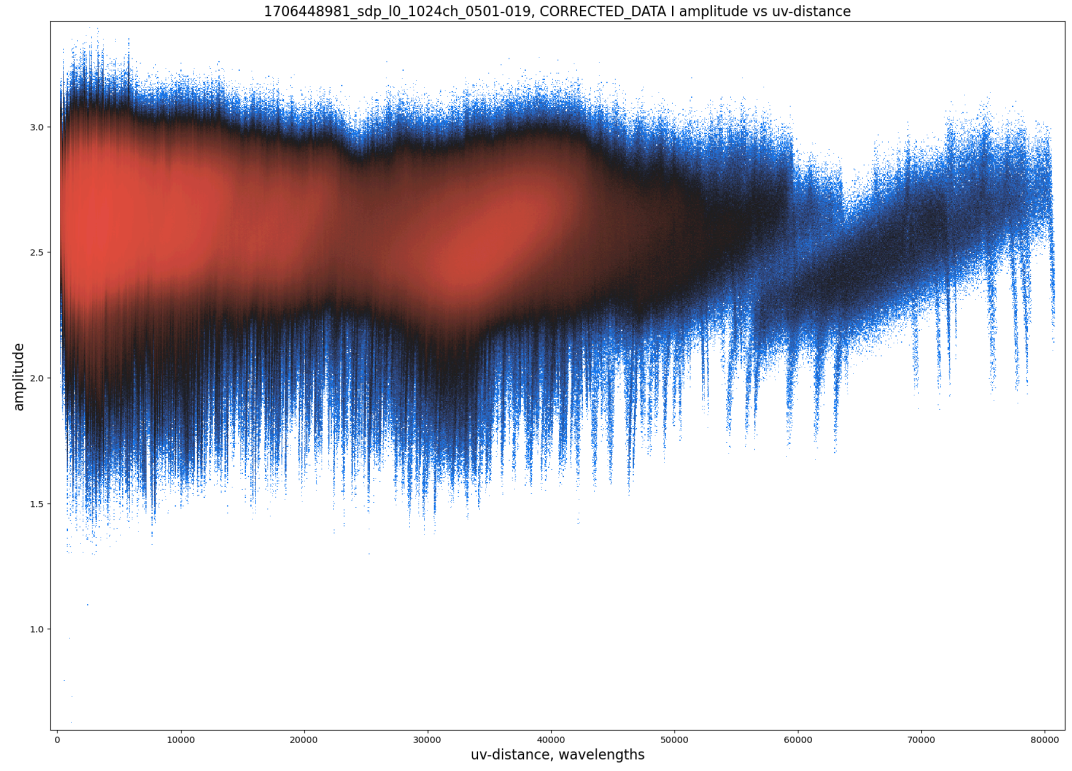

1034-293	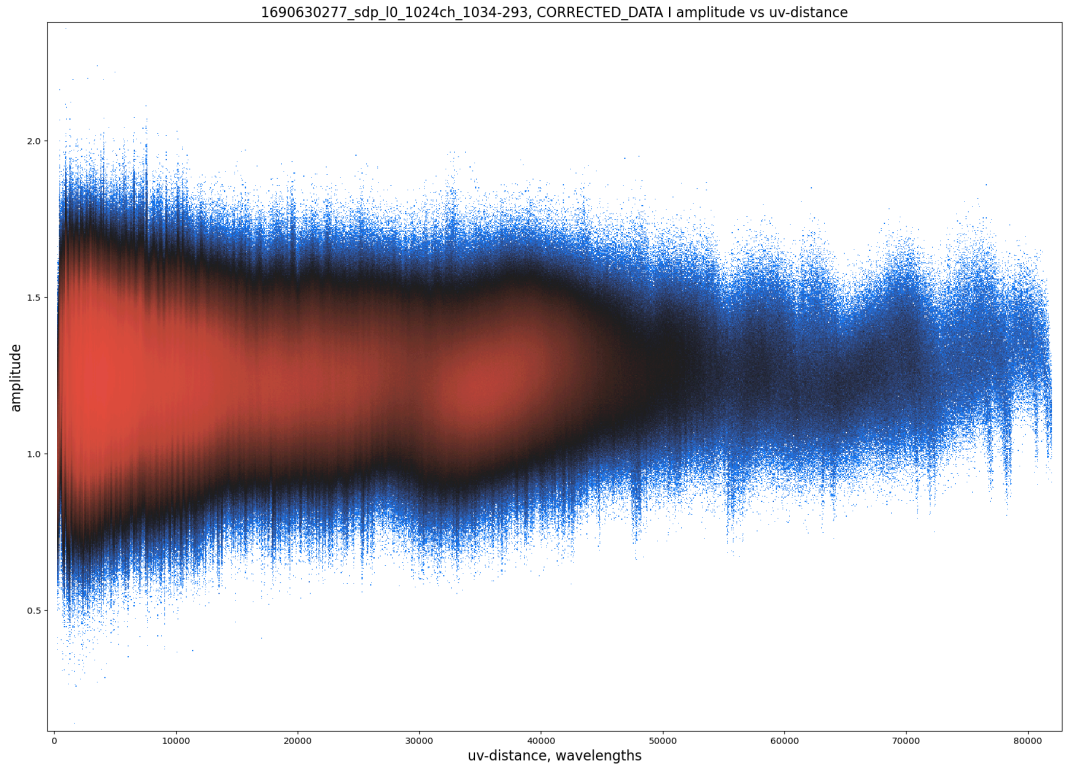
1051-316	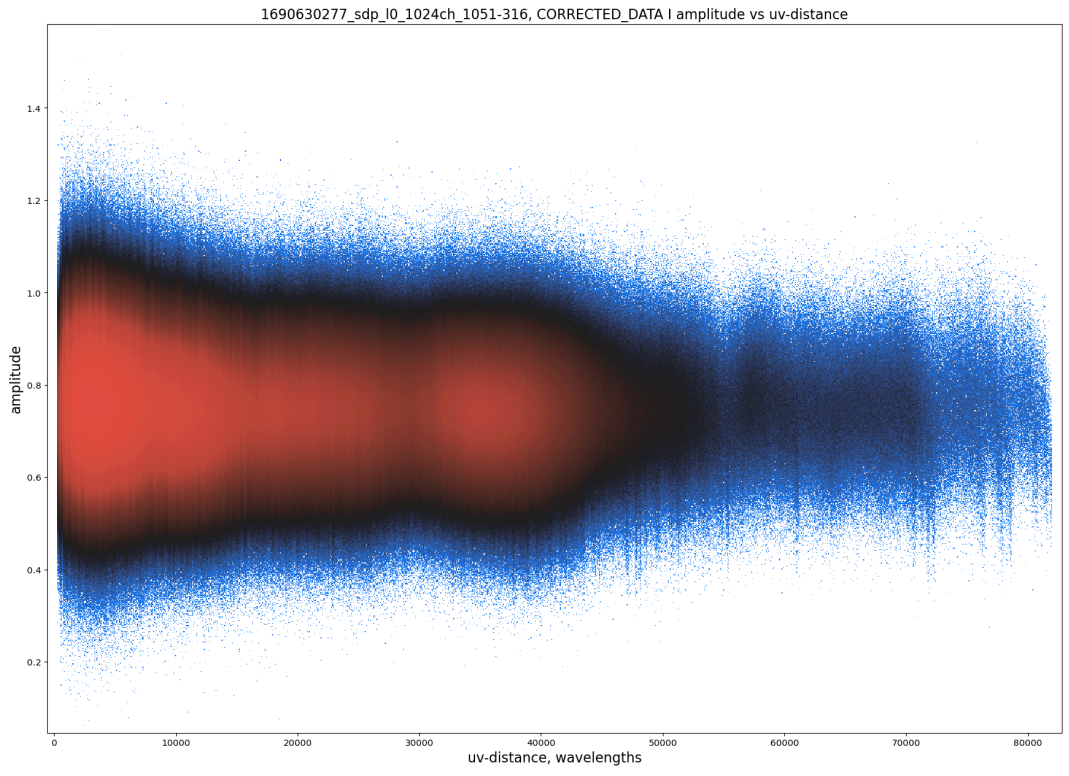

1057-245	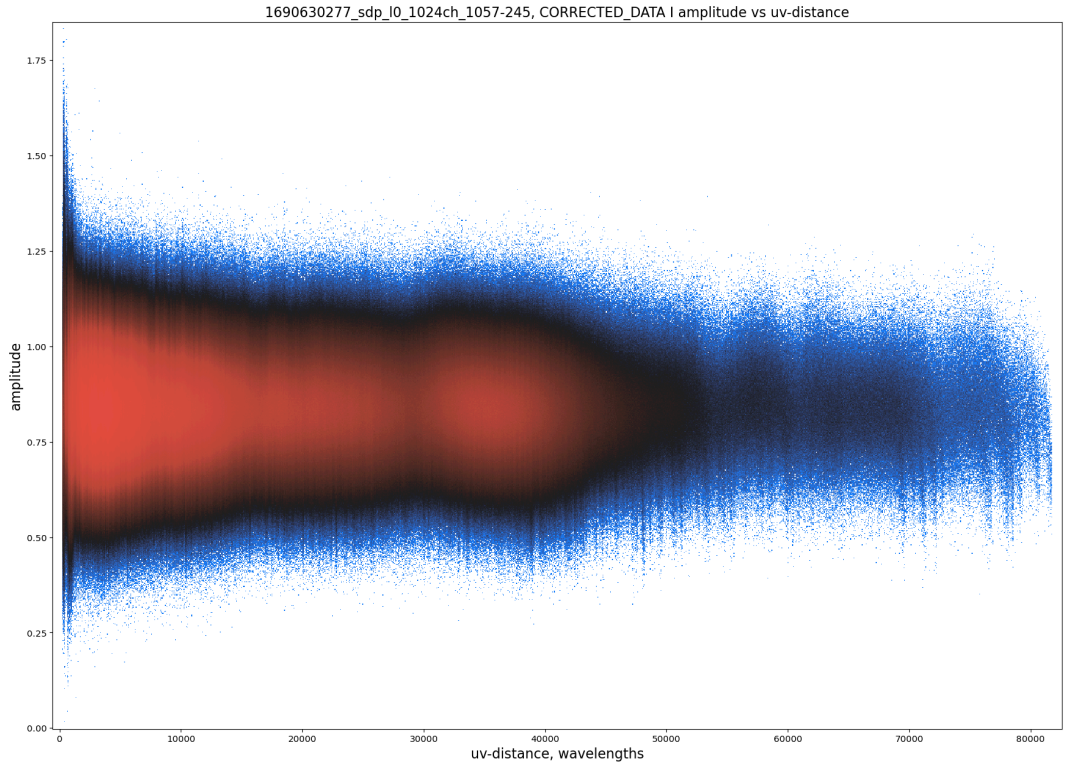
1124-186	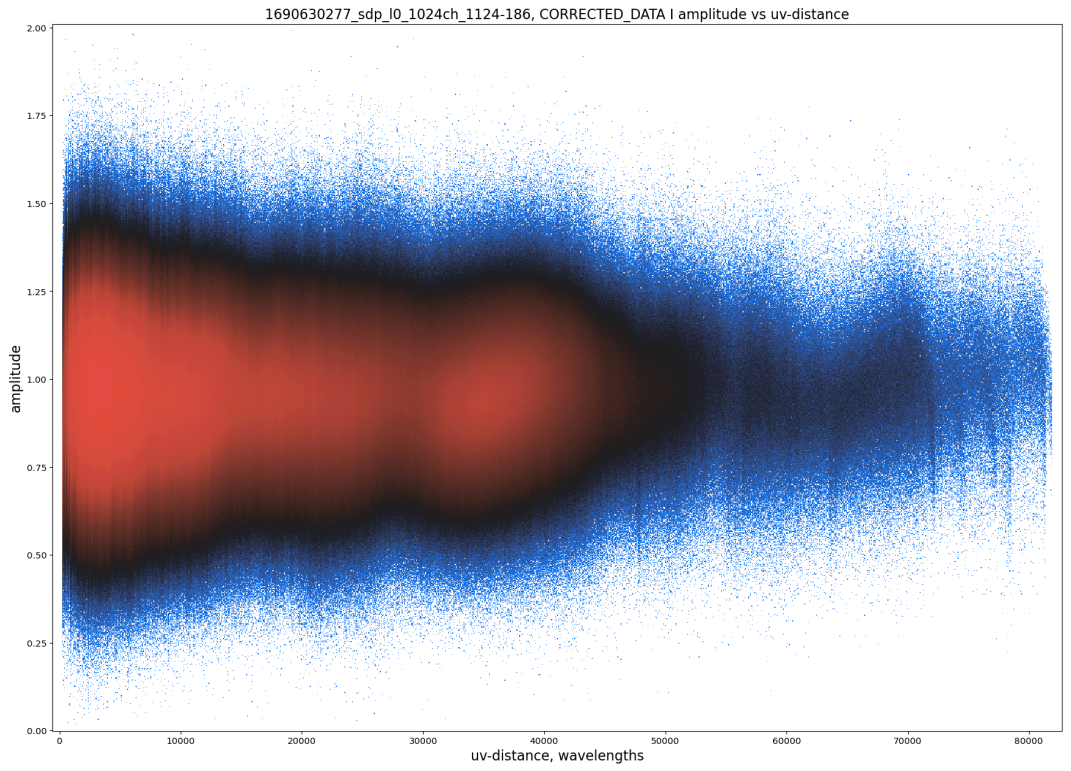

1357-177	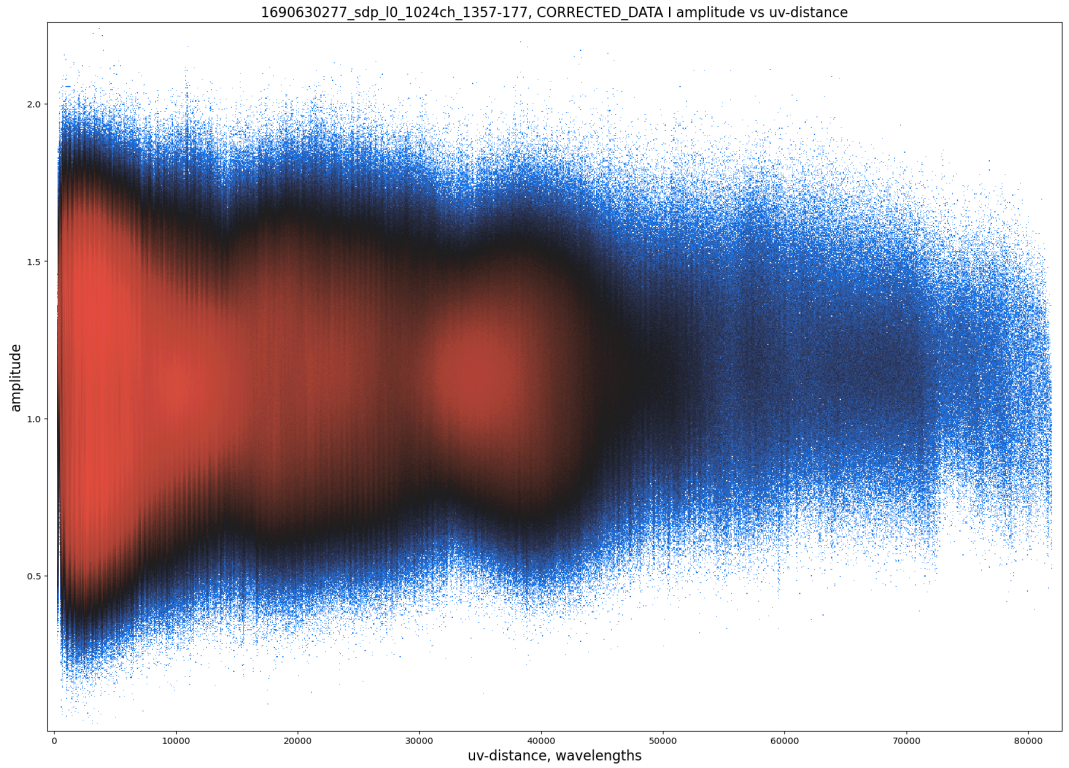
1415+133	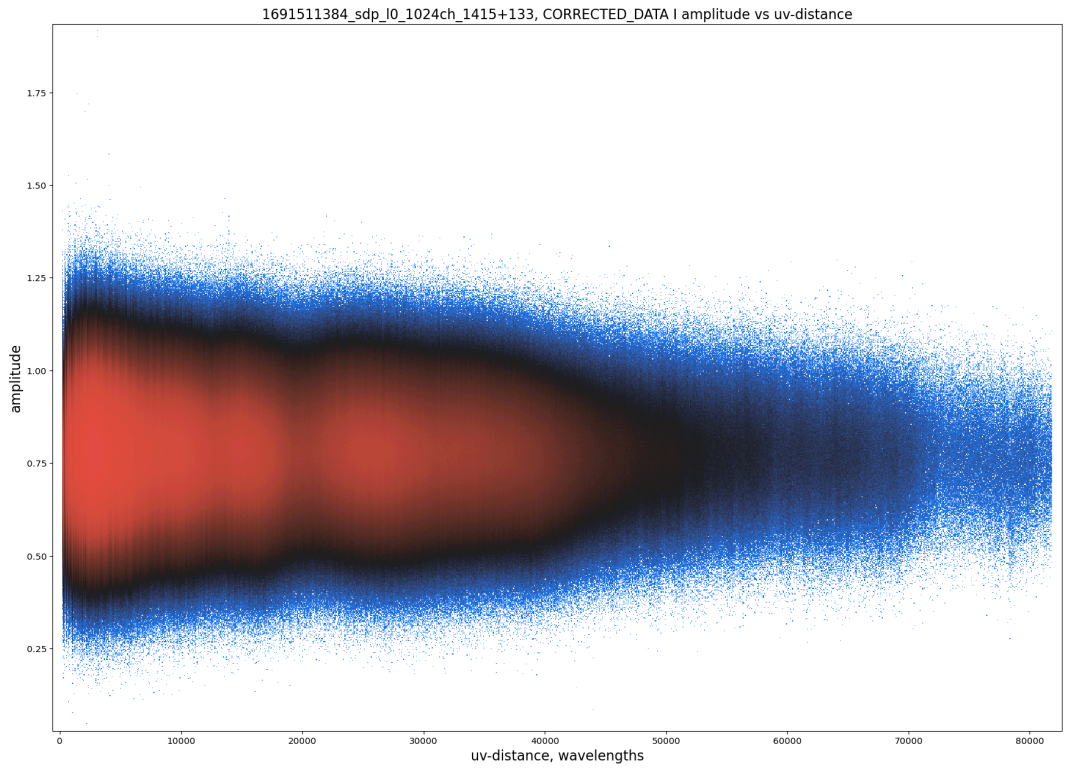

1430+107	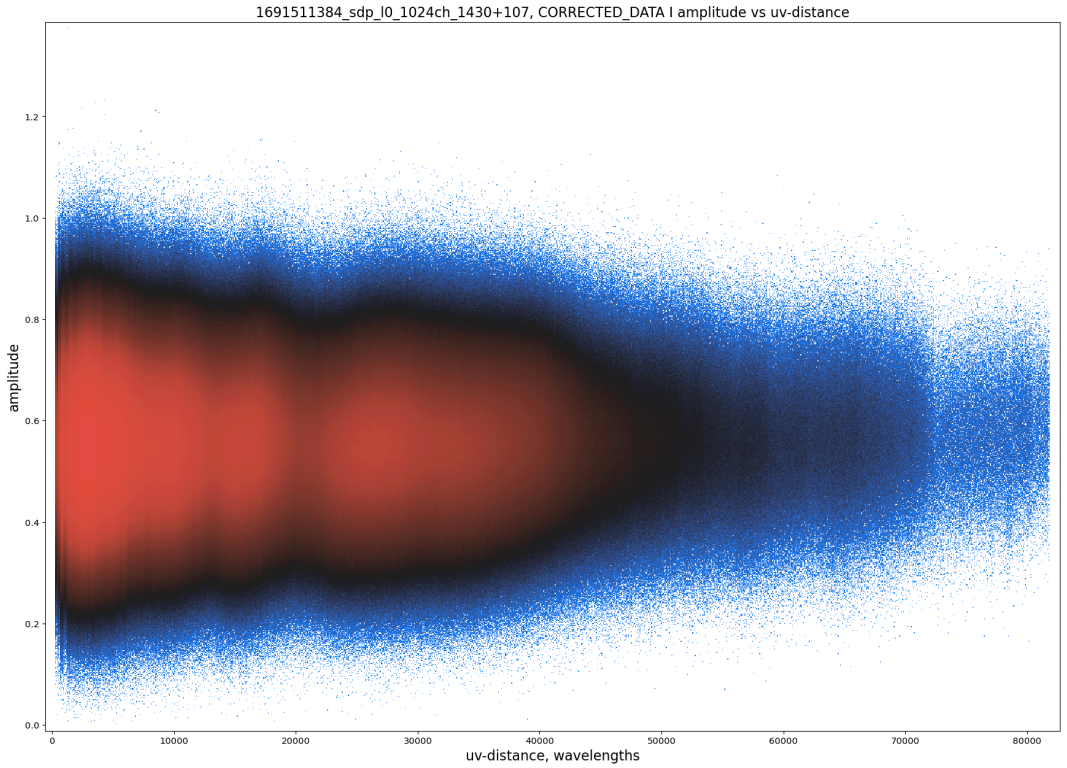
1436+233	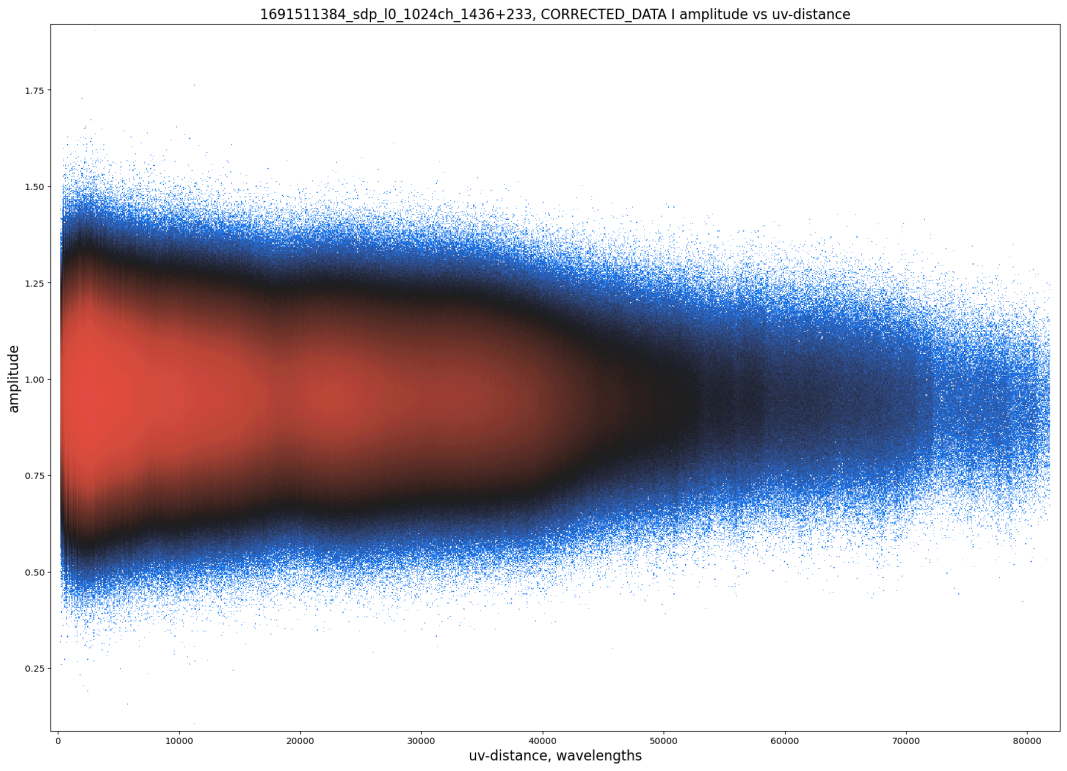

1448-163	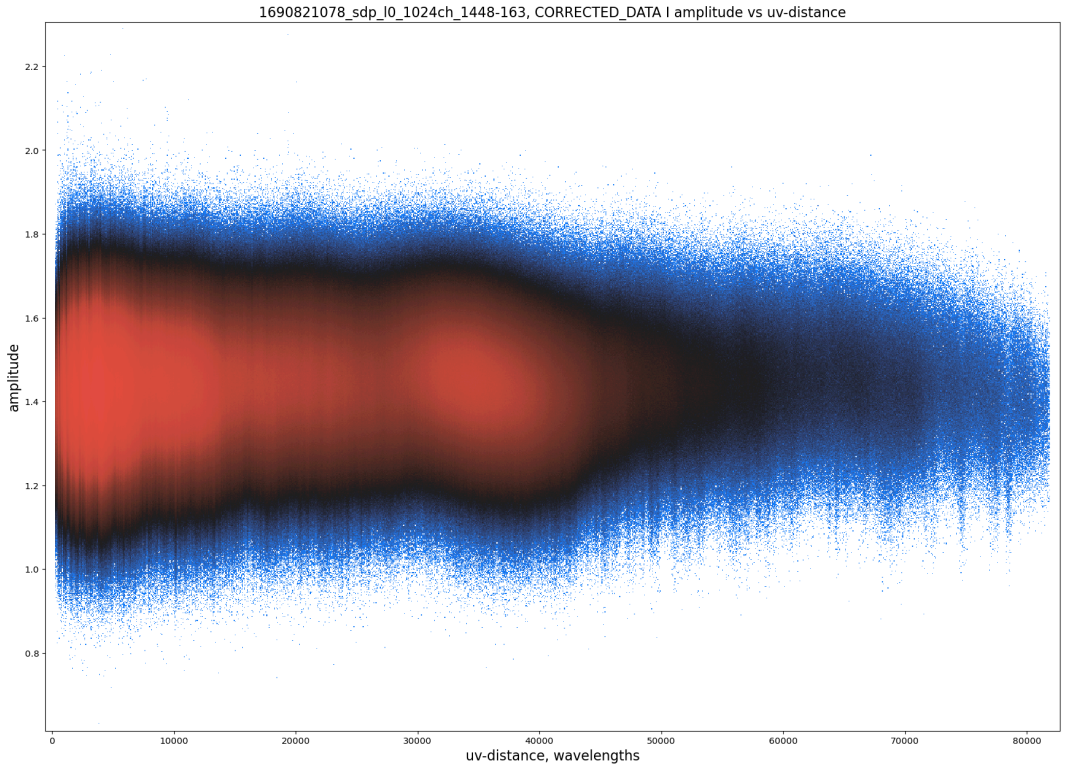
1543-079	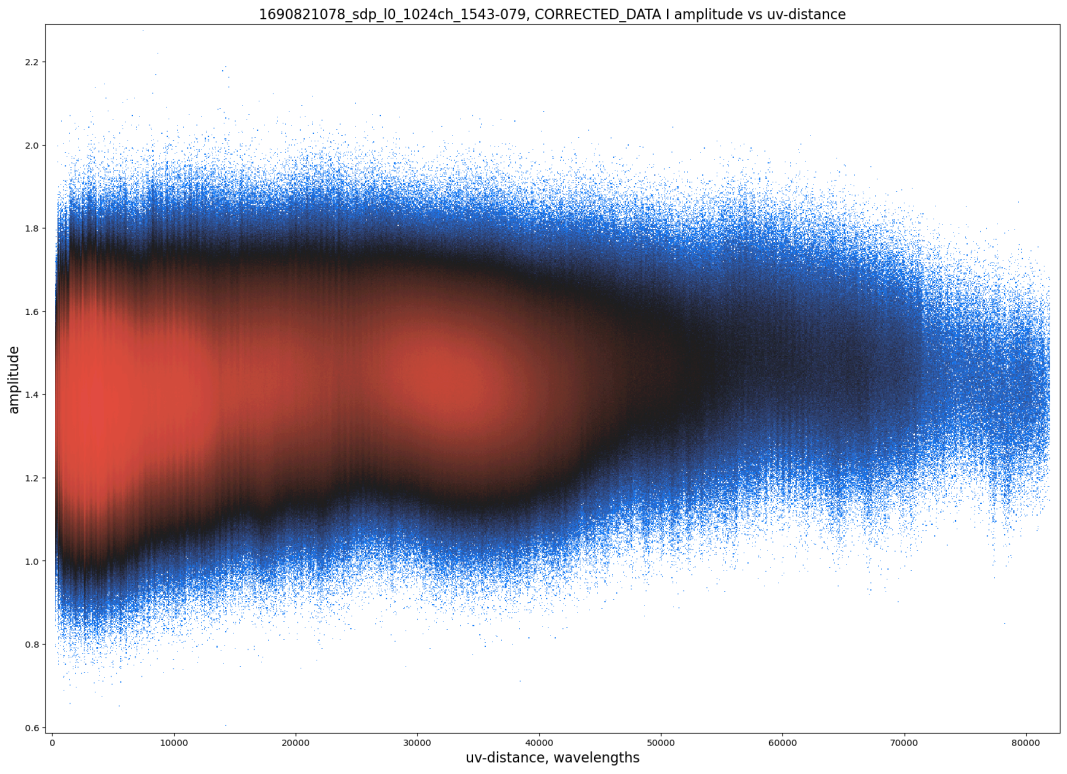

1546 +004	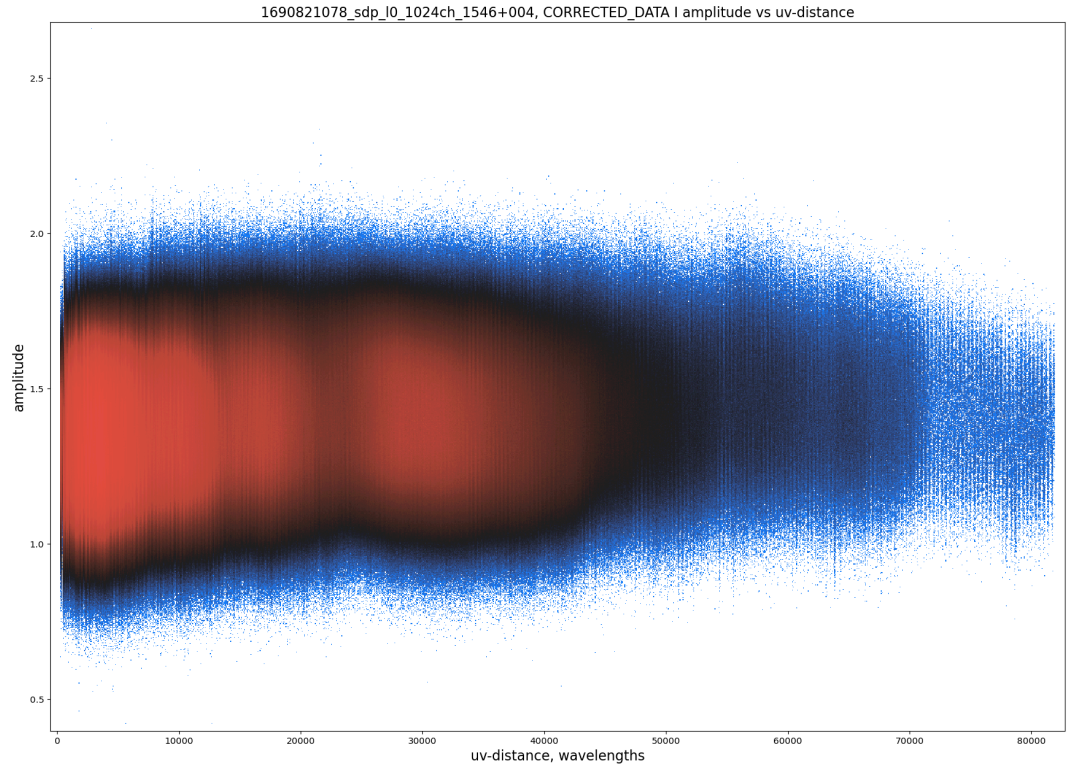
1554-270	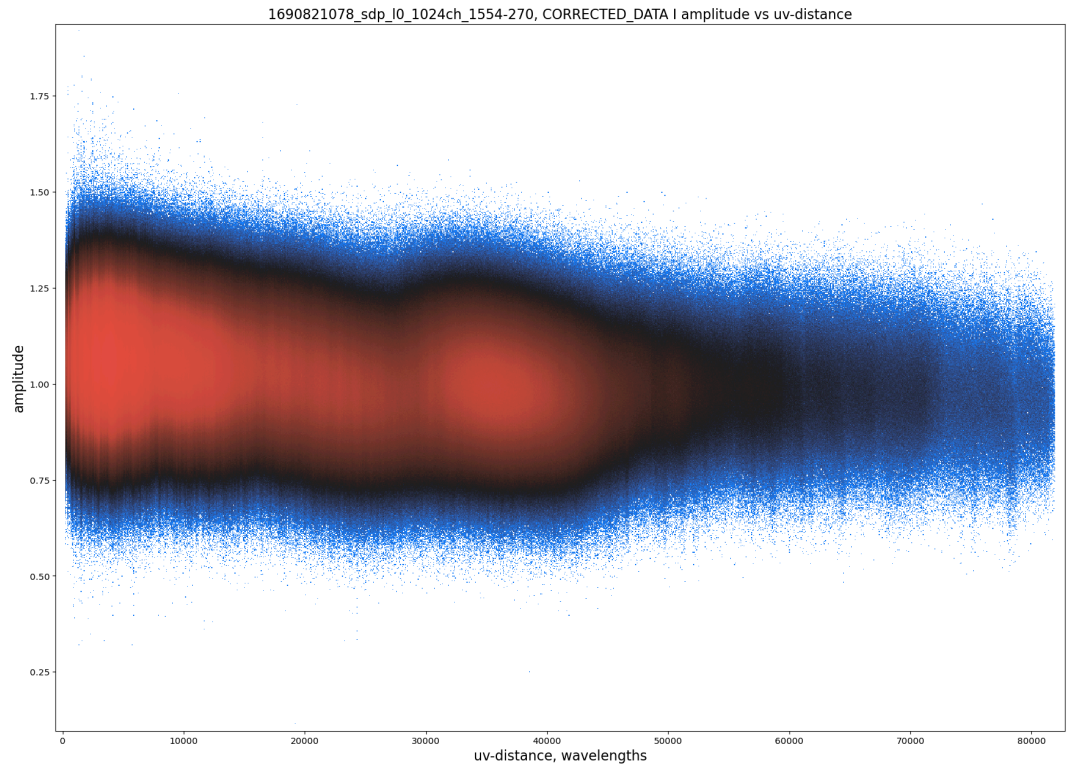

1751-253	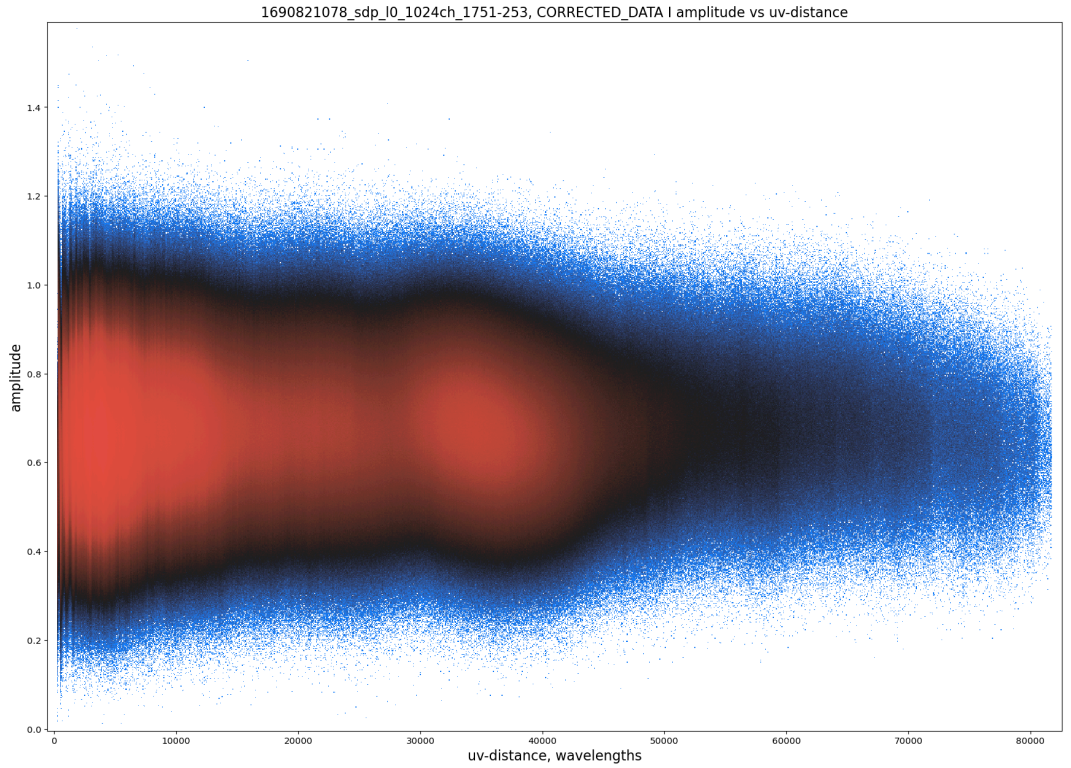
1811-209	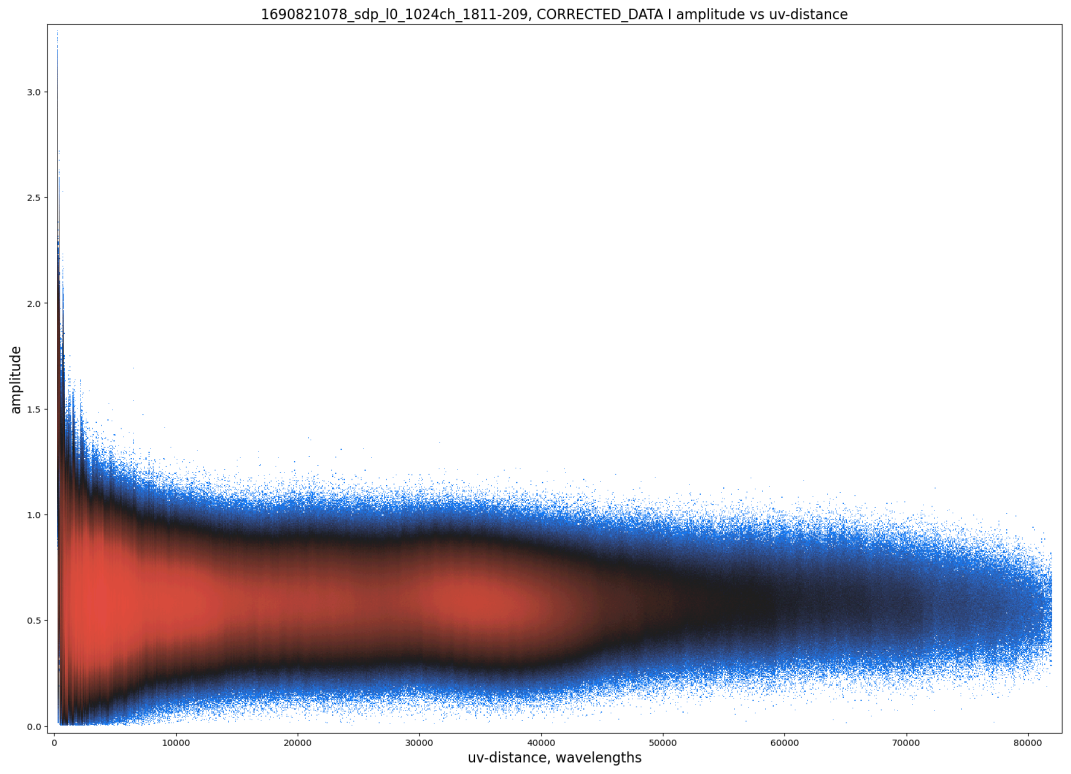

1822-096	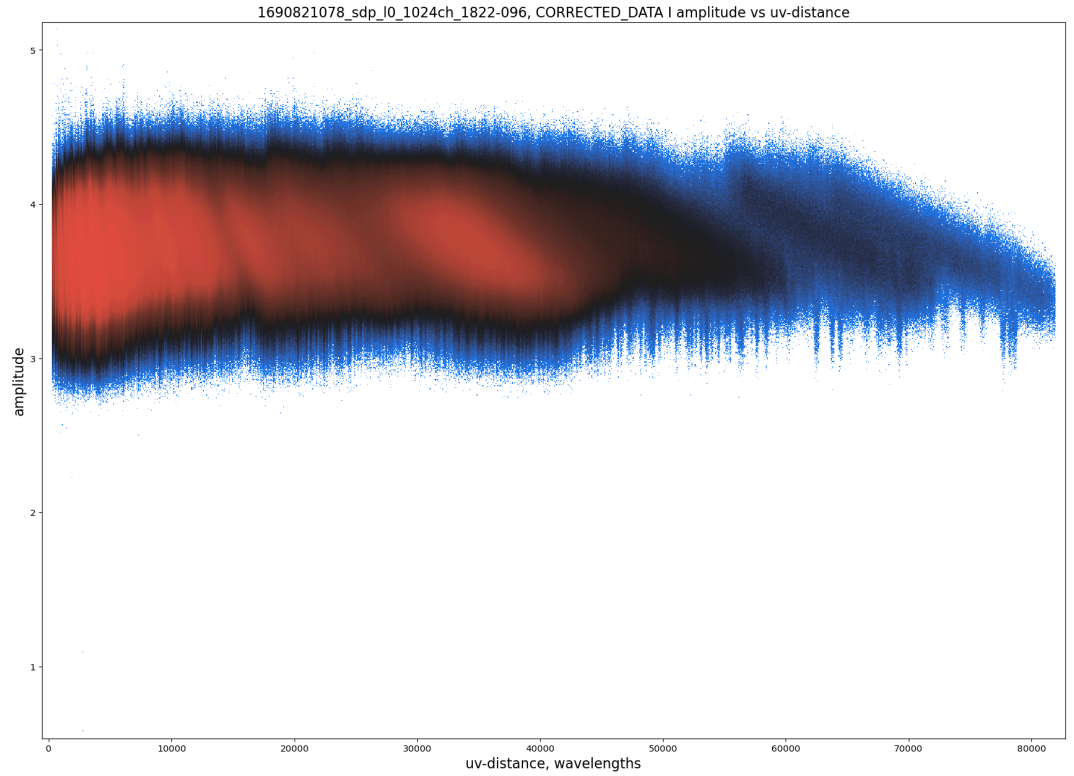
1923-210	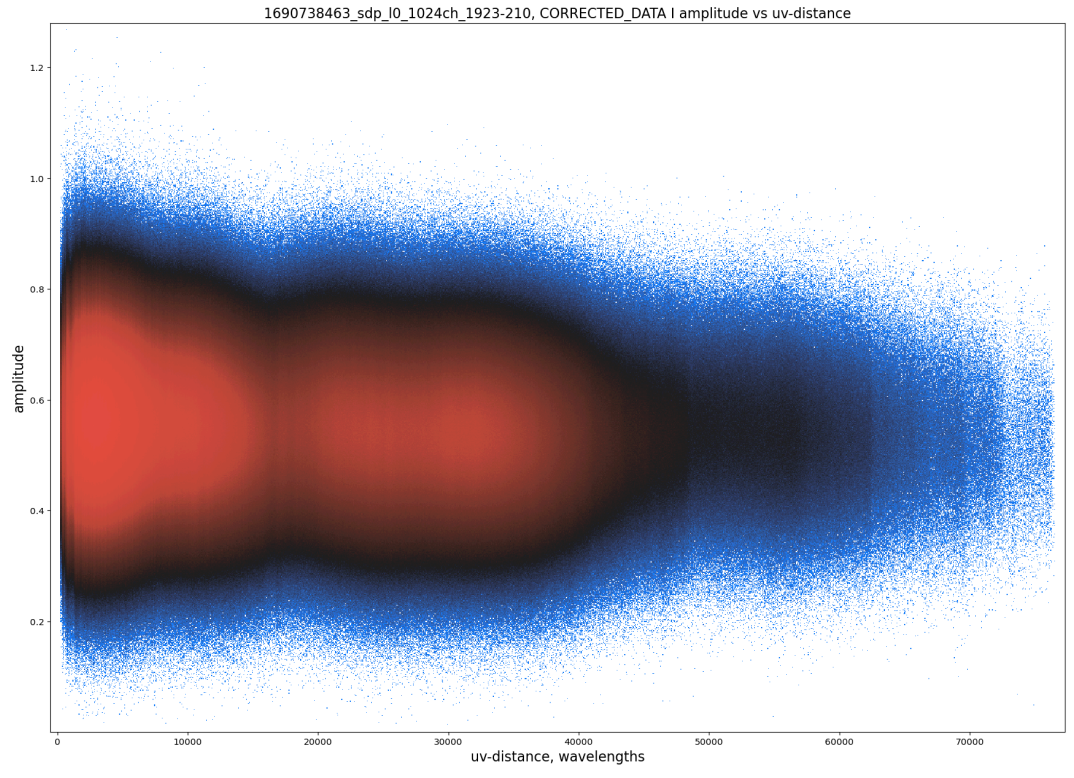

2219-279	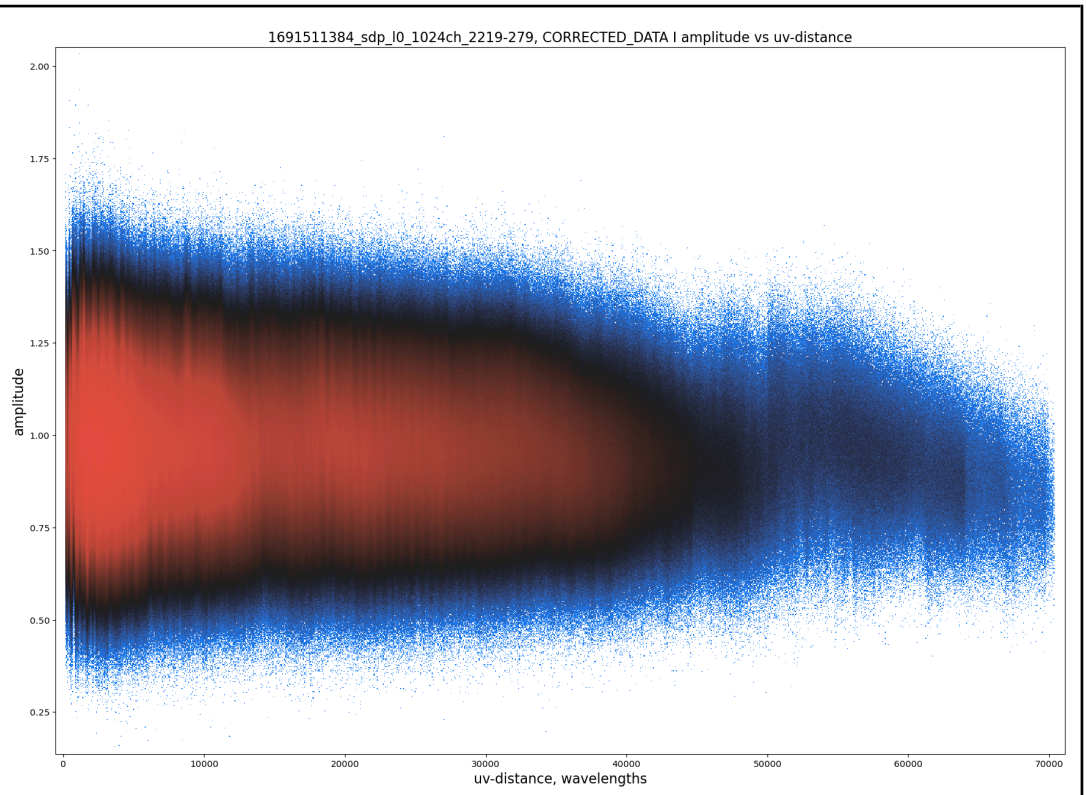
2248-325	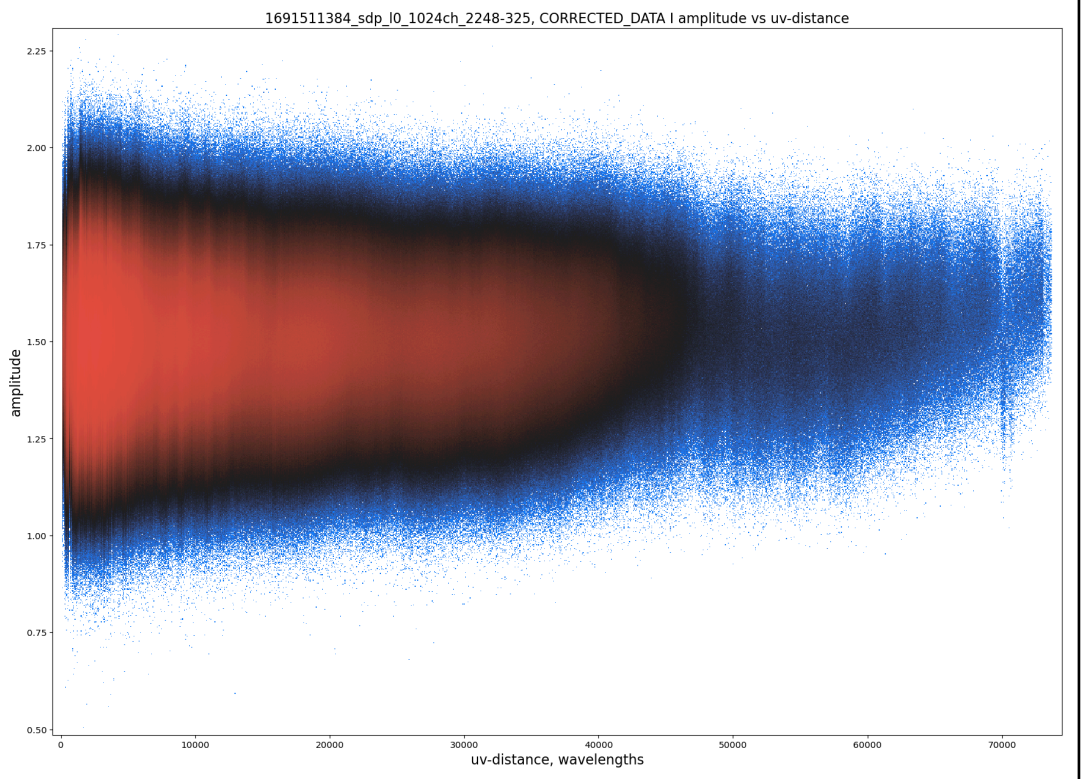

2257-364	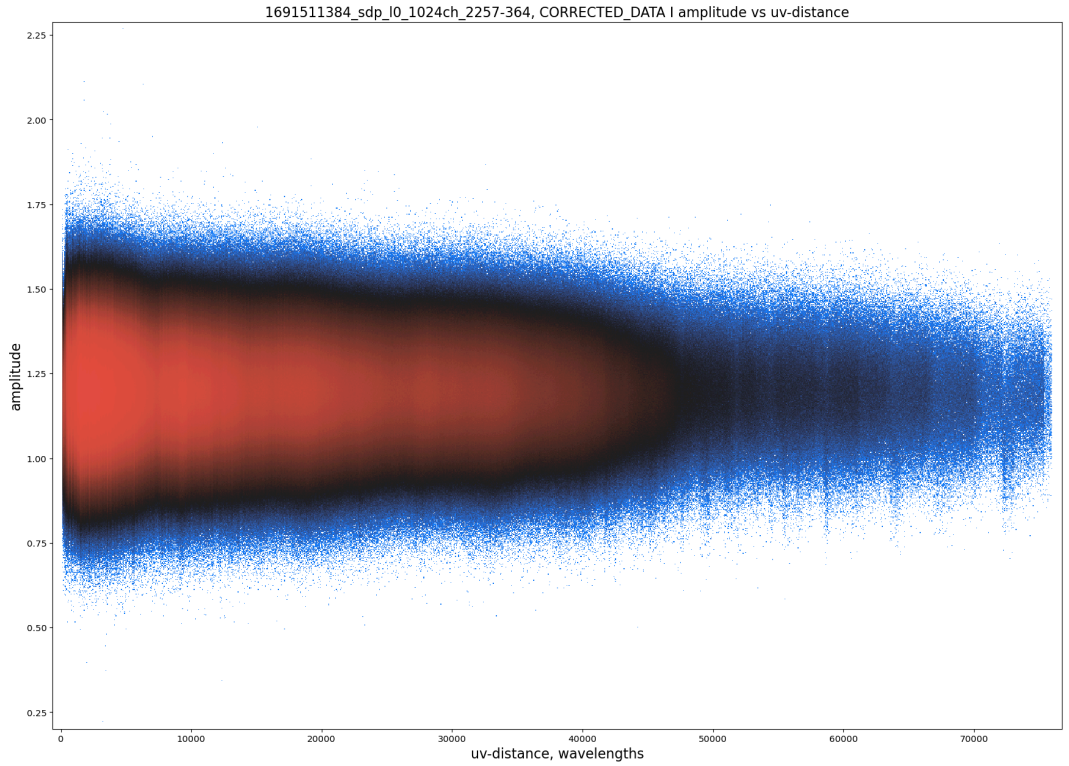
2314-316	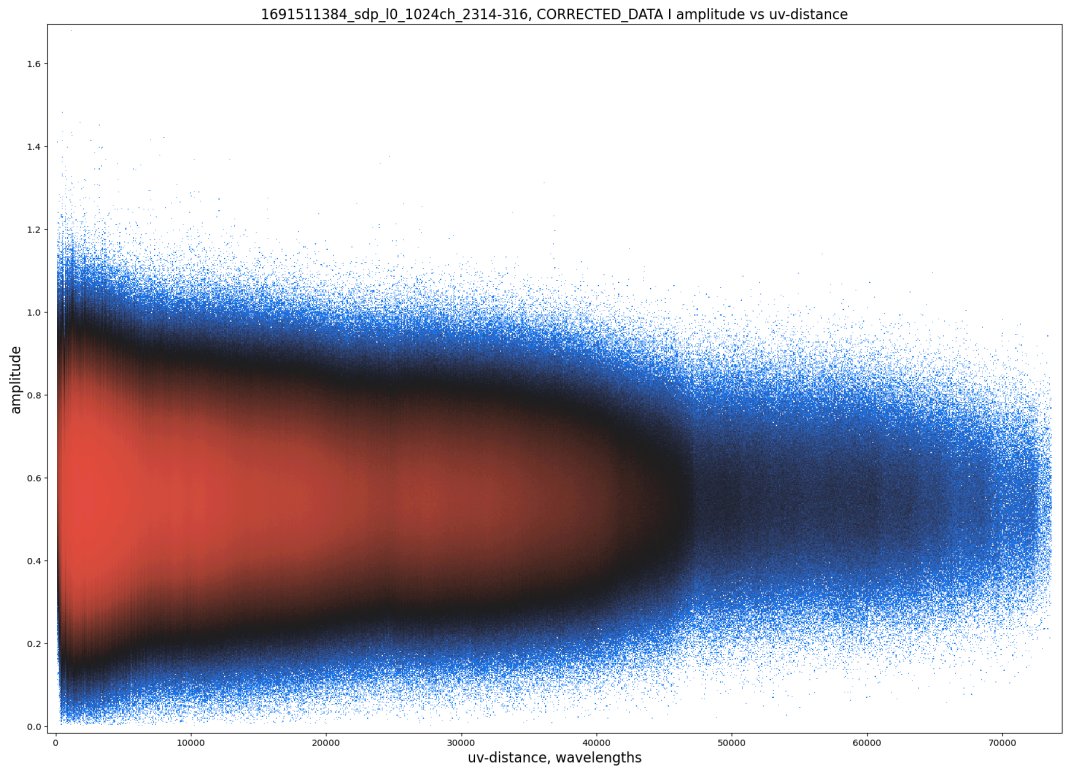

2314-449	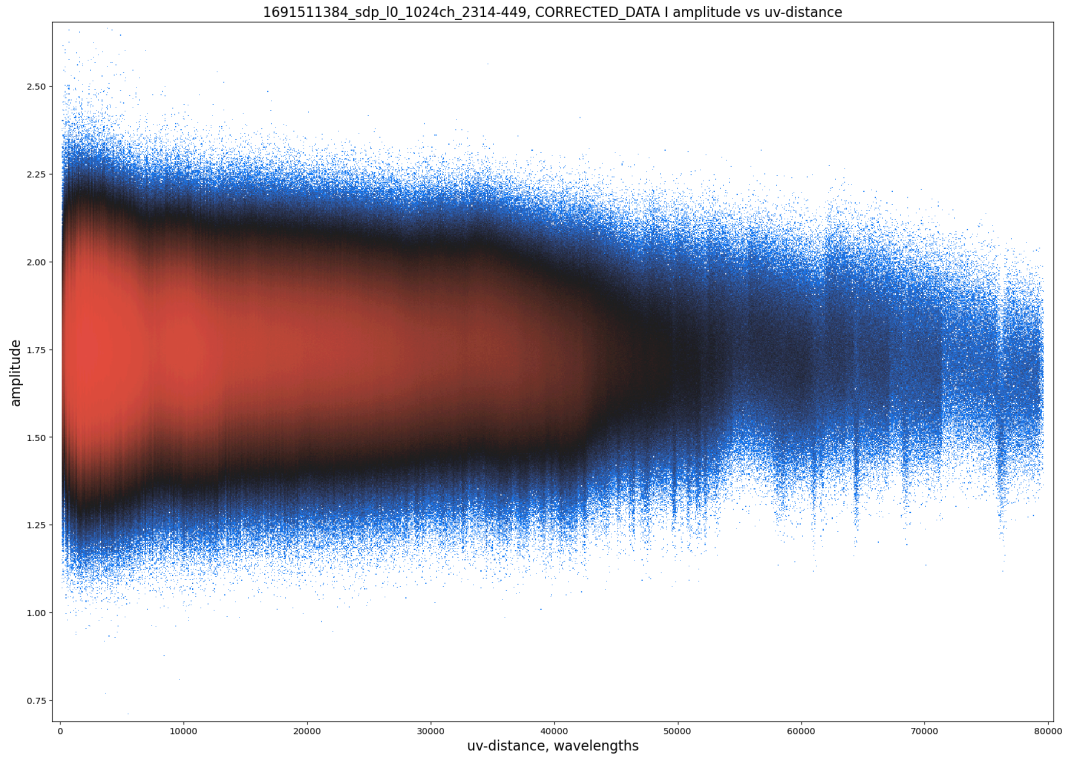
2348-165	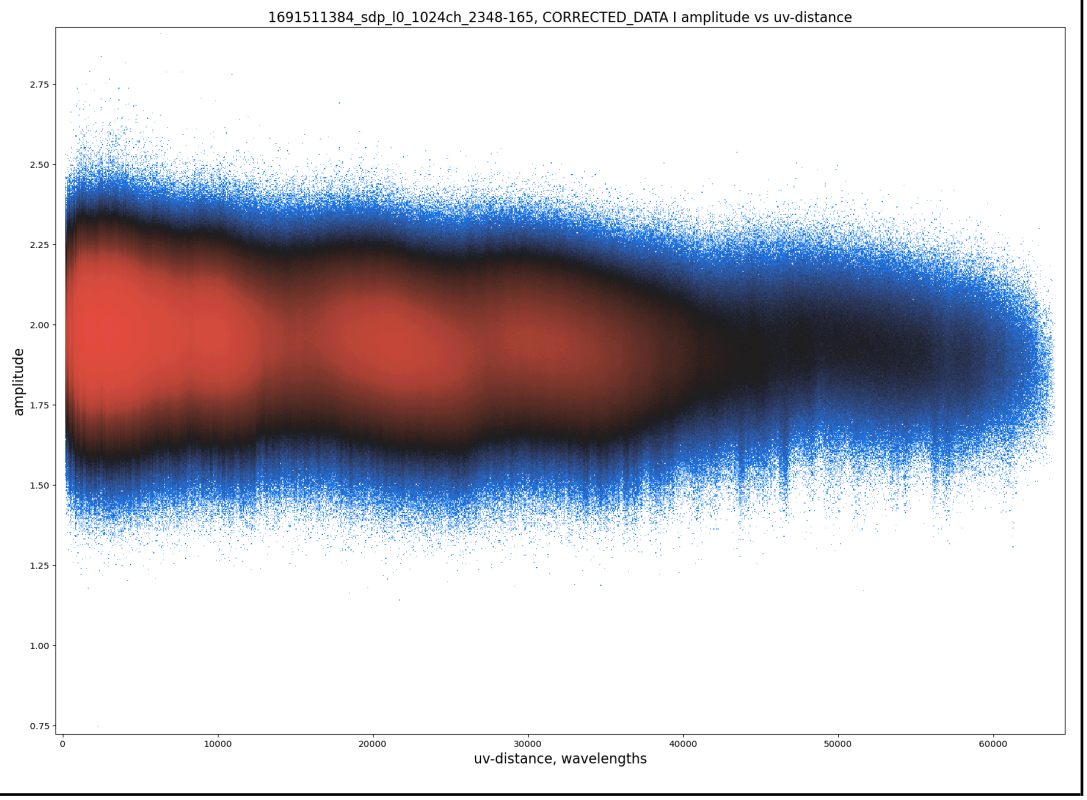

J0449+1121	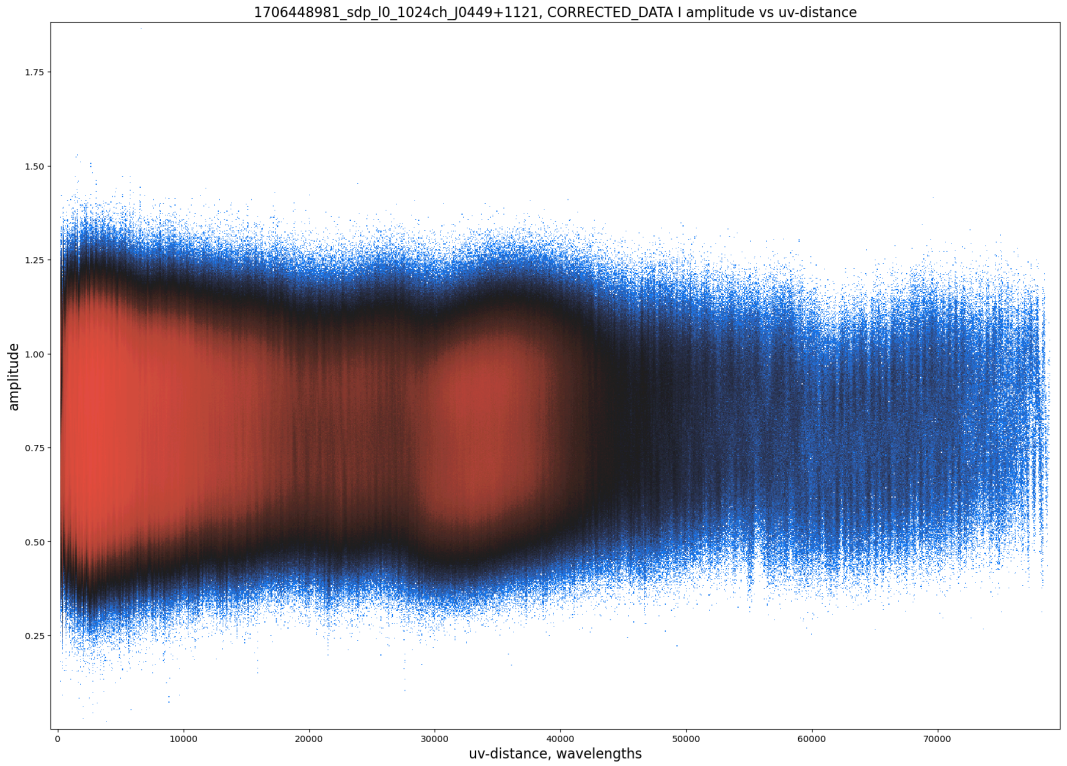
J0459+0229	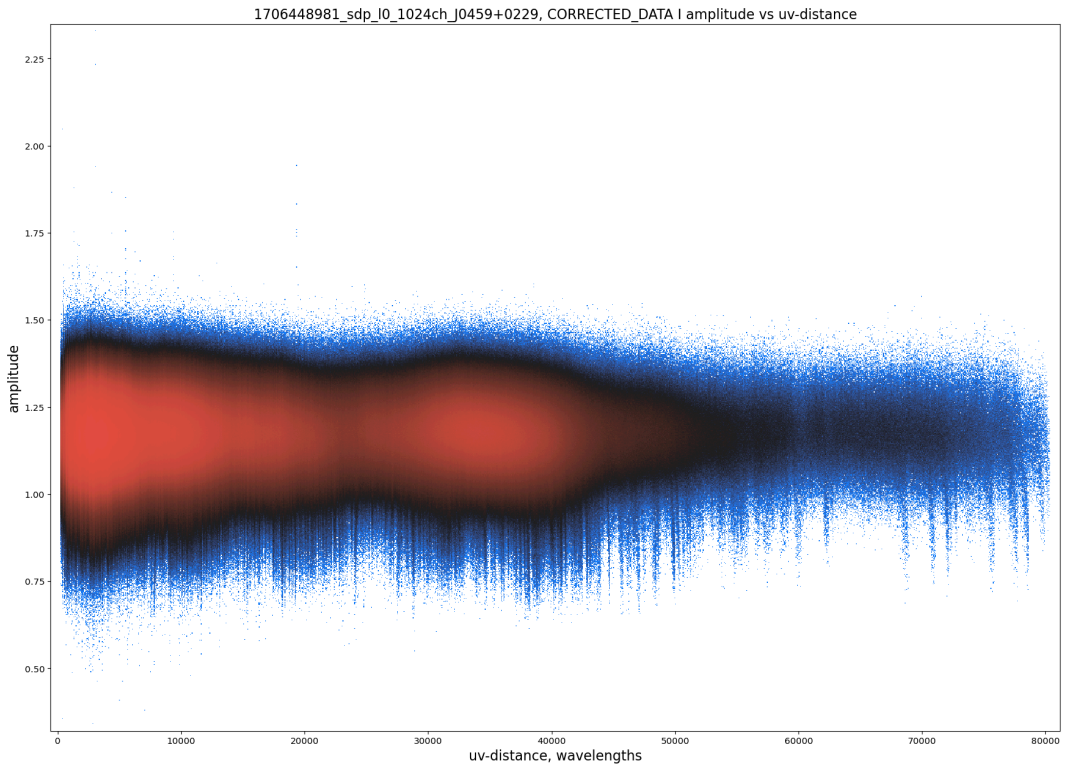

J0502+0609	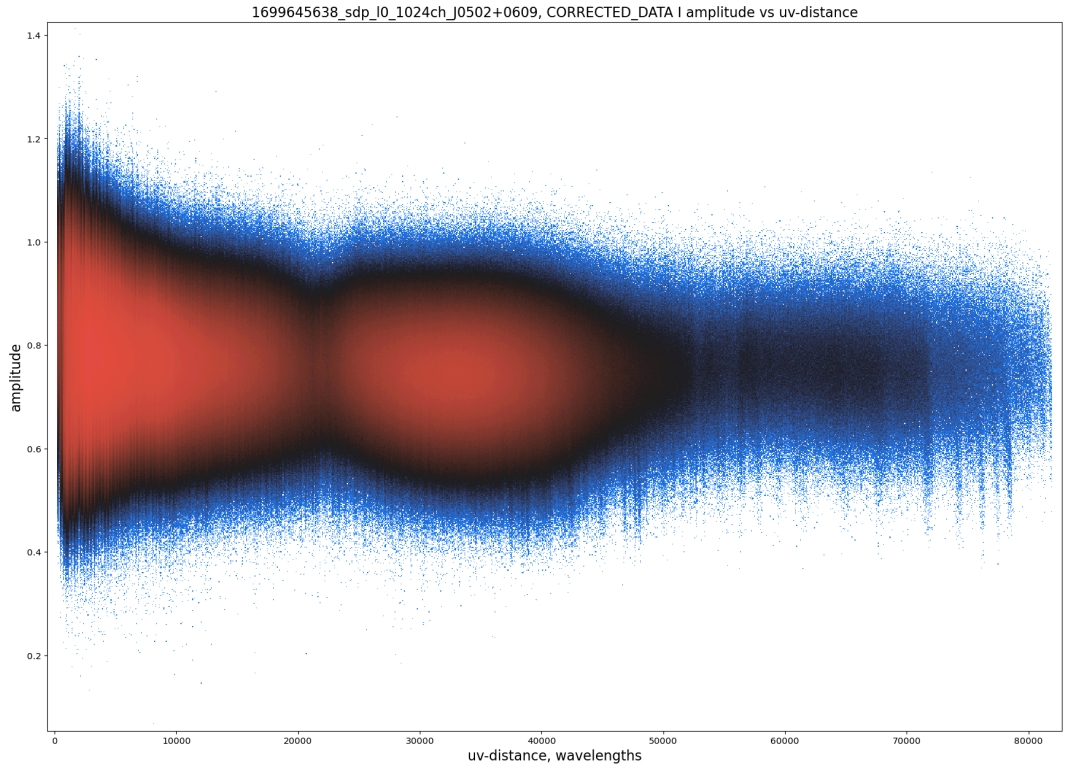
J0505+0459	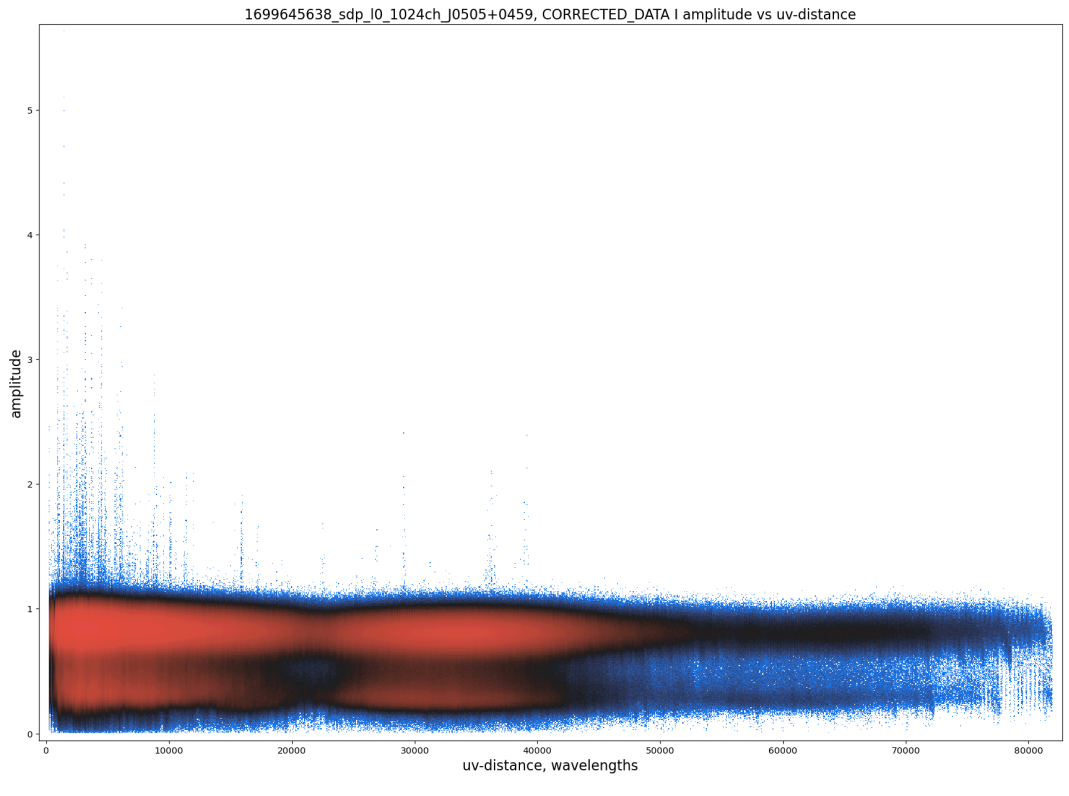

J0509 +0541	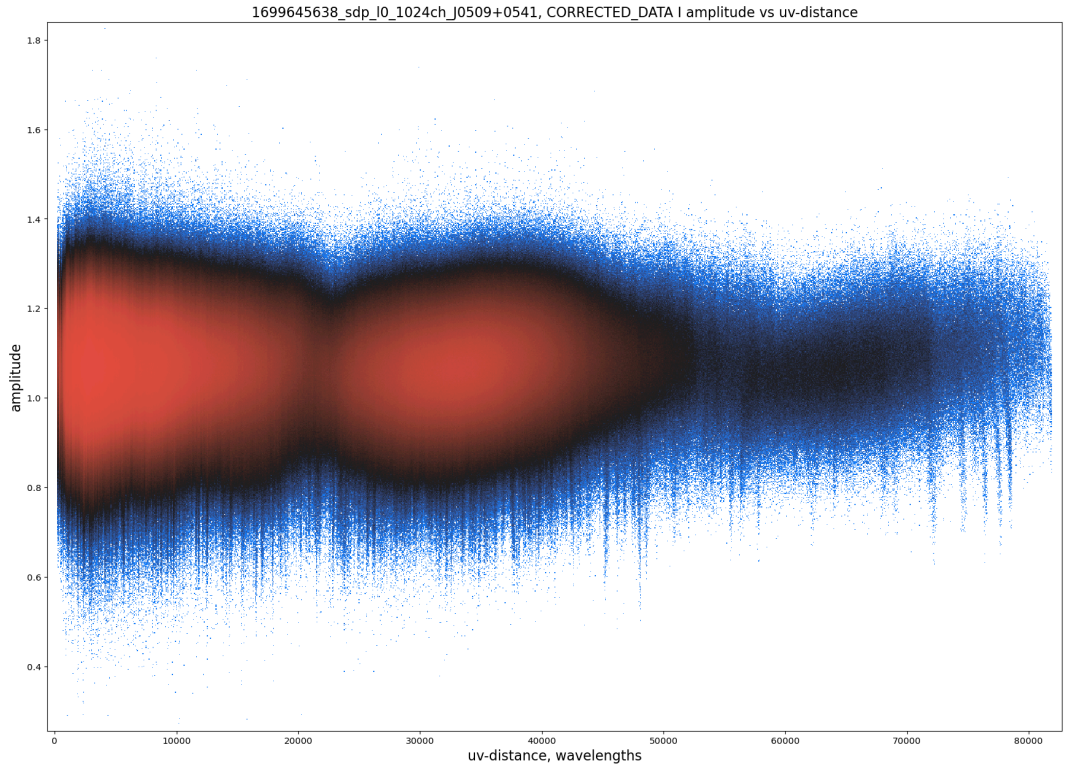
J0522+0113	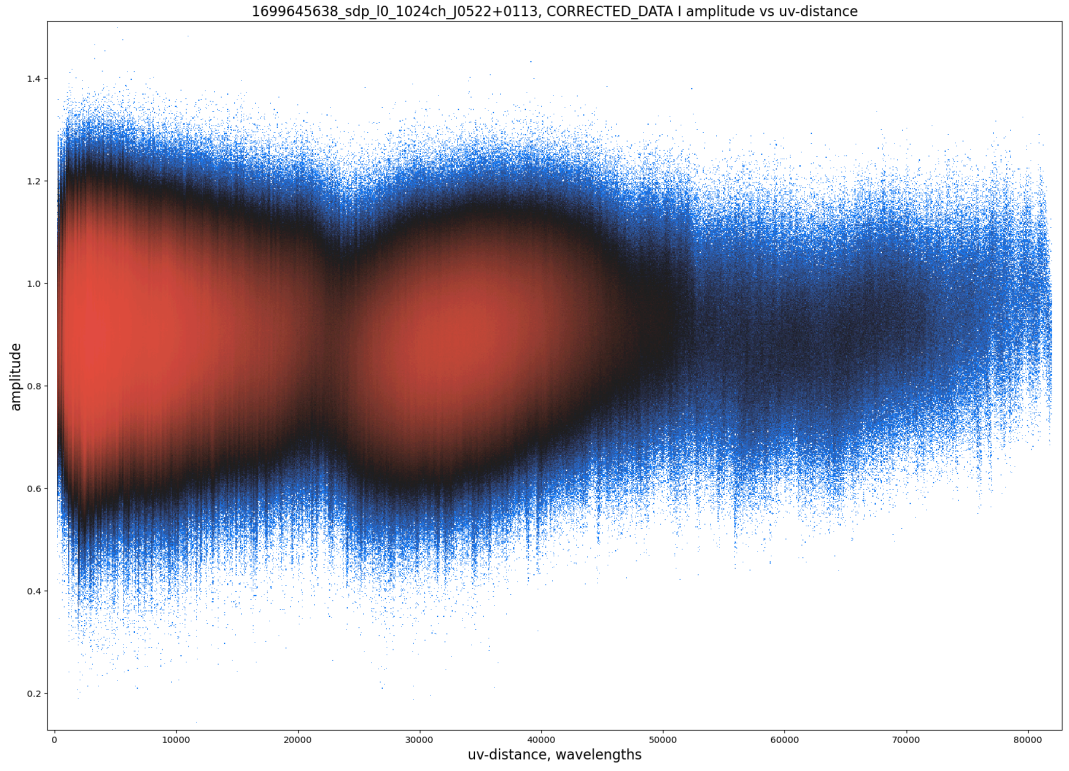

J0524-5658	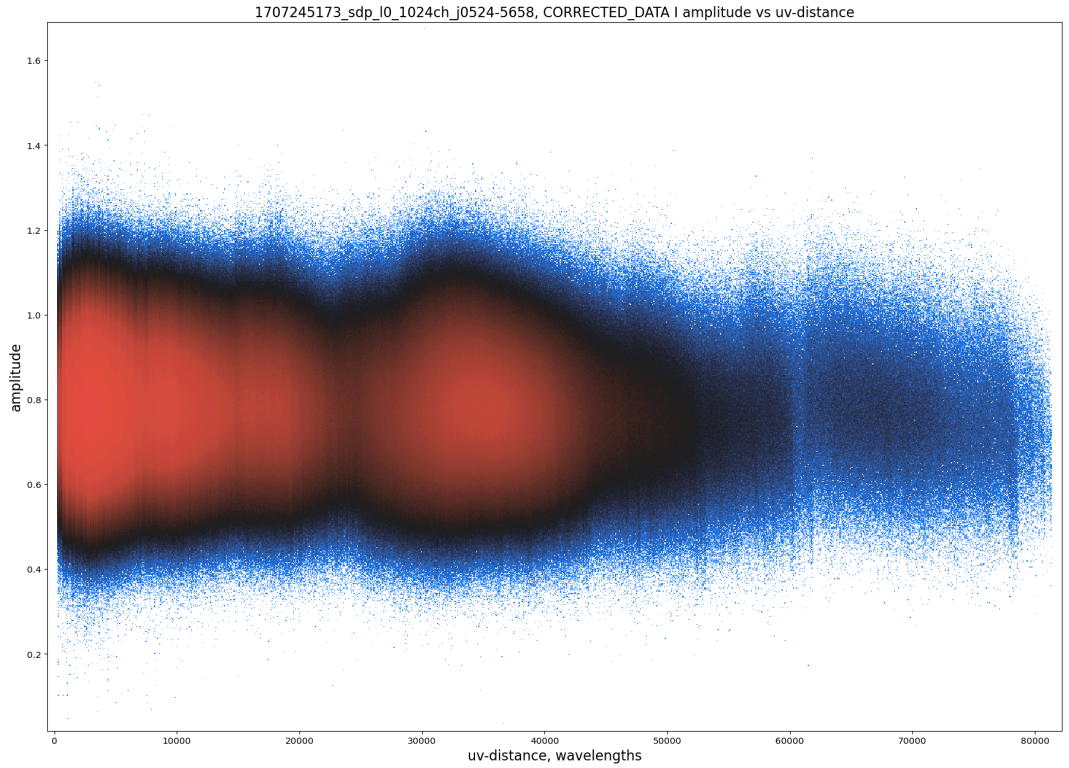
J0607-6031	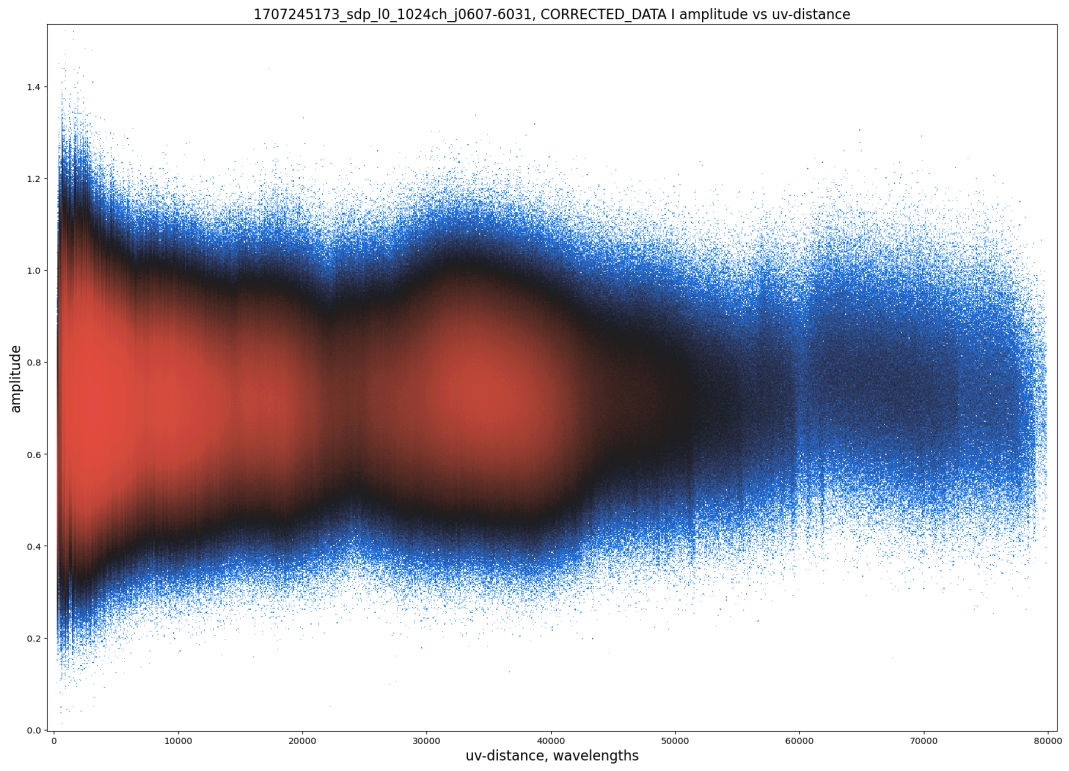

J0909 +0121	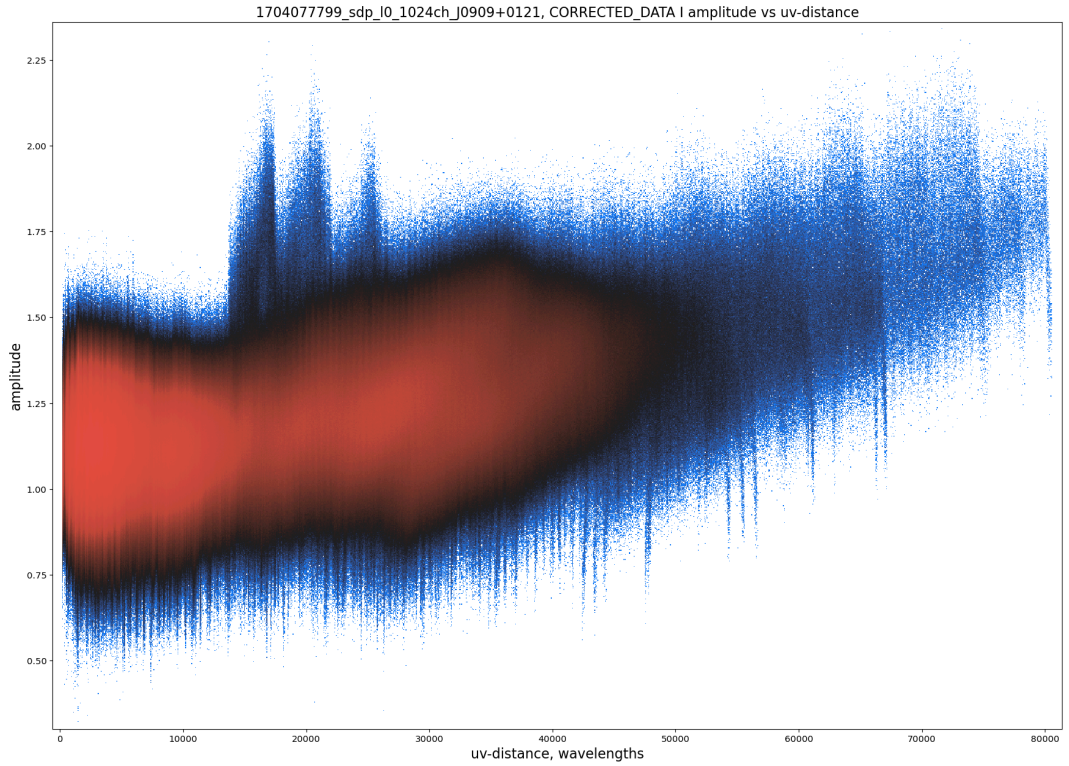
J0954 +1743	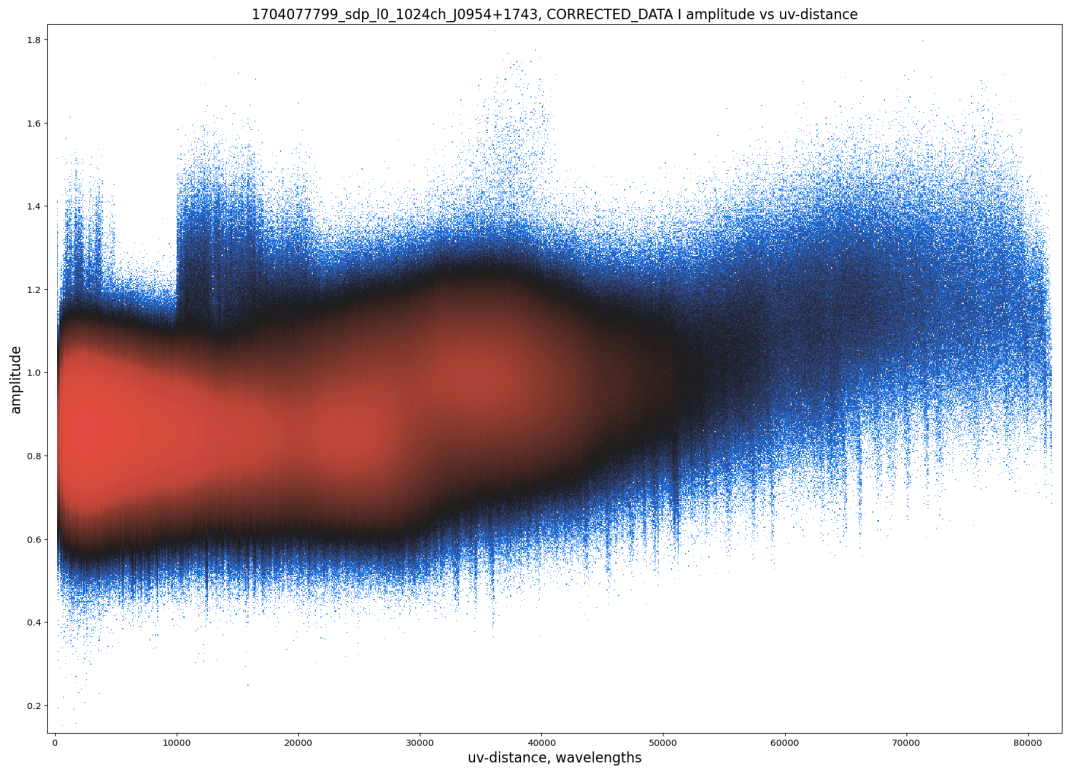

J1109 +3744	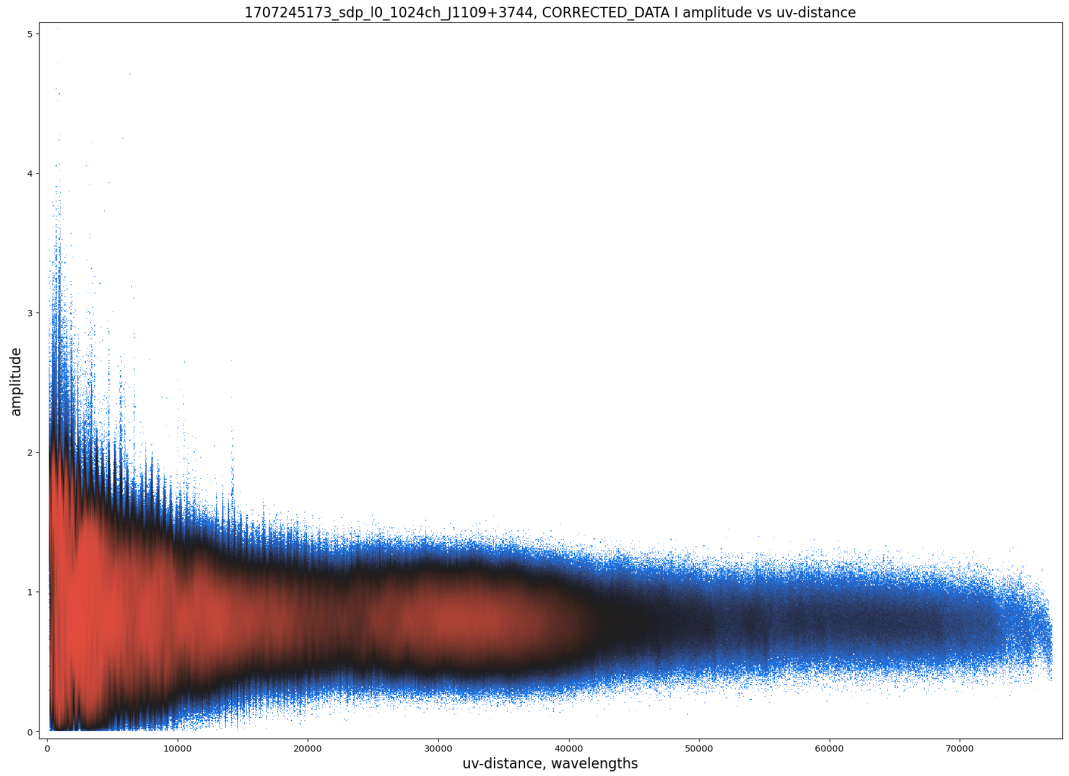
J1640 +1220	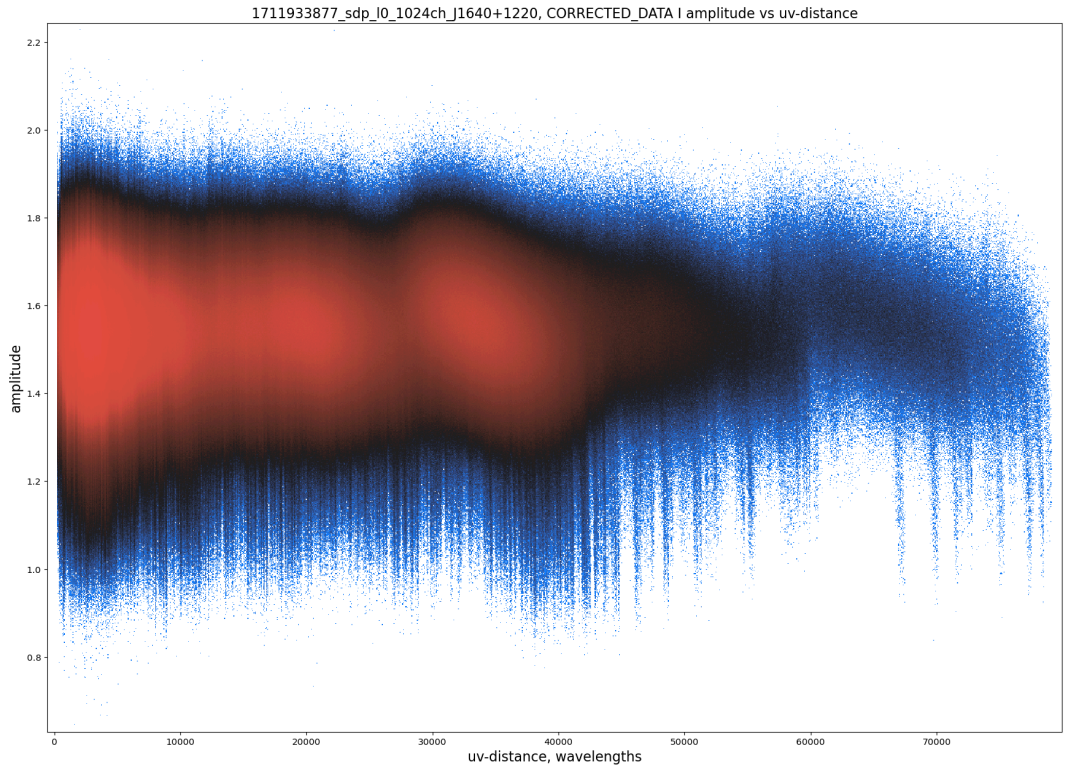

T0735 +2341	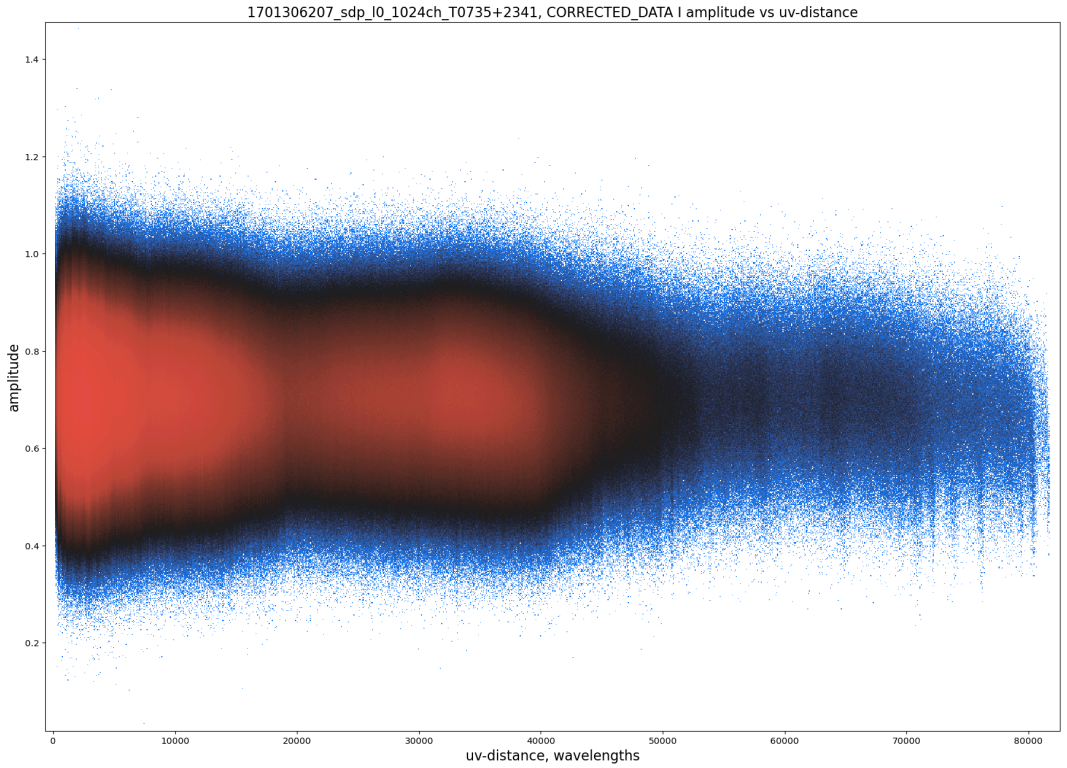
T0952 +2828	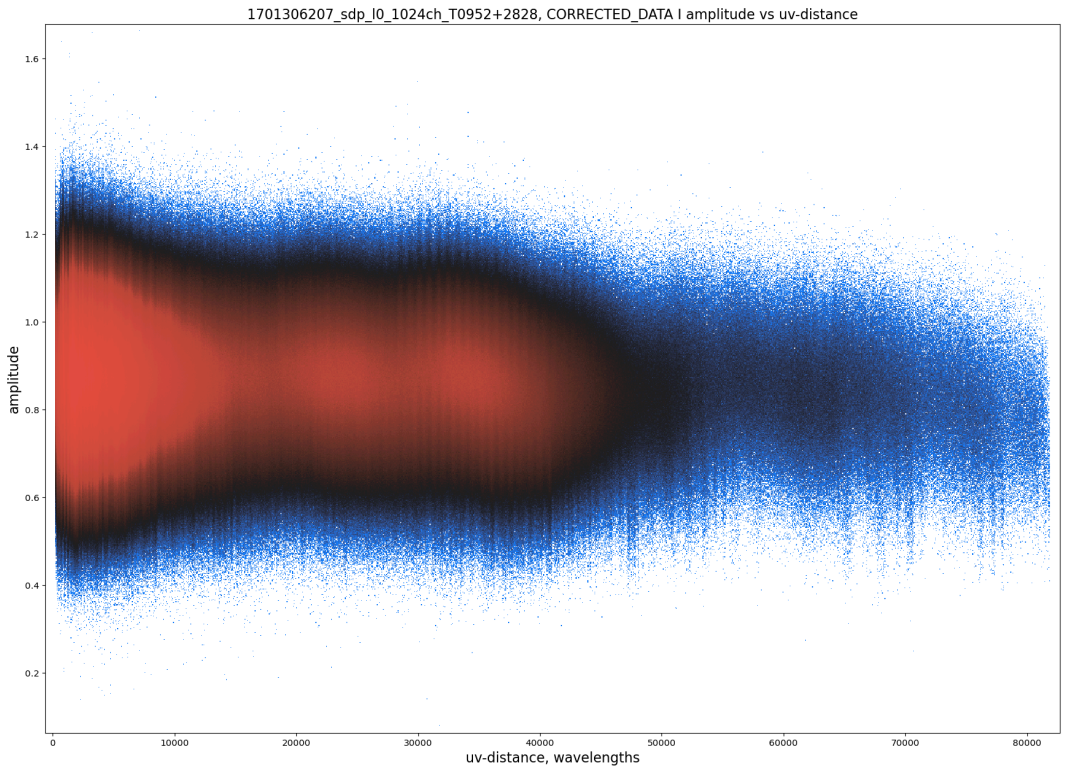

T1126+3345	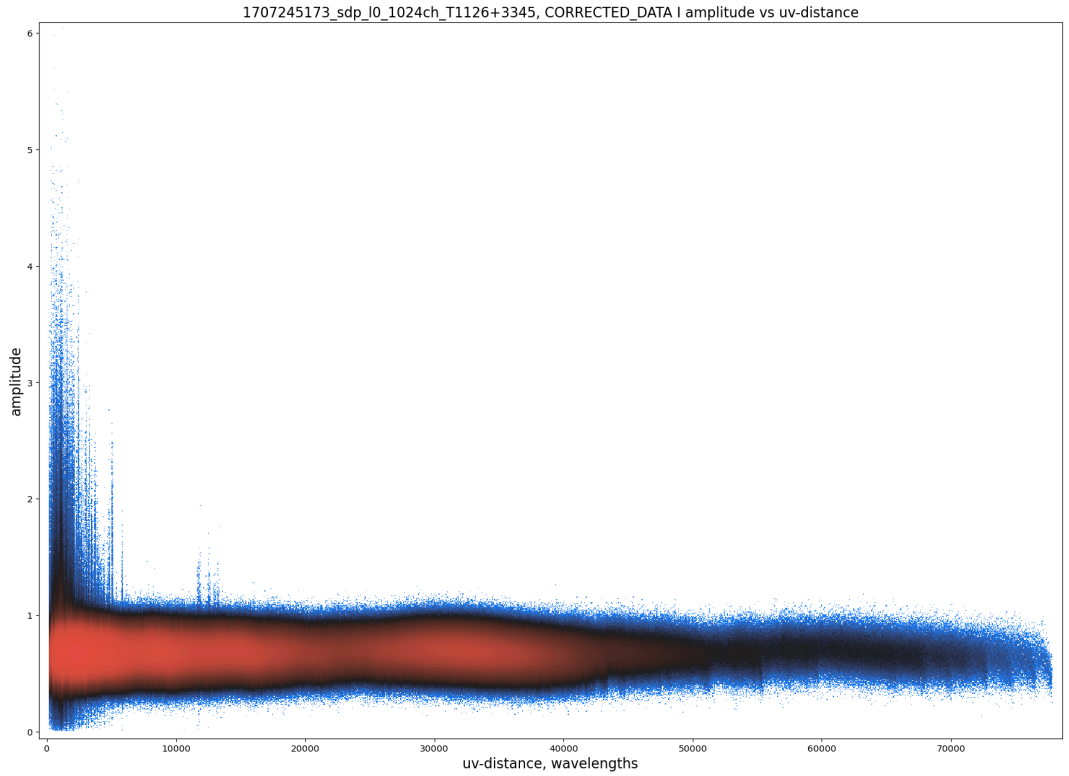
T1352+0232	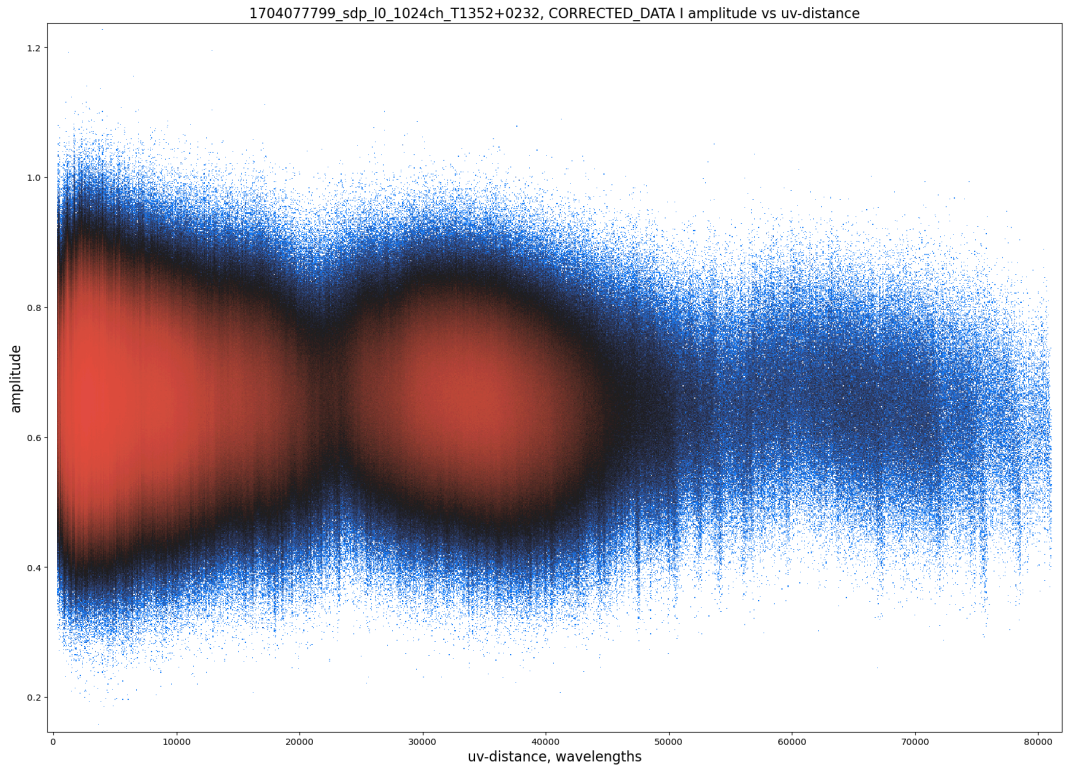

0010+174	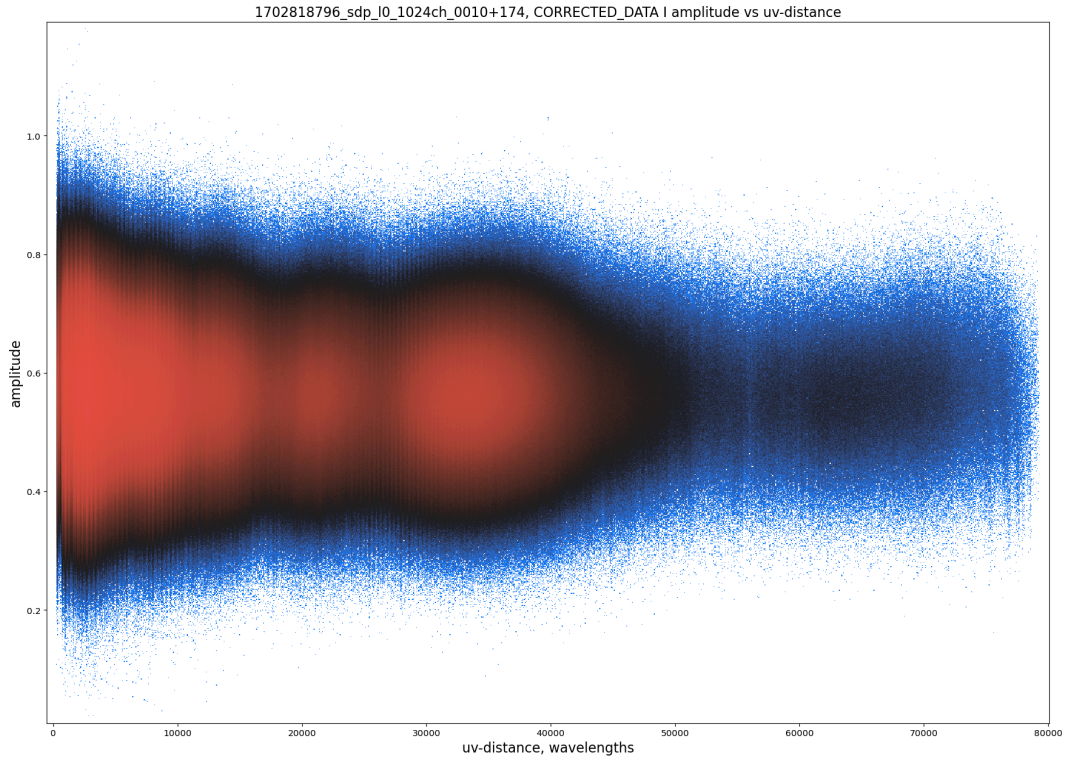
0110-076	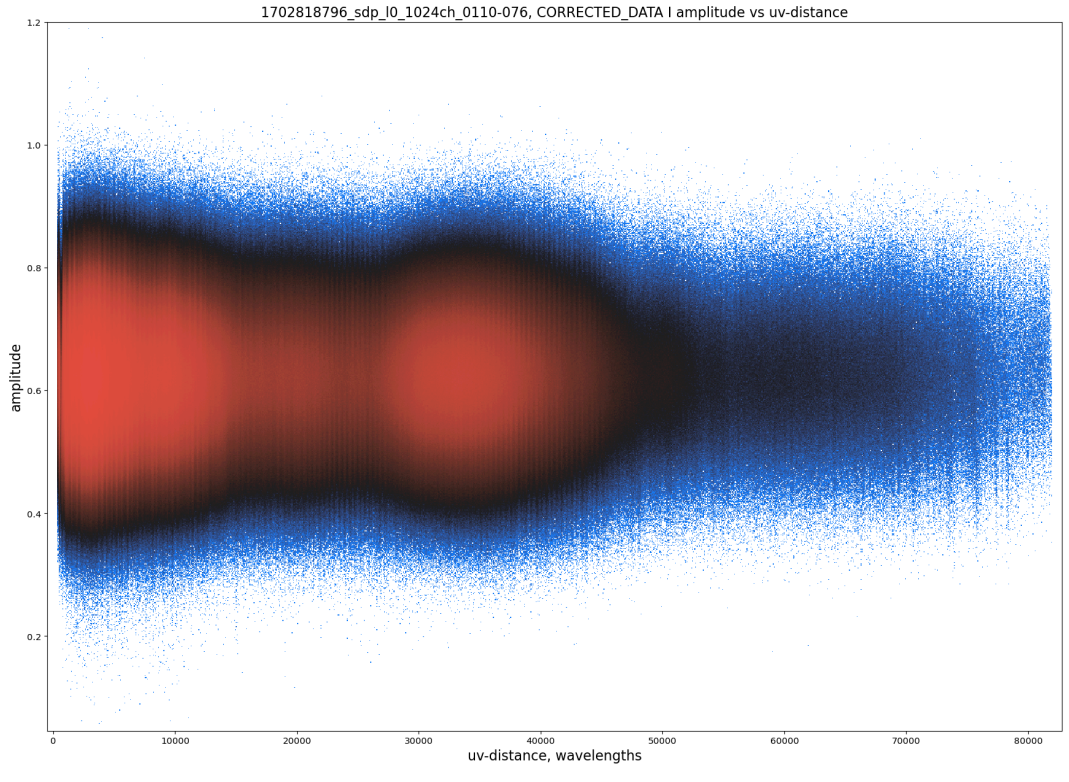

0219+0120	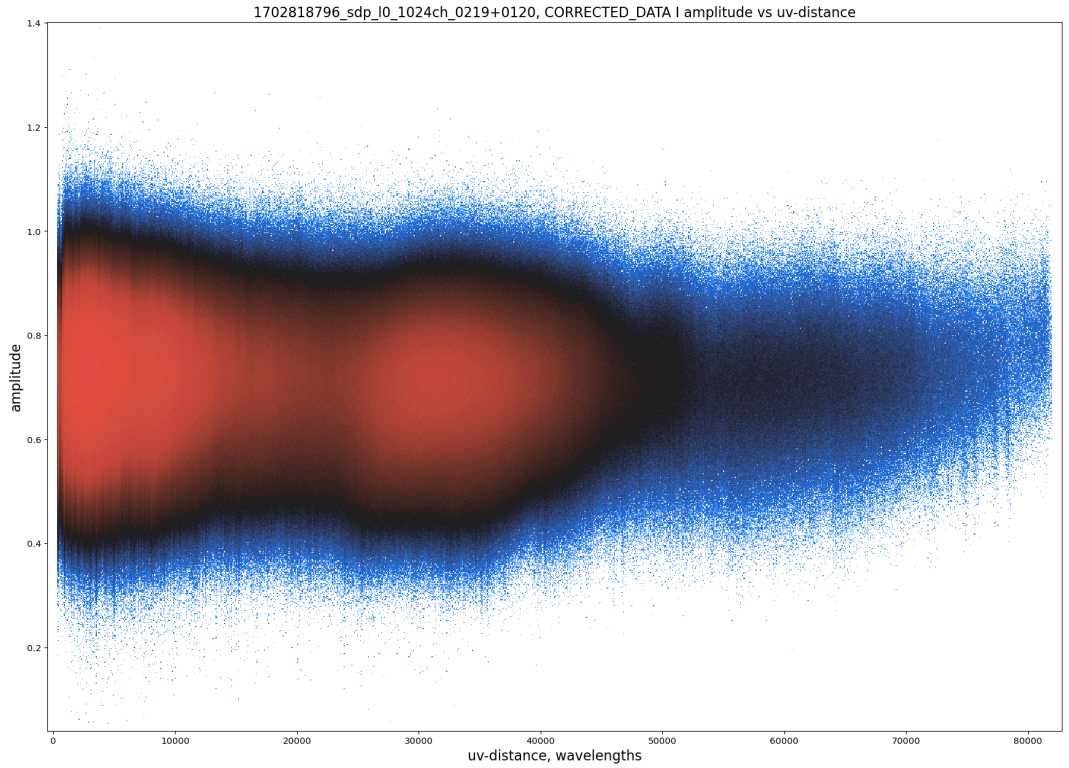
0249+0619	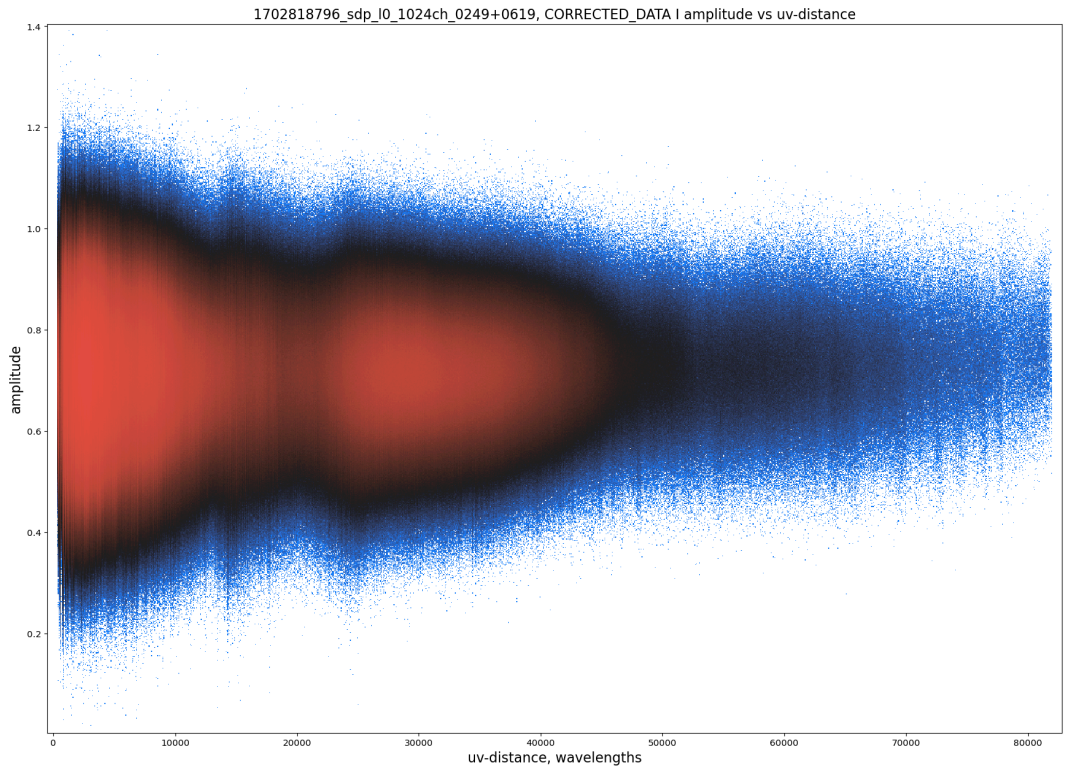

0259+0747	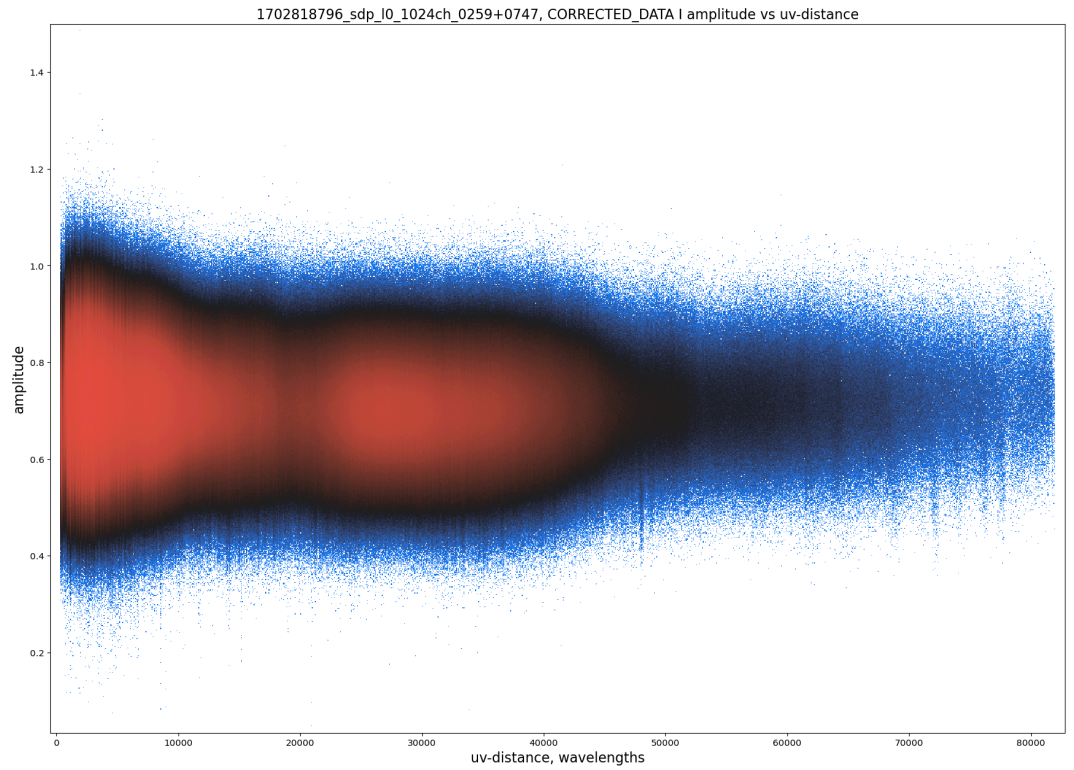
2138-246	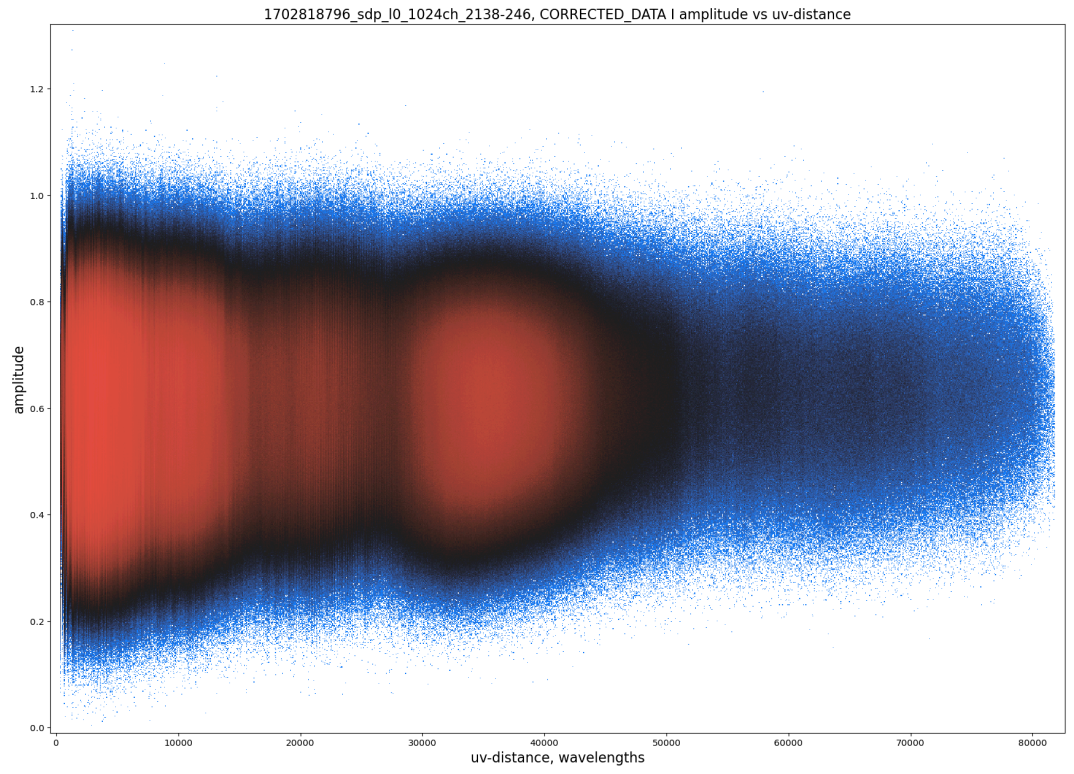

J0403+2600	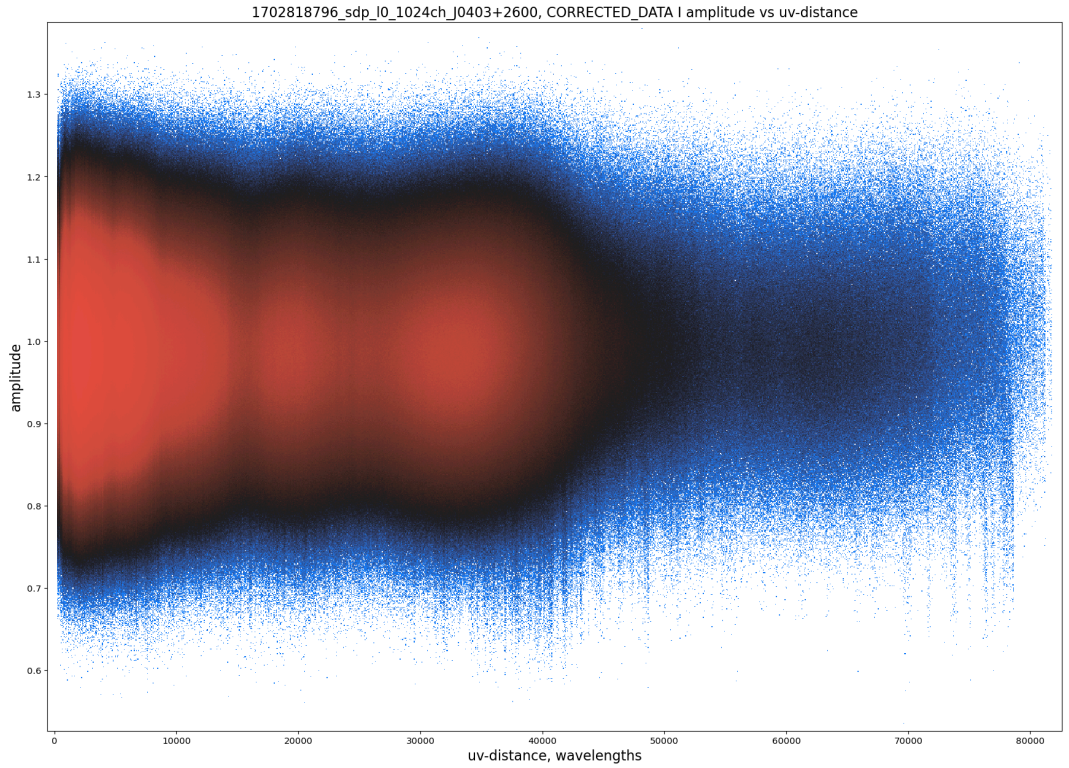
0647-475	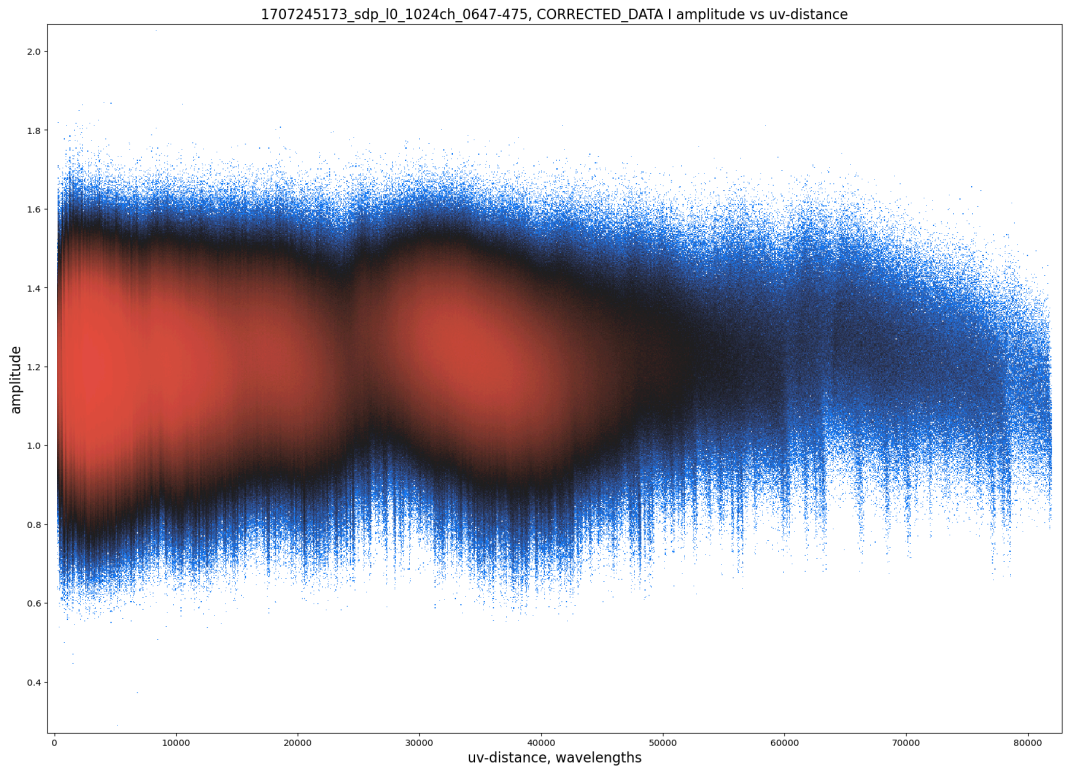

0731-465	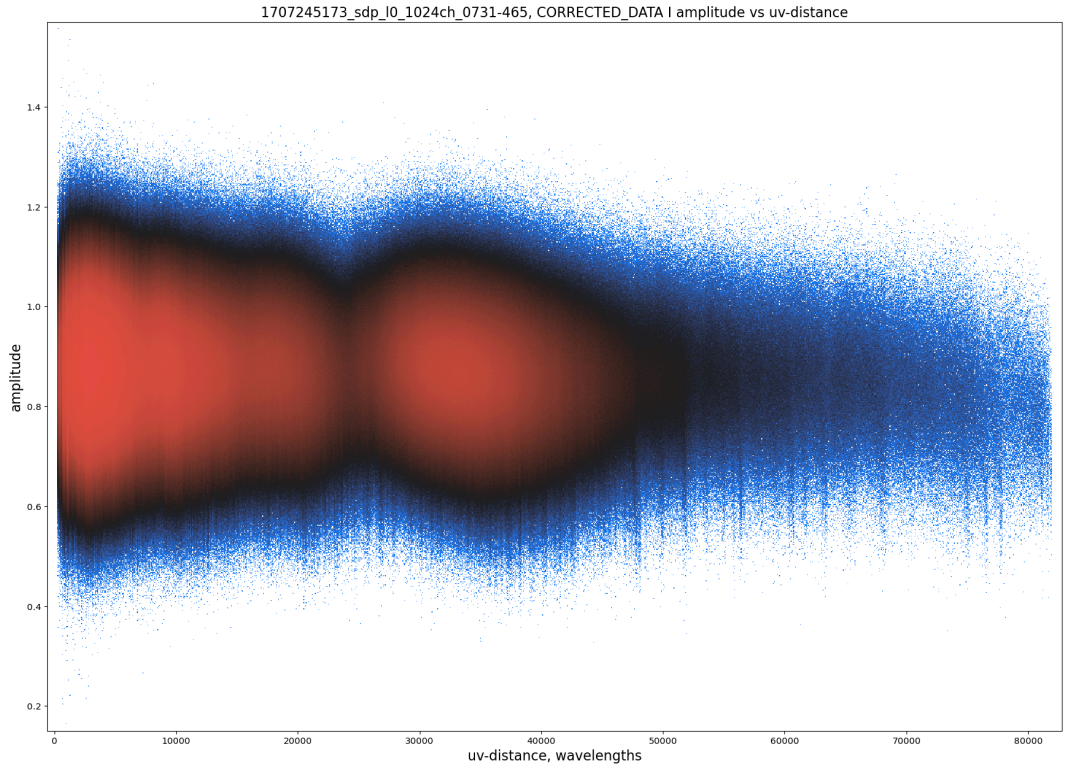
0906-47	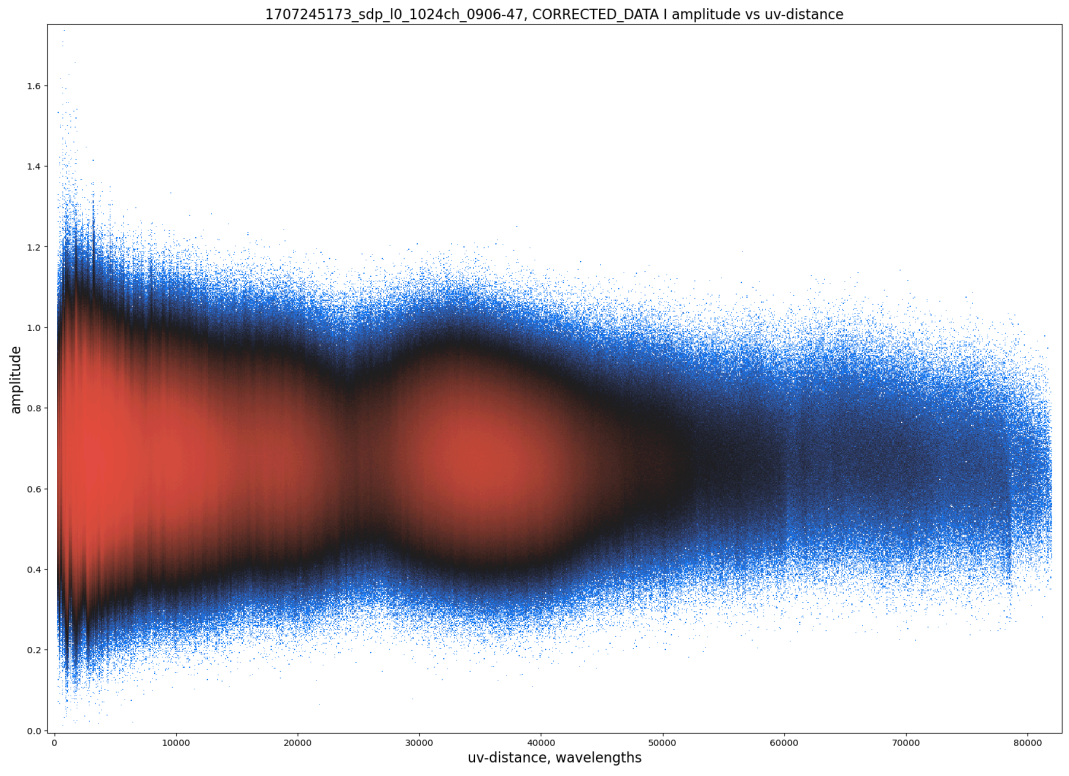

0906-682	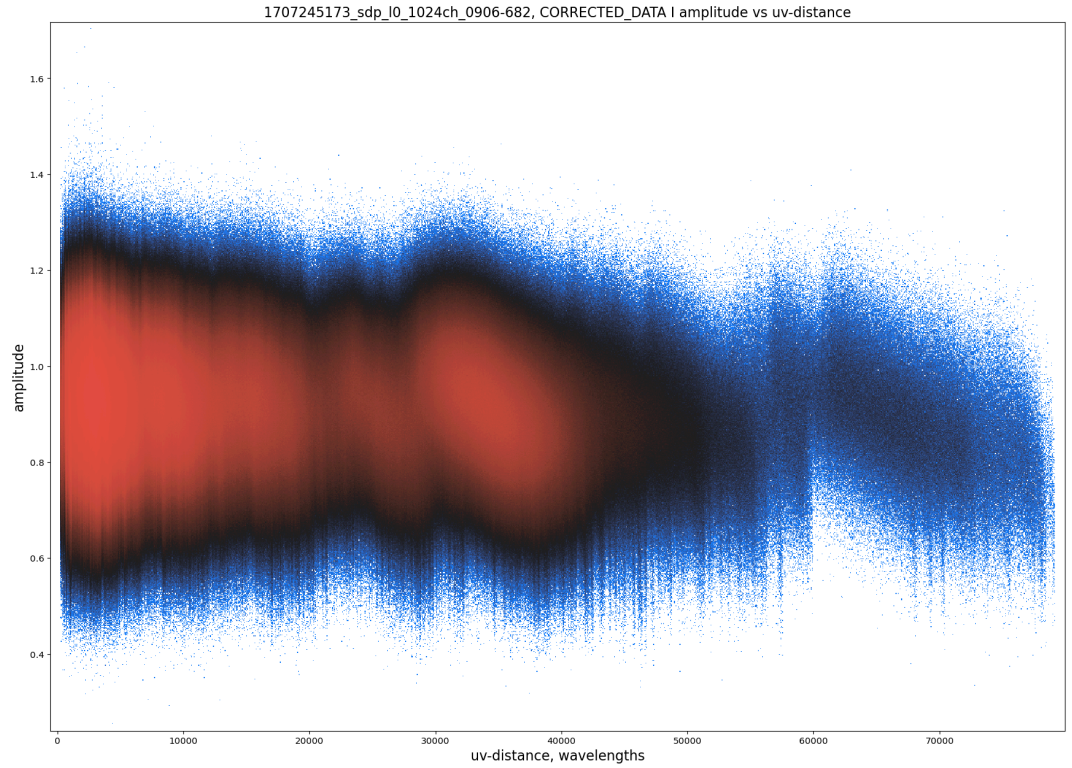
1534+015	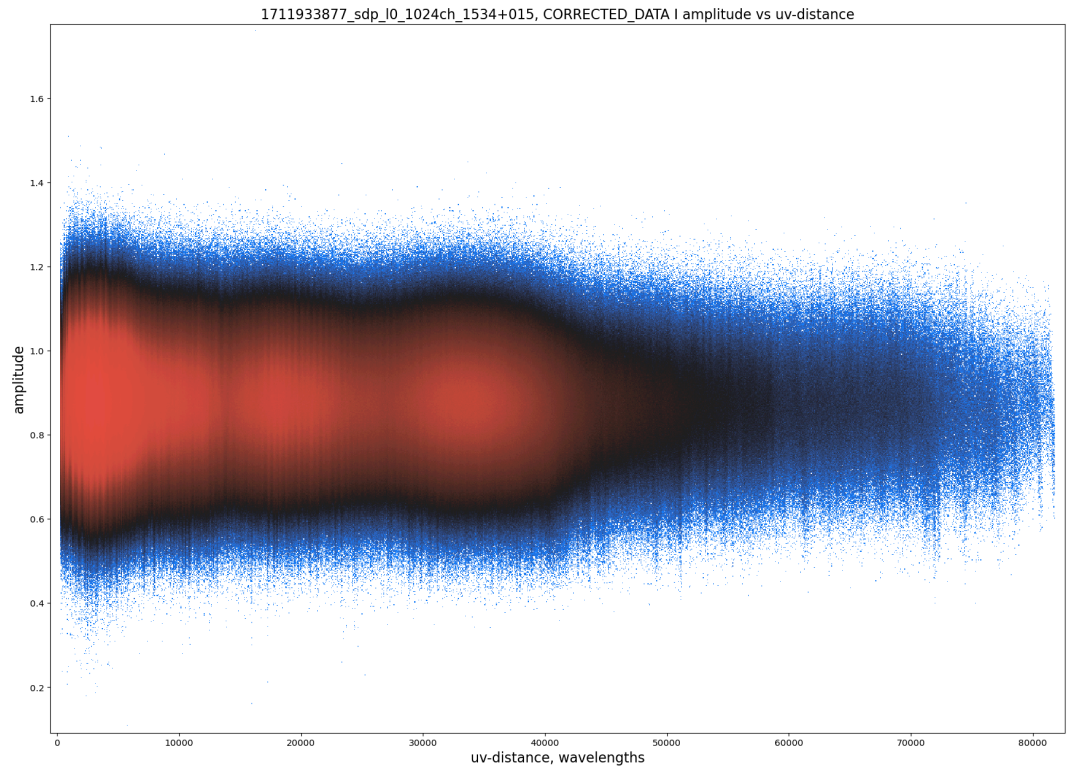

1553+129	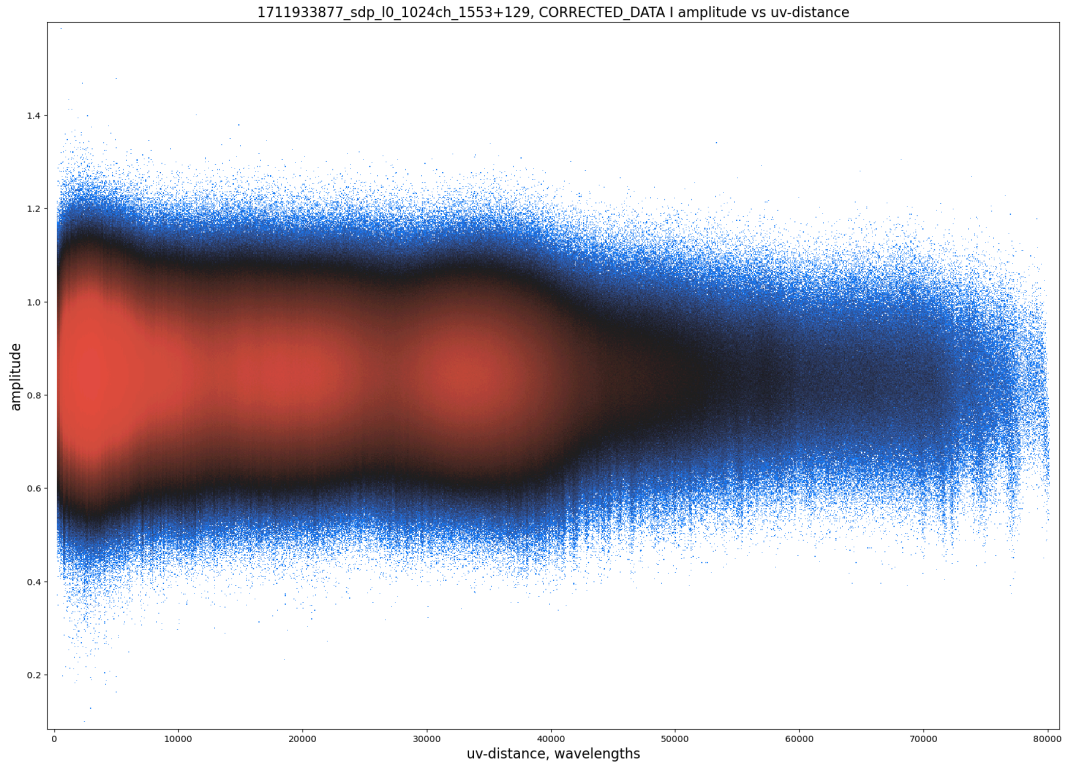
1658-076	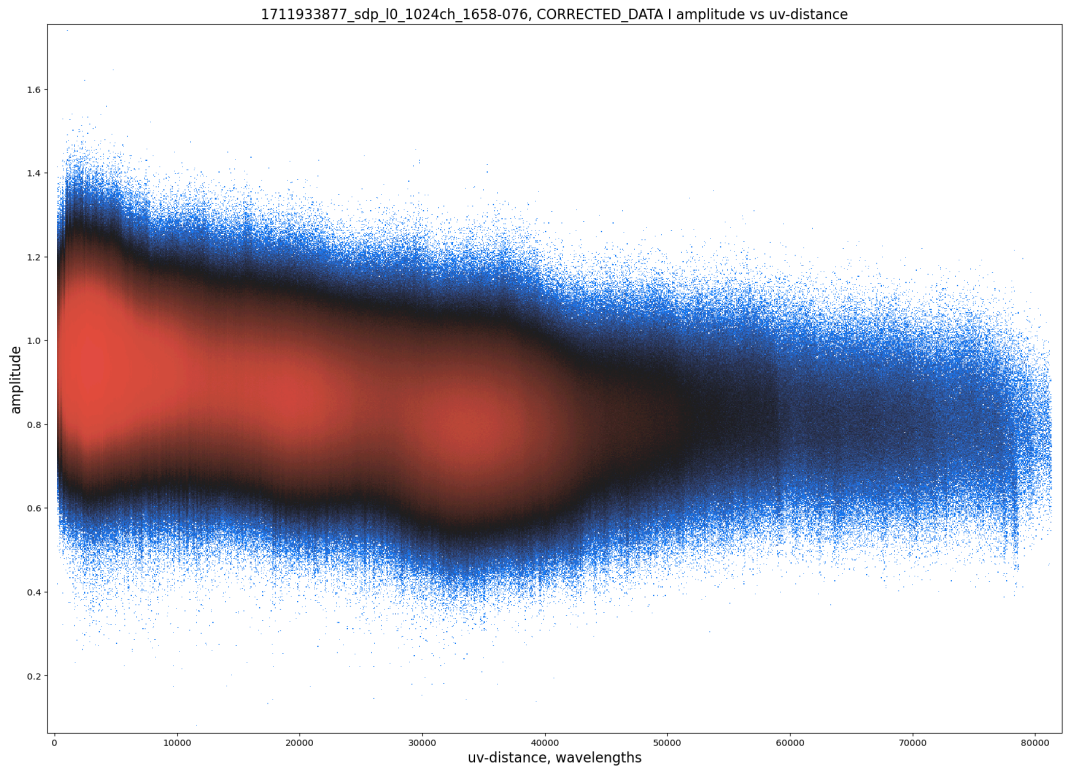

2129-156	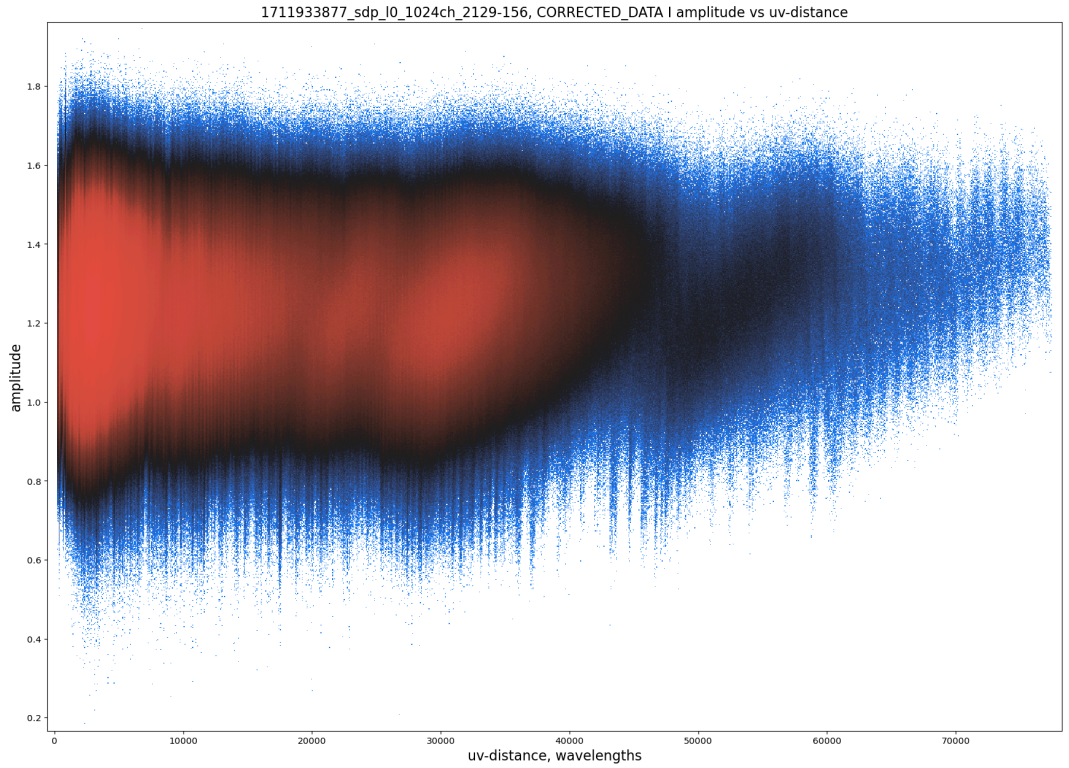
2129-183	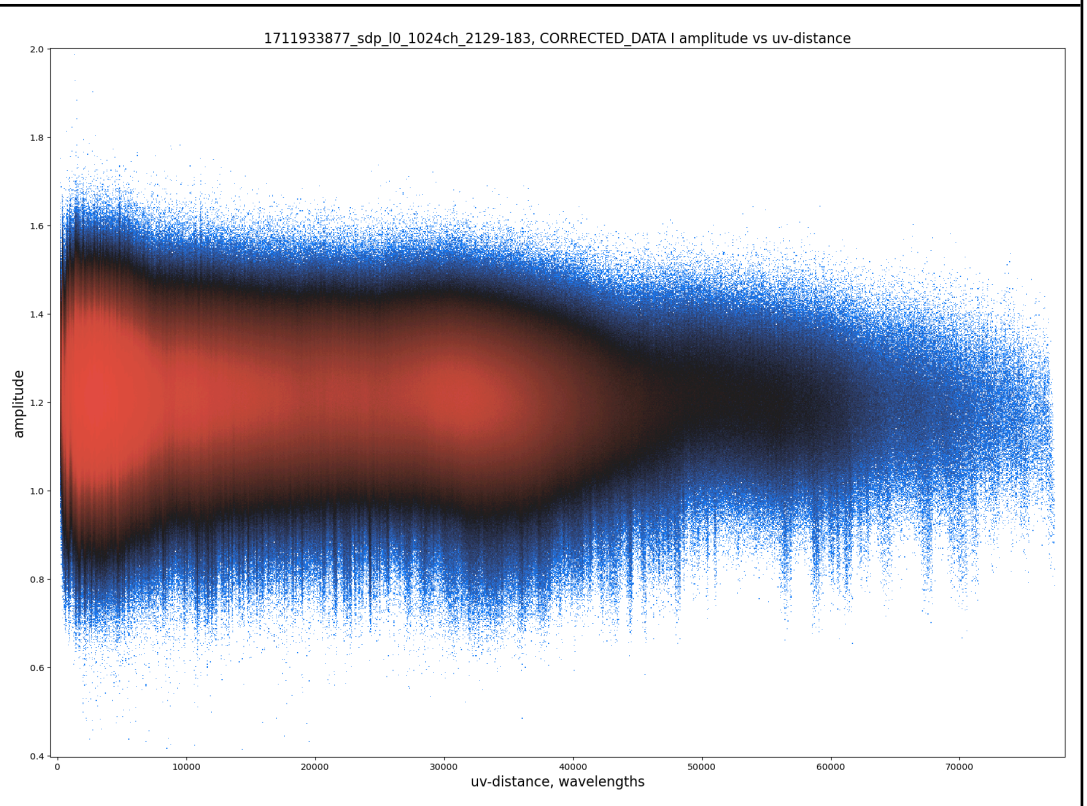

2255-087	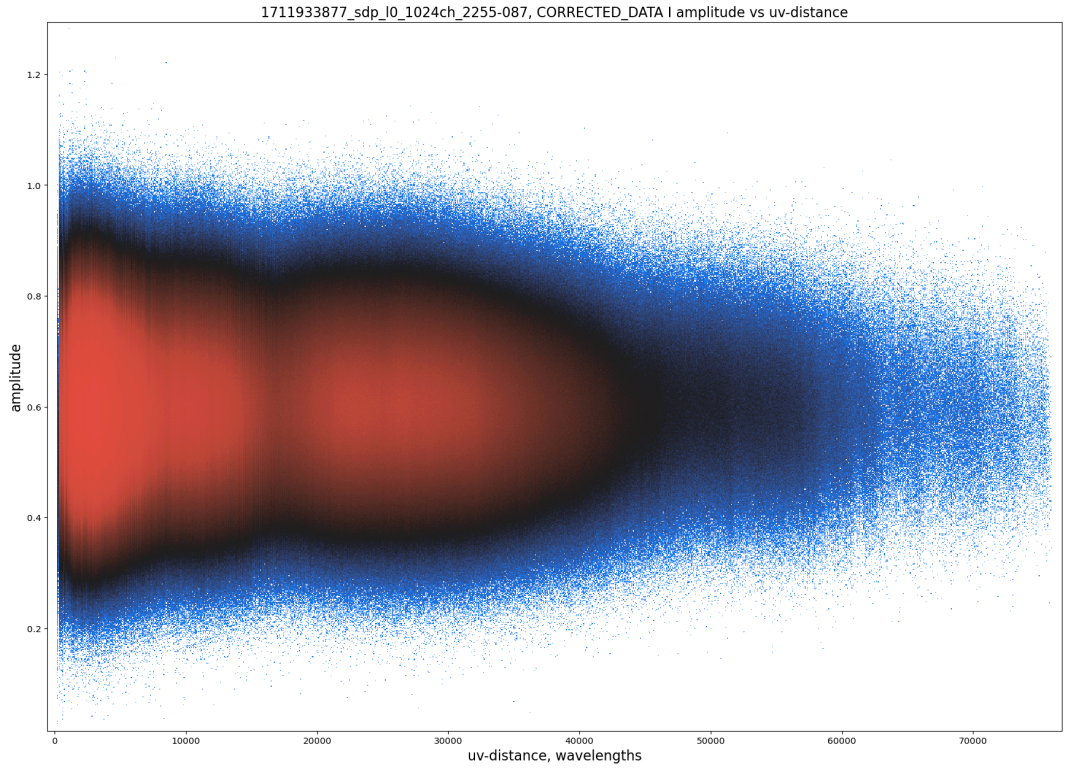
0214-522	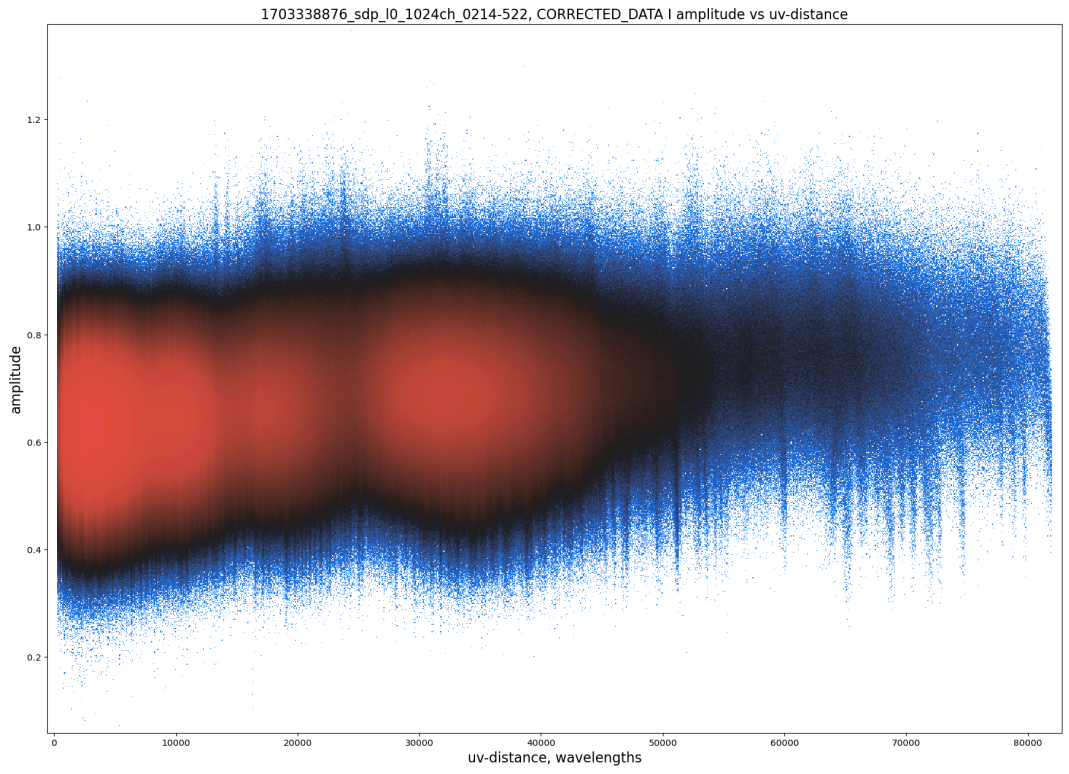

0407-658	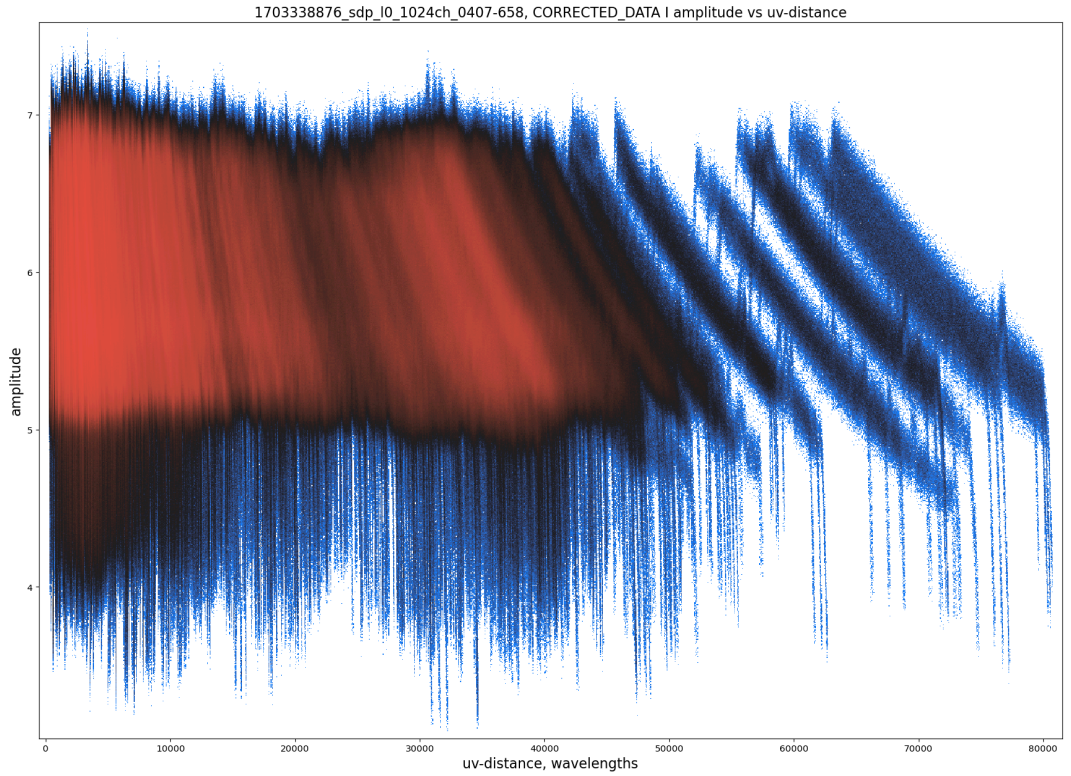
0606-795	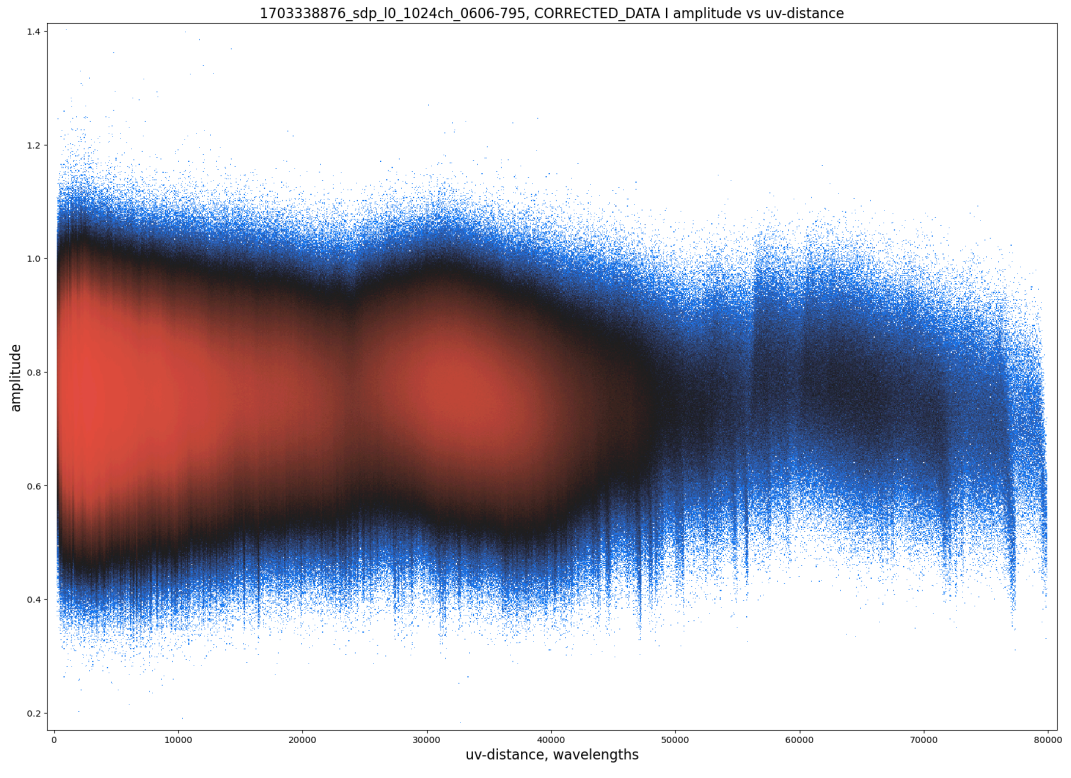

1949-199	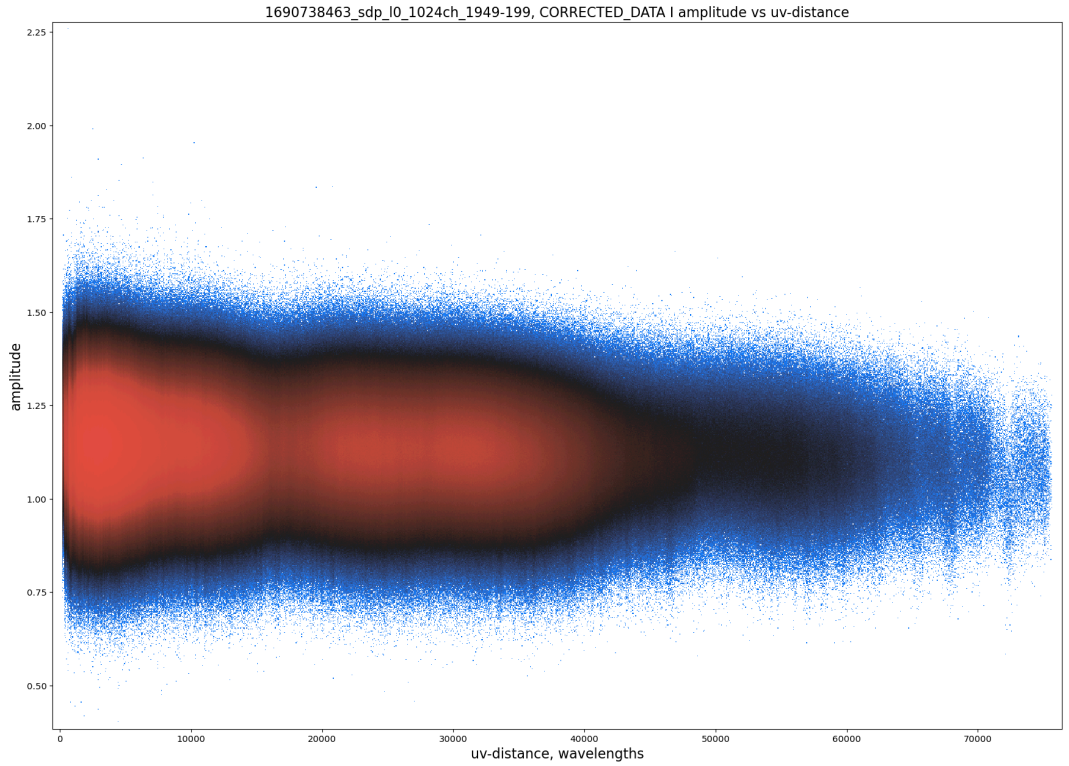
2007-445	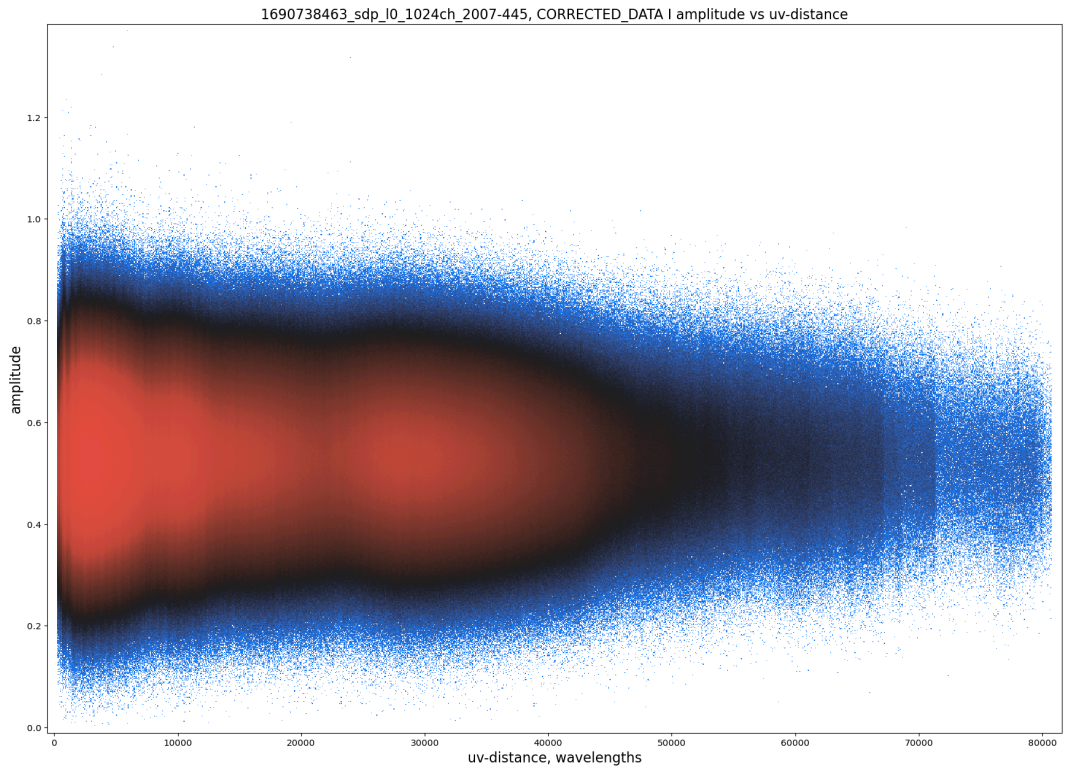

2047-026	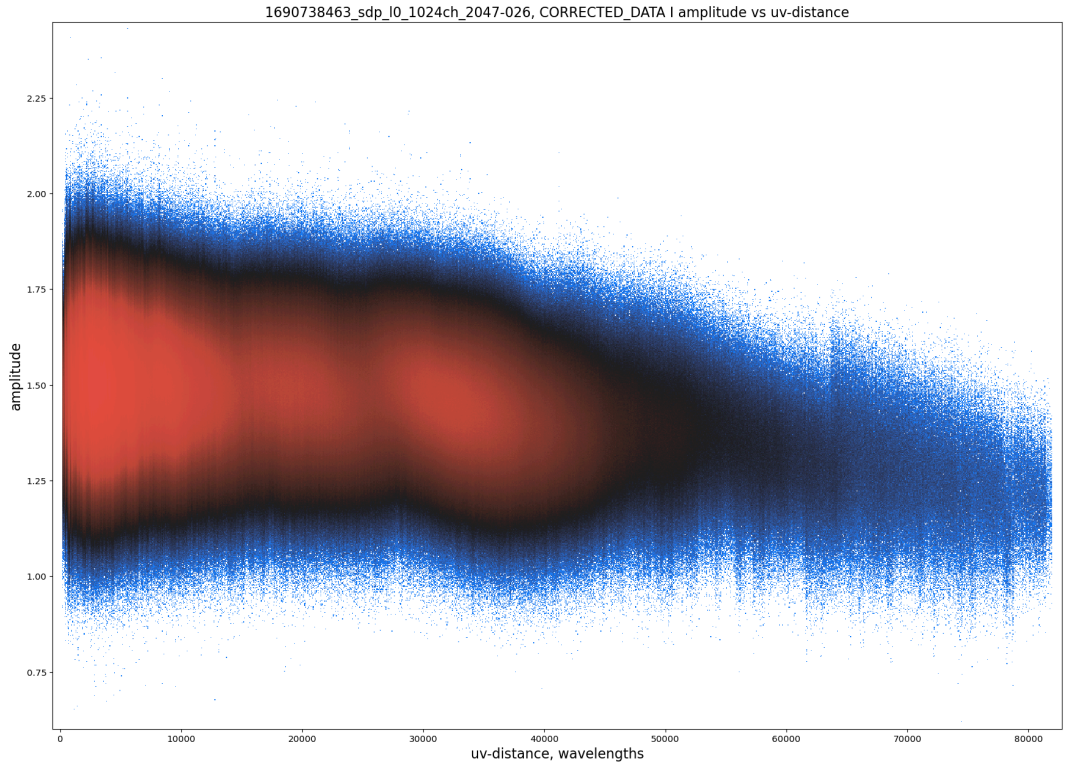
2052-474	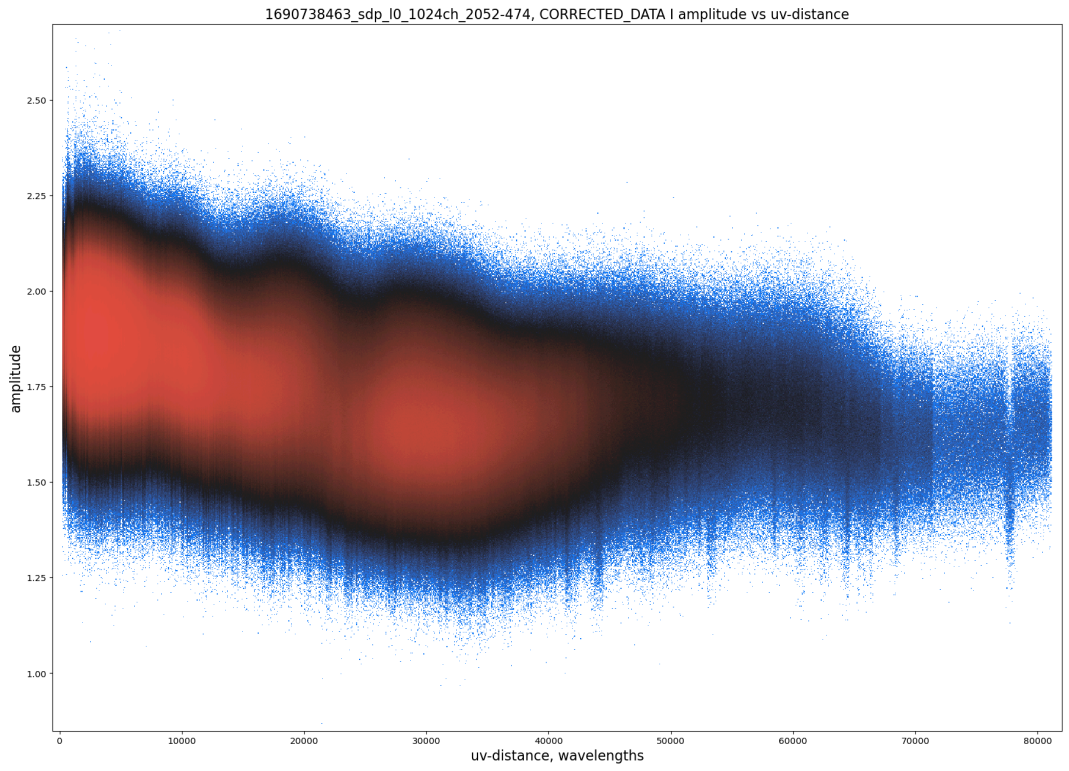

2110-103	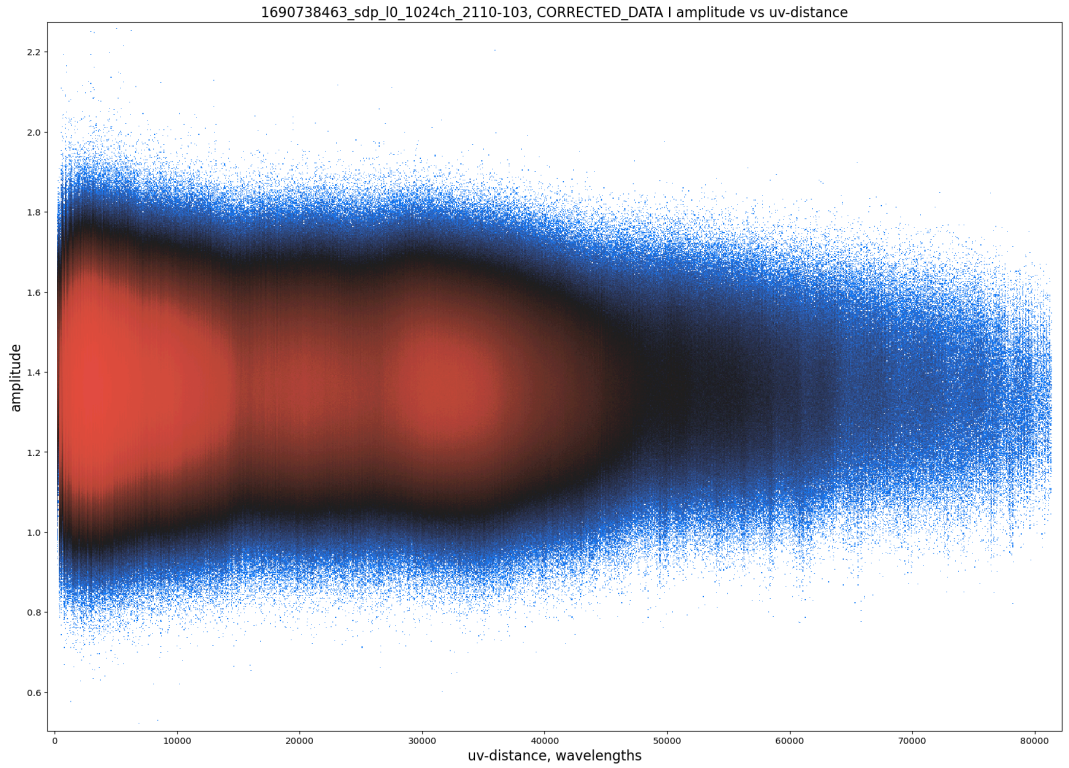
1145-071	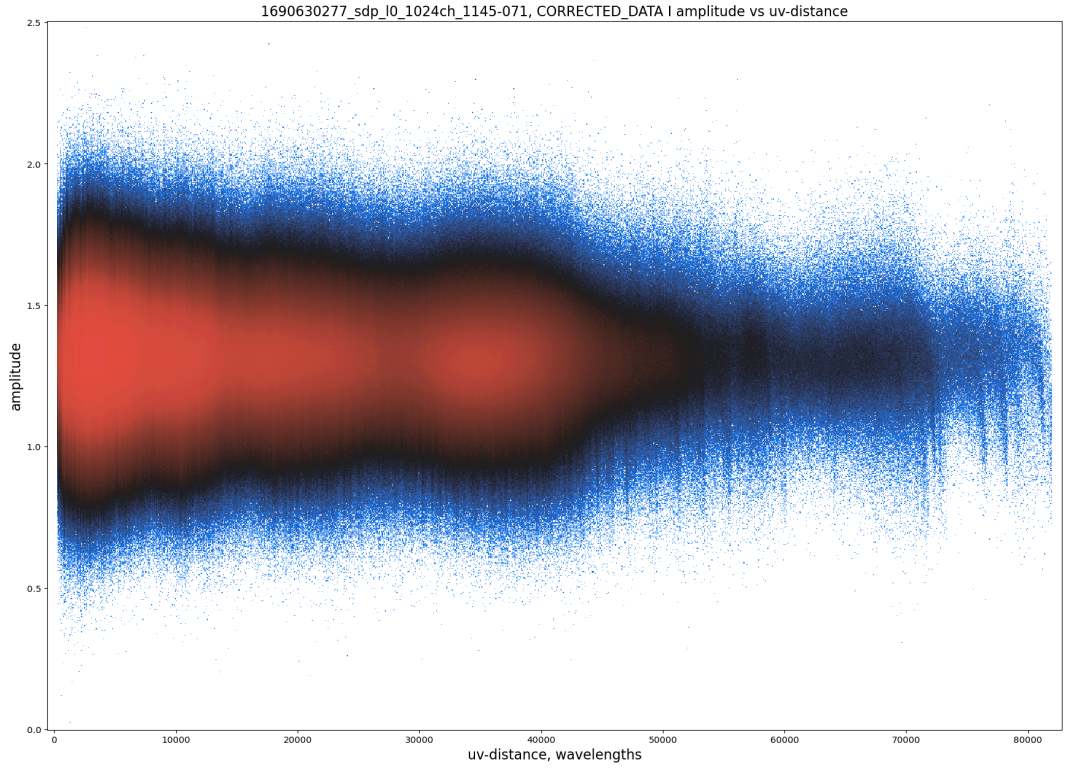

3.4: CLOSURE QUANTITIES

Closure quantities include amplitude and phase. The closure phase is the sum of the measured phases around a triangle (see Figure 1) of baselines connecting three antennas. Mathematically, it is the phase difference between signals on three baselines, and it cancels out any antenna-based phase errors. A sum of three phases around a closed triangle of baselines can be observed by an interferometer and is not affected by telescope phase shifts introduced by atmosphere or optics. Closure phase is a robust observable, useful in self-calibration and improving image quality, especially when phase calibration is difficult or noisy. It also provides accurate information about the source structure, crucial for resolving complex or faint objects.

For a point source at the centre of the field of view, the phase closure should be close to zero as the individual true phases should be zero. If the closure phase is not equal to zero, it can indicate several important aspects regarding the observed source or the data quality in a radio interferometer. Firstly, it could indicate a complex structure rather than a point source. Secondly, it may indicate the presence of interfering sources or background emission affecting the image. However, it's good to note that in the presence of noise, this will never be perfect but it should be close.

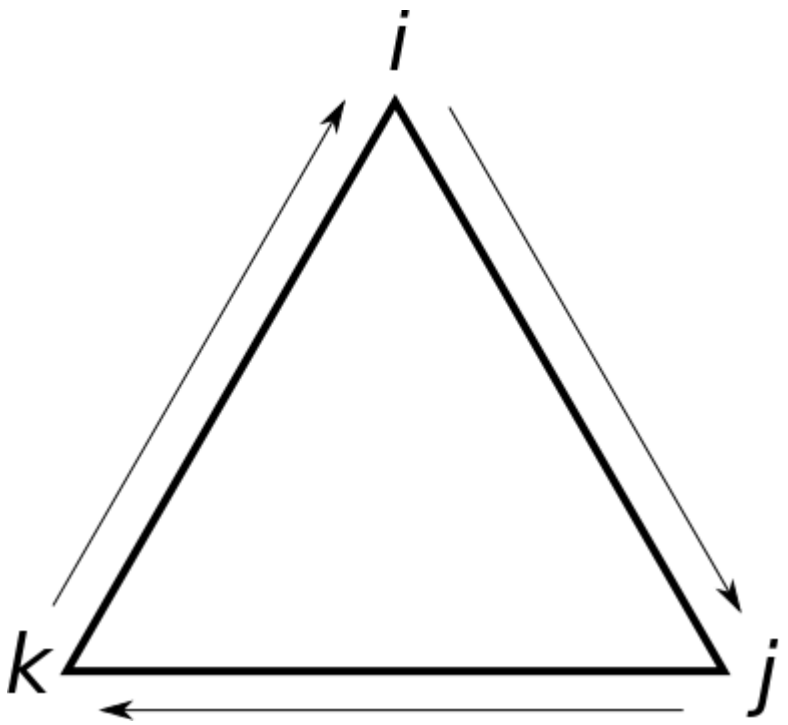

Figure 2: A closure quantity triangle

The closure amplitude is the ratio of amplitudes measured on four baselines that connect four antennas and ideally a constant value that reflects the intrinsic brightness of the astronomical

source. Like the closure phase, it eliminates antenna-specific amplitude errors by comparing the amplitudes between baselines. The measurement removes errors due to antenna gain variations, providing a reliable measure of the source's intrinsic brightness.

For a point source with a known brightness or flux density, the expected closure amplitude should ideally reflect this intrinsic property of the source. In a perfect observational scenario, the expected closure amplitude would be constant across different sets of triangles of baselines if the source remains stable over time and proportional to the flux density of the source being observed, meaning that stronger sources will generally yield higher closure amplitudes. If the source itself changes over time (e.g., due to variability in brightness), the expected closure amplitude may not hold.

For most arrays, phase closure should be less than 2 degrees and amplitude closure should be less than two percent (Fomalont et. al. 1999). However, when applied to point sources, the phase closure should be zero and the amplitude closure unity (Thompson et al. 2017).

Both quantities are determined against time for short and long baselines.
Closure quantities of the measurement files containing these sources were determined using CASA task closure (https://github.com/onsala-space-observatory/closures). These quantities were determined between three antennas, e.g., m001, m033 and m49. Running the closure task with a reference antenna then forms a closure triangle for all the antennas used in the observation. These antennas were selected based on their positions within the MeerKAT array shown below.

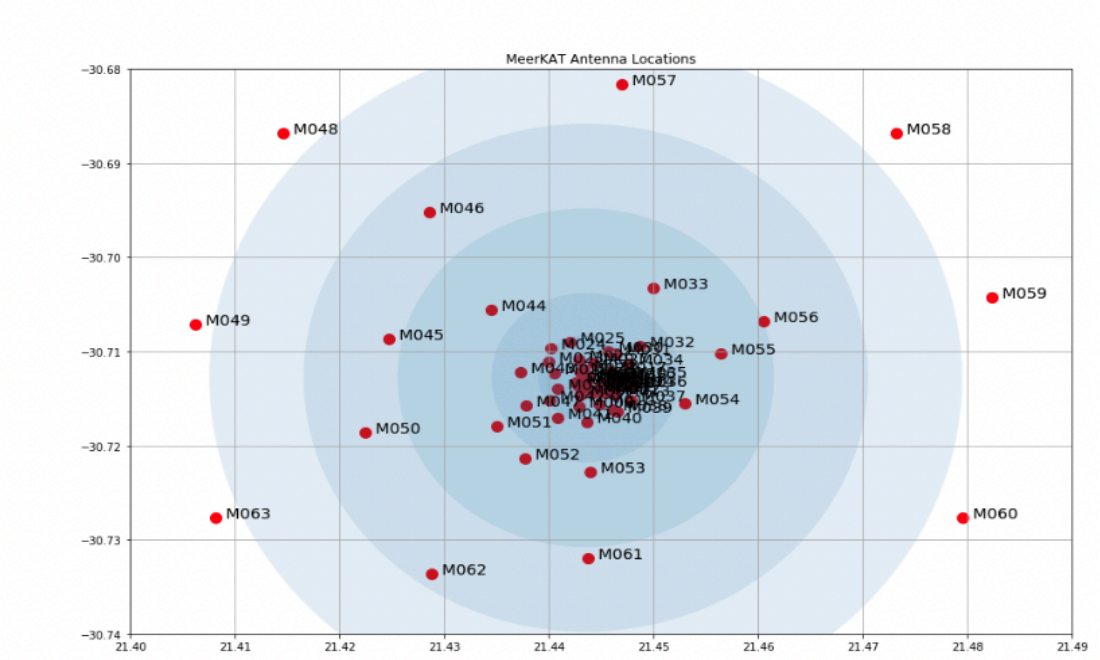

Figure 3: MeerKAT array layout

If several baselines show significant closure quantities using different calibrator sources, then the complex gain is different from unity and closure corrections need to be applied to all visibility measurements unless the values are only associated with baselines for one antenna. If the closure values are mainly associated with short or long baselines, then the calibrator source may not be sufficiently a point source.

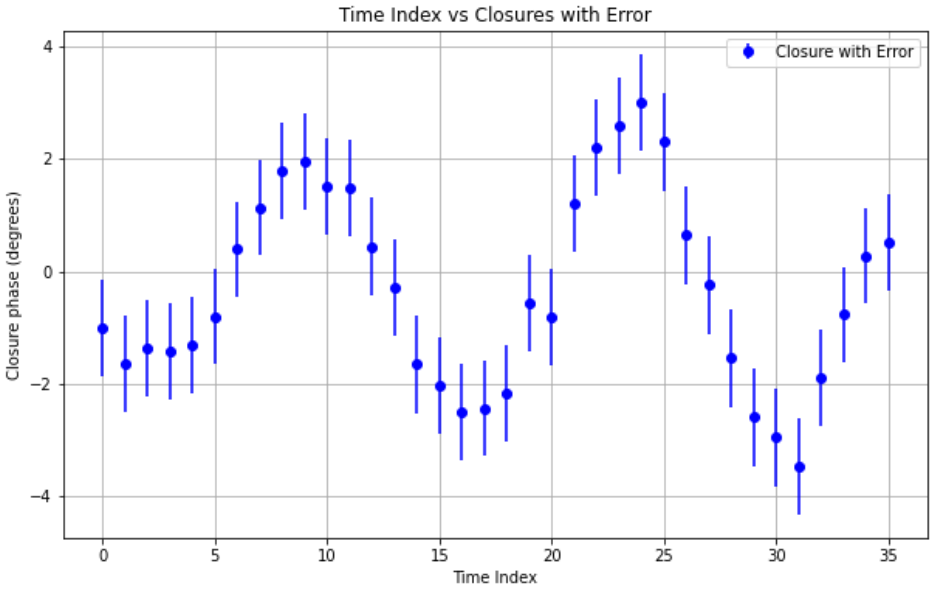

Figure 4: An example of closure phase in degrees for a calibrator source 1034-293 generated for one closure triangle using closure task in casa and manipulated using python. The plot shows an acceptable closure phase for this closure triangle.

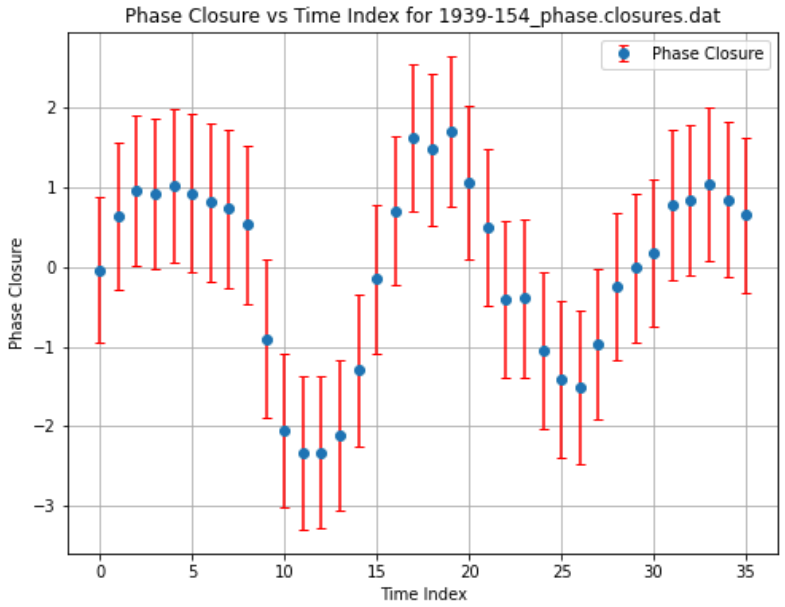

Figure 5: An example of closure phase (XX correlation) in degrees for a calibrator source 1939-154 generated for one closure triangle using a closure task in casa and manipulated using python. The plot shows an acceptable closure phase.

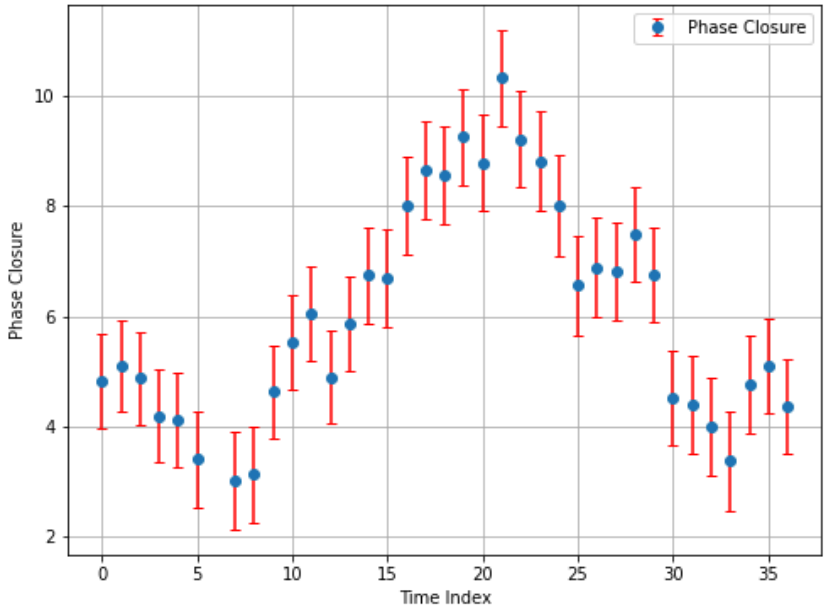

Figure 6: An example of closure phase (XX correlation) in degrees for a calibrator source j0515-4556 generated for one closure triangle using closure task in casa and manipulated using python. The plot shows closure phase greater than 2 degrees which might indicate that the target is resolved or there are bright sources in the field.

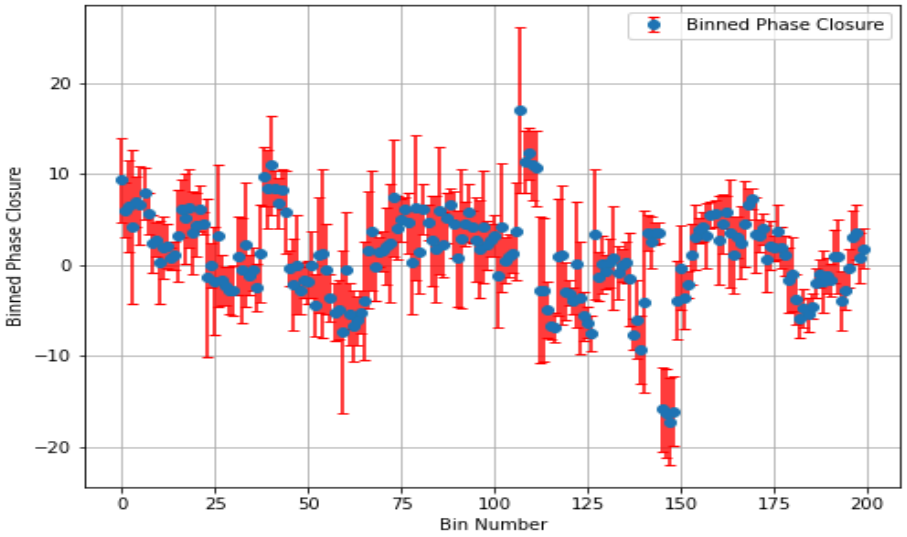

Figure 7: An example of binned closure phases (XX correlation) in degrees for a calibrator source j0515-4556 generated for all closure triangles which includes small and long baselines. The values are average phase closure quantities while the errors are propagated.

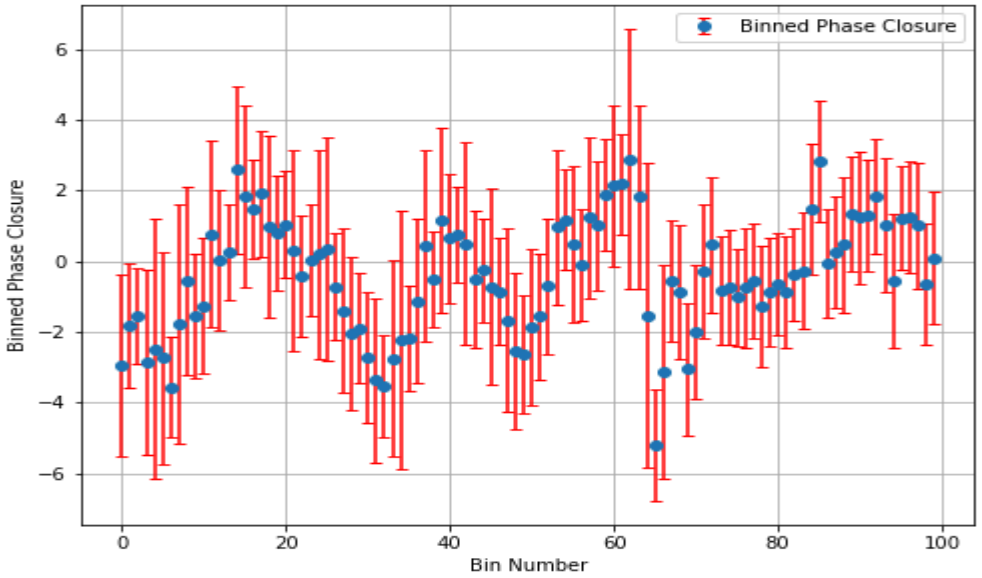

Figure 8: An example of binned closure phases (XX correlation) in degrees for a calibrator source 1305-105 generated for all closure triangles which includes small and long baselines. The values are average phase closure quantities while the errors are propagated.

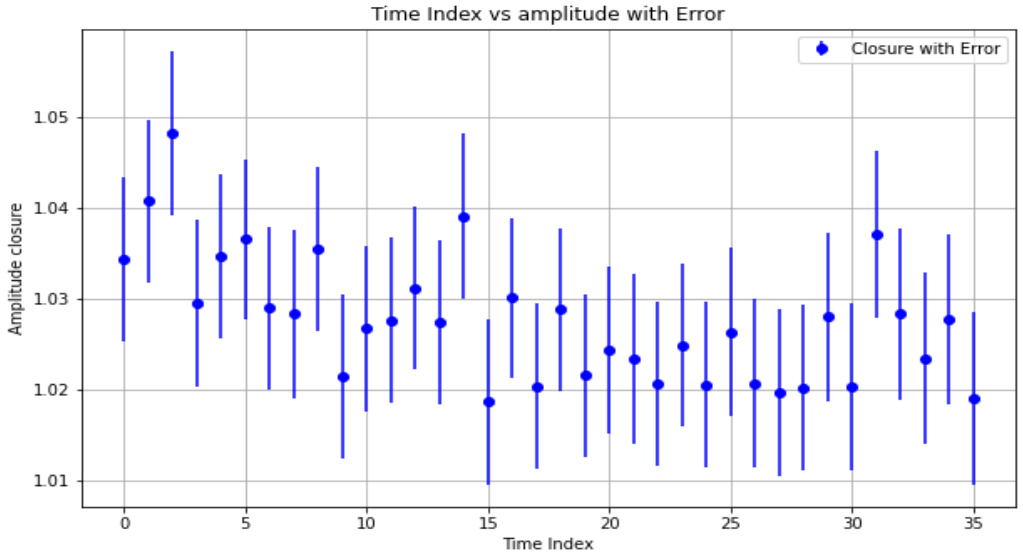

Figure 9: An example of amplitude closure (XX correlation) for a calibrator source 1034-293. generated for one closure triangle using the closure task in casa and manipulated using python. The plot shows acceptable closure amplitude.

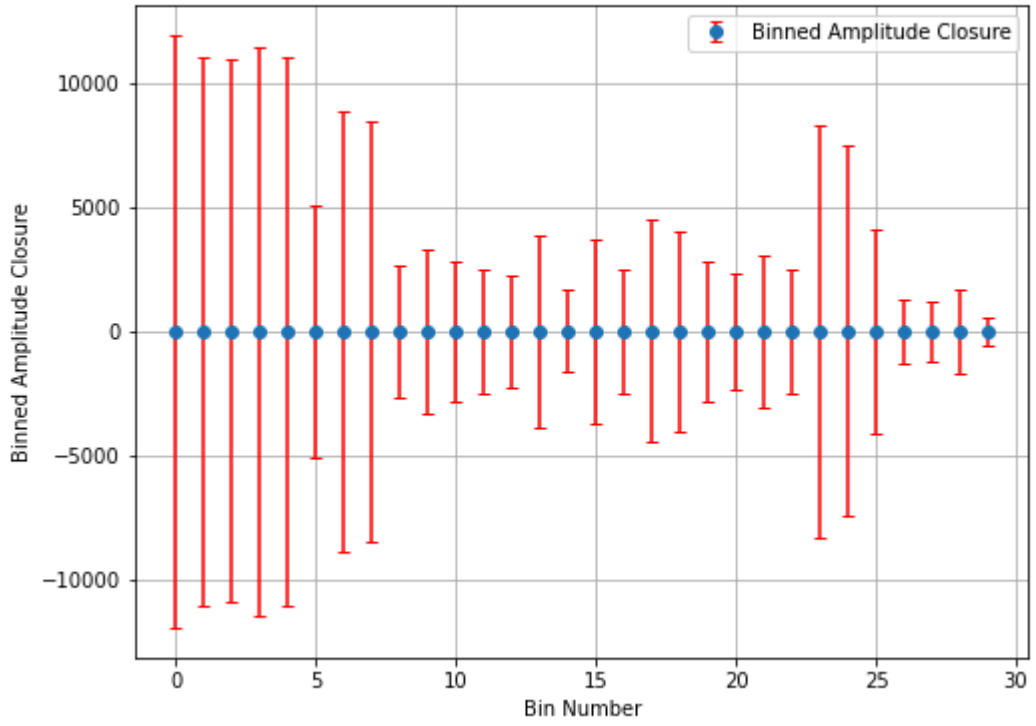

Figure 10: An example of amplitude closure quantities (XX correlation) for a calibrator source J0505 + 0459 generated for all closure triangles which includes small and long baselines. The values are average amplitude closure quantities while the errors are propagated.

To get the average values of closure quantities we use the values computed in the CASA closure task and bin them in python. Binning data refers to the process of grouping continuous data into discrete intervals. Here the closure phase or amplitude are binned and averaging values within predefined ranges or "bins." For example, instead of calculating statistics on individual data points, the data data points are grouped into bins of 10, 30 or 50, and the average closure amplitude or phase is determined within each bin. This helps reduce noise and can make patterns more evident in the data. This is then averaged again to get one value as indicated in Table 4. See similar calculations for ATCA (https://www.narrabri.atnf.csiro.au/calibrators/calibrator_database_documentation.html#measurement-process-closure)

The XX correlation data is utilised here across all the baselines. The values noted in Table 4, indicate the quantity from the closure triangles. Note that there was no significant difference across all the closure triangles.

The errors of each closure quantity were determined using error propagation. Each value in each bin has an associated error, and when calculating the mean for the bin, the errors propagate. The

error for each value is independent, thus the propagated error for the mean in a bin is calculated by square root of the sum of (error of each value)^2 /the number of values in the bin. Intrinsic variance of values within each bin (how much the values deviate from their mean), was included in the calculations.

Once each bin has an associated error, I calculate an overall propagated error for the entire dataset by combining the errors across each bin. The single overall error is therefore the square root of the sum of (error of each bin)^2 /the total number of bins.

In order to quantify the phase closure values, I determine the statistical significance by comparing them with the closure phase mean of zero such that the mean closure value minus the expected value divided by the standard error gives a Z score. For all the selected targets, the Z scores were determined to be less than 2 implying a 2 sigma significance.

Table 4: Average closure quantities (XX correlation) and respective propagated error for selected targets. The given closure quantities are sufficient to show that the selected targets are point sources and there is no interference from bright sources.

Name	Mean closure phase (degrees)	Mean closure amplitude
1034-293	0.571 +/- 0.583	1.076 +/- 0.022
1051-316	-0.448 +/- 0.294	1.093 +/- 0.027
1057-245	-0.218 +/- 0.354	1.078 +/- 0.022
1131-050	-0.916 +/- 0.385	1.271 +/- 0.043
1124-186	-0.144 +/- 0.723	1.171 +/- 0.028
1145-071	0.0035 +/- 0.295	1.034 +/- 0.014
1145-228	0.194 +/- 0.188	1.269 +/- 0.04
1146-247	-0.409 +/- 0.377	1.03 +/- 0.0136
1147-074	-0.0083 +/- 0.298	1.055 +/- 0.015
1305-105	-0.396 +/- 0.41	1.127 +/- 0.025
1351-018	-0.213 +/- 0.319	1.128 +/- 0.031
1357-177	0.356 +/- 1.474	1.308 +/- 0.041
1404-015	-0.055 +/- 0.32	1.174 +/- 0.0434

0016-002	0.282 +/- 0.252	1.095 +/- 0.0072
0040-017	0.402 +/- 2.95	2.591 +/- 0.347
1923-210	0.066 +/- 0.286	1.163 +/- 0.0093
1937-399	-0.0357 +/- 0.304	1.102 +/- 0.0079
1939-154	0.413 +/- 1.193	1.383 +/- 0.06
1958-179	0.126 +/- 0.155	1.0044 +/- 0.004
2011-157	0.011 +/- 0.39	1.051+/- 0.01
1949-199	0.0877 +/- 0.149	1.1304 +/- 0.343
2007-445	-0.0265 +/- 0.289	1.707 +/- 0.512
2047-026	-0.0939 +/- 0.167	1.08 +/- 0.144
2052-474	-0.0764 +/- 0.28	1.061 +/- 0.039
2110-103	0.005 +/- 0.303	1.103 +/- 0.165
0012-399	0.0836 +/- 0.18	1.052 +/- 0.004
1448-163	-0.076 +/- 0.168	1.019 +/- 0.003
1507-168	0.818 +/- 0.753	1.125 +/- 0.018
1522-275	-0.011 +/- 0.166	1.033 +/- 0.004
1543-079	-0.121 +/- 0.338	1.031 +/- 0.007
1546-004	0.094 +/- 0.573	1.066 +/- 0.012
1554-270	-0.025 +/- 0.232	1.044 +/- 0.007
1557-000	-0.053 +/- 0.21	1.094 +/- 0.005
1700-261	-0.0077 +/- 0.119	1.0043 +/- 0.004
1743-038	0.013 +/- 0.116	1.0023 +/- 0.0043
1745-078	-0.075 +/- 0.2	1.0389 +/- 0.005
1751-253	0.132 +/- 0.4	1.1798 +/- 0.024
1811-209	2.153 +/- 1.54	1.582 +/- 0.12
1822-096	0.0128 +/- 0.128	1.0027 +/- 0.005

1415 +133	0.1 +/- 0.448	1.1164+/- 0.01
1430 +107	-0.0133 +/- 0.344	1.190 +/- 0.01
1436 +107	0.466 +/- 0.304	1.0723 +/- 0.0079
1446 +173	0.562 +/- 0.964	1.518 +/- 0.05
1504 +104	0.217 +/- 0.318	1.052 +/- 0.0084
1505 +034	-0.288 +/- 0.459	1.136 +/- 0.01
2219 -279	0.044 +/- 0.708	1.108 +/- 0.015
2248 -325	-0.432 +/- 0.366	1.043 +/- 0.01
2257 -364	0.082 +/- 0.224	1.041 +/- 0.005
2314-316	-0.334 +/- 0.696	1.347 +/- 0.022
2314-449	0.083 +/- 0.248	1.026 +/- 0.01
2324-372	-0.0886 +/- 0.26	1.142 +/- 0.0076
2333 -237	0.2395 +/- 0.227	1.055 +/- 0.0086
2348-165	-0.068 +/- 0.167	1.013 +/- 0.004
2354-152	-0.259 +/- 0.28	1.0977 +/- 0.0064
2359 -315	0.242 +/- 0.554	1.216 +/- 0.014
0121 + 043	-0.018 +/- 0.161	1.127 +/- 0.056
0149 + 059	-0.161 +/- 0.222	1.271 +/- 0.422
0203 + 115	0.091 +/- 0.332	1.392 +/- 0.103
0204 + 152	0.0555 +/- 0.079	1.03 +/- 0.141
0231 + 133	0.194 +/- 0.134	1.069 +/- 1.19
J02111 + 1051	-0.669 +/- 0.458	1.5 +/- 0.117
J0502 + 0609	-1.038 +/- 0.385	1.248 +/- 0.128
J0505 + 0459	**0.7211 +/- 1.51**	**3.86 +/- 1104.77**
J0509 + 0541	0.0168 +/- 0.285	1.256 +/- 3.08
J0522 + 0113	0.814 +/- 0.284	1.19 +/- 0.11
T0237+0919	-0.0904 +/- 0.182	1.082 +/- 0.0357

1432-180	-0.0104 +/- 0.4198	2.028 +/- 2.555
J0659 + 0813	0.0045 +/- 0.419	1.825 +/- 0.058
J0738 + 1742	-0.0063 +/- 0.42	1.69 +/- 0.24
J0745 + 1011	0.00092+/- 0.4	1.67 +/- 0.562
J0839+0319	0.00261 +/- 0.42	1.878 +/- 1.454
T0735 + 2341	-0.00093 +/- 0.42	1.92 +/- 0.134
T0952 + 2828	0.0065 +/- 0.4	1.884 +/- 0.348
0037 - 593	-0.202 +/- 0.266	1.506 +/- 0.061
0048 - 427	0.167 +/- 0.229	1.27 +/- 0.085
0048 - 447	-0.165 +/- 0.347	1.682 +/- 0.36
0131 -522	-0.113 +/- 0.202	1.154 +/- 1.73
0214-522	0.0717 +/- 0.302	1.066 +/- 0.322
0308 - 611	-0.0255 +/- 0.1	1.03 +/- 0.134
0332 - 403	-0.0042 +/- 0.184	1.106 +/- 0.331
0407-658	0.0234 +/- 0.183	1.0013 +/- 0.0076
0606-795	0.0116 +/- 0.206	1.0443 +/- 0.0361
J0044 - 8422	0.178 +/- 0.636	1.53 +/- 0.027
J0246 - 4651	0.025 +/- 0.21	1.232 +/- 0.079
1534 + 015	-0.255 +/- 0.342	1.267 +/- 0.084
1553 +129	0.0089 +/- 0.188	1.315 +/- 0.563
1658-076	-0.048 +/- 0.235	1.28 +/- 0.126
1741 - 038	0.0085 +/- 0.08	1.024 +/- 0.08
2129-156	0.129 +/- 0.372	1.159 +/- 0.089
2129-183	-0.00049 +/- 0.228	1.134 +/- 0.345
2236 - 145	-0.195 +/- 0.21	1.36 +/- 0.05
2255-087	0.082 +/- 0.459	1.707 +/- 0.413
2323 - 032	0.021 +/- 0.162	1.143 +/- 5.93

J1608 + 1029	0.06 +/- 0.927	1.21 +/- 0.21
J1640 + 1220	0.091 +/- 0.142	1.094 +/- 0.1
J1728 + 0427	-0.091 +/- 0.24	1.554 +/- 0.044
J1734 + 0926	-0.191 +/- 0.22	1.12 +/- 0.47
0647-475	0.105 +/- 0.187	1.163 +/- 1.803
0731-465	0.160 +/- 0.256	1.258 +/- 0.085
0843 -54	0.0033 +/- 0.187	1.187 +/- 0.15
0906-47	-0.770 +/- 0.825	1.635 +/- 0.184
0906-682	-0.086 +/- 0.185	1.253 +/- 0.22
J0524 -5668	0.049 +/- 0.334	1.43 +/- 11.54
J0625 - 5438	-0.318 +/- 2.42	1.768 +/- 1.06
J0607 - 6031	-1.397 +/- 0.491	1.498 +/- 0.225
J1109 + 3744	0.0076 +/- 3.29	2.64 +/- 0.271
T1126 + 3345	0.145 +/- 0.35	1.6 +/- 0.179
0222 - 346	0.058 +/- 0.15	1.214 +/- 0.12
0242 -215	-0.016 +/- 0.28	1.23 +/- 0.05
0319 + 1901	-0.037 +/- 0.265	1.45 +/- 1.26
0501 - 019	0.0131 +/- 0.12	1.03 +/- 0.06
J0449 + 1121	-0.379 +/- 1.192	1.42 +/- 0.41
J0459 + 0229	-0.0098 +/- 0.133	1.103 +/- 0.33
0010+174	-0.454 +/- 0.528	1.601 +/- 0.195
0110-076	-0.172 +/- 0.346	1.370 +/- 0.076
0219+0120	0.106 +/- 0.341	1.307 +/- 0.168
0249+0619	0.737 +/- 0.446	1.371 +/- 0.27
0259+0747	0.106 +/- 0.395	1.323 +/- 0.46
2138-246	0.344 +/- 0.714	1.657 +/- 0.394
J0403+2600	-0.008 +/- 0.132	1.171 +/- 0.659

3.5: Rejected targets

Targets that were not considered ideal calibrators include:

- Low values of flux density
- Multi-component sources (resolved)
- Resolved out images

Here, we use two criteria to reject non-ideal calibrators. The first criterion is the brightness. A faint calibrator will have a low signal-to-noise (S/N) ratio, meaning the signal from the source is close to the noise level of the observation. This makes it difficult to accurately measure the source's amplitude and phase. If the complex gain is measured inaccurately, errors in the gain calibration will propagate into the target observations, degrading data quality or leading to incorrect interpretations. To compensate for the low S/N of a faint calibrator, longer integration times are required to improve it by averaging out the noise. However, this introduces issues such as increased observation time for calibration, reducing the time available for science target observations. During long integrations, atmospheric turbulence and instrumental drifts can change, further complicating the calibration process. A faint calibrator may not provide sufficient signal to track short-term variations in antenna gains or atmospheric conditions accurately. In contrast, a bright calibrator can be observed quickly and frequently, allowing for real-time tracking of these variations. If the calibrator is too faint, the phase measurements will be dominated by noise, leading to significant uncertainties or incorrect phase solutions.

Table 5: Rejected sources with low flux densities

Name	Integrated flux density +/- error (2.84 GHz)/ mJy	Ra	Dec	Reason
1146-289	312.7 +/- 1.5	11:46:26.197	-028:59:18.642	Low flux density
1253-055	11082 +/- 84	12:56:11.163	-005:47:21.496	
1357-154	415.6 +/- 2.4	13:57:11.242	-015.27.28.81	Low flux density
J1112-2158	1031 +/- 10	11:12:49.839	-021:58:29.467	
0040-017	666.3 +/- 1.0	00:40:57.619	-001:46:31.888	Two components
0050-094	263.5 +/- 3.8	00:50:41.307	-009:29:05.199	Low flux density
1957-387	2369.7 +/- 1.4	19:57:59.809	-038:45:06.230	Resolved

2109-411	1643.2 +/- 3.4	21:09:33.186	-041:10:20.785	Resolved
2047-166	399.7 +/- 8.6	20:47:19.67	-016:39:05.944	Three components
J0006-0623	3956.0 +/- 6.5	00:06:13.869	-006:23:35.488	resolved
0011-262	265.43 +/- 0.20	00:11:01.232	-026:12:33.182	Low flux density
1513-212	447.00 +/- 0.23	15:13:56.968	-021:14:57.545	Low flux density
1538+003	408.42 +/- 0.98	15:38:15.951	+000:19:05.339	Low flux density
1438-220	482.46 +/- 0.92	14:38:09.468	-022:04:54.69	Three components
1445-164	337.9 +/- 1.4	14:45:53.372	-016.29.01.765	Low flux density
1622-253	1640 +/- 23	16:25:46.895	-025:27:38.131	Resolved
J0823+2928	485.6 +/- 4.9	08:23:41.137	+029:28:28.42	Low flux density
J0827+3525	820.7 +/- 7.7	08:27:38.605	+035:25:05.77	Resolved
J1016+2037	720 +/- 18	10:16:44.32	+020:37:47.471	Resolved
J1103+2203	773 +/- 24	11:03:23.065	+022:03:37.755	Resolved
J1125+2610	747 +/- 32	11:25:53.713	+026:10:20.237	Resolved
T1052+2029	1111 +/- 34	10:52:26.096	+020:29:48.282	Resolved
0047-579	1812 +/- 32	00:49:59.475	-057:38:27.306	Resolved
0039-445	1870 +/- 200	00:42:09.018	-044:13:59.685	resolved
0252-549	847 +/- 12	02:53:29.183	-054:41:51.354	Resolved
0355-669	683.7 +/- 7.9	03:55:47.892	-066:45:33.958	Resolved
2326-477	2612 +/- 29	23:29:17.704	-047:30:19.1	Resolved
j0330-4014	496.3 +/- 6.7	03:30:51.098	-040:14:16.827	Low flux density
J1041+0610	1407 +/- 12	10:41:17.148	+006:10:16.67	Resolved
1344 + 141	559.0 +/- 7.0	13:44:23.738	+014:09:14.999	Resolved
J1038+0512	1020.8 +/- 10.0	10:38:46.765	+005:12:28.889	Resolved

J1445+0958	1.38 +/- 0.20	14:45:16.452	+009:58:36.171	Resolved
J1737+0621	489.4 +/- 2.6	17:37:13.748	+006:21:03.666	Resolved
2137-207	2245.0 +/- 8.9	21:37:49.998	-020:42:31:696	Resolved
0454-463	2599 +/- 80	04:55:50.794	-046:15:58.491	Resolved
0506-612	1598 +/- 69	05:06:44.006	-061:09:41.296	Resolved
0515-674	1001.6 +/- 9.9	05:15:37.559	-067:21:28.008	Resolved
0539-530	675 +/- 17	05:40:25.156	-053:03:46.547	Resolved
0637-752	4360 +/- 120	06:35:46.561	-075:16:16.66	Resolved
0903-573	2455 +/- 78	09:04:53.235	-057:35:04.834	Resolved
J1109+3744	773 +/- 31	11:09:28.866	+037.44.32.442	Resolved
J1130+3815	1858 +/- 68	11:30:53.295	+038:15:19.499	Resolved
J1158+2450	1316 +/- 31	11:58:25.793	+024:50:18.495	Resolved
j0515-4556	872 +/- 20	05:15:45.258	-045:56:43.034	Resolved
j0820-5705	1090 +/- 100	08:20:58.846	-057:05:32.529	Two components
0029+349	1452 +/- 99	00:29:14.233	+034:56:32.795	Resolved
0042+2320	1048 +/- 91	00:42:04.509	+023:20:00.985	Resolved
0111+3906	1.13 +/- 0.23	01:11:37.407	+039:06:29.777	Resolved
0149+3628	489 +/- 80	01:49:46.092	+036:28:32.499	Low flux density

0204-170	1515 +/- 21	02:04:57.682	-017:01:19.720	Resolved
0205+322	1240 +/- 160	02:05:04.946	+032:12:30.610	Resolved
0238-084	1170 +/- 22	02:41:04.797	-008:15:20.586	Resolved
0309+1029	399.7 +/- 4.5	03:09:03.622	+010:29:16.444	Low flux density
0318+1628	4118 +/- 69	03:18:57.8	+016:28:32.9	Resolved
0321+1221	1636 +/- 23	03:21:53.1	+012.21.13.995	Resolved
0336-019	805 +/- 22	03:39:30.955	-001:46:35.67	Resolved
J0426+0518	489.4 +/- 4.9	04:26:36.599	+005:18:19.948	Low flux density
1538+003	388.6 +/- 6.0	15:38:15.956	+000:19:05.471	Low flux density
1549+026	3037 +/- 45	15:49:29.439	+002:37:01.296	Resolved
2142-046	502 +/- 17	21:42:36.873	-004:37:43.9305	Resolved
J1513+2338	1189 +/- 15	15:13:40.177	+023:38:35.29	Resolved
J1716+2152	562 +/- 13	17:16:11.177	+021:52:13.056	Resolved
J1719+1745	759 +/- 19	17:19:13.028	+017:45:05.588	Resolved
J1734+3857	938 +/- 74	17:34:20.598	+038.57.53.014	Resolved
J1753+2848	1910 +/- 170	17:53:42.438	+028:48:04.391	Resolved
J1845+3541	1050 +/- 120	18:45:35.116	+035:41:18.289	Resolved
J2151+0552	887 +/- 40	21:51:37.896	+005:52:13.038	Resolved
T1525+0308	1208 +/- 12	15:25:48.962	+003:08:26.185	Resolved
0239+0416	459.4 +/- 3.0	02:39:51.249	+004:16:21.270	Low flux density
0329+2756	863.3 +/- 3.8	03:29:57.676	+027:56:15.567	Two component

0329+3510	647.8 +/- 5.1	03:29:15.378	+035:10:06.429	Three components
0336+3218	1862 +/- 19	03:36:30.125	+032:18:29.618	Two components
0503+3403	583.0 +/- 7.3	05:03:56.818	+034.03.29.011	Two components
0510+1800	748.6 +/- 3.2	05:10:02.364	+018:00:41.586	Resolved
2146-154	354.0 +/- 5.1	21:46:22.981	-015:25:43.825	Low flux density
2357-114	1875 +/- 19	23:57:31.199	-011:25:39.225	Resolved
2358-103	459.9 +/- 3.9	23:58:10.882	-010:20:08.701	Low flux density
J0429+2724	340.8 +/- 2.7	04:29:52.970	+027:24:37.97	Low flux density
J0443+3441	456 +/- 13	04:43:31.684	+034:41:07.584	Low flux density
J2015+3410	538 +/- 20	20:15:28.878	+034:10:39.076	Resolved
J2025+3343	1589 +/- 45	20:25:10.879	+033:43:00.035	Resolved
J2050+3127	669 +/- 21	20:50:51.16	+031:27:27.218	Resolved
J2052+3635	4130 +/- 160	20:52:52.079	+036:35:35.786	Resolved
J2114+2832	300.6 +/- 6.7	21:14:58.35	+028:32:57.496	Low flux density
J2218-0335	1921 +/- 22	22:18:52.041	-003:35:36.902	Resolved

Two component sources (resolved)

The second criterion for rejecting a calibrator is the presence of structure. Calibrators are not always point sources. Many are bright but resolved. At low resolution and lower frequencies, many sources used as the VLA calibrators are considered point sources with extended emission hence possible confusion with nearby sources. If the calibrator has significant structure across the UV plane, then self-calibration techniques are necessary to derive the complex gain. The calibration process should minimise complexity to avoid prolonged and complex calibration strategies. The calibrators' complex spatial structure introduces variability in the visibility data, making it difficult to obtain reliable amplitude and phase calibrations across baselines. Visibility measurements for extended sources vary with baseline, while ideally, the amplitude should be constant. Any baseline-dependent amplitude variations makes it difficult to distinguish whether the changes in the observed visibility are due to the source structure or instrumental effects. Calibration relies on a stable reference, so any baseline-dependent changes introduce errors. The phase response of an extended source is also complex because different parts of the source

contribute different phases depending on their position relative to the antennas. This leads to inconsistent phase measurements across baselines. Phase variations from extended sources compromise the stable reference needed for reliable phase calibration..

Table 6: Sources with more than one component

Name	Image
J0820-5705	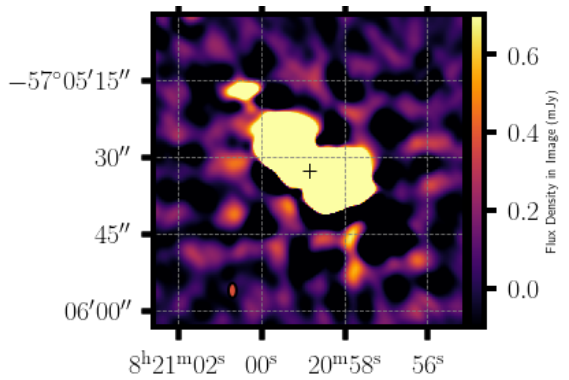
0040-017	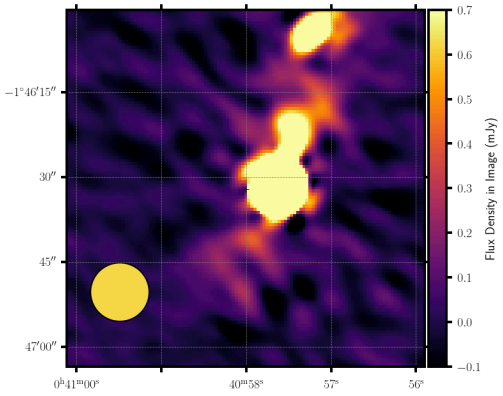
2047-166	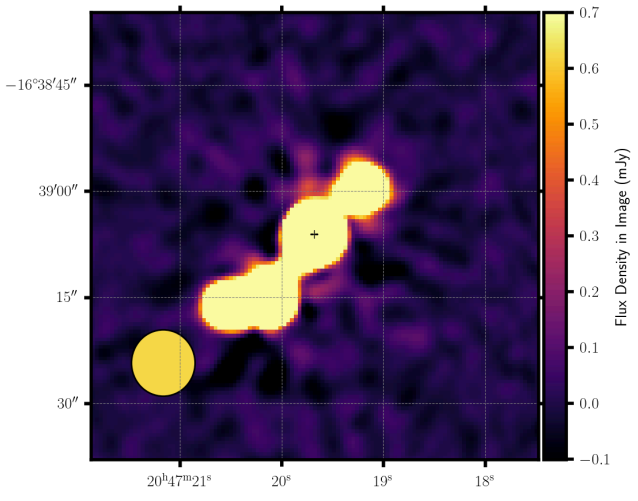

1438-220	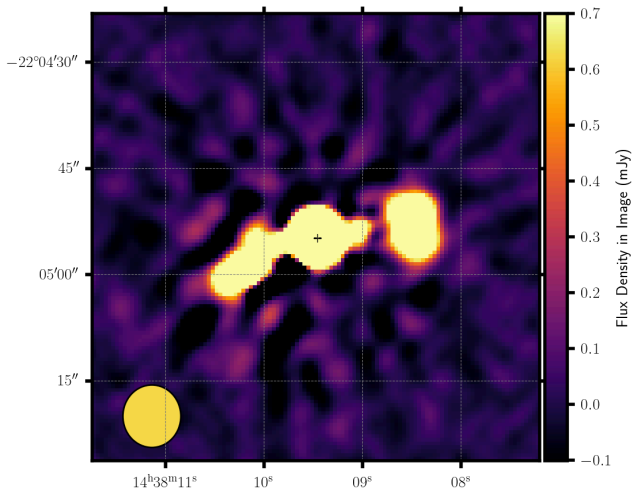

Resolved out images

Finally, some sources are resolved out, resulting in weak or zero visibilities, as the interferometer can no longer detect the source effectively. The sample obtained from the VLA database contained sources that had flux densities > 0.5 Jy at VLA S band (3 GHz). The resolution of the MeerKAT S band is only an estimate between VLA C and B configurations and ATCA's 3 to 9 arcsecs. Consequently, some of the targets were resolved out hence not suitable calibrators.

Table 7: Images that are resolved out.

Name	Ra	Dec	Image
0047-579	00:49:59.48	-057:38:27.31	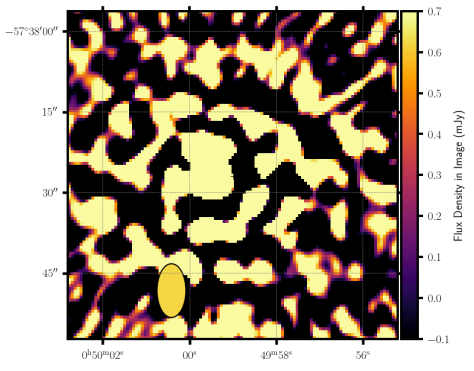

0252-549	02:53:29.18	-054:41:51.35	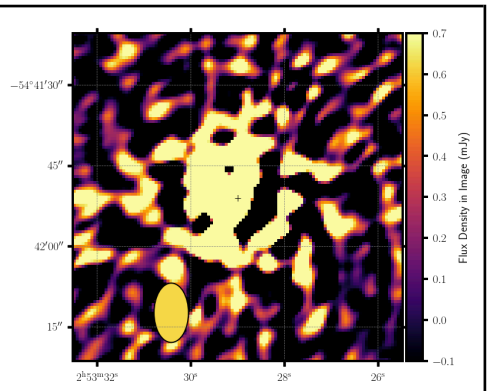
0355-669	03:55:47.89	-066:45:33.96	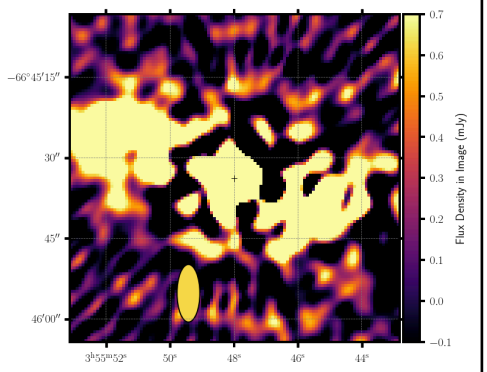
1622-253	16:25:46.9	-025:27:38.13	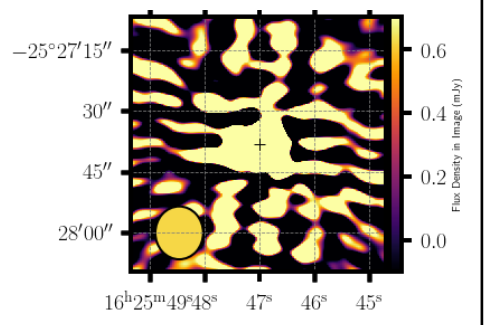
J1016+2037	10:16:44.32	+020:37:47.47	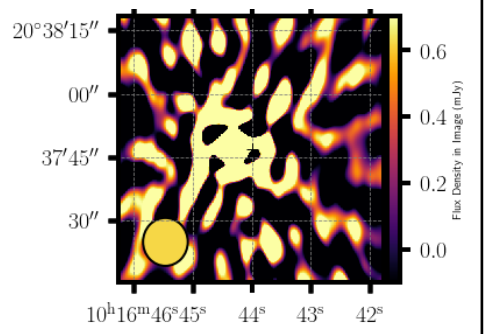
J1103+2203	11:03:23.06	+022:03:37.75	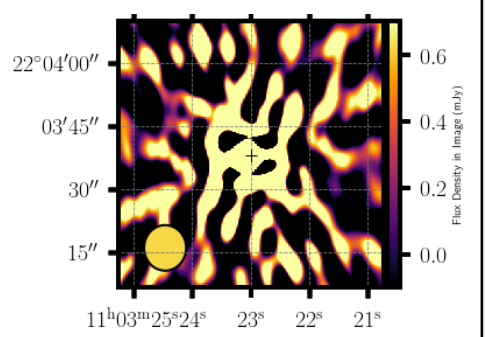

0903-573	09:04:53.2351	-057:35:04.8337	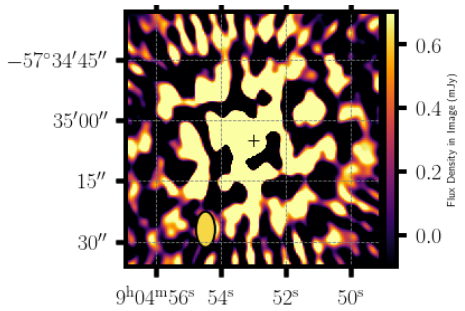
J1130+3815	11:30:53.2949	+038:15:19.4985	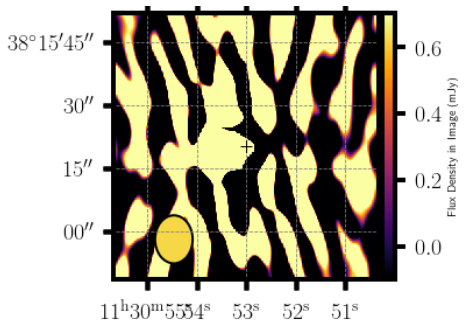
J1158 +2450	11:58:25.7932	+024:50:18.4945	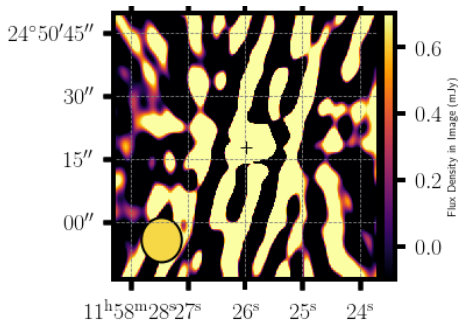
J0515-4556	05:15:45.2579	-045:56:43.0342	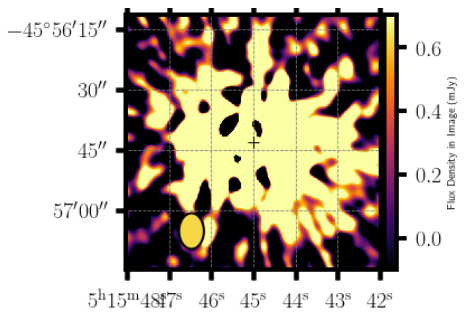

4 Further work

4.1 Polarisation

Each dataset was observed using either the 3C 286 or 3C 138 polarization calibrator. However, polarization analysis was not performed, and the results are not included in this report.

Conducting such analysis would be valuable, as it could expand the pool of sources that can be used to calibrate MeerKAT data as polarization calibrators.

5 References

Beasley A. J., Conway J. E., Diamond P. J., Cotton W. D., Vermeulen R. C., 1994, in Robertson J. G., Tango W. J., eds, IAU Symposium Vol. 158, Very High Angular Resolution Imaging. p. 105
Heywood I., 2020, oxkat: Semi-automated imaging of MeerKAT observations, Astrophysics Source Code Library, record ascl:2009.003 (ascl:2009.003)
Heywood I., et al., 2022, MNRAS, 509, 2150
Hugo B. V., Perkins S., Merry B., Mauch T., Smirnov O. M., 2022, in Ruiz J. E., Pierfedereci F., Teuben P., eds, Astronomical Society of the Pacific Conference Series Vol. 532, Astronomical Society of the Pacific Conference Series. p. 541 (arXiv:2206.09179), doi:10.48550/arXiv.2206.09179
Kenyon J. S., Smirnov O. M., Grobler T. L., Perkins S. J., 2018, MNRAS, 478, 2399
Kovalev Y. Y., Petrov L., Fomalont E. B., Gordon D., 2007, AJ, 133, 1236
O'Dea C. P., Saikia D. J., 2021, A&ARv, 29, 3
Offringa A. R., et al., 2014, MNRAS, 444, 606
Fomalont E. B., Perley R. A., 1999, in Taylor G. B., Carilli C. L., Perley R. A., eds, Astronomical Society of the Pacific Conference Series Vol. 180, Synthesis Imaging in Radio Astronomy II. p. 79
Thompson A. R., Moran J. M., Swenson George W. J., 2017, Interferometry and Synthesis in Radio Astronomy, 3rd Edition, doi:10.1007/978-3-319- 44431-4.